University of Sheffield

Department of Civil
and Structural Engineering

The rapid load testing of piles in fine grained soils

By

Michael John Brown

Supervisor: Doctor Adrian F.L. Hyde

A thesis submitted to
The University of Sheffield
Department of Civil and Structural Engineering
for the degree of Doctor of Philosophy

March 2004

Abstract

The behaviour has been examined of piles installed in clay subject to a rapid load testing method known as the Statnamic test. The Statnamic method is easier and quicker to mobilise than a static test and is less complex to analyse than dynamic pile load tests. This investigation consisted of a laboratory study of the effect of the rate of loading on pile behaviour in clay and a field test of a pile in glacial clay to calibrate the findings of the laboratory study.

The effects of penetration rate and Statnamic loading on model pile behaviour have been studied using an instrumented clay calibration chamber. The effect of rate of loading on the pile's capacity was quantified using constant rate of penetration tests (CRP) at different pile penetration rates. This allowed viscous soil damping characteristics to be determined and a new Statnamic analysis method incorporating rate dependant soil behaviour to be developed. This rate dependant behaviour can be represented by modification of a non-linear rate law proposed by Randolph & Deeks (1992).

A field pile testing facility was developed in glacial till. To test the success of the new Statnamic analysis, a class A prediction of static pile behaviour from prototype pile load testing was undertaken. Encouraging results were obtained for the prediction of ultimate static pile behaviour, but the analysis method under predicted soil-pile stiffness. A soil inertial component was added to the analysis, based upon instrumentation readings, which improved the predicted static soil-pile stiffness.

Results from prototype pile testing show that the stiffness during Statnamic and static load tests was very similar up to 50% of the ultimate static pile capacity. Thus, rapid load testing may be used for verification of pile settlements at working loads in clays. At the present level of understanding of testing in clays, rapid load pile tests should not be carried out in isolation. Ideally, tests should be used in conjunction with a static test that will allow back figured parameters to be derived for analysis.

Keywords: pile testing, clay, rate effects, damping, Statnamic, static loading, rapid

Acknowledgements

My first acknowledgements most go to my supervising team of Dr Adrian Hyde and Prof. Bill Anderson. Again, as I did in my undergraduate thesis, I extend my thanks to Adrian for setting the initial course of the project, whilst allowing me to carry out research, and produce a thesis, that I can truly call my own. Adrian has always been generous with his time and advice on technical, personal and career issues. I am very grateful to Bill for his pragmatic input and the push to explore opportunities outside the bounds of normal PhD study.

Secondly, I would like to thank the Department of Civil and Structural Engineering's technical staff for all their hard work, good ideas and humour during this research. In particular, I wish to thank Paul Osborne, Mark Foster and Shane Smith for their support through leaks (water, kaolin and hydraulic oil), emergency shower visits and guesthouse food poisoning. These people are an asset to the department that cannot be assessed on financial balance sheets alone.

I am grateful to Andy Bell and the directors of the Expanded Piling Company Limited for providing access to their head office facilities to conduct Statnamic testing. The level of support from Andy, as well as the yard and office staff at Expanded made the field study both successful and enjoyable. Thanks are also extended to Ken Cameron and the team at PMC who undertook the Statnamic and static pile testing. I must also mention Mike Justason (Berminghammer Foundation Equipment) and Ed J Garbin (University of South Florida) who never failed to answer my never ending technical questions during preparation for the field study.

During this research, I have enjoyed my time as a member of the Geotechnical Engineering Research Group at the university and have been lucky to enjoy the company of very able researchers from diverse cultural and ethnic backgrounds. In particular, I have enjoyed working and socialising with Juan Balderas-Meca and wish him every success with his future career.

I am grateful to the EPSRC for providing the funding for the initial project (Grant No. GR/M64017/01) and additional funding to carry out the Grimsby field study (Grant No. GR/R46939/01).

Last but most importantly of all, I would like to thank my wife Claire and growing babies Ed and Alice. This process has probably been harder for them than it has for me. Without the support and understanding of Claire, this thesis would never have been started or completed. I hope that with its completion I will be able to become a full time, rather than part time, husband and father.

Contents

List of Tables

List of Figures

Notation

A	activity
A_{base}	pile base area
A_c	cross-sectional area of concrete
A_p	pile cross-sectional area
A_s	cross-sectional area of steel
A_{shaft}	pile shaft area
C	viscous damping constant
D	displacement control
D_{cell}	earth pressure cell diameter
D_p	pile diameter
E_{ct}	tangent modulus of concrete
E	Young's modulus (E_u for undrained loading of soil, E_p for a pile, E_s for steel)
F	flexible boundary
F_a	pile inertial component of resistance to Statnamic loading
F_{base}	pile base resistance to dynamic loading
F_E	flexibility ratio
F_{soil}	soil component of resistance to Statnamic loading
F_{STN}	measured Statnamic force
F_u	equivalent static pile resistance
F_{unl}	pile resistance at the unloading point
F_v	velocity dependant viscous soil resistance
G	shear modulus (G_0 for dynamic shear modulus)
G_s	specific gravity of soil grains
I_L	liquidity index
I_P	plasticity index
I_r	soil rigidity index
$I_{v\alpha}$	viscous damping constant for soil
J	viscous damping constant for soil
K	soil spring constant
K_L	viscous damping constant for soil
K_0	coefficient of earth pressure at rest
L	pile length
M	pile mass
N	rate parameter
N_c	bearing capacity factor
N_k	cone factor
N_s	scaling ratio
N_w	wave number
P	force control

$\dot{P}$	loading rate
P_h	pile head load
P_{hd}	pile head force derived from instrumentation during dynamic testing
$P_{h(total)}$	total pile head force
Q	quake
P_i	axial force at level i in a pile
Q_b	pile base resistance
Q_s	pile shaft resistance
R	pile radius
R_A	average surface roughness
R_f	cone friction ratio
$R_{dynamic}$	dynamic pile resistance
R_d	resistance to dynamic pile loading
R_{ep}	radius of elastic plastic boundary
R_R	force resisting dynamic loading
R_{static}	static pile resistance
R_s	low rate pile resistance
S_w	stiffness coefficient
S_1	sliding shear against a smooth surface
T	duration of Statnamic loading
ΔU	excess pore pressure
V_s	shear wave velocity
Z	pile impedance
a	acceleration
a_0	dimensionless frequency
c	elastic wave velocity
c_u	undrained shear strength
$c_{u\alpha}$	undrained shear strength at a defined low strain rate
c_{ud}	undrained shear strength at an elevated rate
$\dot{e}$	rate of change of void ratio
f_{cu}	concrete cube strength
f_s	cone sleeve friction resistance
k_v	coefficient of vertical permeability
q_c	cone end resistance
q_{cd}	cone end resistance at elevated rates
q_{cs}	cone end resistance at the lowest rate
q_f	deviatoric stress at failure

q_s	ultimate unit shaft resistance
r	radial distance from pile centreline
r_{probe}	"effective radius" of penetrating object
t	time
t_f	time to failure
v	velocity
Δv	pile-soil relative velocity
v_s	lowest velocity
v_0	reference velocity
w	soil water content
w_L	liquid limit
w_P	plastic limit
x	displacement
$\dot{x}$	velocity
$\ddot{x}$	acceleration
x_e	elastic soil deformation
$\ddot{x}_l$	local clay bed accelerations
$\ddot{x}_p$	peak pile acceleration
x_0	amplitude of vibration
z	elevation above pile tip
M	slope of critical state line projected to $q' : p'$ plane
α	viscous damping constant for soil
α_A	adhesion factor for pile friction
β	viscous damping constant for soil
δ	angle of friction
δ_{cell}	earth pressure cell deflection
ε	strain
$\dot{\varepsilon}$	strain rate
ε_f	failure strain
ϕ	design load resistance factor
$\dot{\gamma}_a$	reference shear strain rate
$\dot{\gamma}_d$	elevated shear strain rate
η	Mullins (2002) rate factor
$\overline{\eta}$	Taylor (1942) rate factor
κ	slope of swelling and recompression line
λ	slope of normal consolidation line and critical state line
λ_L	wave length
μ	coefficient of friction
ρ	saturated soil density
ρ_p	pile density
σ_c	chamber confining pressure
σ_h	horizontal stress
σ'_{rr}	radial effective stress
τ	pile shaft shear stress
τ_d	resistance to shear at elevated rates

τ_s	resistance to shear at low rates
ω	circular frequency of oscillation (angular velocity)
υ	Poisson's ratio (υ_u for soil during undrained loading)
ζ	dimensionless parameter after Randolph (1983)

Abbreviations

AOD	Above Ordnance Datum
BD	Clay bed
BGL	Below Ground Level
BH	Borehole
BSPT	British Standard Pipe Thread
CAF	Cell Action Factor
CF	Clay Fraction
CFA	Continuous Flight Auger
CPT	Cone Penetration Testing
CRP	Constant Rate of Penetration test
DAQ	Data Acquisition
DC	Direct Current
EPCL	Expanded Piling Company Limited
EPSRC	Engineering & Physical Science Research Council
ID	Inner Diameter
KSS	Kaolin, Sand & Silt model soil
LRFD	Load and Resistance Factor Design
LVDT	Linear displacement transducer
MLT	Maintained load test
M-UPM	Modified Unloading Point Method
OCR	Over Consolidation Ratio
OD	Outer Diameter
OS	Ordnance Survey
PC	Personal Computer
PCPT	Cone Penetration Testing with pore pressure measurement
PP	Pore Pressure transducer
PSD	Particle Size Distribution
PVC	Poly Vinyl Chloride
QCL	Quick Continuous Load
QLT	Quick Load Test method
QML	See QLT above
RHS	Rectangular Hollow Section
SAW	Statnamic Analysis Workbook
SCPT	Cone Penetration Testing with Seismic measurements
SD	Standard Deviation
SHS	Square Hollow Section
SPT	Standard Penetration Test
STN	Statnamic
SUPERSAW	Segmental Unloading Point Statnamic Analysis Workbook
UK	United Kingdom
S-UPM	Segmental Unloading Point Method
UPM	Unloading Point Method
US	United States of America
1-D	One dimensional

1.0 Introduction

1.1 Preface

It is normal when constructing piled foundations to undertake a design process that results in specification of the pile length and cross sectional area. The main performance criteria are the pile's settlement under a working load and the ultimate bearing capacity. Large factors of safety are often used due to factors such as natural ground variation, differences in construction techniques and the accuracy of estimating axial capacity based upon empirical correlations. To allow more efficient and confident design of piles, it is common to carry out pile load tests prior to or during the design process. Load tests are also carried out during and after the pile construction process to allow verification of construction techniques and quality.

The main types of load test available fall into three categories; static, dynamic and kinematic or rapid load tests. Static tests are slow and infrastructure intensive but have the advantage of being simple to analyse. Conversely, dynamic tests are very fast with little additional infrastructure but they need specialised analysis techniques. Rapid load testing methods have been developed in an attempt to incorporate the advantages of both static and dynamic tests, the most common being the Statnamic test which has a loading duration between that of static and dynamic test.

The Statnamic test works by the rapid burning of a fuel that produces gas in a pressure chamber. This gas accelerates a mass upwards that in turn imparts a downward load on the test pile. The load is applied and removed by the controlled venting of the gas that results in a load duration $\approx$180 milliseconds which is thirty times that of dynamic load testing.

For foundation design, it is necessary to derive the equivalent static load-displacement curve from the Statnamic data due to damping or rate effects. Damping or rate effects may be defined as the enhancement of soil resistance due to increasing rates of testing. Current Statnamic analysis techniques consider both pile penetration rate dependent soil

damping (viscous damping) and acceleration dependent pile damping (inertial damping). However, the current analysis techniques make several assumptions that influence the accuracy of derived static behaviour. These include assuming that the viscous damping model is linear and that inertial effects are limited to the pile. In addition, the effects of excess pore water pressure generation and dissipation during and after loading are ignored.

Although existing methods of analysis have shortcomings, they generally provide excellent correlation with static tests for sands and gravels, but may over predict pile capacities by up to 35% (Holeyman *et al.*, 2001 & Mullins, 2002) for fine grained soils (clays). This is because the shear strength of clays increases significantly with increasing rate of deformation. The rate effect or damping coefficient for clays is highly non-linear resulting in a reluctance to adopt the Statnamic test method for piles installed in clay. The commercial advantages of being able to use Statnamic testing in countries such as the UK, which has large areas covered by fine grained soil deposits, would be considerable. A programme of research was initiated at the University of Sheffield to investigate Statnamic testing of piles in clay deposits.

1.1.1 Laboratory model pile study

An insight into the characteristics of pile-soil interaction during Statnamic and high penetration rate testing was obtained through the development of a fully instrumented model pile and clay bed. This study tackled the problems of Statnamic testing in clays firstly by undertaking Constant Rate of Penetration (CRP) tests at different pile penetration rates in a controlled and repeatable laboratory environment. This allowed the viscous soil damping characteristics to be quantified and a new analysis method for Statnamic testing incorporating non-linear rate dependant soil behaviour to be developed. To verify the performance of the new analysis method, model Statnamic tests were also undertaken.

1.1.2 Full scale field study

A prototype pile testing facility was developed in glacial lodgement till near Grimsby, UK. In order to calibrate the findings of the laboratory study a class A prediction of static pile behaviour from prototype Statnamic pile load testing was undertaken to measure the success of the improved analysis method. Encouraging results were

obtained for the prediction of ultimate static pile behaviour but it was recognised that the new analysis method did not adequately predict soil-pile stiffness. A soil inertial component was added to the new analysis method, based upon instrumentation readings, which produced an improvement in the prediction of static pile-soil stiffness.

1.2 Aims and objectives

The aim of this study was to examine the equivalence of rapid (Statnamic) and static pile load testing methods for fine grained soil types and geological conditions relevant to the UK.

To meet this aim the following objectives were set:

1. To carry out model pile tests in a large clay calibration chamber to determine the effects of rate of testing on effective stresses and pile bearing capacity in clay.
2. To develop a model and analysis method based upon the results of the model pile tests to allow better prediction of static pile behaviour from rapid load tests in clays.
3. To measure the success of the improved analysis by means of a class A prediction of static pile behaviour from prototype Statnamic pile load tests on a pile installed in typical UK clay.
4. To refine the analysis using the prototype load test data.

1.3 Thesis structure

A review of the background literature relevant to this study is presented in Chapter 2. This chapter highlights the need for pile load testing and goes on to introduce some of the common methods employed. Particular emphasis is placed on describing the rapid load testing method known as Statnamic testing. The use, methods of analysis and merits and shortcomings of the test are described. Details of previously undertaken investigations into rate effects as well as analysis methods and models are presented. The chapter ends with a summary of the areas of investigation that are required to improve understanding of Statnamic and other rapid load tests.

Chapters 3 and 4 are concerned with the laboratory experimental investigation with Chapter 3 presenting the programme of model pile testing. Chapter 4 describes the

improvements to existing equipment along with the development of new equipment and testing procedures. This chapter also presents preparation procedures and specification for the materials used to produce clay beds in this study.

The results of Constant Rate of Penetration (CRP) testing at different pile penetration rates and simulated Statnamic testing are presented and discussed in Chapter 5. In both cases the influence of loading and penetration rate on the soil effective stress and the components of pile capacity are investigated. This chapter also includes the selection of a model along with parameters to allow the application of a new analysis method to predict equivalent static pile behaviour from rapid load tests.

Chapter 6 describes the full scale pile testing facility established in glacial lodgement till near Grimsby. This chapter looks at the development and specification of instrumented prototype test piles. Results of Statnamic and top-down static load testing are presented along with discussion of the load test and instrumentation results. Emphasis is placed upon the differences in load transfer characteristics from test to test along with the radial dissipation of accelerations away from the pile during Statnamic testing.

Chapter 7 describes a class A prediction of equivalent static pile load-penetration behaviour from full scale Statnamic load testing results based upon the laboratory model study. This chapter proceeds to discuss the results of the prediction event and presents an improved model for the analysis of Statnamic tests in fine grained soils. This model incorporates both viscous and inertial soil damping components. Recommendations are also made for the improvement of Statnamic field testing.

Chapters 8 and 9 summarise the key conclusions from this study and make suggestions for future research.

2.0 Literature Review

2.1 Introduction

Two comments made at Professor Mark Randolph's (Randolph, 2003) Rankine lecture, "Science and empiricism in pile foundation design", reinforce the need for pile load testing:

"Scientific approaches to pile design have advanced enormously in recent decades and yet, still, the most fundamental aspects of pile design-that of estimating the axial capacity-relies heavily upon empirical correlations."

"....is consistent with my belief that we may never be able to estimate axial pile capacity in many soil types more accurately than about ±30%. We therefore need to rely on pile tests to refine pile design....."

Due to the inherent uncertainty associated with predicting both load capacity and settlement behaviour of piled foundations (Chow, 1997, Anon, 1999 & Wheeler 2000), based on existing design methods it is common to carry out load tests for verification (Fleming *et al.*, 1992). As noted by White (2002) the uncertainty in pile design methods is recognised by Eurocode 7 (EC 7:1997) where design methods that are either analytical or empirical must be verified by static load tests. Although EC 7 states that the static load tests must have been undertaken in similar conditions, it does not clarify if a static test is necessary for each individual design case. It may be argued that all empirical design methods are based upon static load tests at some point in their development.

Poulos (2000) states that the information obtained from pile load testing may be used in a number of ways including:

1. Construction and quality verification.
2. As a means of verifying design information.

3. As a means of obtaining design data on pile performance, which may allow for a more effective and confident design of the piles.

Pile load testing methods include static tests, dynamic tests and kinematic or rapid load tests. There are also less frequently used static load test methods such as the Osterberg Cell (O-Cell). Generally, static pile testing methods are expensive and time consuming (Fleming *et al.*, 1992 & SCI, 1997), but have the advantage of simple analysis and interpretation. Conversely, dynamic and rapid load testing methods are quick to carry out but require more specialised equipment and analysis.

This literature review aims to identify and introduce the main types of pile load testing methods and highlight their advantages and disadvantages, as well as assumptions and parameters required for analysis. The review will focus on the rapid pile load testing method known as Statnamic and its' current analysis method, which does not perform well in clays or fine grained soils due to rate effects. Previous investigations into the behaviour of these materials at elevated loading rates and the effect on soil behaviour are identified. Where models for deriving equivalent low rate material behaviour have been proposed, these are reviewed with key input parameters identified. The review will then look at high loading rate model pile tests in fine grained soils.

2.2 Pile load testing methods

2.2.1 Top-down static load testing of piles

The most common method of pile load testing may take one of two forms. These are the Maintained Load Test (MLT) and the Constant Rate of Penetration Test (CRP). The names of the two tests are derived from their methodology. Since the invention of tests such as the Osterberg Cell method, these types of testing are often referred to as top-down as the loading is applied at the head of the pile.

The MLT works by applying and maintaining increments of load to the head of the pile for a minimum specified time and until a specified rate of settlement criterion is satisfied. At which point the load is either increased or reduced (Tomlinson, 1994). The minimum time for holding of an increment typically varies from 30 minutes to 6 hours. This results in a test that generally takes a minimum of 19 hours but may take much

longer depending on the particular test specification (ICE, 1997). This neglects time required for setting up the test equipment. The magnitudes of the applied load increments are chosen to verify the ability of the pile to carry the design loads associated with the structure to be constructed above the pile (working load). At the same load, the pile settlement must be within acceptable limits. To allow for natural variation of ground conditions, the load applied to the pile is taken to 1.5 or 2 times the working load (Tomlinson, 2001).

Generally, this test method is not used to prove the pile ultimate load (Figure 2.1) capacity or generate "plunge" as it is difficult to maintain constant load during rapid penetration. Additionally, it is typical to increase the pile load in 25% increments of the working load, which may mean the application of many hundreds of kN's between load increments. It is then possible for the actual ultimate load to be missed resulting in an underestimation of ultimate capacity as the pile plunges at a higher load increment. To avoid the underestimation, the load increment may be reduced to 12.5% of the working load but this extends the duration of the test (Wood, 2003).

A typical reaction or anchor pile type arrangement for pile testing is shown in Figure 2.2. Alternatively, the reaction to the hydraulic jack can be provided by placing kentledge above the jacking arrangement. If the pile is a preliminary pile i.e. one that is required to validate the pile construction performance prior to construction of the working piles, then either arrangement of pile test would be suitable. Where load tests are required on piles that will form part of the final structure (working piles) then the test arrangement using kentledge would appear more appropriate. Unfortunately, if several working pile tests were needed, multiple individual test arrangements would be required to avoid time delays. Greater detail regarding pile testing procedure and equipment arrangements are given by Weltman (1980).

The CRP test varies from the MLT test in that a varying load is applied to the pile under a constant rate of penetration. The rate of penetration is chosen to reflect the predominant soil type that the pile installation encounters (Table 2.1). Due to these penetration rates, tests are completed relatively quickly. For instance a 600mm diameter pile installed in clay pile can be taken to a penetration equal to 15% of the pile diameter (90mm) in 2.5 hours. The pile load resistance at a pile penetration equal to 15% of the

pile diameter is a commonly adopted definition of pile ultimate load capacity (ICE, 1997). It can be seen in Table 2.1 that the rates used for CRP in US practice may be 50% slower or faster than those specified for UK use. There are also differences in the way MLT testing is undertaken in the US with an additional test referred to as the Quick Load Test method (QLT) where load increments are only held for 2.5 minutes (ASTM D1143-81:1994).

The CRP test is usually reserved for determining ultimate pile capacity and for research purposes (Tomlinson, 2001). Although testing is faster, it requires greater capacity from the loading and reaction systems to produce plunge. There are also reservations about the relatively high penetration rates and short test duration especially where piles are installed in clay. It has been shown that as the penetration rates in CRP increase so does the ultimate pile capacity and stiffness (Burland & Twine, 1988, Lyndon *et al.*, 1993, Fleming, 1996, England, 2000 & King *et al.*, 2000). Based upon laboratory triaxial element testing Burland & Twine (1988) suggested that penetration rates during CRP testing should be reduced from 0.01mm/s to 1.6×10^{-4}mm/s. England (2000) suggested that the standard CRP penetration rate in clay soils should be reduced by at least two orders of magnitude. The increase in shaft resistance with increasing rate of penetration is shown in Figure 2.3 for a series of four CFA bored piles of 450 to 490mm average diameter. These piles were installed at depths between 7.8 to 11.8m in soft silty clay at the former EPSRC Bothkennar test facility (King *et al.*, 2000). The rate of penetration dependant ultimate capacity and stiffness were also noted in sands and granular soils, but to a lesser degree, by Weele (1993) and Fleming & England (2001).

One drawback of static top-down load testing systems that is often overlooked is the influence of the reaction system on the ground surrounding the pile (Wood, 2003). Poulos (2000) reports that the use of kentledge causes an increase in vertical and lateral stresses acting along the test pile's shaft and at the base. Non-linear finite element modelling in sand suggested that pile ultimate capacity and stiffness might be increased by 10-20% due to the presence of kentledge. Poulos & Davis (1980) showed that the proximity of reaction piles subject to uplift might cause an enhancement of the test pile's stiffness. The influence of the reaction system arrangement may not be considered a problem where the associated loading is similar to that of the final structure, but it may cause problems when comparing pile load testing methods.

2.2.2 Bi-directional static load testing of piles

The bi-directional static load test is an alternative to the top-down static load tests described in Section 2.2.1 (England, 2003). The method varies from the top-down load tests in that the major component of the system is a sacrificial purpose built high capacity jack cast in the pile length. The most common form of this type of system is referred to as the Osterberg Cell (O-Cell), which is claimed to have been deployed over 200 times a year (Loadtest, 2003).

The bi-directional method of testing was originally designed to load the pile from the base rather than from the head as shown in Figure 2.4 (Schmertmann *et al.*, 1998). On inflating the jack, reaction is provided by the pile end bearing capacity to mobilise the pile's skin resistance and vice versa until the capacity of either the jack or the upper or lower components of resistance are exceeded. More recently individual jacks or multiple jacks have been installed at various levels within cast in situ piles to allow testing of different sections of the pile length (England, 2003 & Randolph, 2003).

The system typically works by incorporating the jack within the reinforcement of a cast in situ pile. When pile construction is complete, the jack is then inflated using a hydraulic pump with the oil pressure monitored by a pressure transducer attached to the hydraulic return line. The calibration of this system allows the required loads to be applied. During testing, the separation of the jack is monitored by displacement transducers (LVDTs) mounted between the two faces of the jack. Telltales are also attached to the top of the jack that extend up to the head of the pile, which allow the compression of the pile shaft to be monitored. The movement of the pile head is also monitored. On completion of testing, the jacks can be grouted up to allow the pile to be used as a working pile. The Osterberg Cells come in various diameters from 130mm to 870mm, with capacities from 0.76MN to 27.4MN. Test loads as high as 151MN have been applied using several O-Cells installed at the same level.

The bi-directional type of load test has several obvious advantages over static top-down methods described in Section 2.2.1. The systems require no large surface reaction thus reducing space requirements, set up time and transportation costs. The system is also safer with the loads being applied at depth. There are also reported cost savings with bi-

directional load testing being comparable in cost with top-down static load tests at 5 to 10MN but then becoming much more cost effective at higher loads.

Several disadvantages of the system are reported by Wood (2003). For instance as the test pile requires the jacking system to be pre-installed it is not possible to select a random working pile. Where the jack is installed at the pile tip only, the test is limited by the capacity of the sections being mobilised above the jack and the bearing capacity below the jack. Thus making it difficult to mobilise the full capacity of both sections at once and determine a pile's ultimate capacity. By using multiple jack installations, it should be possible to find individual capacities for both the base and the skin friction components of shaft resistance. It is also assumed that the skin friction component of a pile's capacity is the same when the pile is displaced upwards rather than downwards as is normally the case in working conditions. However, Wood (2003) found that the direction of loading effected both stiffness and ultimate pile behaviour. Poulos (2000) also notes that when the jack is installed at the base it will interact with the shaft resistance resulting in an overestimation of pile stiffness.

2.2.3 Dynamic load testing of piles

The pile load testing methods discussed typically have load application durations in terms of hours. Dynamic pile load testing works by applying a very short duration impact load (5 to 10 milliseconds) to the pile head (Middendorp *et al.*, 1992 & Weele, 1993). If the pile is being installed by pile driving, the load may be applied by the driving hammer (Figure 2.5a), or by large guided drop weights for other pile types. Tests up to 30MN have been undertaken by dropping 20 tonne masses from 2.5m above auger bored piles. Typical loads achieved are 1MN for 1000-1500kg drop weight systems (1.5 to 2% of the applied load) and 3MN for 4000kg drop weight systems. (Holeyman, 1992 & Middendorp *et al.*, 2000).

Measurements are taken during the hammer impact from a pair of accelerometers and strain gauges mounted at the head of the pile (Figure 2.5b). The response of this instrumentation is logged during and after the weight impact (Humpheson & Seaman, 1992 & Stain, 1992). Data from the instrumentation is used to derive the load applied to the pile by multiplying the measured strain by the cross-sectional rigidity of the pile and velocity by integrating the accelerometer readings.

The stress wave produced by the weight impact travels down the pile (Figure 2.6) with force and velocity which are assumed to be directly proportional to one another as in Equation 2.1.

$$P_{hd} = Zv \tag{2.1}$$

where

P_{hd} = force derived from pile head instrumentation

Z = pile impedance = $\frac{E_p A_p}{c}$

v = pile velocity

E_p = Young's modulus of the pile

A_p = pile cross-sectional area

c = elastic wave velocity in the pile = $\sqrt{\frac{E_p}{\rho_p}}$

ρ_p = pile density

Where the movement of the pile is resisted, or there is a change in impedance such as at the pile tip, a wave will be reflected back up the pile. The total resistance of the pile to the stress wave passing up and down the pile has been shown to equal the sum of the downward travelling wave force plus the upward travelling force that arrives at the pile head at time $2L/c$ (where L is the pile length) after the initial peak load (Rausche *et al.*, 1985 & Randolph, 2003).

Several methods are available to analyse the stress wave data obtained from a dynamic load test in order to derive an equivalent static pile capacity. These include signal processing, numerical models and frequency analysis (Holeyman, 1992). One early method of signal processing is referred to as the CASE method (Rausche *et al.*, 1985). This analysis uses close form solutions of one dimensional wave propagation and is empirically correlated with static pile load tests. This approach utilises a soil damping

factor (J) to reduce the measured dynamic pile reaction to a static value. The formula shown in Equation 2.2 is referred to as the CASE method capacity prediction (Stain, 1992) and is similar in format to those discussed by Ferahian (1977) and Rausche *et al.* (1985).

$$R_{static} = R_{dynamic} - J\left(\left(Zv + P_{h(total)}\right) - R_{dynamic}\right) \tag{2.2}$$

where

R_{static} = static pile capacity

$R_{dynamic}$ = dynamic pile capacity (derived peak dynamic reaction)

J = viscous damping constant for soil

v = pile velocity

$P_{h(total)}$ = total force at the time of impact

The equation above has its origins in the analysis of pile driving proposed by Smith (1962). Smith (1962) proposed that static pile loading is represented by an initial elastic compression to a certain penetration, followed by plastic deformation at constant resistance as represented by the dotted line OABC in Figure 2.7a (Gibson & Coyle, 1968). Smith (1962) then went on to develop a mathematical model that accounts for both the static and dynamic soil behaviour represented by the rheological model shown in Figure 2.7b. The model consists of an elastic spring and a plastic friction block in series, connected in parallel to a viscous dashpot. Under rapid compression the soil resistance in the elastic zone is described by Equation 2.3:

$$R_R = Kx_e + Cv \tag{2.3}$$

where

R_R = force resisting dynamic loading

K = soil spring constant

x_e = elastic soil deformation or quake (Q)

C = viscous damping constant

To allow for pile shape and size effects, Smith (1962) defined the viscous damping constant as:

$$C = Kx_e J \tag{2.4}$$

As the pile velocity approaches zero then Equation 2.3 becomes:

$$R_{static} = Kx_e \tag{2.5}$$

If resisting force (R_R) is assumed to equal the dynamic pile capacity ($R_{dynamic}$) and Equations 2.4 & 2.5 are substituted in Equation 2.3 then the peak dynamic pile capacity is represented by Equation 2.6.

$$R_{dynamic} = R_{static}(1 + Jv) \tag{2.6}$$

Although Smith's derivation was initially founded on explaining behaviour in the pile's elastic zone, Equation 2.6 was also used to describe behaviour in the plastic region. Initially, Smith (1962) proposed that the soil viscous damping constant (J) should have a value of 0.15, pending further research. This assumption was later modified such that the value of the viscous damping constant (J) was considered constant, with specific values for certain soil types.

The most common methods of analysing dynamic load tests presently used are based upon lumped parameter finite difference or finite element techniques where the pile is modelled as an assembly of interconnected masses with varying properties. These properties, predominantly soil parameters, are varied until computer simulated pile head forces and velocities match those measured (Holeyman, 1992 & Randolph, 2003). Several computer packages have been developed that utilise this "Signal matching" method such as CAPWAP (Case Pile Wave Analysis Program, Rausche *et al.*, 1985), TNOWAVE (Middendorp *et al.*, 1992) and SIMBAT (Stain, 1992).

Dynamic load testing has benefits in that it is a relatively fast test with quick set up time. In general, the equipment can be mobilised with a crane (30 tonnes capacity) and multiple piles tested in a single day. For loads above 10MN, the testing rate is normally two piles per day (Middendorp *et al.*, 2000). The timesavings and simple equipment result in test costs being two orders of magnitude lower than an equivalent static test (Randolph, 2003). The system may be used to non-destructively test multiple working piles but it is recommended that the method is first calibrated against a static pile test (Fleming *et al.*, 1992 & EC 7:1997). Dynamic load testing is recognised in BS 8004:1986, EC 7:1997, ICE (1997) and SCI (1997), albeit with limited guidance. Where guidance is given, it relates to the need for calibration of dynamic load testing with static load tests on similar piles under comparable ground conditions. Direct mention of analysis methods is not made.

Claims regarding the accuracy of dynamic pile load testing report predictions within 10% of measured static pile capacity (Anon, 1996). The SCI (1997) report that analysis by the CAPWAP program can produce psuedo-static pile head displacement curves that fit static results to ±10%. Early investigations of the CASE method by Ferahian (1977) suggest far less accurate correlation with differences of 50-100%, especially for clay soils.

Although the method is reported to have a relatively high degree of correlation with static pile tests, there are many critics of dynamic testing (Anon, 1996 & 2000). This criticism is generally levelled at the complex and specialist analysis of the test data. As the analysis becomes more complex, there is greater need to input parameters for soil and pile behaviour based upon experience or correlation (England, 2000). This leaves the method susceptible to operator influence. The main focus of criticism is the derivation of the input parameters for the viscous damping constant and the pile material properties. Holeyman (1992) and Rausche *et al.* (1985) readily admit that large conservative damping constant values have been used for clay soils. This is explained as being due to less experience in these soil types. Paikowsky & Chernauskas (1996) stated that the representation of soil dynamic resistance by viscous damping in the analysis of dynamic load tests is inadequate and incorrect. They argued that doing so results in damping constants that do not correlate to soil type because the models used for dynamic analysis make no allowance for the influence of soil inertia. Furthermore,

where viscous damping constants are defined empirically based upon comparison of static and dynamic load tests carried out in the US, care should be taken when applying in the UK. As discussed in Section 2.2.1, UK and US static testing procedures may vary considerably. It would seem necessary to research the past calibration process for any dynamic analysis method before it can be used in the UK.

Problems with test analysis also arise where the method requires knowledge of parameters that relate to the dynamic performance of the pile. These may relate to length, cross-section, mass, density and Young's modulus. These parameters may be relatively easy to define for a steel or a pre-cast concrete pile but they become more uncertain for cast in-situ types where concrete quality and cross section may vary (England & Fleming, 1994 & Middendorp *et al.,* 2000).

Dynamic load testing has also received criticism due to pile damage during the test. This has been reported both for driven and cast in-situ piles (Anon, 2000 & Middendorp *et al.,* 2000). The damage can either be caused by eccentric loading of the pile head due to a misguided impact or by tensile stresses resulting from stress wave reflection. This may lead to piles that are to be tested requiring additional reinforcement or specialised construction. This then limits the flexibility of pile choice for dynamic load testing.

2.2.4 Rapid or kinematic load testing of piles

The major alternative to static and dynamic load testing methods are rapid or kinematic load tests, the most common of these being the Statnamic test (STN). The Statnamic test was conceived in 1985, with the first prototype tests carried out in 1988 through collaboration between Berminghammer Foundation Equipment of Canada and TNO Building Research of the Netherlands (Middendorp, 1993 & 2000[a]). The motivation for the development of the equipment was to overcome problems associated with dynamic testing whilst maintaining the advantages (Bermingham, 1999).

Statnamic testing works by the rapid burning of solid fuel that produces gas in a pressure chamber (Figure 2.8a). The venting of this gas is used to accelerate a mass upward that in turn imparts a load onto the foundation pile below the Statnamic device. The load is applied and removed smoothly by the controlled venting of the gas which results in a load application of 100 to 200 milliseconds. This is 30 to 40 times the

duration of dynamic pile load testing (Bermingham *et al.*, 1994 & Matsumoto *et al.*, 2000). As the duration of the loading is relatively long, piles less than 40m in length remain in compression throughout resulting in negligible stress wave effects and simpler analysis. This also minimises the chance of potentially damaging tensile stresses developing in the pile (Reiding, 1992).

Statnamic devices have been used that are capable of applying loads from 0.1 to 30MN with devices capable of applying 60MN under development (Middendorp, 2000[b]). The reaction mass required to produce a load of 3.5MN is 18000kg, which is approximately 5% of the resulting load (Holeyman, 1992). Displacements occurring during the test are measured by means of a photovoltaic cell mounted on the Statnamic device that is excited by a remotely mounted laser reference beam. The load applied to the pile is measured directly by a calibrated load cell mounted at the base of the Statnamic device.

The Statnamic load test has advantages similar to those outlined for dynamic testing in that it is compact, quick to test and mobilise. A 3MN Statnamic rig (Figure 2.8b), as used in this research can be mobilised with one articulated truck and a 70 tonne crane. Use of Statnamic rigs incorporating hydraulic weight catch mechanisms allow 10 individual piles to be tested in a day or multiple load cycles to be carried out on an individual pile with minutes between cycles (Middendorp *et al.*, 2000). The method also has other benefits in that it can be used to test pile groups and shallow foundations. The system has been used to test inclined piled structures and horizontally to simulate ship impacts on marine structures. Recent developments include over water testing devices that use seawater as the reaction mechanism (Middendorp, 2000[a] & 2000[b]). It also has the advantage over dynamic load testing, that for simple analysis, the measured data is not influenced by pile cross section or material quality.

The data measured directly during the Statnamic load test includes the load applied at the head of the pile and the displacement of the Statnamic device mounted on the pile. From the measurements of displacement with time, it is possible to derive the pile velocity and acceleration by successive differentiation. Maximum pile velocities calculated during a test may be as high as 1000mm/s, with considerable variation of pile velocity throughout the test. Typical measured and calculated results from a Statnamic test carried out on a pile installed in clay are shown in Figure 2.9. It can be seen from

Figure 2.10 that the Statnamic (STN) load deflection curve varies markedly from that of the top-down static testing carried out on the same pile.

Middendorp (1993) first described a method of analysis to derive the static equivalent load-displacement curve from the Statnamic test results. This simple method of obtaining an equivalent static pile response is known as the Unloading Point Method (UPM), which is described in its most commonly used form by Kusakabe & Matsumoto (1995). In this method the pile and soil system are represented by the rheological model shown in Figure 2.11a. The pile and the soil system are modelled as a single lumped pile mass supported by a spring and dashpot in parallel, as often seen in the modelling of single degree of freedom vibrating systems. The spring represents the load-displacement behaviour under static loading (F_u) and the dashpot represents velocity (v) dependant viscous soil resistance (F_v). It is assumed that the pile behaves as a rigid mass (M). The UPM method works by determining a constant damping coefficient (C) that when multiplied by the velocity gives the viscous soil resistance. The equation of force equilibrium is assumed to be:

$$F_{STN} = F_{soil} + F_a = F_u + F_v + Ma \tag{2.7}$$

where

F_{STN} = measured Statnamic force

M = pile mass

a = pile acceleration

$F_v = Cv$ (2.8)

Thus at a given time (t):

$$F_{soil}(t) = F_{STN}(t) - Ma(t) \tag{2.9}$$

The point of maximum displacement on the load-displacement curve in Figure 2.12 is called the "Unloading Point". At this point the pile is said to have zero velocity and thus:

$$F_v = 0 \tag{2.10}$$

and

$$\therefore F_{soil}(t) = F_{unl}(t) - Ma(t) = F_u(t) \tag{2.11}$$

The value of F_u at the unloading point is assumed equivalent to the maximum static pile resistance obtained in the Statnamic test, $F_{u(\max)}$. The damping coefficient (C) is determined at $F_{STN(\max)}$ by assuming $F_u(t)$ is constant between $F_{STN(\max)}$ and F_{unl}. Thus at $F_{STN(\max)}$:

$$F_v = F_{STN(\max)} - F_{u(\max)} - Ma_{STN(\max)} \tag{2.12}$$

substituting Equation 2.12 in Equation 2.8:

$$C = \left[F_{STN(\max)} - F_{u(\max)} - Ma_{STN(\max)}\right] / v_{STN(\max)} \tag{2.13}$$

Simple software that incorporates the above approach referred to as Statnamic Analysis Workbook (SAW) has been developed that can be used with Statnamic test data (Garbin, 1999).

One of the major shortcomings of the UPM analysis is that it relies on the assumption of the pile moving as a rigid body during Statnamic testing. However, if the pile length increases the movement at the top of the pile may not be synchronised with that at the base resulting in stress wave effects. This may also occur if the pile is installed with the tip in stiffer material than is encountered along the shaft (Mullins *et al.*, 2002). To investigate the applicability of applying UPM, Middendorp & Bielefeld (1995) defined

a "Wave Number" (N_w) which is the ratio of wave length to pile length as shown in Equation 2.14:

$$N_w = \frac{\lambda_L}{L} = \frac{cT}{L} \tag{2.14}$$

where

λ_L = wave length

L = pile length

c = elastic wave velocity in the pile

T = duration of the load pulse

Based upon Statnamic analyses using UPM, Middendorp & Bielefeld (1995) & Nishimura & Matsumoto (1995) concluded that UPM gives adequate results where the wave number is greater than 12. This limits the application of UPM to steel piles shorter than 50m (c=5000m/s) and concrete piles shorter than 40m (c=4000m/s) (Mullins *et al.*, 2002).

Where long piles are to be tested (N_w<12) McVay *et al.*, (2003) recommend several modifications to the Statnamic testing and analysis. The first being to increase the duration of the Statnamic load which can be achieved by increasing the venting distance for the gases that drive the reaction mass or increasing the mass itself (Bermingham & White, 1995). The other methods include the application of dynamic pile test analysis methods to the Statnamic measurements (Seidel, 1996 & Esposito *et al.*, 2000).

Where the pile wave number is greater than 12 but the pile does not behave as a rigid body, for example where the tip of the pile is installed as a rock socket, problems may still occur with the UPM analysis. This is a result of the variation in pile velocity and acceleration along its length (Mullins *et al.*, 2002). To overcome this an accelerometer can be incorporated at the pile tip and used in conjunction with pile head calculations to determine the average pile acceleration and velocity. These results can then be

incorporated in the UPM analysis. This method is referred to as the Modified Unloading Point Method (M-UPM) (Middendorp, 2000[a] & Mullins *et al.*, 2002).

Although the M-UPM approach is a refinement addressing some of the problems associated with UPM, it does not address the problem of time lag encountered when testing very long piles (N_w<12). To overcome this, the Segmental Unloading Point Method (S-UPM) was developed (Lewis, 1999, Middendorp, 2000[a] & Mullins *et al.*, 2002). This method is reliant on the pile being instrumented with strain gauges. Incorporating an accelerometer at the pile toe to allow calculation of displacements is also desirable. By incorporating the strain gauges in the pile, it is possible to separate the pile into segments, which are assumed to behave as single degree of freedom systems. Each segment is then analysed using M-UPM and the results from each segment are added together to produce the derived static equivalent pile capacity (Middendorp, 2000[a]). The S-UPM method allows the definition of average acceleration, velocity and displacement that are specific to each pile segment. Software (SUPERSAW) capable of undertaking the S-UPM calculation has also been developed.

One of the main aims of Statnamic analysis was for it to be simple and based upon measured results alone (Bermingham, 1999). This was intended to avoid the criticism of dynamic pile load testing analysis being heavily dependant on user intervention and parameter selection. This said, the original UPM method has several simplifications that may significantly influence the accuracy of predictions.

- The pile is assumed to be a rigid body
- The damping model is simple linear
- The soil is assumed to be perfectly plastic post yield
- The unloading point corrected for inertia is assumed to be coincident with the ultimate static pile resistance
- Inertial effects are limited to the pile, with inertia of the surrounding soil being ignored

The rigid body assumption may be overcome to some extent by incorporating additional instrumentation in the pile. This then allows the use of the M-UPM and S-UPM

methods. The major problem with both M-UPM and S-UPM is that they require pile instrumentation, which adds considerably to the cost of testing and removes the ability to randomly select working piles for load testing. The S-UPM method may also be susceptible to inaccuracies due to assumptions of pile cross section and stiffness similar to those associated with dynamic load testing.

The use of a linear damping model for the UPM analysis may be regarded as an oversimplification although Middendorp (1993) notes that a more complex model may be used, although none are suggested. The problem with a linear approach, as discussed by Hyde *et al.* (2000), is that the viscous damping coefficient for a soil may be highly non-linear particularly for fine grained soils, resulting in the over prediction of static pile capacity.

One of the major considerations that is missing from the analysis is the behaviour of the soil mass during the test. The behaviour of the pile soil interface is included through the viscous soil damping model, as discussed above, but the inertial forces associated with the movements of the soil mass are ignored. This is because the extent of the soil mass accelerated during testing is difficult to determine (Paikowsky & Chernauskas, 1996).

Results from Statnamic testing analysed by the UPM method suggests that it produces acceptable correlations for tests in granular and coarse grained soils (Brown, 1994), but over predictions occur in fine grained soils (Bermingham *et al.*, 1994). Both Holeyman *et al.* (2001) and Mullins (2002) have proposed soil specific reduction factors that may be applied to the UPM derived static equivalent pile resistance to improve results (Table 2.2). These factors varied from 0.96 for piles installed in rock to 0.65-0.7 for piles installed in silts and clays. Mullins (2002) described these factors as "rate factors (η)". These factors were based upon the analysis of previous Statnamic load tests analysed using UPM. Design safety factors (load resistance factors, ϕ) for use in Load and Resistance Factor Design (LRFD) have been defined by McVay *et al.* (2003). The LRFD design method is an extension of limit state design incorporating partial factors. McVay *et al.*, 2003 suggest that for design purposes UPM after correction by Mullins (2002) rate factors should be reduced by the following factors for pile design:

Resistance factor (ϕ) for driven piles in rocks and noncohesive soils = 0.70

Resistance factor (ϕ) for bored piles in rocks and noncohesive soils = 0.65

Resistance factor (ϕ) for driven and bored piles in sands-clays-rocks mixed layers = 0.6

No factor was defined for clay soils due to lack of available data. McVay *et al.* (2003) recommended that Statnamic tests in clay should not be undertaken without calibration against a static load test. Wood (2003) concluded that the UPM method should not be used in its present form where soils have a plasticity index greater than 10. It is apparent from these results that current Statnamic analysis requires refinement especially in fine grained soils where UPM over predicts equivalent static pile capacity by 30 to 35%.

It should be noted that with all forms of dynamic or rapid load testing, loads are applied for a very short duration as the true displacement of a pile under long term load is governed by consolidation and creep (England & Fleming, 1994). ICE (1997) states that dynamic pile load testing will not predict long term pile settlements and that appropriate soil mechanics methods of calculation should be used.

2.3 Rate effects in clay soils

A common problem encountered when comparing pile load tests with the final structural function of the pile as a structural foundation, is the duration of loading. The previous section highlighted this as a particular problem in clay or fine grained soils. The reason this poses a problem to the pile designer is that as the rate of loading of a clay changes so do the fundamental properties that effect pile behaviour. This is generally referred to as the "Strain rate effect" or "Rate effects", and was defined by Whitman (1957) as "The relationship between rapidity of loading and shearing strength of a soil".

These rate effects are well documented by early research in soil mechanics. The effect of loading rate on in-situ shear vane testing results obtained from the testing of soft alluvial clays was noted by Skempton (1948). He concluded that where the test was carried out ten times faster there was a 6% increase in measured undrained shear strength. Where the test duration was extended by five times there was a 2% reduction in undrained shear strength. Casagrande & Shannon's (1948) studies of slope stability

during bomb impacts concluded that the strength of clay increased by 1.5 to 2 times that of static tests with decreasing time of loading. They also found that the shear modulus of a clay subjected to transient loading was twice that of a static test. In contrast, Casagrande & Wilson (1951) found that undisturbed clays crept under sustained loads and ultimately failed at loads considerably lower than those found during tests at normal laboratory strain rates. Skempton & Bishop (1950) suggested that in certain loading conditions, such as the loading of subgrades in roads and runways, shear stresses are applied at rates that may be 1000 or 10000 greater than in the laboratory. They concluded that such transient rates of loading in clay soils may result in shear strength 30 to 60% greater than clays tested at normal laboratory rates.

These early studies suggest quite considerable increases in clay shear strength and material stiffness with increasing strain rate. It is also important to note that although rate effects were noted for sands they were not considered as significant as in fine grained soils.

2.4 Rate effects in laboratory testing

2.4.1 Rate effects in triaxial and multiaxial testing

The rate of shearing has been found to affect the behaviour of clay in several ways. The most commonly noted effect in laboratory triaxial testing was an increase in the peak shear strength with increased strain rate or reduced time to failure (Casagrande & Shannon, 1948, Whitman, 1957, Richardson & Whitman, 1963, Lefebvre & LeBoeuf, 1987, Zhu & Yin, 2000 & Katti *et al.*, 2003). A typical increase in deviator stress of 10% was noted by Richardson & Whitman (1963) when increasing the strain rate from 3×10^{-6} to 13×10^{-3} mm/s. Leinenkugel (1976) defined the increase in shear strength by Equation 2.15 based upon biaxial testing of materials at various rates.

$$c_{ud} \approx \left[1 + I_{v\alpha} \ln\left(\dot{\gamma}_d / \dot{\gamma}_\alpha\right)\right] \tag{2.15}$$

where

c_{ud} = undrained shear strength at an elevated rate

$c_{u\alpha}$ = undrained shear strength at a strain rate of 10^{-5}% or 0.0005mm/s

$I_{v\alpha}$ = viscous damping constant for soil or viscosity index

$\dot{\gamma}_d$ = elevated strain rate

$\dot{\gamma}_\alpha$ = reference strain rate (10^{-5}%)

Triantafyllidis (2001) goes on to describe the soil rate constant as a percentage defined in terms of the soils liquid limit (w_L) as a percentage:

$$I_{v\alpha} \approx -7 + 2.55\ln(w_L) \tag{2.16}$$

Where the soil rate constant has typical values of 0.01 to 0.02 for clayey silt and silty clay and 0.04 for clay (Gudehus, 1981). A summary of rate effect models found during this study is summarised in Appendix 1.

As well as the effect on peak shear strength, both the elastic modulus and pore pressure response were found to be affected by strain rate. Casagrande & Wilson (1951) described a reduction in peak pore pressure magnitude with increasing strain rate. However, both Richardson & Whitman (1963) Lefebvre & LeBoeuf (1987) note that pore pressure is unaffected by rate at small strains (ε <0.5%) and even at peak shear strength where this occurs at low strains. Zhu & Yin (2000) found that the reduction in pore pressure at peak deviator stress varied between 5 to 50% where deformation rates were increased from $42\text{x}10^{-6}$ to $4.2\text{x}10^{-3}$ mm/s. The effect of increasing loading rate on the elastic modulus of clays is well documented (Casagrande & Shannon, 1948, Olson & Parola, 1967 & Zhu & Yin, 2000) with the tendency for modulus to increase with increasing rate.

Although considerable strain rate effects have been noted in triaxial studies, the strain rates are relatively low with maximums of 0.013mm/s. Typically these strain rates correspond to pile penetration rates for CRP static pile testing in clays (0.01mm/s, Section 2.2.1) and do not reflect the velocities encountered in Statnamic or dynamic testing which may be of the order of 100 to 5000mm/s.

In an attempt to check the validity of the Smith model for dynamic pile resistance (Section 2.2.3), Gibson & Coyle (1968) carried out laboratory testing on soils at high deformation rates. Their research concentrated on undrained triaxial testing of sands and clays loaded dynamically by a drop hammer. Deformation rates were varied from those associated with standard triaxial testing to 3600mm/s. Gibson & Coyle (1968) found that the peak dynamic load attained during testing clays increased very rapidly for deformation rates up to 300mm/s and thereafter increased more gradually with increasing deformation rate (Figure 2.13a). To check the value of the of the viscous damping constant (J) proposed by Smith (1962), Gibson & Coyle (1968) studied the effect of varying the deformation rate or velocity on Equation 2.17 which is a Equation 2.6 rearranged:

$$J = \frac{1}{v}\left[\frac{R_d}{R_s} - 1\right] \tag{2.17}$$

R_d = peak elevated rate resistance

R_s = peak low rate resistance

This process showed that the viscous damping parameter (J) was not a constant as proposed by Smith (1962), but varied with velocity or deformation rate (Figure, 2.13b). To maintain a constant value for the viscous damping parameter, Gibson & Coyle (1968) found that it was necessary to raise the velocity or deformation rate to a power N, where $N<1$ (Equations 2.18 & 2.19). The power of the deformation rate (N) was found to be relatively insensitive to soil type with $N=0.18$ for clay soil (Litkouhi & Poskitt, 1980).

$$J = \frac{1}{v^N}\left[\frac{R_d}{R_s} - 1\right] \tag{2.18}$$

or rearranging:

$$\frac{R_d}{R_s} = 1 + Jv^N \tag{2.19}$$

During the initial phase of Gibson & Coyle's (1968) study they made pore pressure measurements for sand samples but not in the clay samples due to poor results. Pore pressure measurements for the sands tested at elevated rates showed an immediate plunge to a limiting negative value, which was assumed consistent with pore water cavitation.

2.4.2 Rate effects measured in other laboratory and field testing

As well as triaxial testing, rate effects have been noted in many other laboratory based studies. To better understand the results of dynamic seabed penetrometer testing, Dayal & Allen (1975) undertook laboratory testing of a cone penetrometer in soil targets of sand and clay. The penetrometer used was designed to measure both tip resistance and skin loads. Velocity of the penetrometer was kept constant throughout individual tests. The range of velocities used during the testing programme was varied from 1.3mm/s to 810mm/s. The effect of penetration velocity on penetrometer resistance was found to be negligible in granular soils. In fine grained soils and clays, the increased penetration rate led to increases in both cone tip and skin friction resistance. The increase was found to be directly proportional to the logarithm of the penetration velocity ratio as expressed in Equation 2.20

$$\frac{q_{cd}}{q_{cs}} = 1 + K_L \log\left(\frac{v}{v_s}\right) \tag{2.20}$$

where

q_{cd} = cone end resistance at elevated velocities

q_{cs} = cone end resistance at the lowest rate used

K_L = viscous damping constant for soil

v = velocity of penetration

v_s = lowest penetration velocity during testing

A similar relationship was defined for the variation of penetrometer skin friction with varying penetration velocity. It was found that the rate effect was greater for the skin component of penetrometer (K_L = 0.17-0.93) than the tip (K_L = 0.03-0.25). The rate effect found for the tip can be summarised as a 10 to 25% increase in capacity per log cycle increase in velocity. There was also a corresponding 10 to 38% increase in skin capacity. For the skin, the rate of increase was relatively constant at this level up to velocities between 13 and 140mm/s. At a point in this range, the rate effect increased markedly to 93 to 100% with log cycle of velocity increase. Similar changes in the rate effect commencing at between 1 to 20mm/s were noted by Lunne *et al.* (1997) during CPT testing.

Similar work was undertaken by Litkouhi & Poskitt (1980) in remoulded samples of London, Forties and Magnus clays. Penetration rates for the model piles used varied between 3mm/s and 180mm/s. They defined the rate dependant variation of tip and skin resistance as per Equation 2.19 originally suggested by Gibson & Coyle (1968). Again, rate effects were found to be greater for the skin friction component of penetration resistance (J=0.19-0.99) than the tip (J=0.12-0.36). Litkouhi & Poskitt (1980) suggested adopting 0.2 as the value for N in equation 2.19 for both the tip and skin in clay soils although it is unclear why, as their results for N varied considerably (N=0.08-0.46). A summary of CPT test findings at elevated rates was presented by Lunne *et al.* (1997).

Skempton (1985) reported the effects of increased shearing rates on residual strengths in clay soils for the ring shear apparatus. Tests were carried out at velocities varying from 0.0002mm/s up to 13mm/s on residual shear planes, established by first undertaking sample displacements of 500mm at the lower velocity. The resistance to shearing at the lowest velocity was referred to as the low rate residual strength. A considerable increase in strength was noted for clays at velocities exceeding 1.7mm/s. Skempton (1985) explained this as being due to the ordered particles at the interface of the shear plane being disrupted due to high rates of shearing, termed "Turbulent" shear (Figure 2.14). The increase in strength prior to this point was 15% for each log cycle increase in velocity and 73% after it. Test results at elevated velocities were characterised by peak strength followed by a lower steady state strength. Skempton (1985) also explained this

behaviour as possibly due to negative pore pressures which dissipated as displacement continued, resulting in the lower than peak steady state strength. He also noted that the rate effects were affected by clay fraction (CF) with higher clay fractions generally displaying greater rate effects.

Although higher velocities were associated with higher peak strengths, this was not the case for post peak strengths at large displacements. Tika *et al.* (1996) defined three types of post peak behaviour: neutral behaviour where, although fast shearing was occurring, the post peak strength reverted to the same as the low velocity residual strength, and positive and negative behaviour where the post peak strengths were lower and higher than the low velocity residual strengths. These varying post peak rate effects were associated with three different modes of shearing identified by Lupini *et al.* (1981):

(a) Turbulent: Soils with high proportion of rotund or platy particles. Shearing involves rotation of the rotund particles and particle orientation has negligible effects. Clay fraction less than 18% (Lemos & Vaughan, 2000).
(b) Sliding: soils with a high proportion of platy low friction particles that orientate readily in the direction of shearing.
(c) Transitional: soil has no dominant particle shape and shearing involves both sliding and turbulent behaviour.

Tika *et al.* (1996) found that soils with turbulent shear modes displayed either positive or negative rate effects depending on the level of normal stress. Transitional soils showed negative rate effects whereas sliding mode soils showed either negative or positive rate effects. Lemos & Vaughan (2000) who carried out ring shear tests against interfaces of various roughness found that the negative rate effect may result in post peak strengths which were one third of the low rate residual strengths. Such reductions in strength were found in tests where displacements were 1000mm.

Large model pile testing undertaken for DOE (1990) where piles were installed by jacking at various rates (1.4 to 8.3mm/s) also displayed rate effects. Here the pile's shaft resistance increased at 5% per log cycle increase in velocity up to 0.8 to 1.7mm/s.

Above these rates the shaft resistance increased at 100% per log cycle increase in velocity. This effect is similar to that noted by Skempton (1985).

As mentioned for triaxial testing, there is limited information regarding the pore pressure behaviour at the penetration rates associated with rapid pile testing. Where pore pressure results are presented for model pile testing and installation, it is normally from long term monitoring after pile installation. Tika *et al.* (1996) presented results for ring-shear testing at 2.7mm/s which showed negative pore water pressures measured for the first 900mm of shearing with a minimum value of –25kPa at 400mm. The pore pressures then returned to positive values with a maximum of 70kPa at 2400mm displacement.

Although it is not a classical soil mechanics case, Palmer (1999) found that cutting speeds during trenching for deep sea pipelines significantly influenced resistance to cutting in saturated silty sand. Palmer (1999) explained the effect as being due to an intense reduction in pore pressure, which occurs during shearing of dilatant sand when it is forced to deform rapidly in an undrained or partially drained condition. The reduction in pore pressure leading to an increase in effective stress. Os & Leussen (1987) measured large negative pore pressures (<-200kPa) on laboratory instrumented cutting blades. Rate effect relationships for dredging similar to those presented by Gibson & Coyle (1968) for the triaxial testing of clays (Figure 2.13) were found by Palmer (1999). Os & Leussen (1987) found that for shallower water depths, cavitation was occurring along the cutting blade, limiting negative pore pressures and effective stress. They then went on to prove that the shape of their cutting force versus blade velocity relationship was due to cavitation (Figure 2.15). Where no cavitation occurred at large water depths, the rate effect was found to increase linearly.

Two main areas that seem to be have been neglected during the previously mentioned studies is the elastic behaviour and the inertial resistance of soils at elevated rates of testing. Stiffness characteristics have been studied at relatively low rates in triaxial studies but no attempt has been made to incorporate them into analysis methods to derive equivalent static behaviour.

2.5 Model pile testing at elevated penetration rates

Much information has been published regarding model pile tests. These studies tend to concentrate on relatively low velocity penetration in unsaturated sands, that have minimal velocity dependant characteristics. As discussed in Sections 2.2.3 & 2.2.4, analysis of both dynamic and rapid load tests are considered less reliable in fine grained soils. For this reason this section will concentrate on model testing of fine grained soils at elevated rates only.

Previous studies by Horvath (1995) compared load-deflection response for model piles installed in clay subject to varying penetration rates. The tests conditions were designed to represent both typical top-down static pile load testing methods used in the US and a simulated Statnamic test. Details of the types of tests are summarised in Table 2.3. To model Statnamic loading, Horvath (1995) used a continuously increasing load (referred to as a Quick Continuous Load, QCL) until the ultimate load was achieved. As shown in Table 2.3 the test duration chosen was similar to that found in the full scale Statnamic test.

The model pile used consisted of a closed end steel pipe 12.7mm in diameter with an embedded length of 508mm. The pile also included a tip mounted load cell as well as a load cell mounted above the pile to allow the determination of pile shaft resistance. The pile was installed in a bed of vacuum pugged pottery clay of low plasticity. To load the pile a servo controlled hydraulic actuator was used driven by a computer control system. Testing was undertaken in a rigid walled cone shaped calibration chamber referred to as a "Frustrum" chamber (Horvath & Stolle, 1996).

Results from the quick maintained Load test (QML10) and the Statnamic simulation (QCL) gave ultimate pile resistances 1.28 and 1.68 times greater than CRP results, respectively (Figure 2.16). For the QML(10) test load increments were held for only 0.5 seconds with pile plunge occurring after 10 seconds. Horvath (1995) then analysed the results using the UPM method described in Section 2.2.4 and obtained a derived equivalent static ultimate pile resistance similar to that measured for the QML(10) test. Thus, the UPM method over predicted the static pile capacity obtained from CRP testing by 28%, which is similar to the correction factor suggested for UPM in clays by

Mullins (2002) and Holeyman *et al.* (2001). The work by Horvath (1995) highlights the rate effects associated with different pile testing methods and the problems associated with analysing the Statnamic tests in clay soils. Unfortunately, results for pile tip and shaft behaviour were not published. Additionally, no attempt was made to investigate the soil or pile-soil interface behaviour during the load testing.

Eiksund & Nordal (1996) carried out model pile testing to look at soil bed response to pile load testing at various penetration rates as well as driven pile installation. The soils used in their investigation were a fine silica sand (Ottawa Sand) and a medium silt (Lebanon Silt). The pile was 1.07m long and 63.5mm in diameter, closed ended and instrumented with strain gauges at different levels as well as containing accelerometers. The soil bed incorporated four Druck PDCR 81 pore pressure transducers installed in advance of the pile. The loading rates investigated varied between 0.8 and 1800mm/s.

Results presented for pore pressure for the tests in sand showed negative pore pressures that increased with increasing penetration up to maximum penetration. The negative pore pressure magnitude was greatest closest to the pile tip and increased with increasing rate of penetration. Maximum negative pore pressures of –35kPa were noted for tests carried out at 800mm/s. Unfortunately, only dynamic impact loads of short duration were presented for the silt. These showed an initial increase to large pore pressures up to 200kPa, which quickly decreased to negative pore pressures 15 milliseconds after commencing loading. Maximum negative pore pressures of -55kPa were noted 20 milliseconds after commencing loading. Results associated with the other pile instrumentation were not presented.

2.6 Points arising from the literature review

Pile design may not adequately predict the capacity of a foundation pile and must be supported by full scale pile testing to add confidence to design and reduce conservatism. Top-down static pile load testing methods are relatively expensive and time consuming. Methods that are quicker and cheaper such as dynamic load testing are under utilised due to a lack of understanding and trust of the relatively complicated analysis methods. The kinematic or rapid load testing method known as Statnamic addresses some of the concerns associated with dynamic testing but suffers from unreliable analysis in fine grained soils.

The unreliability is predominantly due to strain rate or velocity dependant behaviour of fine grained soils. This relationship is non-linear and results in increasing resistance to pile penetration with increasing penetration rate for the velocities associated with rapid pile load testing. Confidence in present analytical methods is further undermined because the components of soil inertia and pore water pressure are largely ignored.

Summary of points that require further research:

- A more appropriate soil damping model is required for analysis of Statnamic load tests based upon the reported performance of the existing UPM method.
- Where input parameters are required for the model these should be consistent with particular soil types and easily defined by laboratory testing.
- Investigation is required of the effective stress regime/pore water pressure behaviour at the interface between a pile and the surrounding soil and how this is influenced by pile penetration rates. More generally, there is little published information on pore water behaviour in soils where rates of shearing or penetration exceed 20mm/s especially in fine grained soils.
- Attempts need to be made to incorporate soil inertial behaviour in the analysis of the Statnamic load test. This will require definition of the mass of soil influenced by the test and the acceleration distribution within the mass.

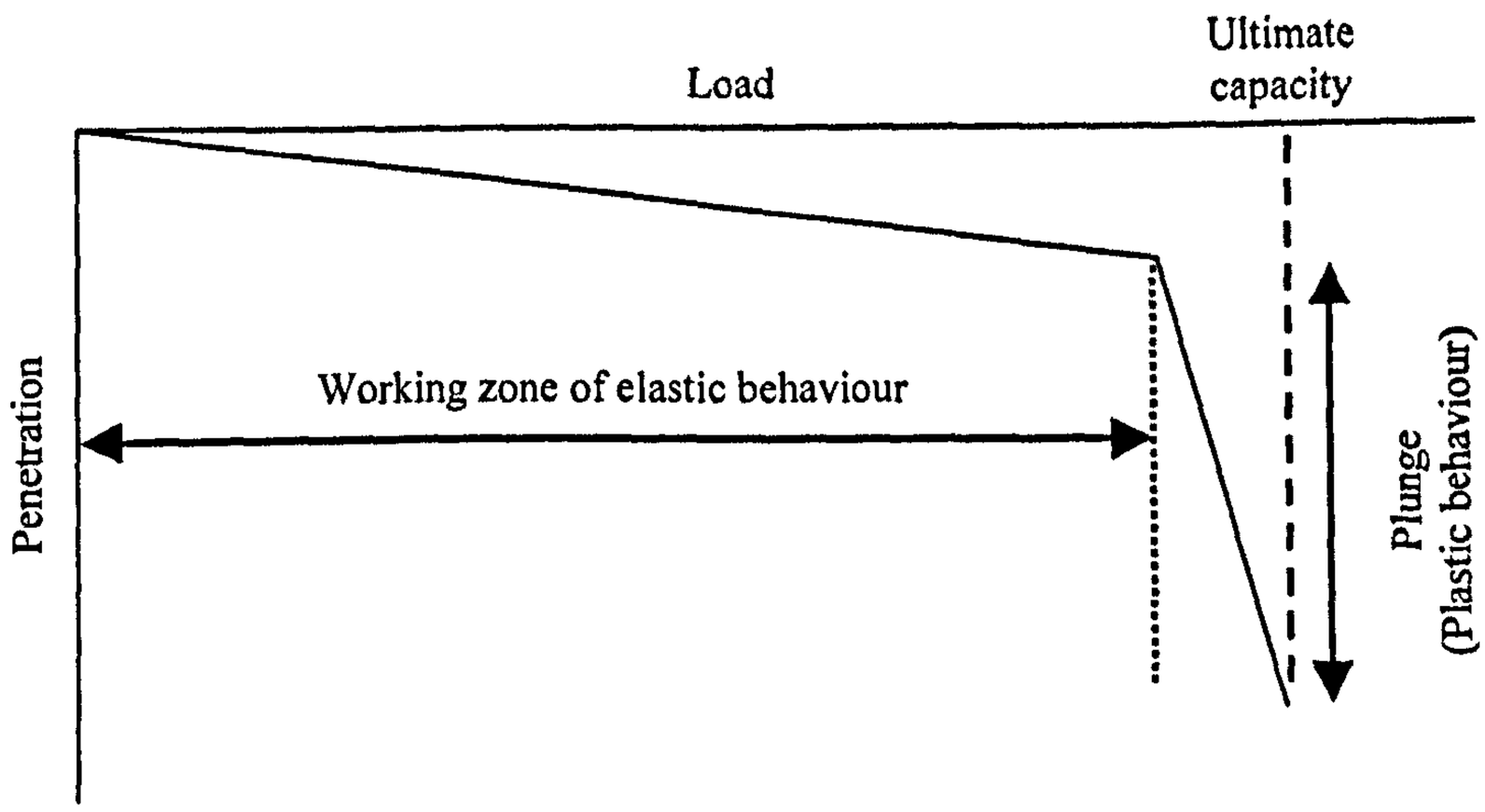

Figure 2.1, Idealised pile load-penetration behaviour.

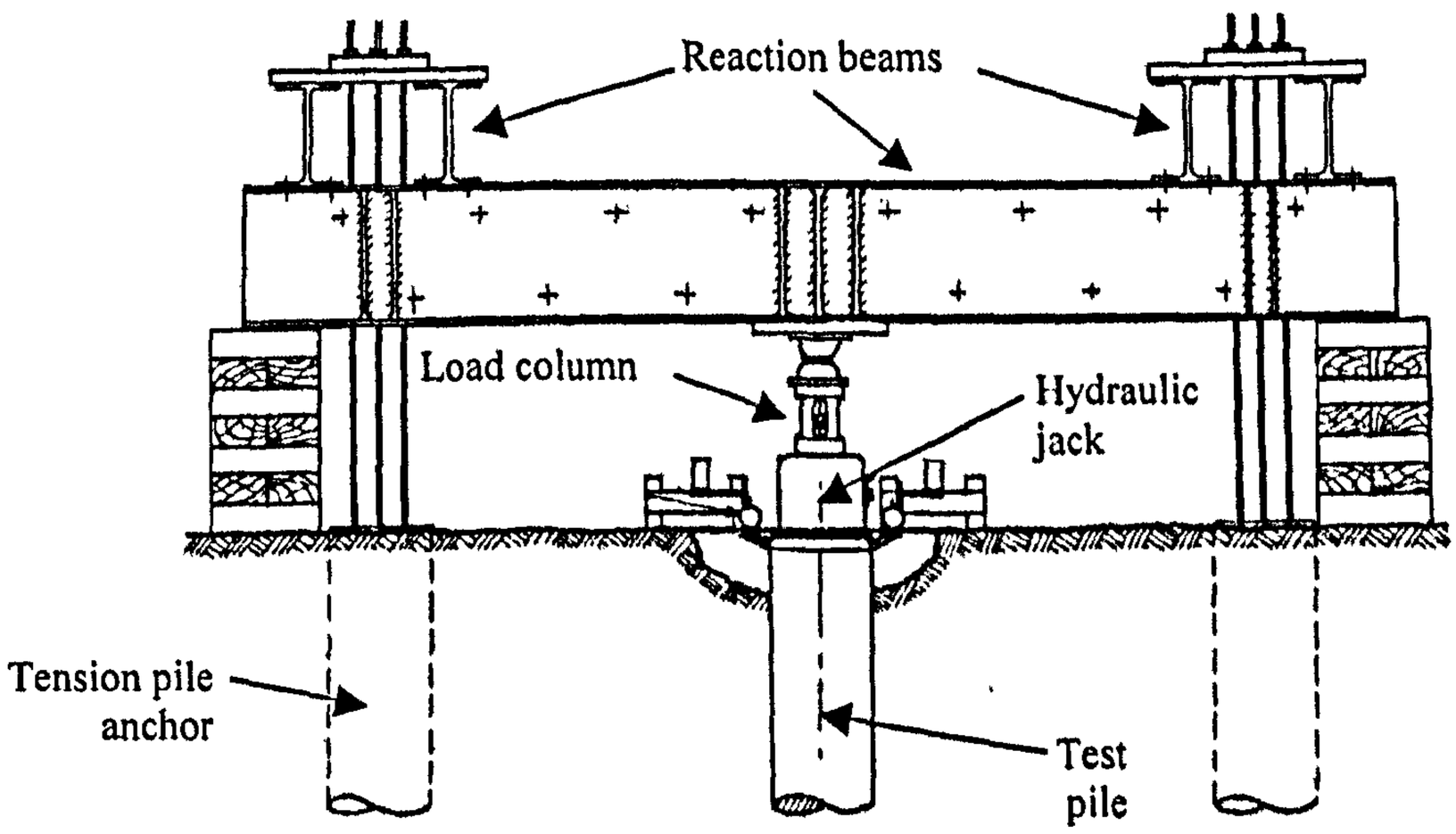

Figure 2.2, Top down static pile testing arrangement utilising a tension pile reaction system (Weltman, 1980).

Major soil type	*Rate of penetration mm/s (mm/min)*		
	ICE (1997)	BS 8004	ASTM D1143-81
Cohesive soils[1]/clay[2]	0.01 (0.6)	0.0125 (0.75)	0.0042-0.021 (0.25-1.25)
Cohesionless soils[1]/sand or gravel[2]	0.02 (1.2)	0.025 (1.5)	0.0125-0.042 (0.75-2.5)

[1]ICE (1997) & ASTM D1143-81:1994 terminology
[2]BS 8004:1986 terminology

Table 2.1, Recommended pile penetration rates to be used during CRP testing.

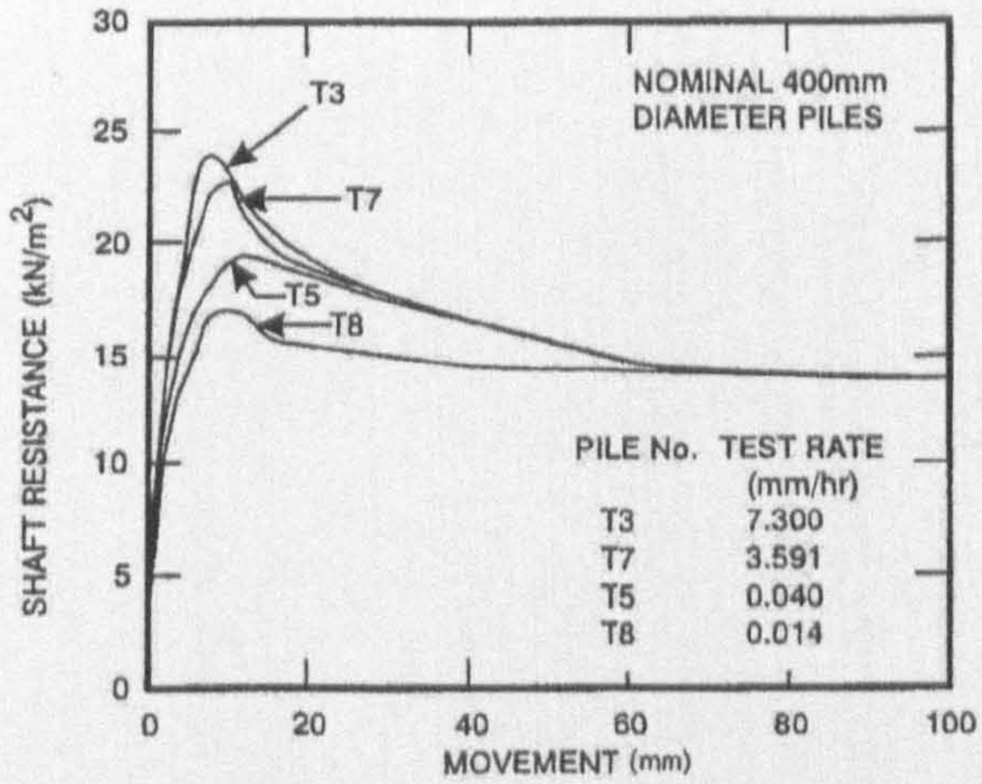

Figure 2.3, Pile shaft resistance versus penetration during CRP testing at different rates (King et al., 2000).

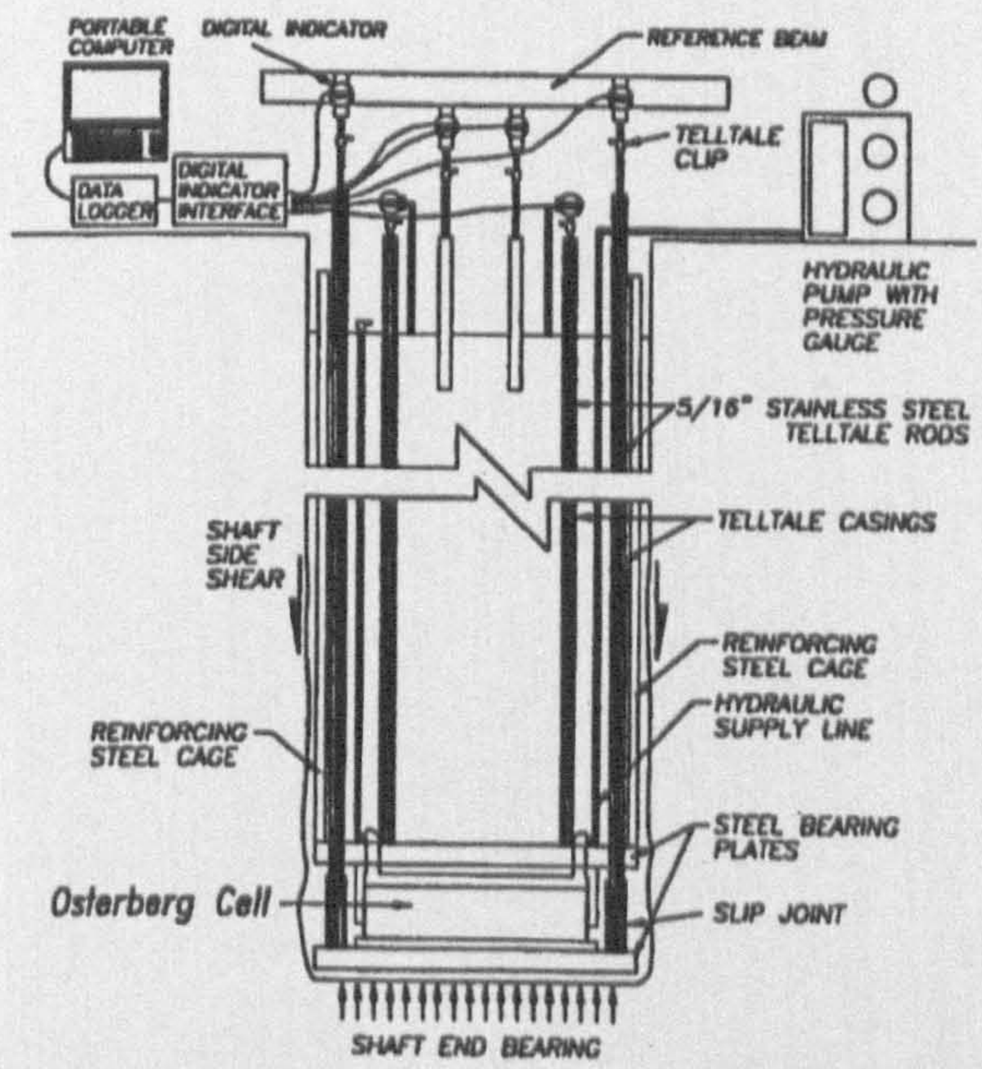

Figure 2.4, Schematic of Osterberg load test equipment (Osterberg, 1999).

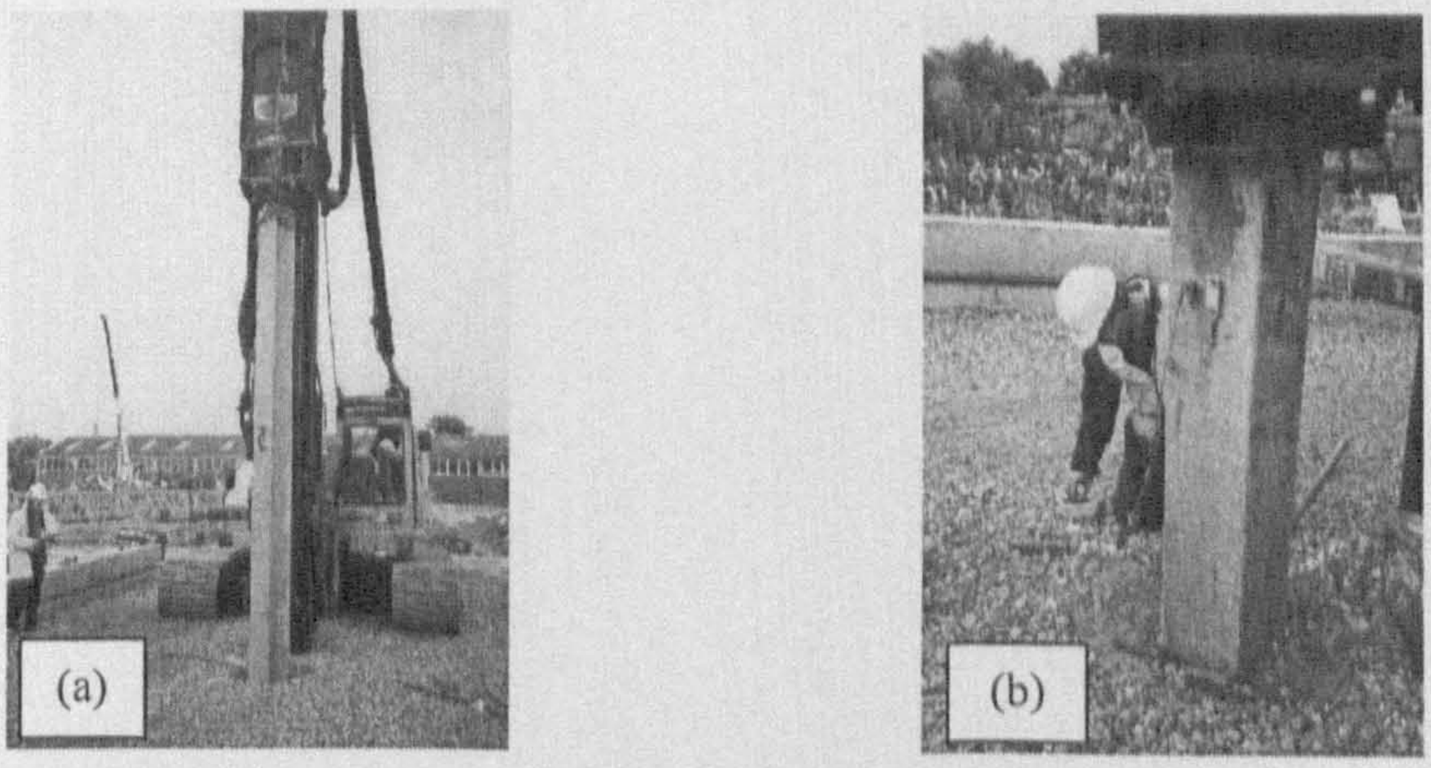

Figure 2.5, (a) Driven pile installation prior to dynamic load testing, (b) Installation of instrumentation to a precast concrete pile for dynamic pile load testing.

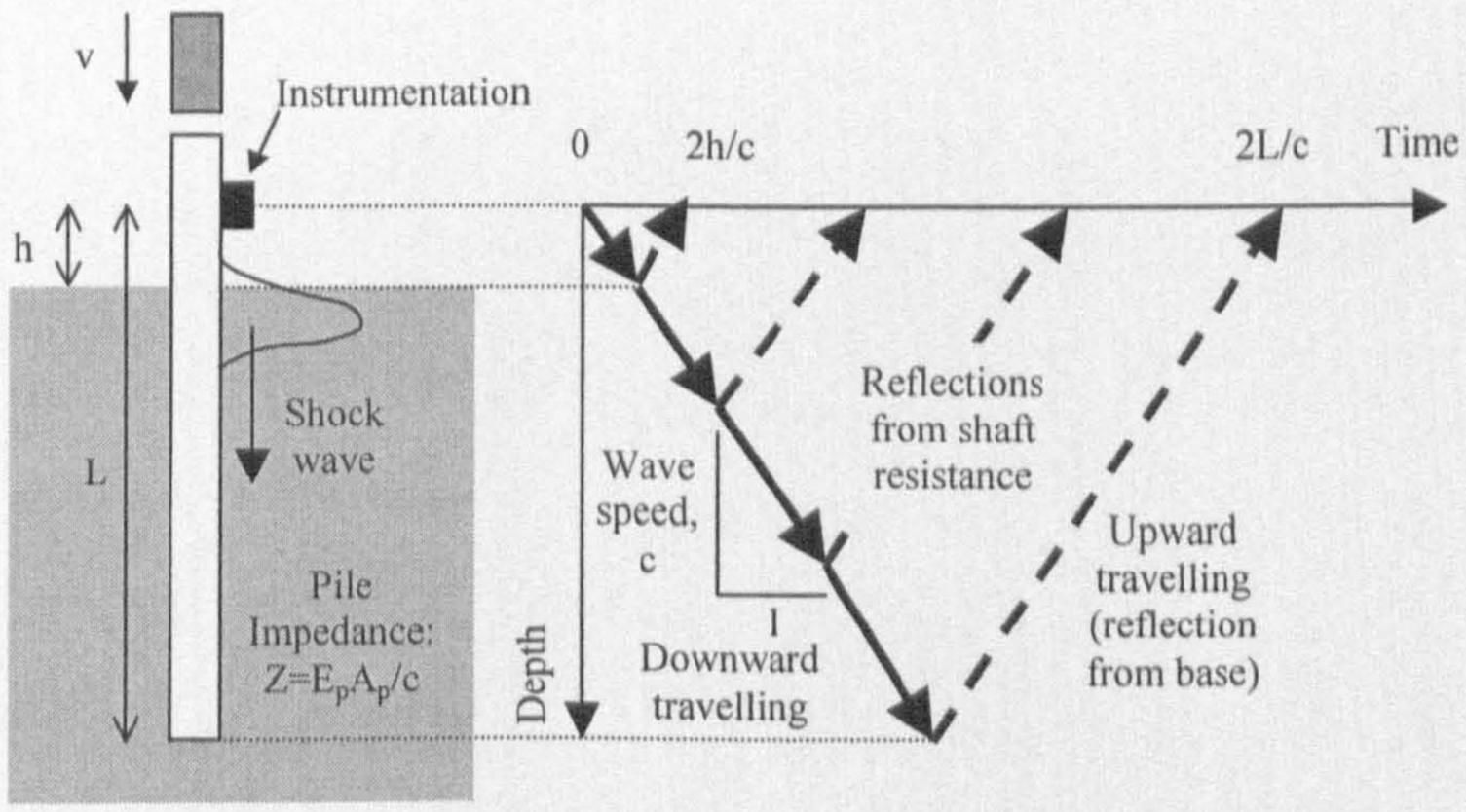

Figure 2.6, Schematic of stress wave travel down a pile (Randolph, 2003).

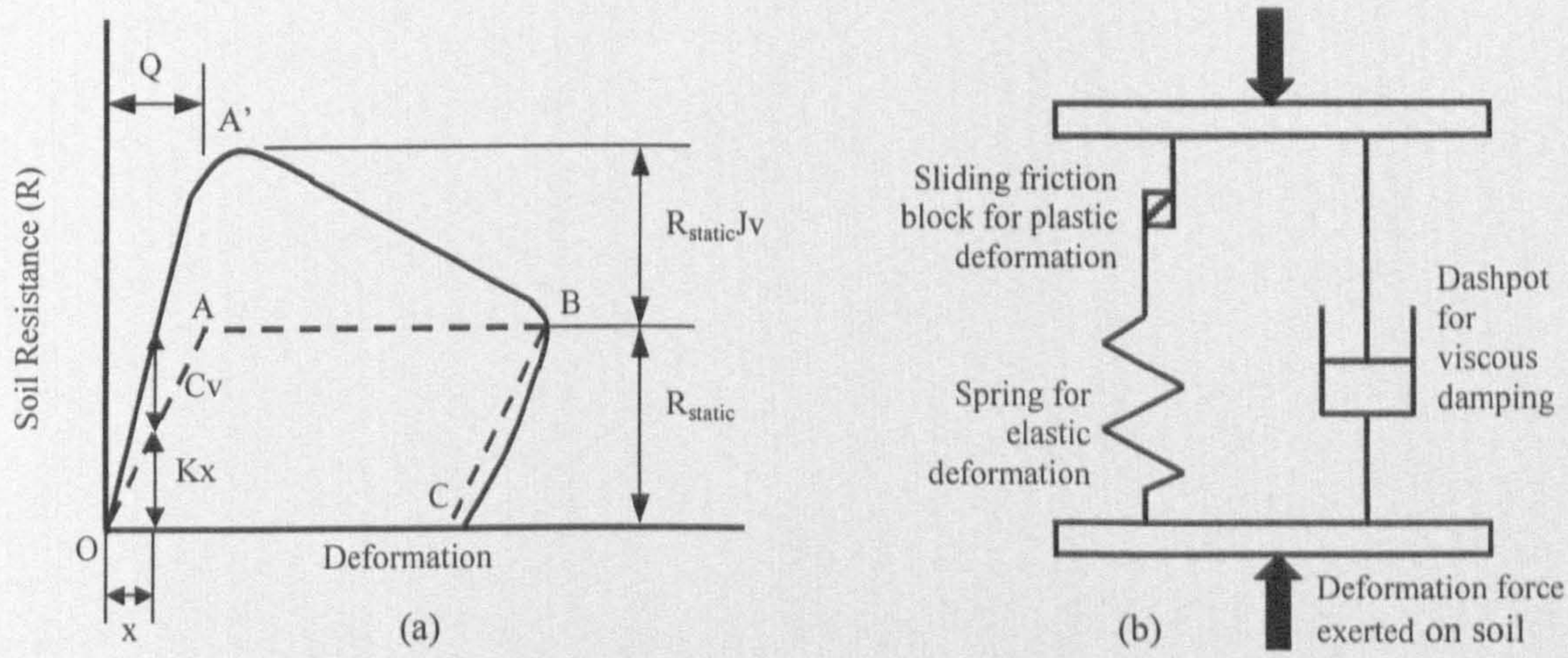

Figure 2.7, (a) Static and dynamic soil resistance versus deformation, (b) Smith's rheological model (Gibson & Coyle, 1968).

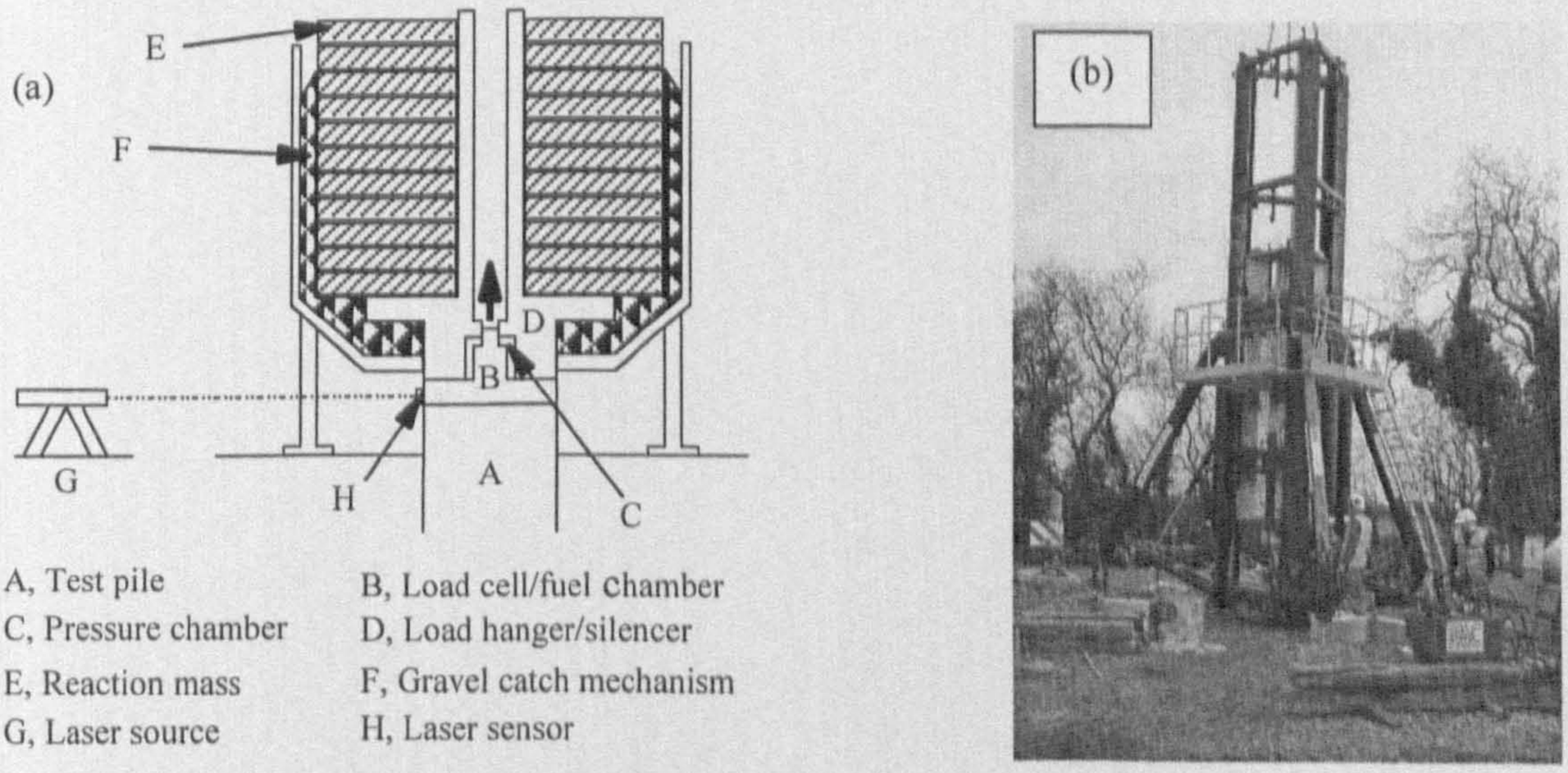

A, Test pile
B, Load cell/fuel chamber
C, Pressure chamber
D, Load hanger/silencer
E, Reaction mass
F, Gravel catch mechanism
G, Laser source
H, Laser sensor

Figure 2.8, (a) Schematic of the Statnamic device with gravel catch mechanism, (b) 3MN Statnamic rig with hydraulic catch mechanism.

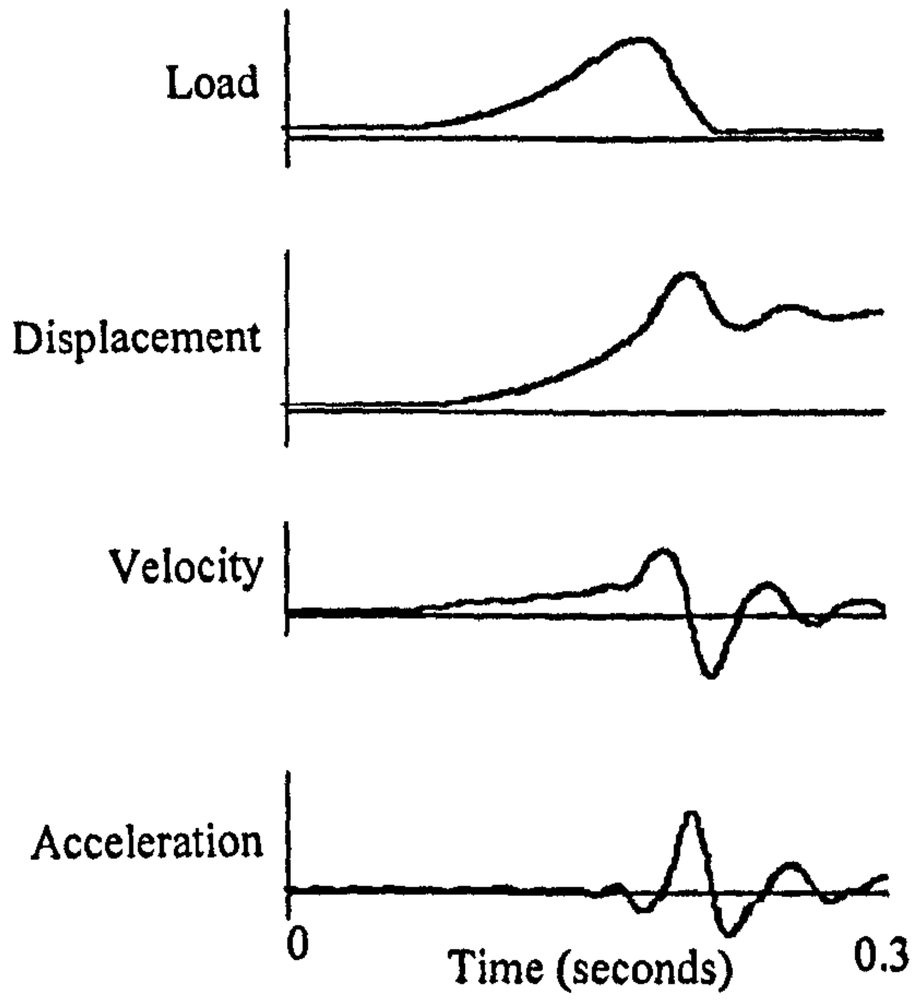

Figure 2.9, Measured and calculated results from a Statnamic test.

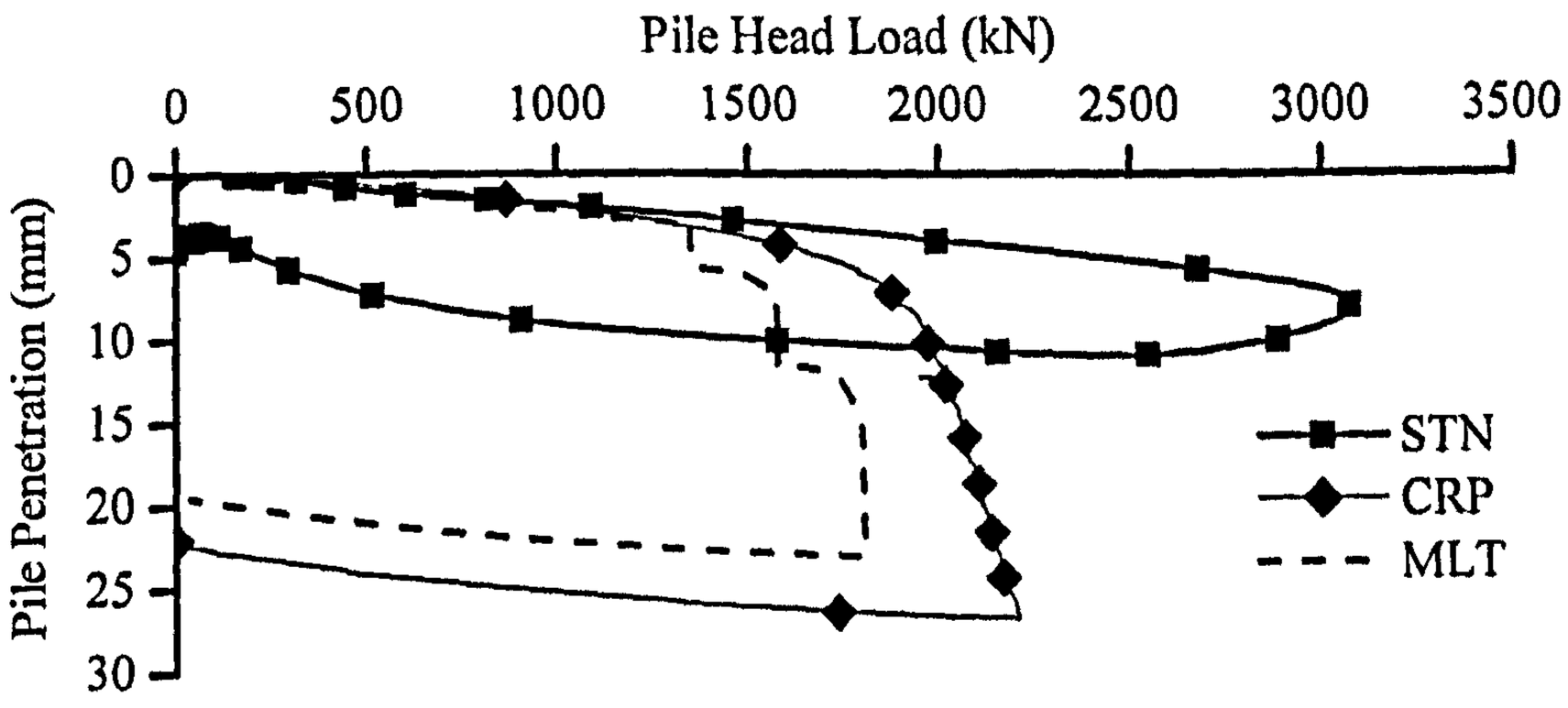

Figure 2.10, Results from a 3000kN Statnamic load test compared with MLT & CRP static load testing. Testing undertaken on an auger bored pile installed in Glacial Till (Brown, 2003).

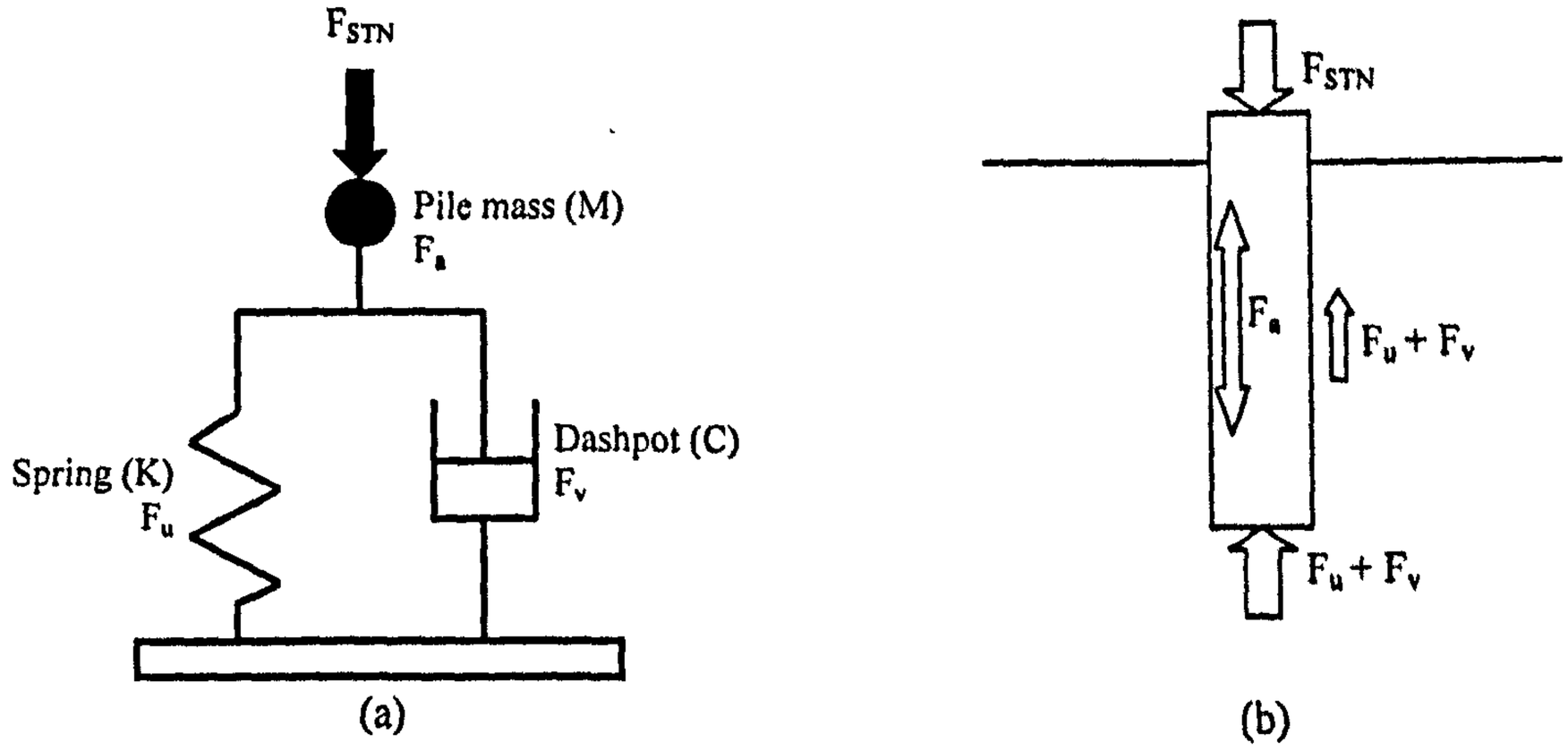

Figure 2.11, (a) UPM Rheological model, (b) Schematic of pile load distribution from UPM analysis (Middendorp, 1992).

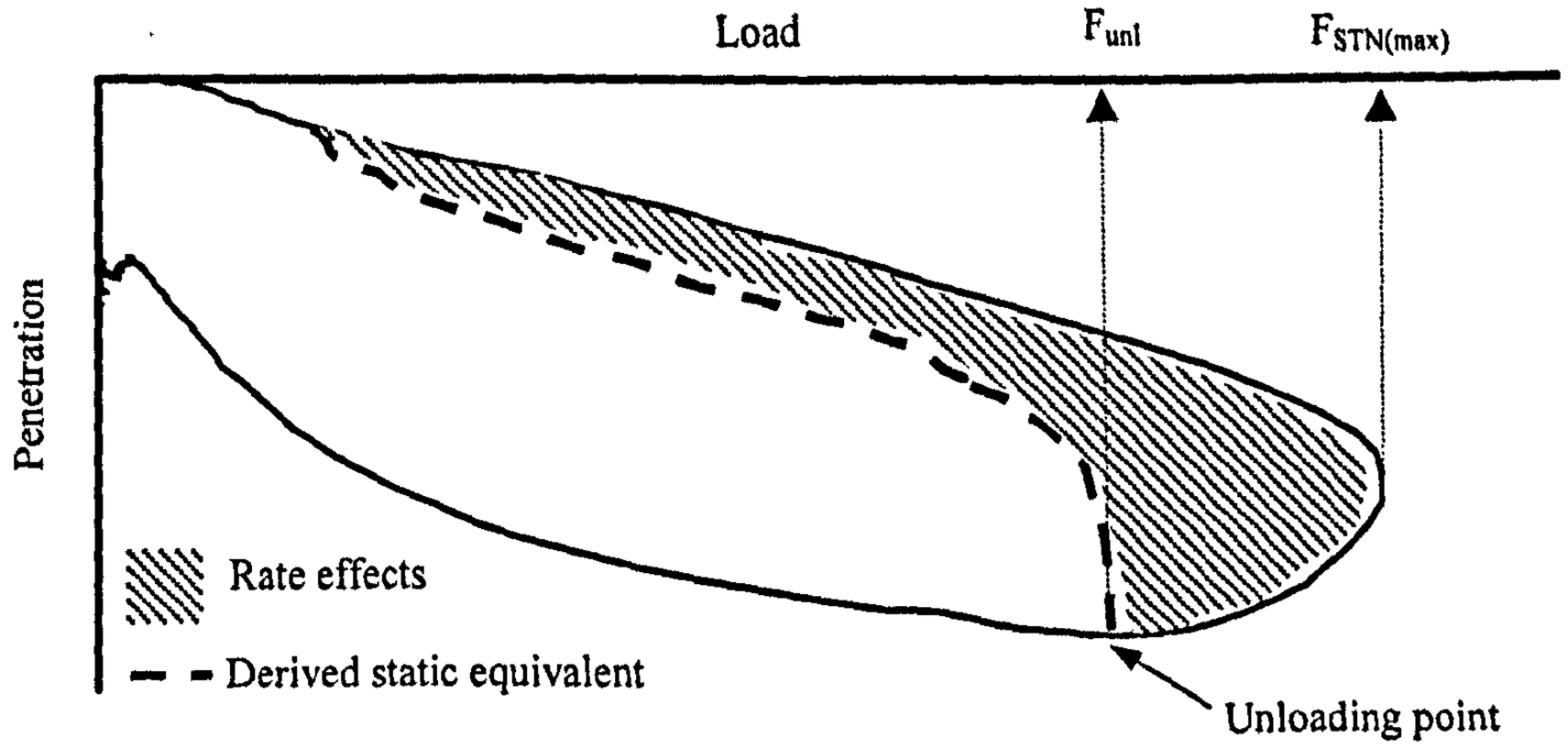

Figure 2.12, Statnamic load-displacement behaviour showing components of UPM analysis.

Soil type	*UPM correction factors*	
	Rate Factor (η), Mullins (2002)	Holeyman *et al.* (2001)
Sands	0.91	
Silts	0.69	
Clays	0.65	0.7
Rocks	0.96	

Table 2.2, Correction factors required for equivalent static pile capacities derived by Holeyman et al., (2001) and Mullins (2002).

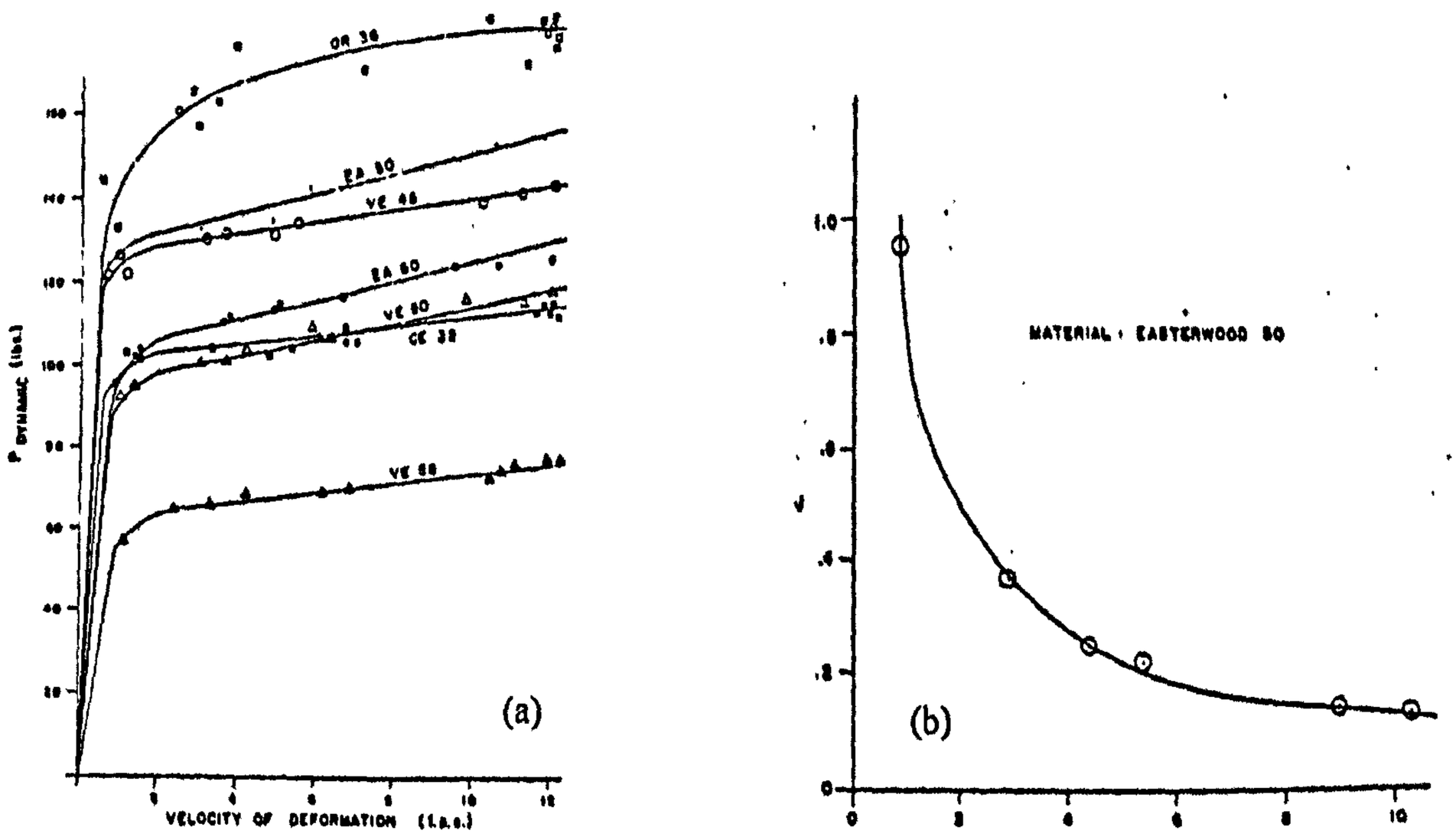

Figure 2.13, (a) Variation of peak shear strength for clay with increasing velocity of deformation, (b) Variation of viscous damping parameter J with velocity of deformation (Gibson & Coyle, 1968).

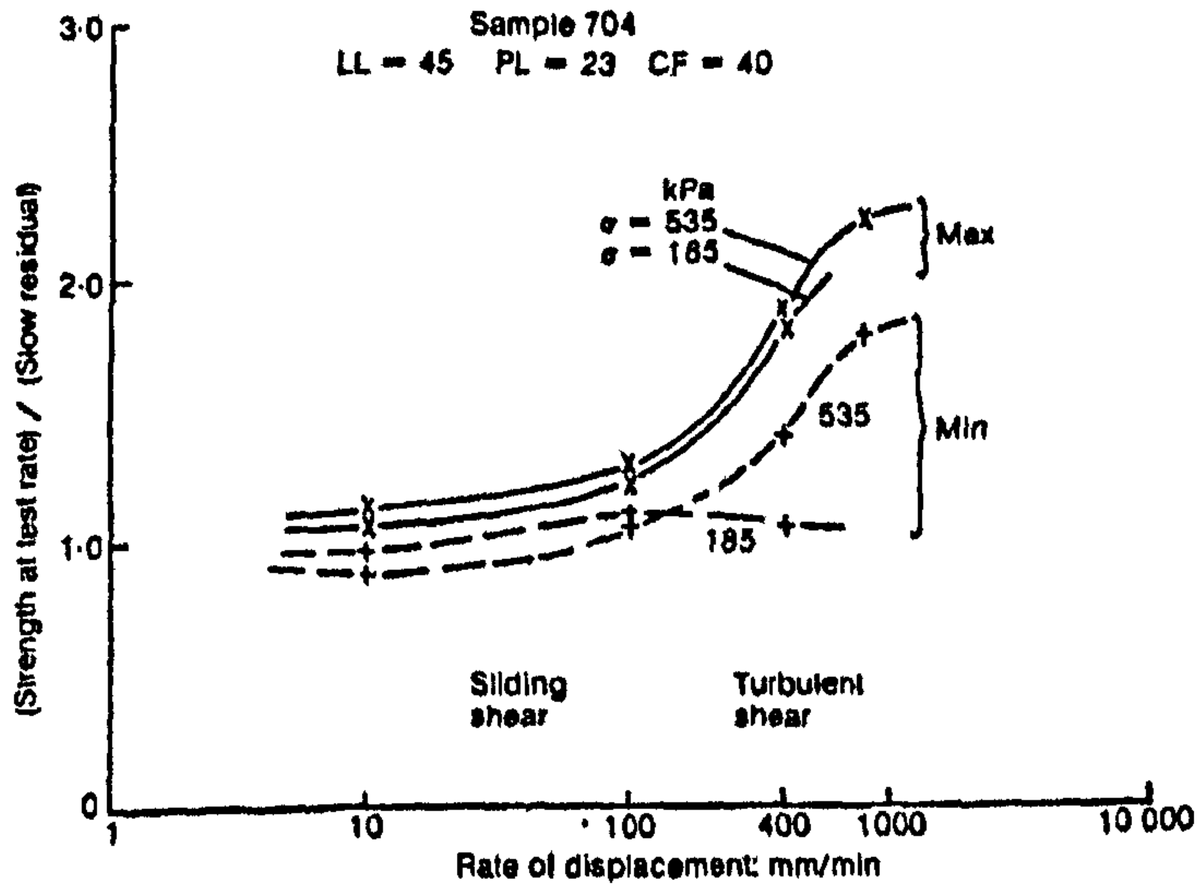

Figure 2.14, Results of ring shear tests on residual shear planes at different rates (Skempton, 1985).

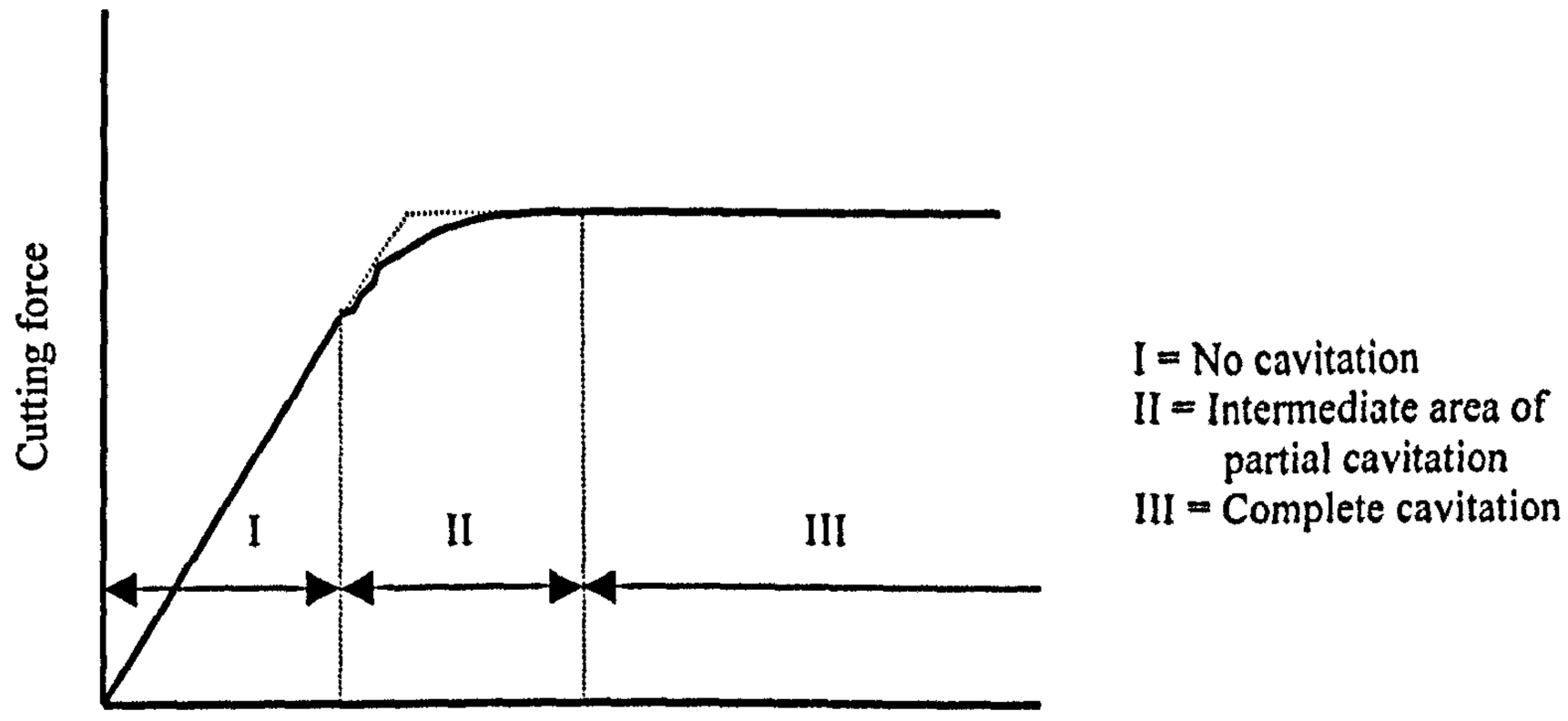

Figure 2.15, Schematic of rate dependency of cutting forces, with cavitation behaviour shown (Os & Leussen, 1987).

Test type	*Penetration rate (mm/s)*	*Test duration (s)*	*Time to failure (s)*
CRP[1]	0.033	15	15
QML (1000)[2]		1000	475
QML (100)		100	55
QML (10)		10	7
QCL (0.1)[3]		0.1	0.06

[1]CRP- Constant Rate of Penetration Test
[2]QML- Quick maintained Load Test, ASTM D-1143:1994(5.6), QLT
[3]QCL- Quick Continuous Load (Statnamic simulation)

Table 2.3, Testing regime adopted by Horvath (1995).

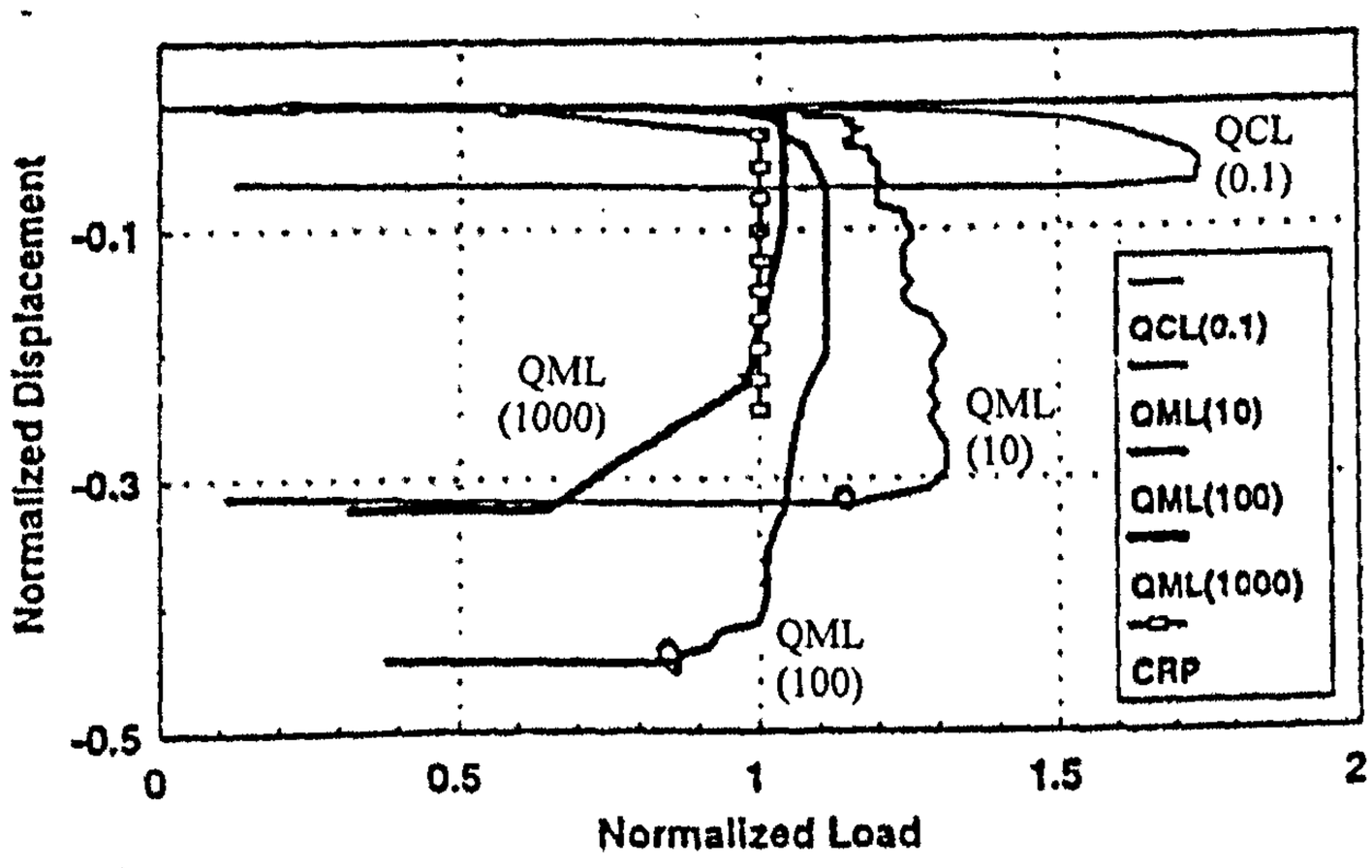

Figure 2.16, Results from Statnamic model pile testing (QCL) compared with different static load tests. See Table 2.3 above (Horvath, 1995).

3.0 Testing Programme

3.1 Introduction

Following the review of previous literature, a testing programme for model pile testing in clay was devised whereby the elevated pile penetration rate on pile-soil behaviour could be determined. This programme had three broad aims:

1. To undertake model pile testing at various penetration rates to quantify the effect of pile penetration rate on pile resistance.
2. To develop a model and analysis method based upon the results of the model pile tests to allow prediction of static pile behaviour from simulated model Statnamic (STN) tests in clays.
3. To gain an insight into the pile-soil behaviour at elevated rates of penetration with particular attention to soil effective stress and inertial behaviour.

To investigate the effect of pile penetration rate on pile resistance and soil effective stress, Constant Rate of Penetration (CRP) testing was undertaken with various target rates from the slowest rate of 0.01mms up to 500mm/s. To gain further understanding of the Statnamic tests, cycles of Statnamic loading were applied to the pile with target peak loads from 10 to 35kN.

Due to the extended periods required for large clay bed preparation, a series of both CRP and Statnamic tests was carried out consecutively in each bed. After each individual load test, the load to the pile was removed and the clay sample allowed to re-consolidate. The re-consolidation was considered complete when the clay bed transducers showed pore water pressures close to the pre-drive values. In all cases, a minimum of 24 hours was left between pile tests. Throughout the pile testing programme the clay beds were subjected to a confining pressure of σ_c = 280kPa. The clay bed preparation methods and material specification also remained unaltered.

3.2 Bed preparation and model pile testing series

During the research project, five clay beds were prepared. These are referred to as Bed 1 to 5 (BD1-5). The first bed (Bed 1) was prepared prior to the development of the pile loading equipment. This was to allow familiarisation with the bed preparation procedures and to test consolidation chamber modifications. No model pile testing was undertaken in this bed. The second bed (Bed 2) was used to develop the model pile and loading systems as well as identifying the important CRP penetration rates for future tests. The remaining beds (Beds 3, 4 & 5) were used to meet the objectives of the research project. The series of tests undertaken in each bed is shown in Tables 3.1 to 3.4.

Throughout testing in the different beds, instrumentation consisting of both pore pressure transducers and accelerometers were incorporated in the clay bed during preparation. In general, pore pressure transducers were located at approximately a quarter, half and three quarters of the bed height. Those at three quarters bed height were in advance of the pile tip at the beginning of testing. The two bed accelerometers were installed at sample mid-height in Beds 2 and 3 and at three quarters of the bed height in Bed 4. In Bed 5, one accelerometer was installed at three quarters bed height whilst the second accelerometer was placed in the pile to verify pile accelerometer readings and velocity calculations.

3.2.1 Constant Rate of Penetration tests

The CRP tests were undertaken with target pile penetration rates of 0.01, 1.0, 10, 25, 50, 100, 200, 350 and 500mm/s. The rates used were changed between clay beds to provide a greater spread of data for the relationship between pile penetration rate and pile resistance. During each series of tests in an individual bed, the lowest rate of pile penetration (0.01mm/s) was undertaken regularly to allow definition of a low rate or static pile resistance benchmark to calibrate the elevated rate tests. Generally, the 0.01mm/s test was the first and last test undertaken in a bed. The 0.01mm/s test was also undertaken after CRP testing and before STN testing.

3.2.2 Statnamic testing

Simulations of pulse load tests were carried out similar to those recorded during prototype Statnamic testing. The pulses maintained the same load duration (≈180ms) but with different target peak loads of 10, 15, 20, 25, 30 and 35kN. The 35kN (target) test was only undertaken in Bed 2 as this exceeded the dynamic performance of the pile loading system. In Bed 4, Statnamic tests were carried out prior to the elevated penetration rate CRP tests. This was to obtain results from Statnamic tests where the soil would be less disturbed than if the results were obtained after a series of CRP tests. A similar regime of re-consolidation was undertaken between each individual load pulse.

Test Number	*Test Reference*	*Type*	*Target Penetration Rate (mm/s)*	*Target Peak Load (kN)*	*Comment / Purpose*
1	BD2/1/CRP-0.01	CRP	0.01		Definition of low rate benchmark
2	BD2/2/CRP-1	CRP	1.0		
3	BD2/3/CRP-10	CRP	10		
4	BD2/4/CRP-100	CRP	100		
5	BD2/5/CRP-0.01	CRP	0.01		Definition of low rate benchmark
6	BD2/6/CRP-500	CRP	500		
7	BD2/7/CRP-0.01	CRP	0.01		Definition of low rate benchmark
8	BD2/8/STN-10	STN		10	
9	BD2/9/STN-15	STN		15	
10	BD2/10/STN-20	STN		20	
11	BD2/11/STN-25	STN		25	
12	BD2/12/STN-30	STN		30	
13	BD2/13/STN-35	STN		35	
14	BD2/14/CRP-0.01	CRP	0.01		Definition of low rate benchmark

Table 3.1, Model pile testing series undertaken in Bed 2.

Test Number	*Test Reference*	*Type*	*Target Penetration Rate (mm/s)*	*Target Peak Load (kN)*	*Comment / Purpose*
1	BD3/1/CRP-10	CRP	10		
2	BD3/2/CRP-0.01	CRP	0.01		Definition of low rate benchmark
3	BD3/3/CRP-50	CRP	50		
4	BD3/4/CRP-50	CRP	50		
5	BD3/5/CRP-100	CRP	100		
6	BD3/6/CRP-100	CRP	100		
7	BD3/7/CRP-200	CRP	200		
8	BD3/8/CRP-500	CRP	500		
9	BD3/9/CRP-0.01	CRP	0.01		Definition of low rate benchmark
10	BD3/10/STN-10	STN		10	
11	BD3/11/STN-15	STN		15	
12	BD3/12/STN-20	STN		20	
13	BD3/13/STN-25	STN		25	
14	BD3/14/STN-30	STN		30	
15	BD3/15/CRP-0.01	CRP	0.01		Definition of low rate benchmark

Table 3.2, Model pile testing series undertaken in Bed 3.

Test Number	*Test Reference*	*Type*	*Target Penetration Rate (mm/s)*	*Target Peak Load (kN)*	*Comment / Purpose*
1	BD4/1/CRP-0.01	CRP	0.01		Definition of low rate benchmark
2	BD4/2/CRP-0.01	CRP	0.01		Definition of low rate benchmark
3	BD4/3/STN-10	STN		10	
4	BD4/4/STN-15	STN		15	
5	BD4/5/STN-20	STN		20	
6	BD4/6/STN-25	STN		25	
7	BD4/7/STN-30	STN		30	
8	BD4/8/CRP-0.01	CRP	0.01		Definition of low rate benchmark
9	BD4/9/CRP-100	CRP	100		
10	BD4/10/CRP-200	CRP	200		
11	BD4/11/CRP-50	CRP	50		
12	BD4/12/CRP-500	CRP	500		
13	BD4/13/CRP-0.01	CRP	0.01		Definition of low rate benchmark
14	BD4/14/CRP-100	CRP	100		
15	BD4/15/CRP-0.01	CRP	0.01		Definition of low rate benchmark

Table 3.3, Model pile testing series undertaken in Bed 4.

Test Number	*Test Reference*	*Type*	*Target Penetration Rate (mm/s)*	*Target Peak Load (kN)*	*Comment / Purpose*
1	BD5/1/CRP-0.01	CRP	0.01		Definition of low rate benchmark
2	BD5/2/CRP-0.01	CRP	0.01		Definition of low rate benchmark
3	BD5/3/CRP-350	CRP	350		
4	BD5/4/CRP-0.01	CRP	0.01		
5	BD5/5/CRP-200	CRP	200		
6	BD5/6/CRP-25	CRP	25		
7	BD5/7/CRP-350	CRP	350		
8	BD5/8/CRP-25	CRP	25		
9	BD5/9/CRP-500	CRP	500		
10	BD5/10/CRP-10	CRP	10		
11	BD5/11/CRP-0.01	CRP	0.01		Definition of low rate benchmark
12	BD5/12/STN-10	STN		10	
13	BD5/13/STN-15	STN		15	
14	BD5/14/STN-20	STN		20	
15	BD5/15/STN-25	STN		25	
16	BD5/16/STN-30	STN		30	
17	BD5/17/CRP-0.01	CRP	0.01		Definition of low rate benchmark

Table 3.4, Model pile testing series undertaken in Bed 5.

4.0 Model Testing Equipment and Procedures

4.1 Introduction

For this study, an existing clay calibration chamber was modified to allow simulation of Statnamic pile loading tests. Previously the chamber was used to investigate the behaviour of the self-boring pressuremeter at full-scale. Further details of the University of Sheffield's clay calibration chamber are reported in Anderson *et al.* (1989) and Anderson *et al.* (1991). Modifications included refurbishing the existing chamber, fabrication of a model pile and the introduction of a loading system capable of rapid pile loading (Brown *et al.*, 2002). To aid further understanding of the Statnamic pulse loading it was decided to carry out constant rate of penetration tests (CRP) at different rates to discern how the behaviour of the clay varied with pile penetration rate.

4.1.1 Calibration chamber testing

The use of a large calibration chamber has the advantage over field studies in that repeatable beds of clay with known composition and stress histories can be prepared. The use of calibration chambers does have limitations though, such as the maximum practical bed size and the nature of the boundary conditions. Their use has real advantages in the simulation of complicated full-scale field events. For these events, repeating tests would prove particularly costly and of limited scientific value due to test-to-test variability.

The use of a 1g system, compared with the now popular centrifuge systems, has the advantages of relatively low cost, simpler scaling laws and the ability to investigate testing events associated with high accelerations. A centrifuge system may encounter problems when attempting to carefully control the movement of bodies through the non-linear acceleration field associated with this test (Bell, 1987). Two of the shortcomings associated with using 1g clay calibration chambers are the long durations required for bed preparation and the limited vertical stress variations over the chamber height (Taylor, 1995). The model in this study only considers pile tip behaviour and adjacent

skin resistance of a pile section installed at some depth equivalent to the applied effective vertical stress.

Examples of small 1g clay calibration cells for modelling field events are relatively numerous (Steenfelt *et al.*, 1981, Anderson *et al.*, 1985, Procter & Khaffaf, 1987, Huang *et al.*, 1988, Horvath, 1995, Hird & Moseley, 2000) whereas the number of large clay calibration chambers is limited, especially those with flexible boundaries (Anderson *et al.*, 1991, Smith, 1993).

4.1.2 Boundary effects

The boundary arrangement for the chamber used in this study may be described as $F_r^f P_p$ using the nomenclature proposed by Houlsby (1984). The F used here describes the flexible boundary at the cylinder edge, superscript f, the top flexible membrane and subscript r, the rigid base plate. The boundary control is also described as either displacement control (D, d) or force control (P, p). In this study, the boundaries were allowed to move but the applied pressure remained constant throughout. To aid understanding of the principle, Houlsby (1984) gives the examples $F_r^r P_d$ to describe a strain controlled triaxial compression test and $R_r^r D_p$ for the oedometer test. Unfortunately, this simple system has seen little use but increased use would greatly aid quick comparison between calibration chambers.

To replicate field conditions in the laboratory for any penetrating or embedded object, it is necessary to minimise boundary influence. This can be done by having a clay bed that is sufficiently large that the existing boundaries do not influence testing or by using boundaries that can be controlled (Smith, 1993). Large beds have the limitation of high mass and space requirements along with preparation problems. The probe diameter to bed diameter ratio along with the type of test to be performed also influences the effect of boundaries on test results. In order to minimise the boundary effects, Smith (1993) made assumptions based upon undrained cavity expansion theory to define the outer diameter of the clay bed:

$$\frac{R_{ep}}{R} = \sqrt{I_r} \tag{4.1}$$

Where

R_{ep} = radius of the elastic-plastic boundary

R = effective radius of the probe

I_r = rigidity index of the soil = G/c_u

G = soil shear modulus

c_u = undrained shear strength

Smith (1993) suggested that if the boundary of the elastic-plastic yield occurs before the outer bed boundary then the soil distortion at the boundary and subsequent boundary influence would be minimised. Theoretical studies of cone penetration testing (CPT) by Teh & Houlsby (1991) used a range of rigidity indexes up to 200 whilst Smith (1993) suggests a maximum value of 500. This places the extent of the radial elastic-plastic boundary for a bed between $14.1R$ and $22.4R$. More typical values for the chamber used in this study may be derived from test results for the rigidity index of London Clay (Wroth *et al.*, 1979) of 36 (Over Consolidation Ratio, OCR=1) up to 120 (OCR=32). Taking the lower value at OCR 1, results in the elastic-plastic boundary being $6R$ from the penetrating object. Modelling of cylindrical cavity expansion for pile driving by Wroth *et al,* (1979) showed that for London Clay at OCR 8, radial stress distributions were significantly altered up to $20R$. This implies that interference by a fixed stress at the boundary would influence the penetration induced stress change. What is unclear from the literature is the nature and extent of interference with test results for clay soils when the chamber boundaries fall within the plastic stress/displacement fields, as discussed above. The model pile used in this study was designed with a diameter of 70mm to be installed in a bed of 780mm diameter. If at this stage we assume that the material has a comparable rigidity index with that of London Clay at OCR 1, then the elastic-plastic boundary would lie at a radius of 210mm, which is well within the existing clay bed.

The base boundary utilised in the chamber was a rigid steel plate, which is not ideal in a study concerned with penetrating objects. It has been suggested by Peterson & Arulmoli (1991) that the CPT can "feel" hard or soft strata up to 10 or 20 cone diameters ahead. The theoretical study of cone penetration testing undertaken by Teh & Houlsby (1991) found that for higher angles of cone apex (60 & 120°) their predictions of elastic-plastic boundaries compared well with spherical cavity expansion approaches. Where the cone had a very narrow point (10°), the boundary of the elastic-plastic yield coincided with the cone tip at rigidity indexes below 150. Based on their findings the boundary of the elastic-plastic yield surface lies between $2.6R$ and $5.6R$ below the penetrating objects for rigidity indexes varying from 25 to 200. Again taking the rigidity index for London Clay as above would place the boundary $3.1R$ below the tip of the penetrating object. For a pile of 70mm diameter the boundary would be 108mm above the base of the chamber.

4.2 The clay calibration chamber

4.2.1 The consolidometer

To prepare the clay bed the chamber had to go through two major consolidation stages referred to as one dimensional consolidation (1-D) and isotropic. The first being the consolidometer as shown in Figure 4.1 & 4.2. To produce uniform and repeatable beds of clay it was necessary to produce a slurry of 1.5 to 2 times the clay material's liquid limit (Sheeran & Krizek, 1971). Due to the resulting high water content, large volume changes occurred during the consolidation process. To accommodate this volume change, a consolidometer consisting of a glass reinforced plastic pipe (1700mm long, 785mm internal diameter and 23mm wall thickness), was clamped between the top and bottom end plates of the consolidometer. The pipe was manufactured by centrifugal casting of a mixture of sand and resin reinforced with glass, sandwiched between 4mm thick layers of resin and glass fibre on the inner and outer surfaces. The resulting pipe had a high degree of circularity and circumferential stiffness whilst being able to deform under its own weight when laid on its side. Smith (1993) describes this as advantageous as the pipe would be able to accommodate any non-verticality in piston travel during consolidation. Although the resulting inner surface of the pipe was relatively smooth, a

layer of silicon grease was smeared on the inside of the pipe prior to filling with slurry to reduce any loss of axial stress within the bed.

To achieve 1-D consolidation, the clay slurry was subjected to pressure by means of a hydro-pneumatic rigid piston, which consisted of a 20mm thick steel loading plate. Above this was a water filled concertina membrane similar to that proposed by Rowe & Barden (1966). This membrane was sealed against the top end plate and loading plate by steel retaining rings incorporating a rubber o-ring seal. The membranes were fabricated by building up to 25 layers of brushable latex on a wooden mould. The latex was then protected by the addition of two layers of flexible polyurethane to both the inner and outer faces. To guide the movement of the piston during consolidation, a 50mm diameter hollow piston rod, passing through an o-ring sealed bush bolted to the top end plate, was bolted to the piston loading plate. The piston rod allowed drainage from the top of the bed and manual measurement of the bed's settlement during consolidation. As the water within the concertina membrane was maintained at a pressure higher or equal to that of the slurry, no additional sealing detail was incorporated at the annulus of the piston loading plate. The use of the flexible membrane allowed a vertical piston stroke of up to 700mm.

The design of the chamber permitted bed drainage from both the top and the bottom of the bed throughout all stages of preparation and subsequent testing. Drainage from the top of the bed was assisted by the addition of a 2mm thick Vyon F circular porous plastic filter membrane. The average pore size for this material was 30μm, which minimised slurry leaching during the early stages of consolidation. The clay beds were separated from the base end plate by a similar layer of porous plastic underlain by a 15 to 20mm thick sand layer to aid drainage. These porous plastic filters were de-aired by boiling for a minimum of 3 hours immediately before placement in the chamber. Bottom drainage was via an outlet in the base end plate.

To remove disturbance of the bed due to transducer installation, the transducers were located in the consolidometer prior to slurry addition. To control their position the transducers were mounted on hollow thin walled metal tubes (6.5mm outside diameter) that were located in holes in the base end plate. The base end plate incorporated

nineteen 7mm diameter holes (Figure 4.1). These holes were used to place transducers at various heights and radial positions within the bed as well as allowing outlet routes for the transducer cables. The rods were then clamped and sealed in place using Wade male stud couplings. To minimise inclusion effects of the rods and to avoid damage during the large consolidation volume changes, the rods were smeared with silicon grease.

4.2.2 Triaxial consolidation

The second stage of the consolidation process was triaxial consolidation in the chamber shown in Figure 4.3. The calibration chamber body consisted of a 1030mm outer diameter steel pipe, 13mm thick with web reinforced welded flanges at each end. A flanged rubber membrane, similar to that used in a triaxial test, was placed over the 1-D consolidated clay. The void between the membrane and the outer calibration chamber body was then filled with water. The membrane was fabricated by gluing sheets of 1mm thick natural rubber together with waterproof polychloroprene rubber adhesive. The flanges of the membrane were sealed between the outer calibration chamber body and the top and bottom end plates by o-ring seals. To apply vertical pressure to the bed a rubber membrane made from the same material as the horizontal membrane was clamped to the top end plate. Again, the void between the end plate and the membrane was filled with water to allow pressure application. This upper membrane was designed to accommodate bed settlements of up to 100mm.

To allow the installation of the pressuremeter in the previous study (Anderson *et al.*, 1991), the top end plate had been designed with a 100mm diameter central hole, through which the guide piston rod passed during 1-D consolidation. During this second stage of consolidation, a piston cutter was fitted in the top plate access hole. To allow the application of uniform vertical stress to the bed in this area, and to provide top drainage, a piston was run down inside the cutter. The piston, pressurised from the same source as the top membrane, ensured a relatively uniform stress to be applied to the upper surface of the bed. The mobile seal between the pressurised water and the piston was formed from a rolling Bellofram.

To allow for the slight difference in heights of the bed at the end of 1-D consolidation, a sand layer was placed on top of the bed, separated by a porous plastic filter membrane. The sand layer allowed pressure to be applied to the bed, as well as acting as a drainage path. During cell assembly, a sand retaining ring was placed outside the horizontal flexible rubber membrane to retain the sand layer during isotropic consolidation.

4.2.3 Calibration chamber services

To apply pressure to the clay bed during both 1-D consolidation and triaxial consolidation, the chamber was connected to two identical systems (Figure 4.4). These consisted of an air/water reservoir cylinder with a water capacity of 27 litres, with pressure supplied via an external regulator valve. Compressed air was provided from a main supply circuit. During the initial 1-D consolidation stage, the two systems were linked together to supply the large water volumes associated with bed volume change. The reservoirs still required regular filling during this initial stage. When linked together, the systems were regulated by one valve that was used to maintain a consistent air supply to the two systems. For triaxial consolidation, the systems were separated by a pressure-switching block, with pressure regulated by individual regulators.

For monitoring the pressure, two wall mounted pressure gauges were used. To allow comparison of the pressure readings taken throughout the test, the pressure gauges were mounted at the mid-height of the clay bed with all other pressure readings corrected to this height. These gauges were used in conjunction with two Druck PDCR 810 general-purpose pressure transducers mounted on the membrane pressure bleed lines.

Water expelled during consolidation was collected in two separate volume change units mounted such that the mid-height of the clay bed was the outflow level. These units were calibrated with a visual scale that was monitored at intervals. Due to the large volumes of water expelled during initial consolidation, these units required regular emptying.

4.2.4 Clay bed material

The bed material used in this study was similar to that used by Rossato *et al.* (1992 & 1994) which consisted of a mix of kaolin, sand and silt, referred to as KSS. Where

possible these materials were sourced from the same suppliers as used by Rossato *et al.* (1992 & 1994) to allow comparison with their findings. The kaolin was Speswhite Powder China Clay supplied by WhitChem, Staffordshire. The sand was Buckland P30 Silica Sand (Hanson Aggregates, Kent), a Lower Greensand sourced from Heath & Reach, Bedfordshire. The silt was Oakamoor HPF4 Silica Flour, manufactured from grinding dry quartz sand supplied by Hepworth Minerals and Chemicals, Cheshire. Similar materials have been proposed by McManus & Kulhawy (1991). A summary of the individual material properties as provided by the suppliers can be found in Appendix 2.

The mix proportions (by weight) used to form the clay beds were 50% kaolin, 25% sand and 25% silt. Index properties for this material are shown in Table 4.1. The clay itself was formed by producing slurry at 55% moisture content, which was equivalent to 1.5 times the liquid limit. This is similar to the previous study (Anderson *et al.*, 1991) where kaolin was prepared at 1.5 times the liquid limit, although this is noted as the lower limit of the water content suggested by Sheeran & Krizek (1971) for the preparation of consistent slurries. Using a lower moisture content has the benefit of lower consolidation times and a bed that does not need topping up with slurry as consolidation progresses.

This material, rather than pure kaolin, was used as a model soil for several reasons. Although kaolin has the benefit of being widely available and has an extensive record of use in research, it has several shortcomings. Rossato *et al.* (1992 & 1994) summarise these as very high clay fraction (80%) and easily orientated particles during consolidation and shear. Kaolin also displays fully developed residual behaviour at strains as low as 12% independent of sample size. This behaviour may be particularly favourable in certain studies, but may have detrimental effects in large model studies where simulations of natural soils are required.

4.2.5 Clay bed preparation

Initially, the transducers required within the bed were placed on thin walled rods set at various heights and radial positions above the chamber base end plate (Figure 4.5). The pore pressure transducers were kept in a modified triaxial cell used for de-airing until chamber assembly commenced. To avoid the pore pressure transducers becoming re-

aerated they were smeared with KSS slurry and sealed in plastic bags. The base drainage was constructed as discussed in Section 4.2.1 and the consolidometer body lowered into position (Figure 4.1). Prior to placing the consolidometer body, it was thoroughly cleaned and smeared with silicon grease.

Slurry preparation was undertaken in a large concrete pan mixer in a manner designed to reduce dust and avoid material segregation. Firstly, the required volume of de-aired and de-ionised water (50 litres) followed by the kaolin (45.5kg) and silt (22.75kg) were added to the pan. This was then mixed for 5 minutes to form slurry. After this time the sand was gradually added to the pan with continuous mixing which was then continued for a minimum of 30 minutes. Smith (1993) recommended a period of 2 hours but it was felt that this would excessively extend the filling time of the consolidometer and threaten the saturation of any exposed pore pressure transducers. Throughout the mixing process, samples were taken from each slurry batch to check the moisture content. The slurry was transferred to the consolidometer using a Mono-Merlin slurry pump through a 50mm ID smooth bore flexible plastic hose. The hose was used to place the slurry in the consolidometer under de-aired water to reduce air entrapment. When the pore pressure transducers became covered by the water layer or rising slurry, their protective covers were removed. Eight mixes were required to prime the pump and fill the consolidometer to approximately 1.4m above the base. Transducer installation and consolidometer filling was generally completed within two days. Once slurry addition was complete, any excess water was removed and the top drainage filter membrane added (Figure 4.1). The top end plate holding the loading plate and concertina membrane arrangement were then lowered onto the slurry and the top end plate bolted in position.

Initially the vertical pressure applied to the bed was maintained at 75kPa for three to four days. This allowed the system to bed in and limit the degree of initial piston settlement and the resulting demands on the pressure supply and drainage water collection systems. After this stage, the pressure was increased to 280kPa. Continuous system monitoring throughout this period included bed drainage volumes, piston settlement, applied pressure and bed pore water pressures. Where installed, a similar approach was used with the earth pressure cell. During the 1-D consolidation stage approximately 160 litres of water was expelled from the slurry.

Previous work by Anderson *et al.* (1991) using kaolin found that 6 to 7 weeks were required for the slurry to reach 90% consolidation under 1-D conditions. To avoid long delays, consolidation was stopped after approximately 3 to 4 weeks when the clay bed was found to be self-supporting. The termination conditions used by Anderson *et al.* (1991) were:

1. Clay bed height equal to or less than 1m.
2. Average degree of consolidation, as indicated by the clay bed pore pressure transducers, greater than 40%.
3. Mid-height excess pore water pressure less than 200kPa.

The termination conditions for the KSS bed were similar to these but mid-height pore pressure transducer readings were allowed to fall to 150kPa. This was achieved in the relatively short time of 18 days.

When these termination criteria were satisfied, the drainage valves to the bed were closed to minimise swelling and the consolidation pressure slowly reduced to zero over a period of 30 minutes. The water was then siphoned from the concertina membrane followed by the removal of the top end plate with the loading plate clamped in place. To remove the consolidometer from the bed, uplift was provided initially by placing a hydraulic jack between the bed and a square hollow section (SHS) section bolted across the top of the consolidometer. To protect the bed, a sheet of plywood was placed between the base of the jack and the bed. Once the jacking system had overcome the friction between the clay bed and the consolidometer pipe, lifting was completed using an overhead gantry crane. The outer test chamber body was then removed and the freestanding bed was ready for conversion to the triaxial phase of consolidation shown in Figure 4.3.

The bed was then carefully fitted with the flanged rubber membrane as described in Section 4.2.2, which was sealed between the top and bottom end plates. Once the membrane was in place, the outer test chamber body was replaced and the space between the membrane and the body filled with water. This offered limited support to the bed during cell construction. A sand-retaining ring was placed around the top of the

bed, up against the membrane. This ring provided support for the sand that was placed on top of the bed to act as a spacer and a drainage layer. The top end plate, from which had been removed the concertina membrane and loading plate arrangement, was fitted with the flexible rubber membrane and piston cutter as shown in Figure 4.3. This arrangement was lowered onto the sand layer in the position it was to be bolted down. The top end plate was then raised and voids identified between the top end plate and the sand layer. Where these voids occurred additional sand was added and the process repeated. Once the cell top was bolted down, excess sand was excavated from inside the piston cutter. The void was then filled with the piston and rolling bellofram seal arrangement. At the interface between the sand layer and the piston, a sheet of saturated porous plastic was inserted. Drainage could then occur up through the piston via a coil of flexible nylon piping running from the upper face of the piston. Above the piston was placed a "top hat" arrangement that sealed against the flange of the bellofram with an o-ring seal in its base flange. The void between the "top hat" and the piston was filled with water and pressurised from the top flexible membrane supply. This pressurised water was used to maintain similar pressure at the piston/sand interface as that applied by the flexible membrane. After cell assembly, but prior to pressurisation, the transducer support rods and Wade fittings were carefully removed and the cables sealed in the bottom end plate using Plasticon fittings. Due to the different stages of consolidation and the need to remove the support rods, the Druck pore pressure transducers wiring were not terminated in connectors but left free (Pigtails) with connections made using screw connectors.

Consolidation was then allowed to continue with 280kPa being applied both horizontally and vertically. During this phase drainage occurred from both the top and the bottom of the bed, with volume change and bed pore pressure readings throughout. A bed consolidation of 90% was reached in less than 8 days of isotropic consolidation, which compares with 12 days for the previous study, at which stage it was considered suitable to begin model testing. For this study, consolidation was allowed to proceed past 90% due to the timesavings mentioned.

4.2.6 Performance of the clay calibration chamber during bed consolidation

Along with system and equipment development, five test beds were produced during this study, the first of which was used to practice chamber assembly and consolidation. In general, the system performed well after 1-D consolidation. Problems and delays did occur at the 1-D stage predominantly due to leaks associated with the water filled concertina membrane. The problems usually manifested themselves as tears appearing in the membrane or small leaks that could not be traced. These small leaks were probably due to the membrane pulling past o-ring seals at the location of punched holes used during membrane clamping. Tears occurred that resulted in cell strip down and membrane replacement, which could be achieved in two days. Attempts to reinforce the membrane locally by incorporating Hessian mesh in the layers of latex did not improve the situation. Similar problems were noted in the previous study (Anderson *et al.*, 1989).

The triaxial stage of consolidation worked very well with the chamber remaining in this mode throughout consolidation and testing. Initial problems were encountered with top membrane failures. These were put down to excessive membrane movement due to poor localised compaction of the sand drainage layer and existing surface damage to the central retaining ring. To avoid this, a new ring was fabricated. Additionally, a central ring of membrane material was added at the inner clamping point to provide an additional layer of rubber between the membrane and the ring. One area that could be improved is the degree of the top sand layer saturation after cell assembly. To minimise the chances of bed swelling and resulting softening, the sand layer was placed dry and inundated with water just prior to top end plate sealing. This resulted in the bed not being saturated. This in turn resulted in a lag between top drainage and bottom drainage.

In the final test bed, (Bed 5) problems were encountered in the form of bed pore pressures increasing after consolidation was complete. The chamber was stripped down, the outer membrane replaced, and the top membrane checked. On re-building the chamber and re-pressurisation, little improvement was noticed which was reflected in the effective stresses encountered during testing (Table 4.2).

4.2.7 Consolidation behaviour and bed uniformity

Although it did not particularly hinder consolidation, marked differences occurred between the volumes of water expelled from the top of the bed during 1-D consolidation. The amount of water expelled from the top of the bed was typically 55 litres less than that at the bottom or 41% of the total water expelled from the bed. The top drainage output when plotted against logarithmic time suggested that primary consolidation was near completion, whereas this was not seen for the bottom drainage. This was also confirmed by higher than average pore pressure readings from transducers located 750mm above the base of the chamber. Variations did occur in the previous study by up to 20 litres but only one test result was available to check this (Anderson *et al.*, 1989). This lag may have influenced the uniformity of the clay bed at the end of 1-D consolidation. This was probably caused by the difference between the detailing of the two drainage layers.

Initially it was intended to end 1-D consolidation at similar degrees of consolidation for each bed to aid comparison of results. This was achieved for Beds 2 and 3 where 1-D consolidation was terminated at 41.4% and 42.9% average consolidation as indicated by the pore pressure transducers. Unfortunately due to technical difficulties, this was not achieved with Beds 4 and 5 whose 1-D consolidations were terminated at 79.3% and 60.9% respectively. A summary of the bed states during the different stages of testing can be seen in Table 4.2. The effective stress and percentage consolidation are based upon pore pressure readings for transducers located throughout the beds.

To check for bed uniformity, readings were compared for bed pore pressure transducers located close to mid-height of the bed. Transducers located at 475mm above the base end plate in sets of three typically registered within 4kPa of each other throughout 1-D and isotropic consolidation. This would suggest relative uniformity of consolidation on the different horizontal levels of the bed. Greater differences were noted of up to 20kPa after the pile-testing programme had been completed.

As well as checking the uniformity of the bed using the embedded pore pressure transducers, the bed was carefully stripped down over a two-day period at the end of testing. During this strip down moisture content samples, hand vane tests and thin

walled push samples (38mm and 100mm diameter) were taken at various positions throughout the bed. A summary of the results for each bed can be seen in Table 4.3. Although disturbance of the bed would occur during pile testing, tests carried out at 250mm from the pile were assumed to give a good representation of the bed uniformity. This lies outside the plastic zone as suggested in Section 4.1.2. For instance, Bed 2 had an average moisture content at this radius of 23.7% with a standard deviation (SD) of 0.7%. If all the samples are used including those close to the pile, the average moisture content was 22.6% with a standard deviation of 1%. Results from hand vane testing (Bed 4) suggested an average undrained shear strength of 53kPa (SD=5kPa) at 250mm out from the pile with a residual shear strength of 29kPa (SD=2.5kPa) at this position. This was confirmed by results from 38mm quick undrained triaxial tests for Bed 4 that give an average shear strength of 55kPa (SD=9kPa). Variations in these values from bed to bed were due to drainage occurring throughout the pile-testing programme. In each case, the programme of tests varied, as did the duration. The results from the above tests, especially moisture content would also be influenced by the time taken to strip down the beds. Uniformity may also be influenced by the change in bed effective stresses during bed unloading and strip down.

Measurements from the earth pressure cell during 1-D consolidation were monitored, typically at five-minute intervals. Fluctuations were noted by the previous investigators in the form of cyclical pressure build up and release (Anderson *et al.*, 1989). Similar results were noted in this study but after normalising the results of the stress readings by the applied vertical stress, it was found that the cycles had a very consistent 24-hour period. This would suggest that the phenomenon was more likely to be due to external influence on the earth pressure cell, such as temperature change. What was of note from earth pressure cell readings was that the measured stress reduced by 36kPa during 1-D consolidation, whereas reductions were only 15kPa in the previous study. This difference may be due to higher friction between the clay bed and the consolidometer body resulting from the granular content of KSS. As the bed was only partially consolidated at the end of 1-D consolidation, any non-uniformity in the bed due to vertical stress variation would be overcome during the triaxial stage.

Similar cyclic behaviour of the earth pressure cell was noted during the isotropic stage with cycles of 24 hours and peak-to-peak variation in pressure of 10kPa. This further

reinforces the assumption that the cyclic behaviour is a measurement error rather than a physical change of the bed conditions. If the earth pressure cell is to be used in future studies, the long-term drift of the unit along with the influence of external factors such as temperature should be studied.

4.2.8 Clay bed instrumentation

The instrumentation consolidated in the bed was of three types; instrumentation designed to measure pore pressure variation, local accelerations and earth pressures. Measurements of pore pressures were achieved by using miniature series Druck PDCR 81 transducers (Taylor, 1995). Typically, up to eight of these units were incorporated within the clay bed. These transducers have been widely used in physical modelling due to their small size (11.65mm long, 6.4mm diameter and 2.3mm diameter vented cable), rugged nature and proven reliability. The size of the units and low cross section of the flexible cable minimises their interference during testing. These units were also employed in the previous chamber study (Anderson *et al.*, 1991).

These units operate on the differential pressure approach where atmospheric pressure is present one side of a flexible strain gauged diaphragm. The other side of the membrane is subject to the pressure to be measured and the diaphragm deflects according to the difference in pressure. The atmospheric reference pressure is supplied to the rear of the diaphragm via a hollow tube. As Taylor (1995) notes, due to the design, the integrity of the tube itself and the tube/transducer interface must be checked regularly.

The ability of the transducers to monitor rapid loading events was investigated by Bond *et al.* (1991) and it was found that the probes had a 99% response to a pressure change of ± 800kPa within 10 to 400 milliseconds, depending on the quality of saturation. The response time would also be affected by the movement of the pore fluid through the porous ceramic filter that isolates the pore fluid for measurement (Taylor, 1995). The performance of the filter can be further degraded by blockage due to clay particles. The filter elements used in this study were the ceramic type supplied with the units, which were not removed during this study. In order to saturate the transducers they were placed in a specially modified triaxial cell full of previously de-aired water and subjected to a vacuum for a minimum of 24 hours. De-aired and de-ionised water was used for saturation, as this was the pore fluid within the clay bed.

Kulite were also approached to manufacture a specially ruggedised version of their XT-123C-190-7-BAR-A miniature pressure transducer. This type of transducer does not reference back to vented atmosphere but to an on-board sealed in pressure, thus removing the need for tube venting. The modifications carried out by the manufacturer included enclosing the diaphragm in a waterproof coating. The units also incorporated full screening of the input/output wiring which was not present on the Druck transducers. These units initially performed better than the Druck transducers due to low noise on their output signals. Unfortunately, after long periods of energisation during consolidation, the units stopped working, this led to the units no longer being incorporated in the bed. It would appear that the problems encountered with the transducers were due to embedment in the clay as when the transducers were used in non-embedded locations they performed well. To reduce noise input to the signals from the Druck transducers, it was decided to feed all the output cables through a length of screened flexible conduit running from the base of the chamber to the signal acquisition equipment.

The bed also incorporated up to two Kistler 8704B50 piezoelectric accelerometers of the ceramic shear type (Figure 4.6a). The rated frequency response range for these transducers was 3Hz to 7kHz. This range corresponds to ±5% (useable range) variation in transducer output at varying frequencies referenced to its output at 159Hz (1000 rads/sec). Frequency response calibrations from the manufacturer for the individual transducers give deviations of –0.9% at 20Hz and 1.0% at 10kHz. These units were chosen due to their hermetically sealed titanium construction, small size, low mass and flexible cabling. The low mass being important to minimise any frequency alteration or "mass loading" associated with incorporating the instrument in the vibrating soil. It is recommended that the mass of the accelerometer be kept below 10% of the mass of the vibrating body. As it was not clear what proportion of the soil mass would be vibrating, it was decided to minimise the inclusion mass where possible.

Initially, these units were placed in the clay bed supported on metal rods. It was assumed that the o-ring sealed 10-32 type (Microdot) connection between the wire and the accelerometer was sufficient to stop water ingress. After stripping down of the first

bed, condensation build up was found within the connector and this practice was dropped. To avoid this situation the accelerometers were placed in stainless steel sealing units that slid over the top of the accelerometer and sealed close to the base of the unit with an o-ring (Figure 4.6b). This left the base of the accelerometer exposed to the clay bed. The drawback of incorporating the sealing device was that it increased the mass of the accelerometer inclusion. The cable passed through a watertight Plasticon fitting that screwed into the top of the sealing unit.

One limiting factor of the accelerometers as specified is that, when mounted in the chamber, they could only monitor acceleration in the vertical direction. Horizontal mounting was not attempted at it was felt that the increased profile would lead to distortion of the mounting rod, and subsequent cable damage, during the consolidation phase. Triaxial mounted accelerometer packages could be introduced but they are generally quite large, heavy and expensive.

A Kulite 0234 soil pressure cell with a fluid filled low deflection diaphragm was introduced for the final test bed (Bed 5) to look at the influence of the rigid base boundary of the chamber on test results. It had a central sensing zone of 37.9mm diameter (1128.2mm^2), an outer diameter of 54.8mm (2358.6mm^2) and a thickness of 15.6mm. The unit was placed at the centre of the bed, above the porous plastic filter and sand layer. The problem with any attempt to measure earth pressures is that the inclusion of the measuring device influences measured pressures due to its geometry and any movements associated with measurement (Hanna, 1973). The ratio of measured stress to the value that would have existed if the cell had not been included is referred to as the Cell Action Factor (CAF), for a simple diaphragm cell (White, 2002). As noted by Clayton & Bica (1993) generally the CAF is based purely on aspect ratio of the cell with little regard to the stiffness properties of both the cell and the soil. As reported by White (2002), the CAF can be related to the flexibility ratio (F_E) of the soil-cell system where the stiffness and thickness of the cell diaphragm material are known. In this case, the calculation of the flexibility ratio (F_E) and subsequent determination of the CAF were hindered by lack of knowledge of the internal arrangement of the pressure cell and how applicable this approach is to fluid filled diaphragms. This problem was also noted by Take & Valsangkar (2001). What can be deduced from the work by Clayton & Bica

(1993) is that as the stiffness of the cell increases, the CAF approaches unity. Hanna (1973) suggests that the stiffness of the cell should be such that the ratio of the deflection (δ_{cell}) at the centre of a cell to the diameter D_{cell} is limited to 1/5000 or even greater. In the case of the cell used in this study, the deflection is a maximum of 0.0025mm at 700kPa (δ_{cell}/D_{cell} =1/21920).

4.3 Instrumented model pile

The instrumented model pile used in this study (Figure 4.7) was designed with the aims of being able to:

1. Determine the effects of rate of testing on effective stresses and pile bearing capacity in clay.
2. Directly measure both skin friction and pile tip loads independently of each other.
3. Combine with the existing clay calibration chamber with minimal modifications.
4. Utilise commercially available components but with majority of fabrication carried out in house.

Historically there have been many model pile studies incorporating instrumented devices capable of measuring different aspects of pile behaviour. The measurements may include tip loads (Cooke & Whitaker, 1961, Morrison & Taylor, 1994, Borghi *et al.*, 2001, White, 2002), skin friction or load distribution (Coop & Wroth, 1989, Bond *et al.*, 1991, Taylor, 1995, Nicola & Randolph, 1999, Mendoza *et al.*, 2001), contact pore pressures (Steenfelt et al., 1981, Anderson et al., 1985, Coop & Wroth, 1989, Bond *et al.*, 1991, Mendoza *et al.*, 2001) and surface stress (Anderson *et al.*, 1985, Coop & Wroth, 1989, Bond *et al.*, 1991, Mendoza *et al.*, 2001).

The pile used for this study was split into four major sections, two of which incorporated instrumentation. The sections included the pile tip, skin friction sleeve, pile top end plate seal (Bellofram) and the actuator pile connection (Figure 4.7 & 4.8). The pile was 70mm in diameter throughout its embedded length and 1295mm from tip to actuator connection. Typical embedded lengths were initially 720mm, with the pile being advanced to 840mm during testing. The pile was fabricated throughout from

stainless steel unless otherwise noted. In Bed 2, the pile was 120mm longer than for the remainder of the study. The pile was shortened because it was found that, to achieve the required number of tests, the pile tip came to within 93mm of the end of the rigid chamber bottom end plate. This would place the bottom boundary within the high distortion plastic yield zone as discussed in Section 4.1.2.

Based upon the undrained triaxial results from Beds 2 and 4, an estimate was made of the material rigidity index as discussed in Section 4.1.2. This was achieved by calculating the undrained Young's Modulus (E_u) of the material at 0.2% strain from triaxial testing. By using the equation:

$$G = \frac{E_u}{2(1+\upsilon_u)} \qquad \text{(Atkinson, 1993)} \qquad (4.2)$$

Where the undrained Poisson's ratio (υ_u) is assumed to be 0.5 (Tomlinson, 2001) for undrained clay. The rigidity index was then found from:

$$I_r = G/c_u \qquad (4.3)$$

The average rigidity index for Bed 2 and 4 were 30 and 36 respectively. The average value 250mm away from the pile's disturbance was 34 and 36 respectively. The upper value of 36 was deemed the most relevant for cylindrical cavity expansion. This corresponds with the value assumed earlier. As it was difficult to sample under the tip of the pile, no specific rigidity index was determined for this zone. Assuming increased rigidity below the pile tip due to the proximity of the base drainage layer a value of 49 was proposed for the rigidity index based upon the maximum single value obtained from the two beds. Based upon Teh & Houlsby (1991) this would place the elastic-plastic boundary 123mm below the pile tip. The minimum separation of pile tip to base was 182mm in Bed 5.

4.3.1 Pile tip section

The load applied at the pile tip was measured by compression of a miniature Entran ELHS load cell that was connected to the pile tip end plate, which was allowed

to move within the pile outer sleeve (Figure 4.9a & 4.9b). The dimensions of this unit were one of the predominant factors that governed the diameter of the pile. White (2002) adopted a similar approach, as the more common method of strain gauging the pile outer wall just above the tip may result in spurious readings due to local high shaft friction. The pile tip end plate was free to move whilst being sealed with an o-ring to avoid water leaks. All of the joints and o-ring seals associated with the pile were pressure tested to 800kPa prior to pile installation. The pile tip load cell was calibrated as assembled to allow for any frictional losses that may occur due to the o-ring seals. These seals may have offered different resistance at different rates of pile testing but calibration at rates up to 500mm/s, with correspondingly small deflections, was considered impractical.

The pile tip also included a Kulite pore pressure transducer, located in the tip faceplate. In front of the transducer-sensing element was a silicon fluid (Dow Corning, 200/20cS) filled void that was separated from the clay bed by a silicon fluid saturated, sintered stainless steel porous filter element (6mm diameter, 3mm thick, 40μm max. pore size). A vacuum was applied to the filter elements immersed in de-aired silicon oil for a minimum of 24 hours to allow saturation. Several different saturation fluids were tried prior to choosing silicon oil. These included Glycerine, de-ionised water as well as silicon fluid of different viscosities. The use of glycerine was dropped after the first bed due to the visible traces of bacteria associated with the filter elements and surrounding clay. Silicon oil was the preferred fluid as it has a density similar to water. It has been used in similar studies (Penumadu & Chameau, 1998) and is commercially used in cone penetration testing operations (CPT). It was also preferred as several authors suggest that silicon fluid saturated transducers may respond better after cavitation than would water (Bond *et al.*, 1991 and Lunne *et al.*, 1997). Where cavitation is often associated with rapid pile installation (Bond *et al.*, 1991). The silicon fluid used for this study had a kinematic viscosity approximately 17 times that of water, which compares with 20 to 30 times used by Bond *et al.* (1991). The use of this fluid rather than water may raise concerns about signal attenuation and response during high frequency loading. Lee (1990) showed that, for a similar transducer arrangement saturated with silicon fluid with a viscosity 20 times that of water, a loss of only 5% of measured pressure for a pressure fluctuation at 1kHz would occur. The phase lag for a fluid with a viscosity of

50 times that of water (50W) was reported as 26°. What was also of note was the significance of degree of saturation. If the saturation of the system was reduced to 50% with 50W fluid, the phase lag increased to 56° and the signal attenuation increased by 50%.

Additionally, the pile tip base plate had two 4mm diameter holes drilled through it which were connected to two nylon tubes (4mm ID) which extended through the pile length to the outside of the chamber. One of these tubes was filled with water whilst the other one was left empty. Both tubes could be sealed by a manually operated valve located outside of the pile. These tubes were designed predominantly for use during the pile installation phase, with the air filled tube providing an outlet for air trapped in advance of the pile. The second tube was rarely used but was provided as a flushing port in case of saturation concerns. In both cases, the hole in the pile tip base plate was sealed with a porous plastic bung.

The pile tip was also designed to incorporate a Kistler accelerometer that was fixed rigidly to the pile. This measured the pile's acceleration and allowed checking of the accelerations calculated from penetration measurements.

4.3.2 Pile skin friction sleeve

The skin friction sleeve (Figure 4.10a) measured the skin friction resistance over a 302mm length of the pile body. This section was designed to measure the skin friction over a known pile length, without influence from the components of the pile capacity, above or below the measuring zone. This was achieved by placing a strain gauged aluminium "Dumb bell" load cell outside the central structural cylinder of the pile. The central cylinder transferred the load developed below the skin friction zone up the pile. The aluminium load cell was designed to pass over this with clearance. The friction sleeve was bolted to the load cell without connection to the rest of the pile (Figure 4.10b). To compress the load cell, the skin friction sleeve was located such that the load cell was permanently in contact with the pile at its top. The lower load cell was identical to that above, but was free to move over the pile central shaft and within the friction sleeve (Figure 4.10a & 4.10b). This cell acted as a "Dummy" cell within the strain gauge bridge arrangement, which compensated for temperature change

(Vaughan, 1975). The skin friction load measuring arrangement was initially calibrated for a full-scale load of 5kN, but this was exceeded in the early tests so it was re-calibrated for a maximum of 12kN. The skin friction sleeve was sealed at both ends by o-rings as well as compressible rubber soil seals, which were designed to protect the movement gaps. Located directly above the skin friction sleeve was another pore pressure transducer similar to that placed in the pile tip. This unit was used to measure the local pore pressures at the pile-soil interface. The transducer was mounted 534mm above the pile tip.

4.3.3 Remaining pile components

The pile then extended as a hollow tube to the interface with the calibration chamber top and the outside. To minimise the frictional resistance to pile movement, a rolling Bellofram seal was incorporated similar to that used for sealing the cutting shoe piston in the triaxial phase (Figure 4.11). O-ring seals were not adopted, as it was felt that they would offer too much frictional resistance and potentially have varying resistance with pile penetration rate. The sealing boss for the Bellofram also incorporated an outlet for top drainage during consolidation after pile installation.

At the top of the pile was a simple connection between the pile and the actuator load cell. The pile was connected to the actuator by a U-shaped receiver with a pin connection. At the base of the actuator was a swivel ball eye type connection through which the pin was placed and locked in position. The U-shaped connector at its lower edge was screwed into a 40mm OD hollow stainless steel extender rod that in turn screwed into the pile. This rod acted as the exit point for the pile's instrumentation cabling and pipe work from within the pile. The simple eye-pin connection between the actuator load cell and the pile proved unsuitable, as it was very difficult to remove the pin at the end of the loading phase. The connection detail was revised such that the swivel eye-pin connection remained permanently fixed to the pile throughout the testing sequence. Connection was instead made by screwing a round 15mm thick stainless steel plate with a screw fixing machined on one face to the bottom of the actuator load cell (Figure 4.8). A similar plate was fixed to the top of the eye-pin connection with the two plates being brought together for loading and secured by eight M10 bolts.

4.3.4 Pile installation

It was initially intended to install the pile as soon after conversion from 1-D to triaxial consolidation to minimise the effects of installation through further consolidation. In two out of the four piled beds this was achieved in 6 days with average bed consolidation of 93-95% (Table 4.2). Unfortunately in the case of Bed 2, there was considerable delay between the change to triaxial consolidation and pile installation due to delays with equipment development. This resulted in the bed having a degree of consolidation of 99.3%. The degree of consolidation in Bed 5 was 88.7% but it is thought that this was due to a water leak (Section 4.2.6).

Prior to introducing the pile, the actuator loading frame minus the actuator was bolted to the top of the chamber (Figure 4.12). Next, the chamber top and side membrane pressures were slowly reduced to zero. The Bellofram "Top hat" was then de-pressurised, drained and removed followed by the piston. The sand within the piston cutter was carefully excavated down to the porous plastic membrane, which had been slightly penetrated by the piston cutter. The porous plastic visible within the piston cutter was then cut out to expose the clay bed. Pile installation proceeded by installing a thin walled (1.6mm) casing tube of 73.3mm ID through the hole in the top plate (Figure 4.12). Vertical guidance and depth control for the casing installation was provided by a guiding plate attached to the top of the casing that ran down the threaded mounting rods of the actuator loading frame.

Initially, the casing was held in contact with the top of the clay bed (Figure 4.13). A void was then excavated to approximately 90mm below the casing tip by means of an auger, 90mm long and 68mm diameter, lowered down the inside of the casing. Once the void had been excavated, the casing was advanced under manual pressure to support the void and the process repeated until the tip of the casing was coincident with the final required pile tip depth (Figure 4.13). During casing advance, it was occasionally noticed that thin trimmings would enter the casing but these were removed during auger withdrawal. During auger operations, it proved very difficult to remove the auger due to the clay-casing seal and resulting vacuum. To overcome this, the auger was modified with a tip that could be forced out prior to raising the auger. This then created airflow through the stem of the auger to balance the pressure either side of the auger. The base

of the excavation was inspected and then trimmed flat using a flat-headed cutter. Any material left after this operation was removed using a vacuum cleaner. A pre-measured volume of de-aired and de-ionised water was tremied to the base of the excavation in attempt to maintain saturation. The volume was chosen to reflect the annulus between the pile and the casing but, terminated below the top sand drainage layer to avoid wash out of the sand into the void between the pile and the clay. The pile was then carefully lowered into place using a block-and-tackle (Figure 4.12 & 4.13). This method of installation would cause minimal soil fabric and stress field disturbance during the casing installation stage. Relatively large disturbance to the existing stress field would be caused by the closure of the void around the pile during horizontal stress application (Chandler & Martins, 1982). Further consolidation post pile installation would serve to minimise the effects on pile testing.

Before pile installation, the pore water pressure measuring devices within the pile were assembled with de-aired components having remained under vacuum. As the pile was lowered into position, the valve for the air-filled tip flushing tube was left open to allow any air in advance of the pile to escape. This valve was then closed when the pile was in position. The casing was then gradually removed using two manually operated scissor jacks mounted between the actuator loading frame and the casing guiding plate. The resistance to casing extraction was proof that minimal over-break had occurred during excavation.

Once the pile was in place, the rolling Bellofram seal attached to the pile was clamped down along with the Bellofram sealing boss. The pile was then restrained vertically with an aluminium clamp around the pile extender rod, which was seated on top of the Bellofram sealing boss. Vertical positioning of the pile was chosen such that the top of the Bellofram sealing ring on the pile was level with the top of the Bellofram sealing boss or slightly lower (Figure 4.11). This allowed the maximum Bellofram travel of 120mm to be achieved. The pressure was gradually re-applied to the bed and consolidation allowed to continue.

4.3.5 Pile instrumentation

The instrumentation within the pile was briefly described in Section 4.3.1 & 4.3.2. Further details are given here.

The resistance to pile penetration at the tip was measured by a miniature Entran load cell (ELHS-T4M-25kN/Z1/L5M). This unit had a specified maximum deflection of 0.012mm at maximum load (±25kN) which is equivalent to δ_{cell}/D_{cell} =1/5833, based upon a 70mm diameter pile tip (Figure 4.9). The unit was 25mm high and 25mm in diameter. The construction included 25mm long M16 threaded attachments at both ends of the load cell. This made the unit simpler to incorporate in the pile. The unit also had the added advantage of having a relatively high full-scale output of 200mV.

The pile also contained two Kulite XT-123C-190-7-BAR-A miniature pore pressure transducers (Figure 4.9 & 4.10). These units were 15.5mm long and 9.5mm in diameter. To allow ease of mounting and saturation, a standard mounting detail was used for both transducers. Further description of these units is given in Section 4.2.8.

Where required a Kistler 8704B50 piezoelectric accelerometer was incorporated in the pile above the tip load cell. This was identical to the unit mentioned in Section 4.2.8.

Electrical resistance strain gauges were applied to the aluminium "Dumb bell" load cells in the skin friction measuring region of the pile (Figure 4.10). The aluminium load cells were 127mm in length with a central measuring zone of 57mm. The wall thickness in the region of strain gauge application was 3mm. This geometry resulted in a length to external diameter ratio of 3.1 that was considered adequate to minimise end effects (Hanna, 1973). It would have been better to have had reduced length load cells such that the skin friction could have been measured over a smaller area. The separation of end bearing skin friction measurements resulted in load cell diameter being dictated by the internal structure of the pile. Shorter load cells could have been used but these would have become susceptible to end effects. The load cells were fabricated from aluminium due to its Young's modulus being lower than a steel alternative. This resulted in higher strain gauge outputs than would be achieved with steel.

Four strain gauges were applied diametrically around each load cell to remove bending strain effects. The gauges used were 120Ω Kyowa KFG type (KFG-30-120-C1-23) with temperature compensation for aluminium. The units were wired in a full Wheatstone

Bridge arrangement using an excitation of 5v rather than 10v to increase the life of the gauges. The gauges were fixed to the load cells using Kyowa PC-6 thermosetting phenolic adhesive, chosen for its long-term stability. The use of this adhesive required the gauges to be pressure clamped to the load cells and baked at successively higher temperatures for several hours. To aid protection and minimise moisture take up the gauges were then coated with Measurements Group's M Coat A air-drying polyurethane. On top of this coating was painted a layer of hot Kyowa C-4 moisture proofing wax.

4.3.6 Model pile performance during installation and consolidation

Generally the pile performed well throughout testing with minimal modifications and redesign required during the project. Where modifications were required, they centred on the pile tip load cell and the skin friction zone.

Due to the design of the Entran tip load cell it, was not advisable to apply any torque to the device during pile construction. This made detailing of the connection within the pile tip difficult. Initially the unit was fixed by threading it into the tip of the pile with locking nuts to maintain the correct position of the pile tip. These locking nuts had a tendency to come loose even when grub screw locking pins were added. The final solution was to make up two cylinder spacers that the load cell could be screwed up against, with their lengths chosen to maintain the pile tip load cell in the correct position. This modification worked well but there was a tendency for the arrangement to tighten up during loading. This problem also occurred at several of the joints throughout the pile.

The interface between the pile and the top of the skin friction "Dumb bell" load cell was modified during the testing programme by introducing two locating pins fixed on top of the load cell. These were incorporated to stop the load cell rotating during pile handling and tightening of the sections, which could result in damage of the instrumentation cabling. Unfortunately, this occurred just prior to installation in one of the test beds resulting in the wiring being severed to the load cell.

As for the pile tip, o-ring seals were used throughout the pile and in particular at the seals for movement of the pile tip and skin friction sleeves. These seals may have given variable resistance to movement and their behaviour may have changed with varying rate of pile testing. The effect of this was not assessed due to the high velocities involved, and the very small movements of the components of the measuring devices.

4.3.7 Servo-hydraulic loading system

To apply the required loading patterns to the pile, a servo-hydraulic loading system was used. The system was arranged as shown in Figures 4.8, 4.14 & 4.15. The system centred around a Kelsey 50/36 TestLab unequal area servo actuator capable of applying loads of 41.4kN statically and 27.3kN dynamically with a total stroke of 150mm. Oil flow to the actuator was provided by a mobile LOS Series 60 hydraulic power pack capable of oil flows of 20l/min at 210 bar. A servo valve rated for oil flows up to 70l/min was used to control flow supply from the pump to the actuator. To aid response of the system both the pressure and return hydraulic flow lines were fitted with accumulators (Figure 4.8 & 4.15). At the tip of the actuator rod (36mm diameter), a 41.4kN fatigue rated load cell (Type T5139N423) sat between the pile and the actuator during testing. The load cell was used to measure the total resistance of the pile as well as acting as a feedback signal during load control tests. The actuator also incorporated an internal 150mm stroke linear displacement transducer (LVDT) that was used to provide a feedback signal during displacement-controlled tests. The actuator system was controlled by a Kelsey K7500 digital servo-controller, which allowed closed loop control of the pile loading. This unit also provided excitation and signal conditioning for the actuator load cell and LVDT. Signals from both of these two sources were then available as output from the unit for logging purposes. Additionally, the controller was capable of receiving an external 0 to 10v DC input command for driving the unit.

The actuator, and key components including the accumulators, were mounted on a 40mm thick cross head plate that incorporated a lifting eye in its top face. This was used to quickly add or remove the actuator system when required and aided resetting the height of the actuator (Figure 4.8 & 4.15). The actuator assembly was supported by a specially designed loading frame bolted to the chamber top end plate. The frame consisted of two rectangular hollow sections (RHS celcius 90x50x6.3), spaced 382mm apart and connected by a 25mm thick plate (410mm square) welded between the two

sections. Mounted at each corner of the plate were four high tensile 38mm diameter smooth rods that were externally threaded at the ends. These threaded rods were used to locate the actuator crosshead plate and manually adjust the position of the actuator above the pile. The plate between the two RHS sections was bolted to the chamber top end plate around the bellofram sealing boss. Two additional plates, welded across the ends of the sections, were bolted through the normal end plate bolting positions.

Although the travel of the actuator (150mm) exceeded that of the pile (≈120mm), the actuator crosshead required lowering halfway through pile testing. This was because the actuator was initially set with a gap between itself and the pile connection. This precaution was taken as the actuator had a tendency to creep down towards the pile when the system was switched off resulting in the actuator being in contact with the pile prior to commencing testing. The tendency of the actuator to jerk slightly on start up meant that this contact was not ideal. At all stages when the pile was not in contact with the actuator, it remained vertically restrained to avoid any accidental loading. Due to the crosshead re-set and slight vertical movement of the pile between tests, the internal actuator LVDT was not considered suitable for monitoring the absolute pile position throughout testing. To keep track of the pile's position, manual distance readings were made between a reference point on the pile relative to the pile Bellofram sealing boss. The measurements were made using a Mitutoyo 100mm digital vernier calliper.

As penetration during pile loading was limited generally to 15mm and in exceptional circumstances to 30mm, the 150mm long LVDT incorporated within the actuator was considered too long for measuring the pile's penetration. There were also concerns about how load cell and connection detail compression would affect the pile top penetration measurements. To remove the uncertainty, a MPE LVDT was mounted rigidly on an arm, clamped to the pile extender rod. Measurements of penetration were then made relative to the connection plate between the two RHS sections of the loading frame. Two LVDTs were used; either 20mm or 50mm stroke depending on the length of the pile test. The 50mm LVDT was calibrated and conditioned to give a full-scale output at 40mm.

4.4 Equipment calibration

The summary in Appendix 2 shows the instruments calibrated and the piece of standard equipment used. Calibration of the Kistler accelerometers was not undertaken in house, as this requires specialist equipment. Results from calibration were logged by LabVIEW and transferred to Microsoft Excel where linear regression was undertaken. The calibration constants generated were then fed into LabVIEW for test logging in engineering units. Calibration was undertaken regularly at six-month intervals and additionally when equipment had been stripped down and/or repaired.

In all cases, the instrumentation was connected to the PC logging system using the same arrangement adopted during consolidation and testing. To avoid errors due to different wiring lengths and types, all cables were assigned to the same transducer throughout the project. These in turn were connected to the same channel for excitation and signal conditioning.

To improve the resolution of the instrumentation readings during testing, the transducer outputs were amplified to give 10v outputs at the full scale levels anticipated during testing. For instance, a bed pore pressure transducer would be amplified to give a 10v output at 300kPa rather than at 700kPa, which was the normal maximum operating range for the unit. The unit would then be calibrated using the amplified outputs.

Both the pile tip load cell and the skin friction sleeve arrangements were calibrated when assembled ready for testing. Both the assembled pile tip and the skin friction section were calibrated against a 15kN proving ring (PR4873) with load applied by an Amsler 100kN universal testing machine. Specially fabricated aluminium mounting pieces were made to aid mounting of the sections.

4.5 Logging and control systems

4.5.1 Signal conditioning

To acquire data from the different transducers and output channels previously discussed, a PC based computer logging system was used (Figure 4.14). Conditioning of the majority of the output signals from the various instruments was required prior to

logging. For the pressure transducers and pile outputs, this was done within the Fylde Micro Analog 2 (MA40) unit (Fylde, 1999). The unit was mounted with nine FE-366-TA DC conditioning cards and one FE-H366-TA card. This gave the capability to condition and excite twenty individual channels. Separate mention is made of the FE-H366-TA card as this was a high-speed version of the standard amplifier and was capable of 100kHz response at all gain levels. The fast card was designed for conditioning the strain gauge output signals as these were amplified by up to 5000 times to produce signals with full scale outputs of 10v. The gains attainable from the cards were up to 5000 in preset steps (jumper set) plus an additional 2.5 times (vernier set). Power supply for the transducers was also provided by the cards fixed at either 5v or 10v per card. The combined outputs from the different transducers were then output from the Fylde via a multi-core cable. One additional benefit of using the Fylde system was that it converted the two differential input lead signals into single ended outputs referenced to one common point. Whereas the differential outputs require two channels to be read by the data acquisition board, the single ended only require one channel and a reference connection. This resulted in only half of the available logging channels being required.

A similar function was undertaken by the Kistler power supply/coupler for the Kistler accelerometers. This unit was capable of accepting the output from up to four accelerometers (Kistler, 1997). Outputs from the Kelsey K7500 servo-controller were internally conditioned and required no further treatment. Voltage outputs from both this unit, the Kistler and the Fylde were then passed to the PC for logging via a purpose built interface unit. This unit was also designed to output drive signals created by the PC output channels.

One of the reasons the relatively small signals produced by the transducers were amplified was to aid high-speed logging. As the data acquisition card (DAQ card) logs, a scan is made of the channels being sampled. The maximum scanning rate is mainly defined by the number of channels to be logged but, the rate may be reduced by the magnitude of the signals on each channel. If one channel outputs a low millivolt signal and the adjacent one outputs 10v, the logging/switching time between the channels will be greater than if both channels were of a similar voltage magnitude. In extreme cases, this may result in the actual scanning rate varying from the required rate.

4.5.2 Data acquisition and control

Data acquisition of the signals from all the transducers was carried out by a PC fitted with a National Instruments PCI-6071E DAQ card. The card was capable of accepting 64 single ended or 32 differential channel inputs, sampling at 1.25 Msamples/sec with 12-bit resolution (National Instruments, 1999). The DAQ card also included two analogue output channels of 12-bit resolution. The unit was limited to 12-bit due to the high logging rates and number of channels required.

Control of the data acquisition was carried out using National Instruments LabVIEW software Version 5.1.1 (Base Package) that allowed the development of bespoke programs. In this study, two different programs were designed to suit the different types of loading applied to the pile along with programs for logging calibration and consolidation.

Briefly, the first type of test was a constant rate of penetration (CRP) test as discussed in Section 2.2.1 which was carried out at different rates up to 400mm/s. Control of the actuator movement during these tests was undertaken by the Kelsey K7500 controller in displacement mode. The function of the PC during this type of test was to log the outputs from the various channels during the test and for some pre-defined period after. A flowchart describing the logging program used can be seen in Figure 4.16. As the loading stage and the post-load consolidation phase had varying durations, the program was designed in two parts. It was not considered practical to manually switch from one type to the other so this operation was achieved by monitoring the pile LVDT position. Once this had reached a position corresponding to the known test end penetration, the software changed to slow logging.

The second type of test was a Statnamic (STN) type load pulse as described in Section 2.2.4. During this test, the Kelsey K7500 controller acted in load control with command signals generated in LabVIEW and fed to the Kelsey via one of the DAQ card analogue output channels. The command signal was produced by simply inputting user-defined coordinates, which specified the turning points of the load pulse. After generating the STN command pulse, the program waited for a triggering signal from the Kelsey K7500 controller before continuing. The triggering signal was generated by the

closure of a relay within the Kelsey that was automatically operated when the test start button was pressed. The power for the triggering signal was provided by fixing one of the monitor outputs from the Kelsey at its 10v calibration output. The actual rise in triggering signal was logged at the DAQ card on a channel defined as a triggering channel. LabVIEW continued with the program once a rising voltage reached a certain pre-set voltage on the trigger channel. The STN command pulse was then fed to the Kelsey K7500 controller external command input channel as a DC voltage from one of the DAQ cards analogue output channels, and synchronised acquisition occurred. The command signal lasted for approximately 180msecs but high-speed logging was allowed to continue for 20 seconds. High-speed acquisition stopped when all the data filled a preset buffer size. At this stage the data contained in the acquisition buffer was written to the hard drive and the results displayed (Figure 4.17). This differed from the CRP logging program that wrote information to disk throughout the logging operation. The reason for writing and displaying after the fast acquisition was that both of the operations are relatively slow and would interrupt the high speed logging process. Again, at the end of fast logging, the program automatically started slow logging to monitor post-test bed consolidation.

In both cases, the data was written to text files. The channel information was separated by commas so that the data could be easily imported into Microsoft Excel for processing.

4.6 Pile testing procedure

Immediately prior to pile testing, a record was made of all of the pile and clay bed instrumentation values. Slow consolidation type logging was then stopped and the appropriate logging program loaded for the test to be undertaken. The logging/control software was run several times to confirm that it was operating satisfactorily and the data was being written to text files. This was undertaken at the logging rate and write to buffer rate to be used in the test.

The initial pile position was then measured manually relative to the top of the Bellofram sealing boss and the pile LVDT reset. The limits of both load and penetration were entered in the Kelsey unit. In the case of the CRP test, the test target penetration was input and the time required to reach maximum penetration. The pile penetration at the

end of the test was entered in the software to allow switching from fast to slow logging. The hydraulic pump was started in low pressure then brought to high pressure. Throughout this, the manual oil dump valve on the pump was set such that no pressure was applied to the actuator system, although both the pump and the Kelsey were operating as if high pressure was applied. The dump valve was then slowly adjusted to close to the rated pressure of the hydraulic hoses. This operation was undertaken because there was a tendency for the actuator to jump if the oil pressure was maintained during switching pressures. This could have resulted in accidental loading of the pile. The actuator was then brought slowly into contact with the pile and connected. To aid operation a manual inching pendant, fitted to the Kelsey meant that it was possible to control the position of the actuator without standing at the Kelsey unit.

Throughout the CRP test, the Kelsey was in displacement control mode with manual actuator movements made using the set point function. Prior to removing the pile clamp, the load applied to the pile was checked. The set point was then altered until the load was close to zero. At this point the pile clamp was removed and the system gains increased to test levels. As the gains were increased, the pile moved to close the gap to the set point position. This could have resulted in considerable load on the pile. To avoid this the gains were increased gradually and the set point adjusted in reaction to the pile's movements. The start button was then pressed on the Kelsey and the test left to run, logging was started immediately before this. Further description of the procedure for pile testing is included in Appendix 2.

On completion of the CRP test, the gains were slowly reduced to pre-test levels and loading plate between the pile and the actuator was quickly undone. Reduction of the gains was required prior to disconnection due to the sudden change in stiffness of the system. This was done quickly as, at the end of the test the actuator returned to its pre-test absolute position, which would result in pulling of the pile. This need for the actuator to return to its pre-test load or displacement is a standard safety feature of the Kelsey controller. This feature can also prove a limitation and disruptive to the required test profile (Vega, 2001). It would be better if, at the maximum penetration during a CRP test, the Kelsey controller could be changed to load control and then the load reduced to a small value in a controlled manner. With the present mode of operation, a relatively high load is maintained for a short period at the end of the test. To allow time

for disconnecting the actuator, a large time delay was set in the static fade out which controlled the time taken for the actuator to return to the set point. The actuator was then withdrawn to its upper limit and the pile re-clamped. The final position of the pile was recorded and logging (1 second intervals) left to continue for approximately three hours. At this stage the data was recovered from the PC and logging re-started at 5 minute intervals until the next test. Typically, a minimum of period of 24 hours was left between tests to allow bed pore pressures to return to their pre-test levels.

For a Statnamic type test a similar procedure was adopted to bring the pile into contact. Rather than adjusting the pile displacement to give zero load it was left with a small compressive load and the Kelsey placed in load control mode. Care had to be taken that the set point at this stage had a small compressive load rather than zero load, as the system could not achieve zero load. Again, the load gains were slowly brought to the test levels with corresponding adjustment of the set point. The logging software was started and a graph showing the load pulse to be applied to the pile displayed. At this point the start button was pressed on the Kelsey. The stop button was not pressed on the Kelsey until the 20 second post test logging period had been completed and the system outputs displayed on the PC screen. The stop button was then pressed and the Kelsey returned to displacement mode. The pile could then be disconnected and a similar procedure followed as for CRP. As the Kelsey was returned to a low gain displacement mode at the end of Statnamic testing there was no need to reduce the load gains. It was necessary to reduce these to just above unity prior to carrying out another test.

After testing was complete, the pump was shut down in reverse order to the start up procedures. This was because the hydraulic lines had a tendency to jump violently if the pump was switched directly from high to low pressure rather than gradual reduction at the pump dump valve. This was probably due to accumulator input to the system trying to accommodate a sudden pressure drop. To minimise risk from this event, the hydraulic lines between the pump and the actuator were restrained wherever possible.

4.7 Bed dismantling

4.7.1 Chamber deactivation

On completion of testing the drainage valves were closed to the top and bottom of the bed and the confining pressure reduced to zero. The actuator and loading frame was then removed. The remaining components of the chamber were then removed with the clay bed containing the pile left standing on the chamber base plate. The exposed bed was then wrapped in plastic sheeting to limit drying of the clay.

4.7.2 Bed dismantling and sampling regime

After completion of testing each clay bed was carefully dissected to allow exposure of the embedded transducers, material sampling and final measurements. The bed was slowly excavated to expose each individual transducer and to record the final position of the transducers relative to the pile and the chamber base plate. Although the position of the transducers was controlled prior to filling the consolidometer with slurry, it was found that their final positions did vary from their initial.

Sampling of the clay bed was undertaken for the determination of moisture content and shear strength. Samples for moisture content determination were usually taken at 100mm vertical intervals and at the pile-soil interface as well as 85, 150 and 275mm from the pile. Samples for moisture content were taken at closer vertical intervals of 20mm under the pile for up to 80mm from the pile tip. Additional radial samples at 20, 40 and 60mm from the pile were also taken at these heights.

Samples were taken for triaxial shear strength determination with thin walled sample tubes manually pushed into the sample. The sample tubes were installed at the same radial distances from the pile as used for the moisture content determination. Vertical and inclined 100mm diameter samples were also taken by Balderas-Meca (2004) for use in triaxial rate effect testing and one dimensional consolidation tests. To advance these larger sample tubes, a weight was lowered onto the tubes by an overhead gantry crane. To minimise disturbance and aid installation the external surfaces of the sample tubes were smeared with silicon grease prior to installation. The ends of the sample tubes were sealed with wax immediately after excavation and then sealed in plastic bags.

As well as sampling, in-situ determinations of shear strength were also undertaken with a large Pilcon hand shear vane and in the final bed with a small hand vane (Torvane). The large vane was manually driven 100mm into the sample at the same radial distances as the moisture content determinations. Determining shear strength closer to the pile was not possible due to the diameter of the Pilcon vane's reading dial. A small hand vane (Torvane) was obtained for the final bed and used to measure shear strength on the surface of the exposed clay. This device was predominantly used under the pile tip.

The final measurement taken in the bed was the position of the pile tip at the end of testing relative to the chamber base plate. This measurement was used to back check the embedded length of the pile for the cumulative pile testing.

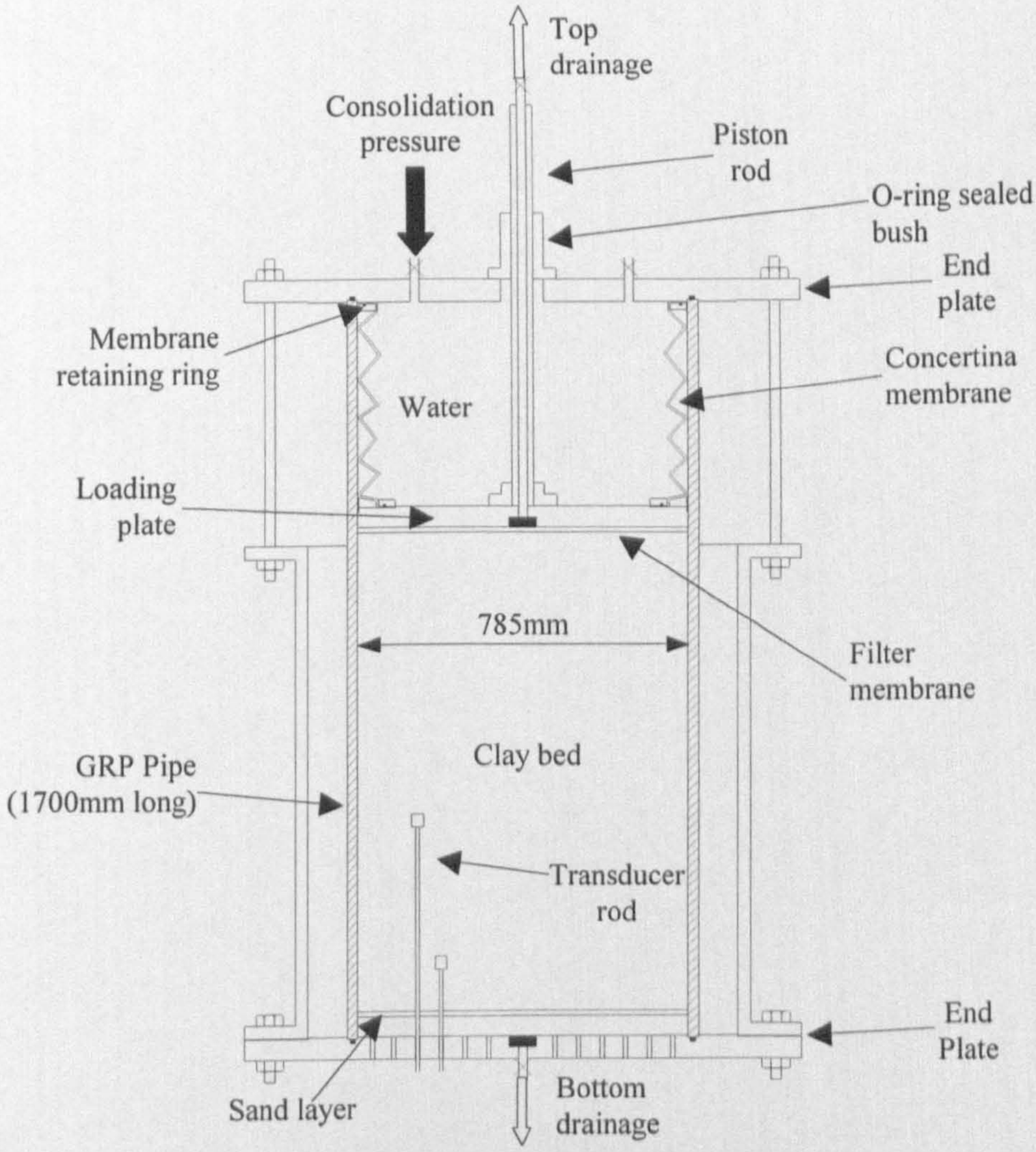

Figure 4.1, Calibration chamber consolidometer.

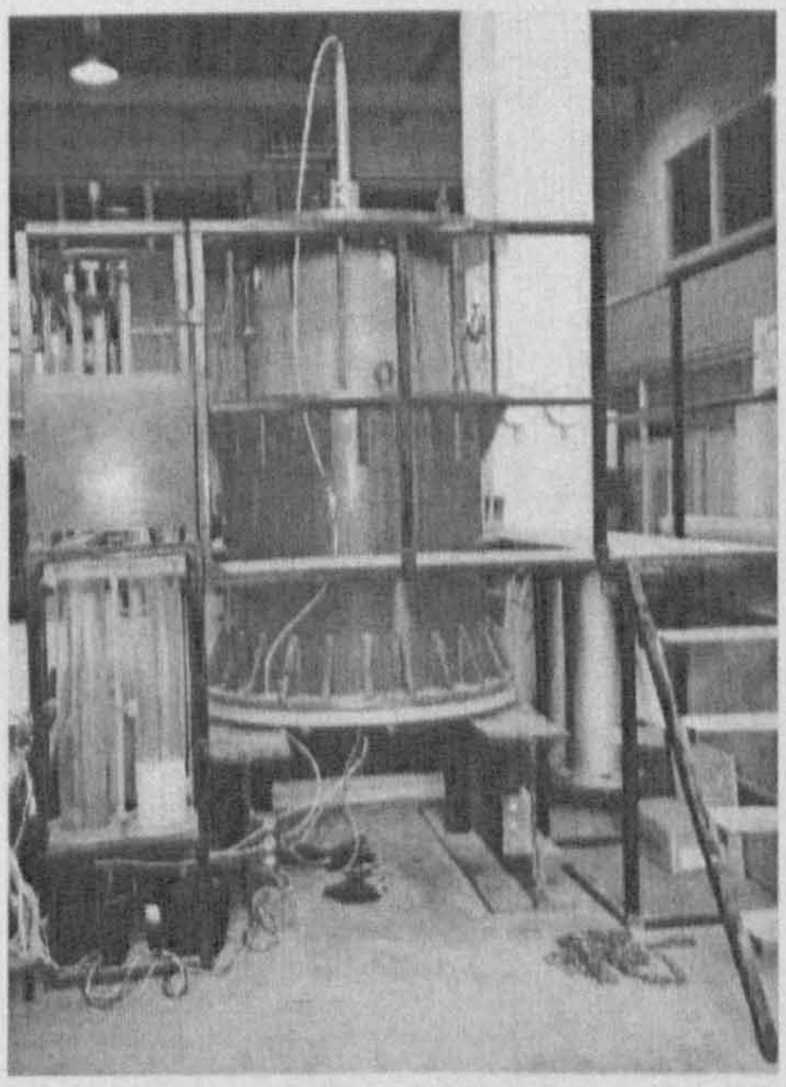

Figure 4.2, Calibration chamber in consolidometer mode shown in the laboratory.

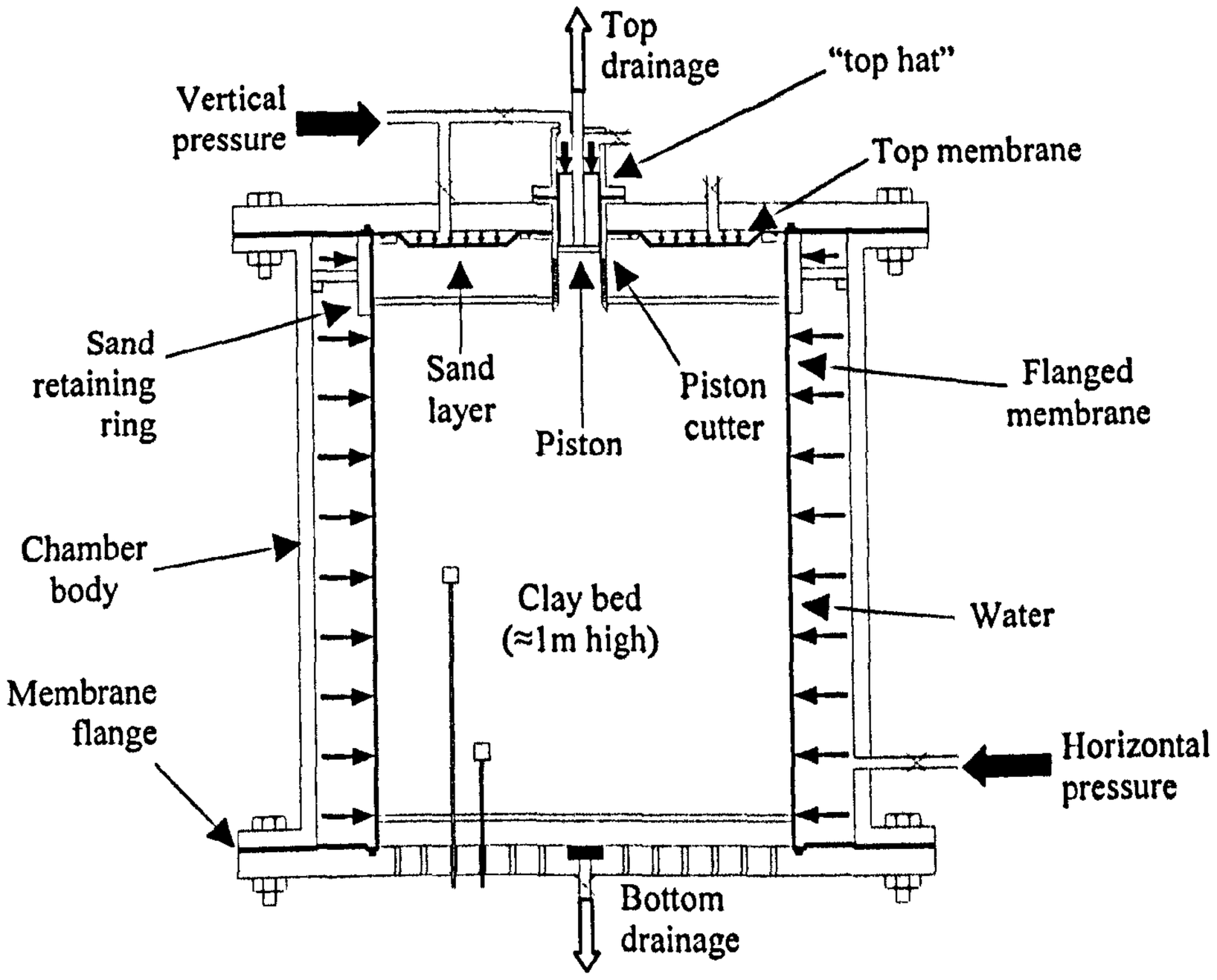

Figure 4.3, Calibration chamber in triaxial mode.

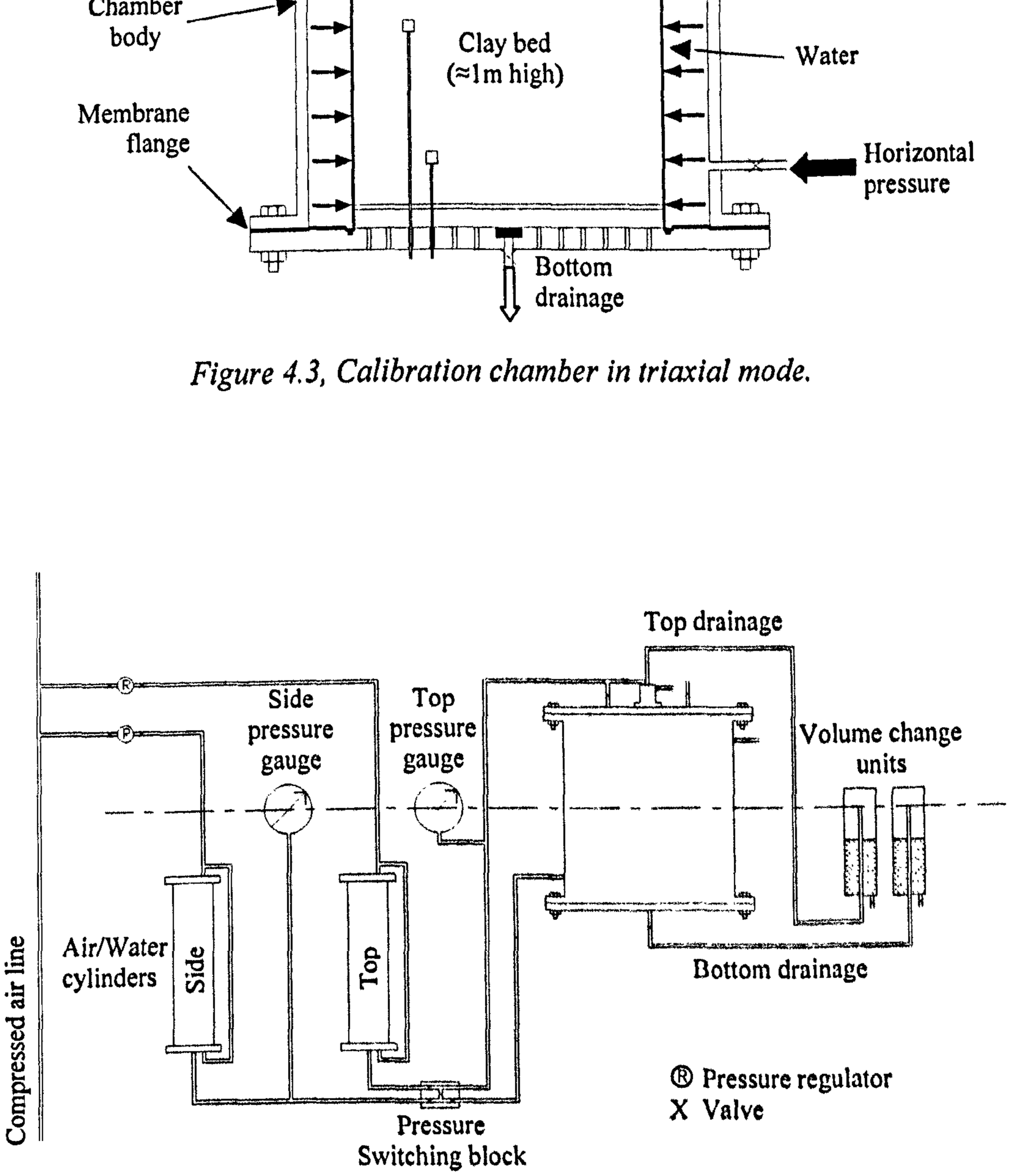

Figure 4.4, Pressure supply and drainage arrangement for the calibration chamber.

Property	*Symbol*	*Value*
Liquid limit	w_L	37%
Plastic limit	w_P	17%
Plasticity index	I_P	20%
Specific gravity of solids	G_s	2.64
Clay fraction (%<2μm)	*CF*	38%
Activity	*A*	0.53
Coefficient of vertical permeability in terms of void ratio (e)	k_v	$6.32e^{3.31}x10^{-9}ms^{-1}$
Slope of consolidation line	λ	0.10
Slope of swelling line	κ	0.03
Slope of critical state line	M	1.05 $\phi'=26.5^{o}$

Table 4.1, Summary of strength and mechanical properties for the KSS material.

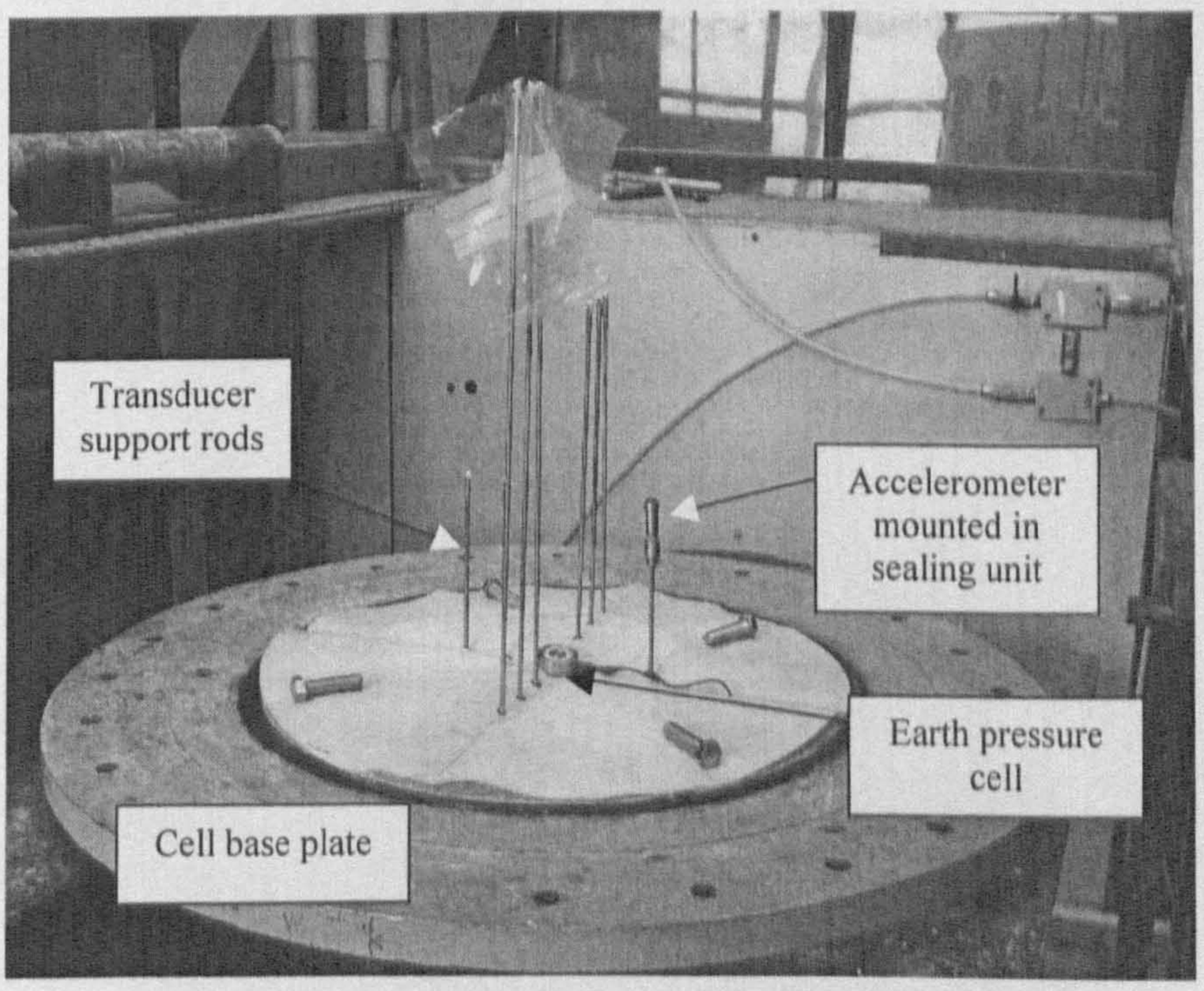

Figure 4.5, Base plate preparation and transducer mounting for K_0 consolidation.

	Test Stage					
	Termination of 1-D Consolidation		*Pile Installation (Triaxial)*		*Commence Pile Testing (Triaxial)*	
Test Bed	*Effective Stress (kPa)*	*% Consolidation*	*Effective Stress (kPa)*	*% Consolidation*	*Effective Stress (kPa)*	*% Consolidation*
2	116	41.4	278	99.3	277	98.9
3	120	42.9	267	95.4	268	95.7
4	222	79.3	260	92.9	261	93.2
5	171	60.9	249	88.7	236	84.3

Table 4.2, Summary of bed stress and consolidation states during chamber operations.

Test Bed	*Average Undrained Shear Strength (c_u, kPa)*			*Average Water Content (%)*
	Pilcon Shear Vane		*Triaxial Compression*	
	Peak	*Residual*		
2	46 (2)*		52 (2)	22.6 (1.0)
3	46 (3)	29 (2)		24.0 (1.7)
4	53 (5)	29 (3)	55 (9)	24.8 (1.1)
5	59 (6)	31 (2)		23.4 (2.1)

** Values shown in parenthesis() denote standard deviation.*

Table 4.3, Comparison of shear strength and moisture content determination between different beds.

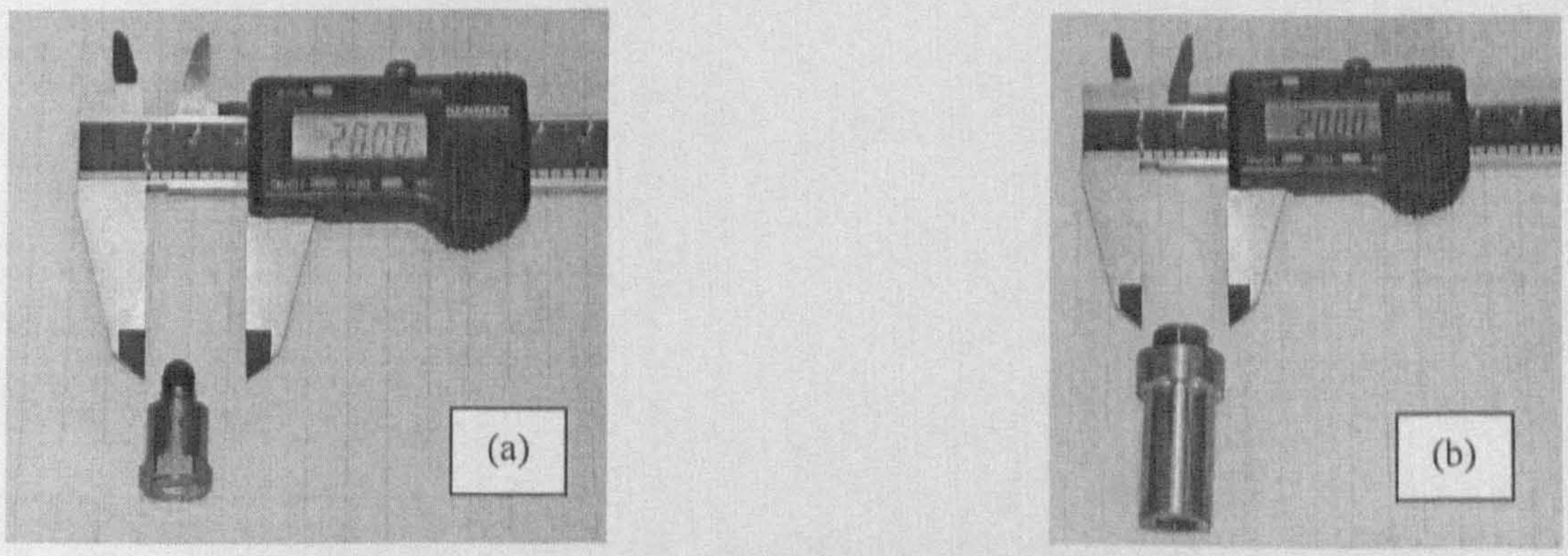

Figure 4.6, (a) Kistler accelerometer as installed in the pile, (b) Accelerometer with stainless steel sealing detail for bed installation.

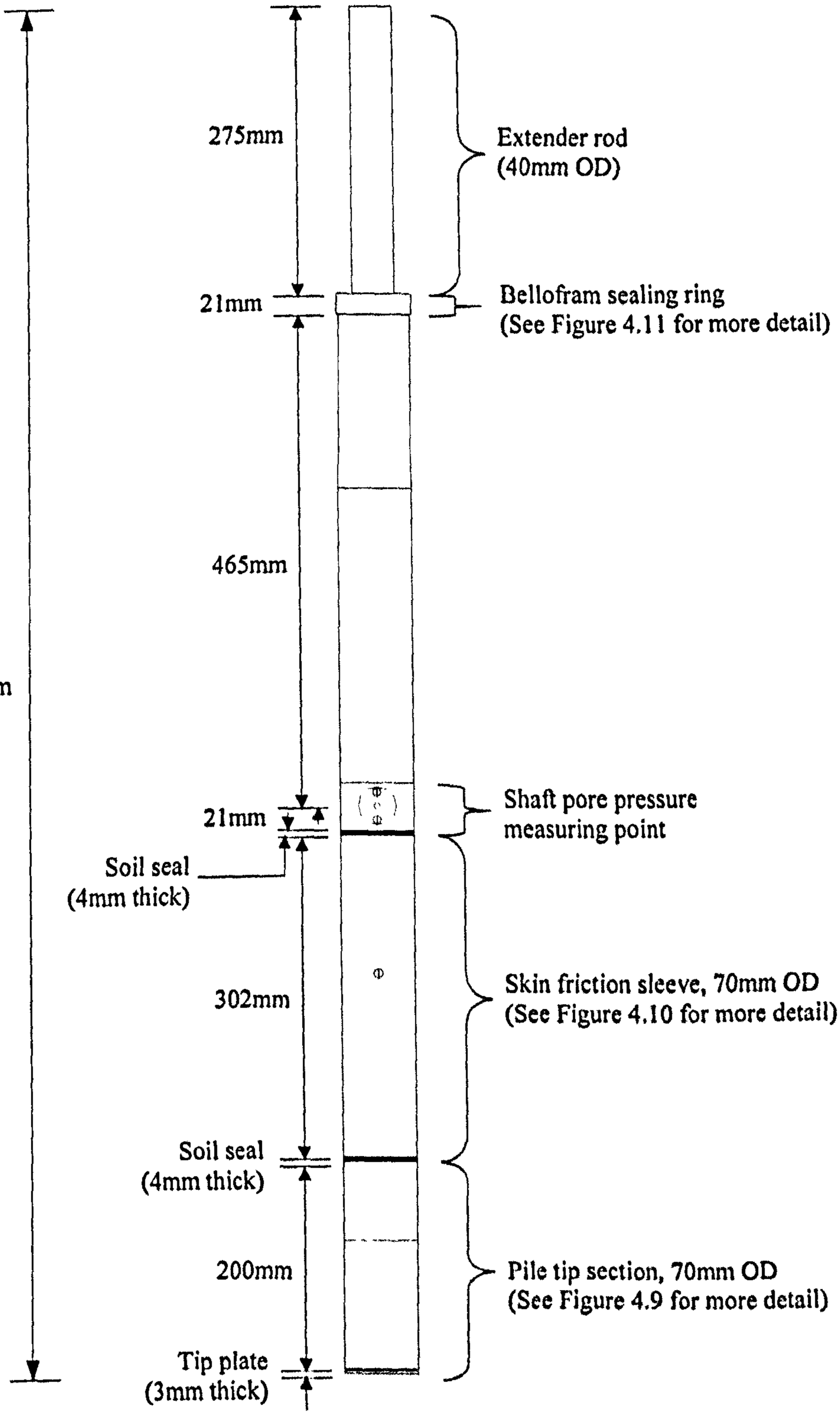

Figure 4.7, General arrangement of the model pile.

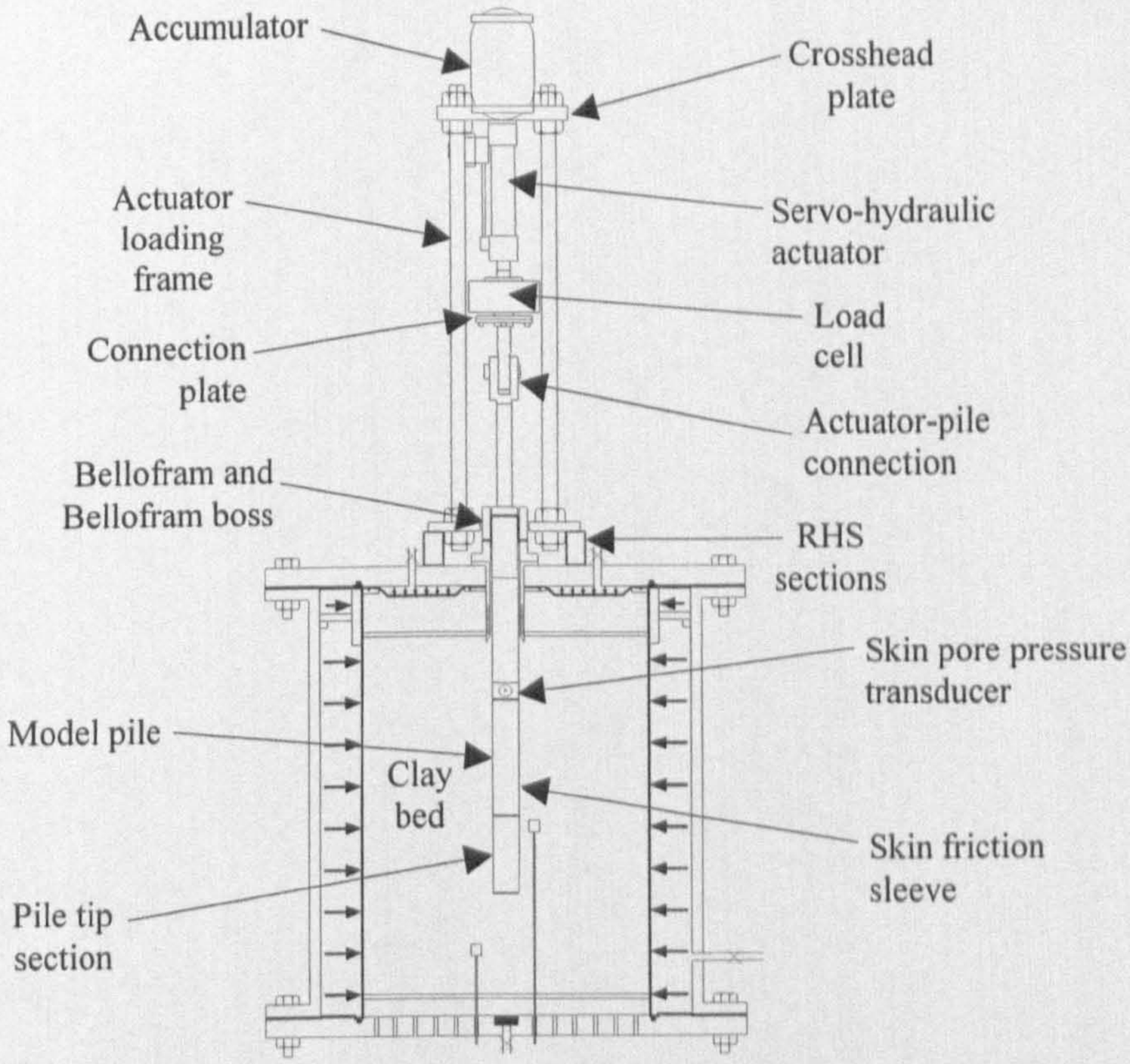

Figure 4.8, Calibration chamber in pile testing mode.

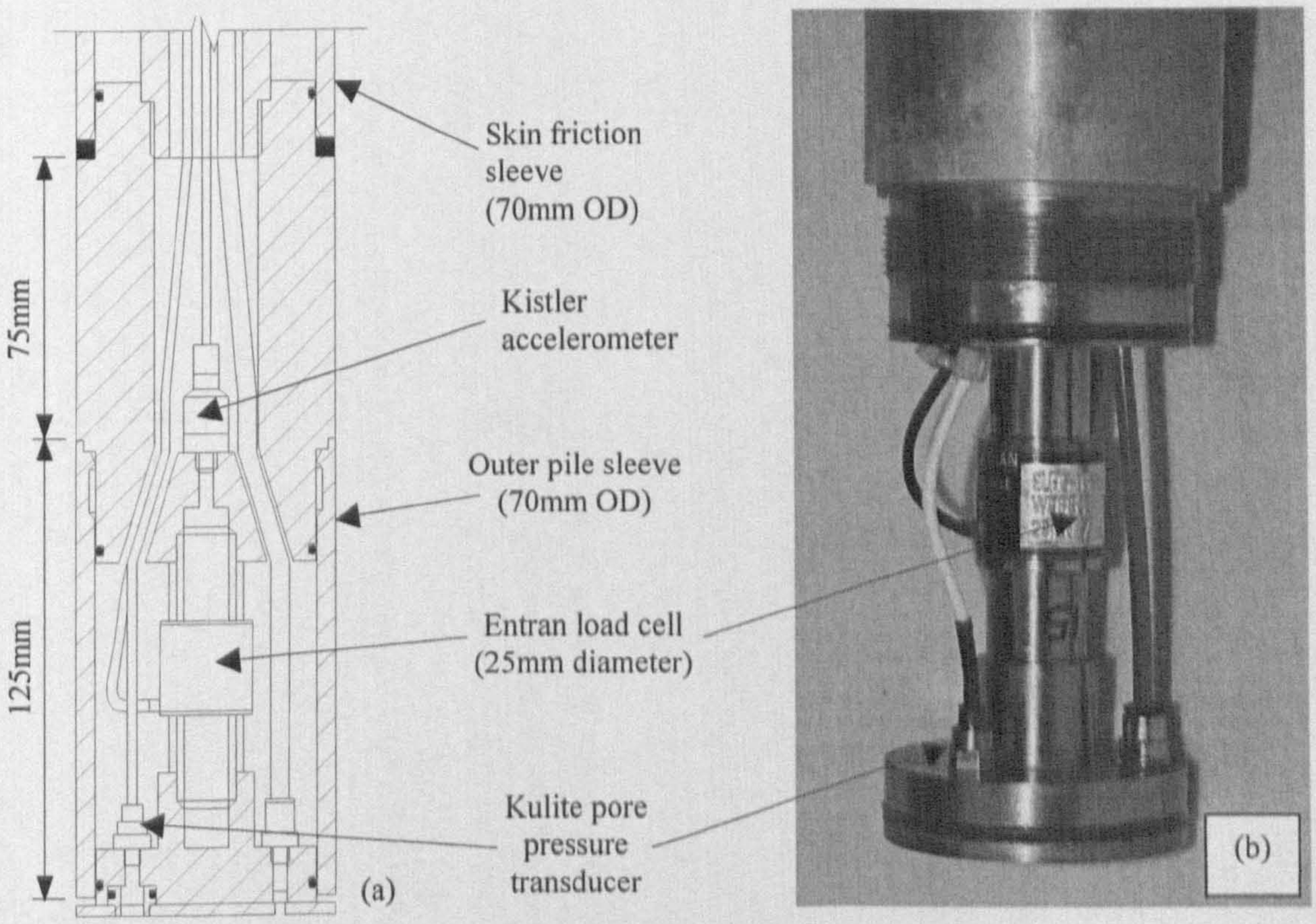

Figure 4.9, (a) Pile tip detailed cross-section, (b) Pile tip with outer sleeve removed

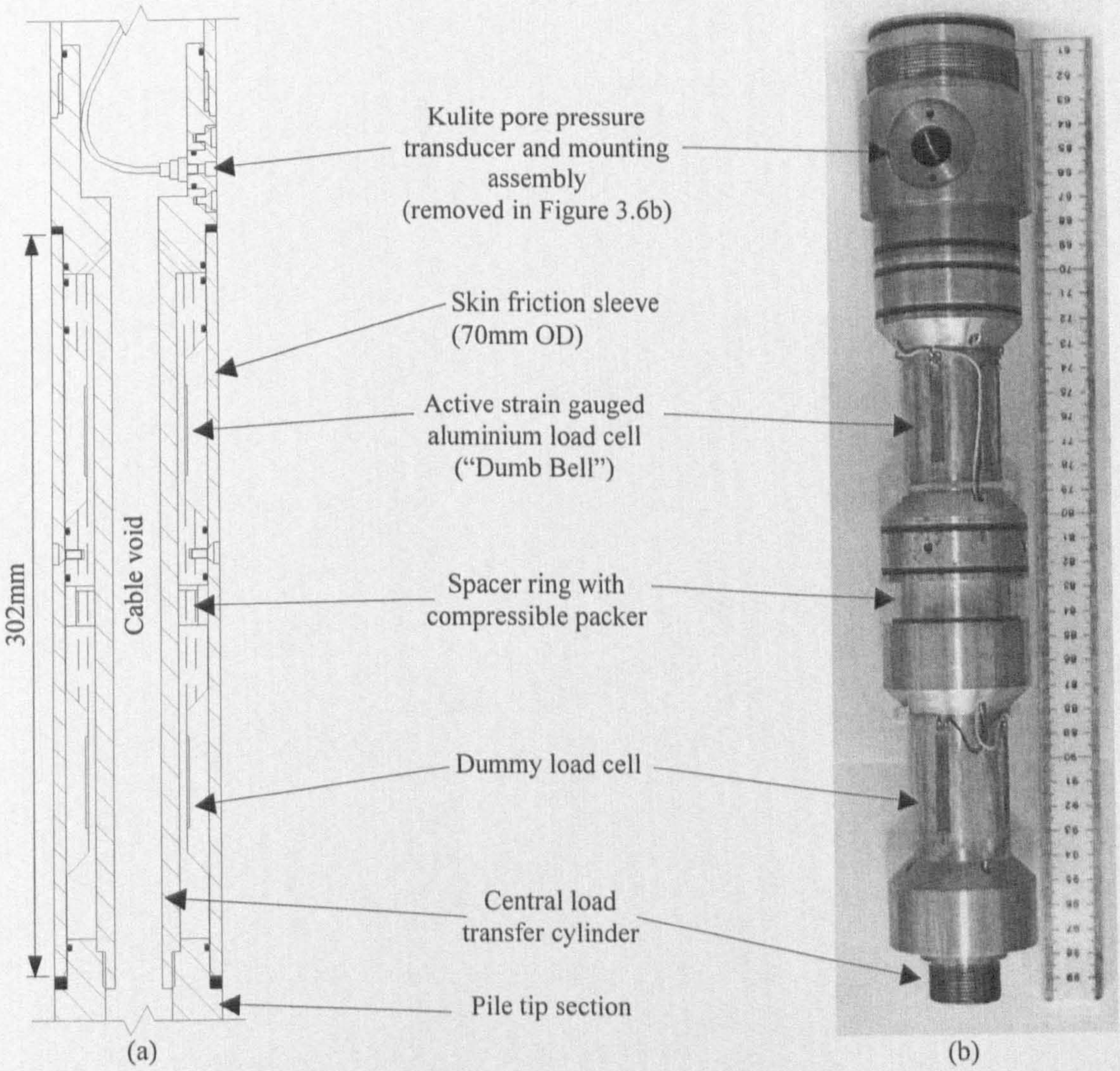

Figure 4.10, (a) Pile skin friction section, (b) Pile skin friction section with outer sleeve removed.

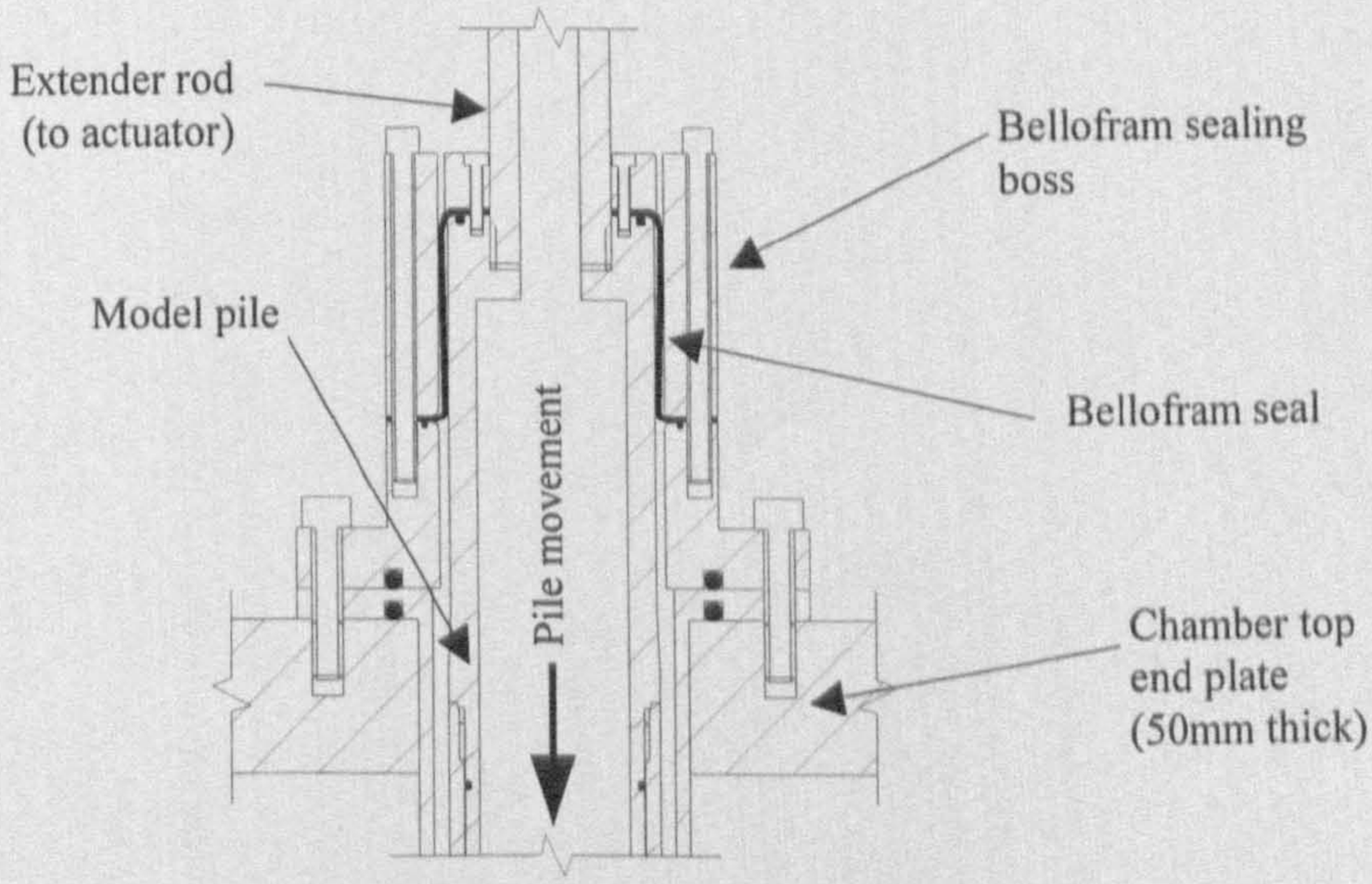

Figure 4.11, Section through pile-Bellofram sealing detail.

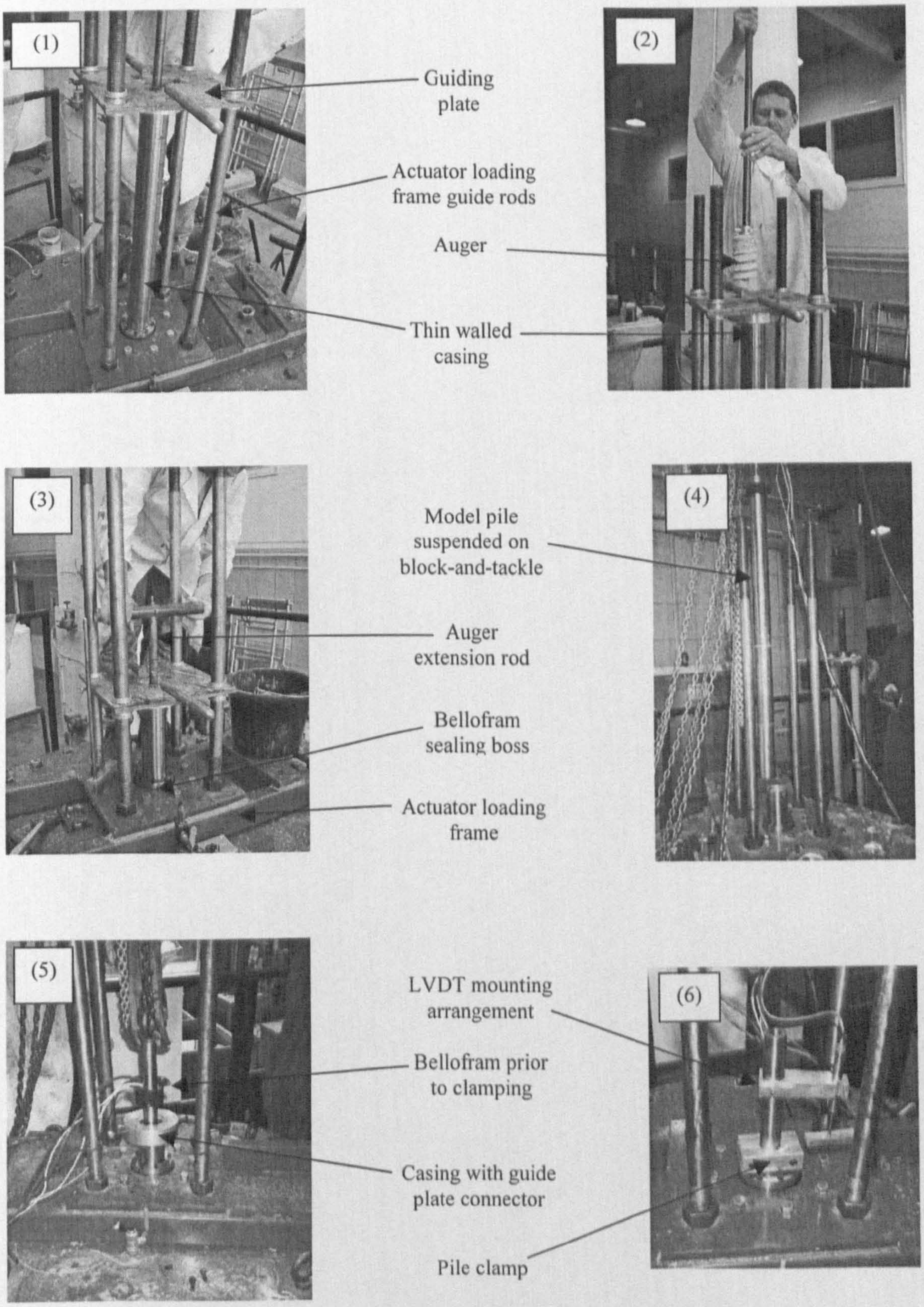

Figure 4.12, Model pile installation sequence, (1) Excavation support casing installation, with actuator loading frame bolted to chamber top plate, (2) Auger after clay excavation, (3) Advancing casing down load frame guide rods, (4) Excavation complete with model pile supported on block-and-tackle, (5) Model pile installed awaiting casing removal, (6) Model pile clamped in final position for completion of isotropic consolidation.

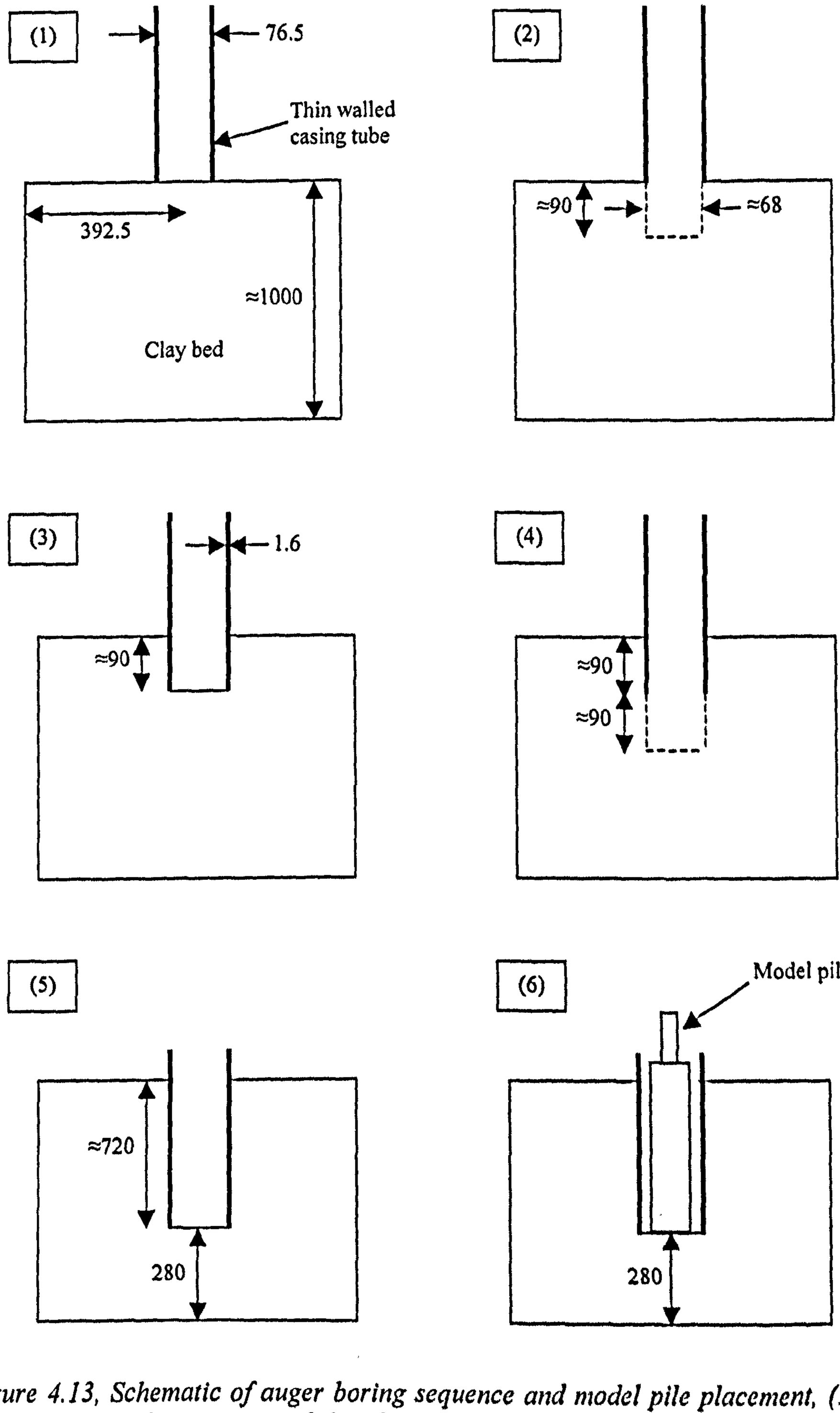

Figure 4.13, Schematic of auger boring sequence and model pile placement, (1) Thin walled casing place on top of the clay bed, (2) Soil excavated to 90mm below the casing, (3) Casing advanced over the excavated length, (4) Repetition of excavation stage, (5) Process repeated until base of casing coincident with the required pile tip level, (6) Final pile position awaiting casing withdrawal. All dimensions in mm.

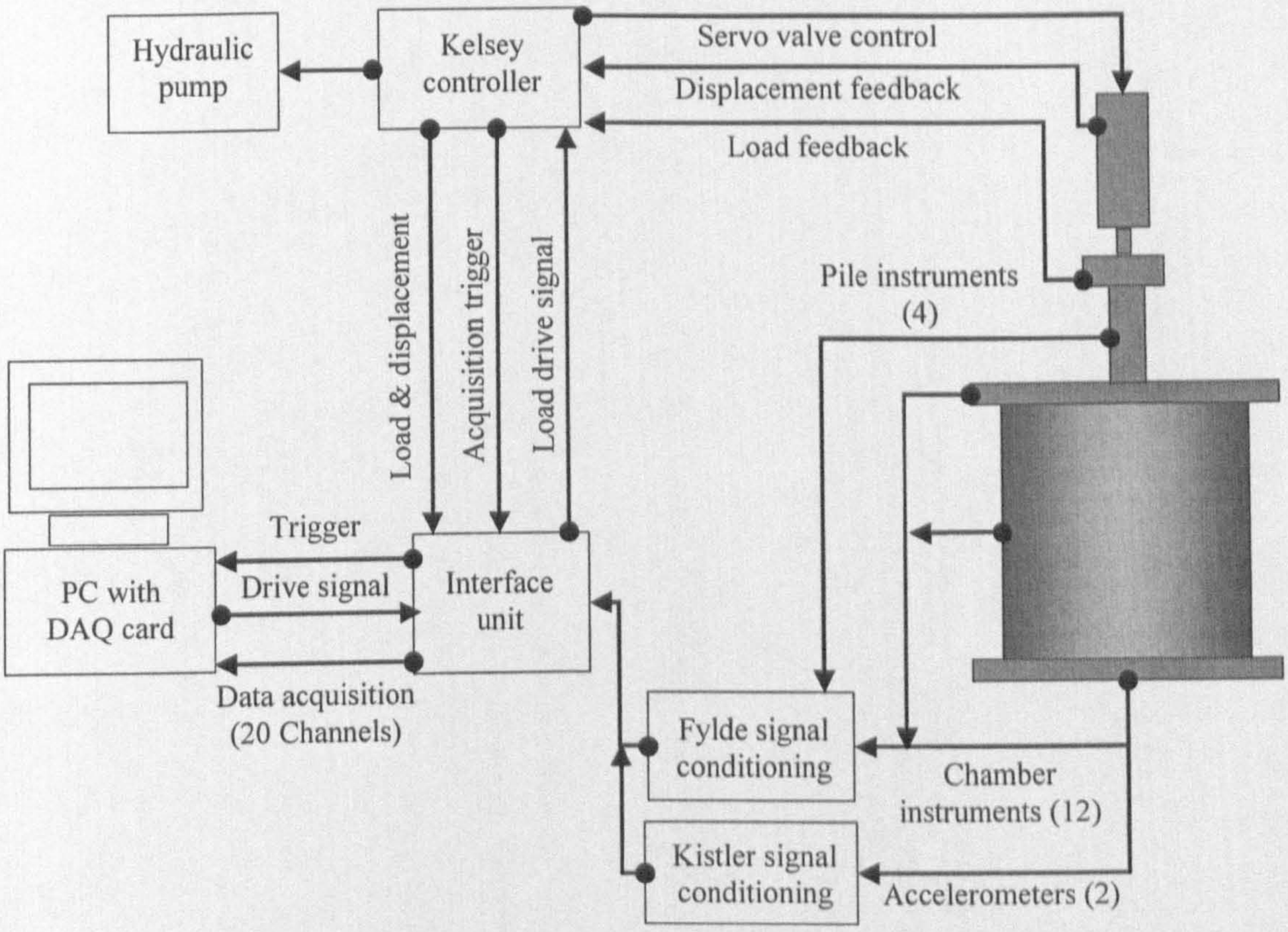

Figure 4.14, Control and data acquisition system for model pile testing.

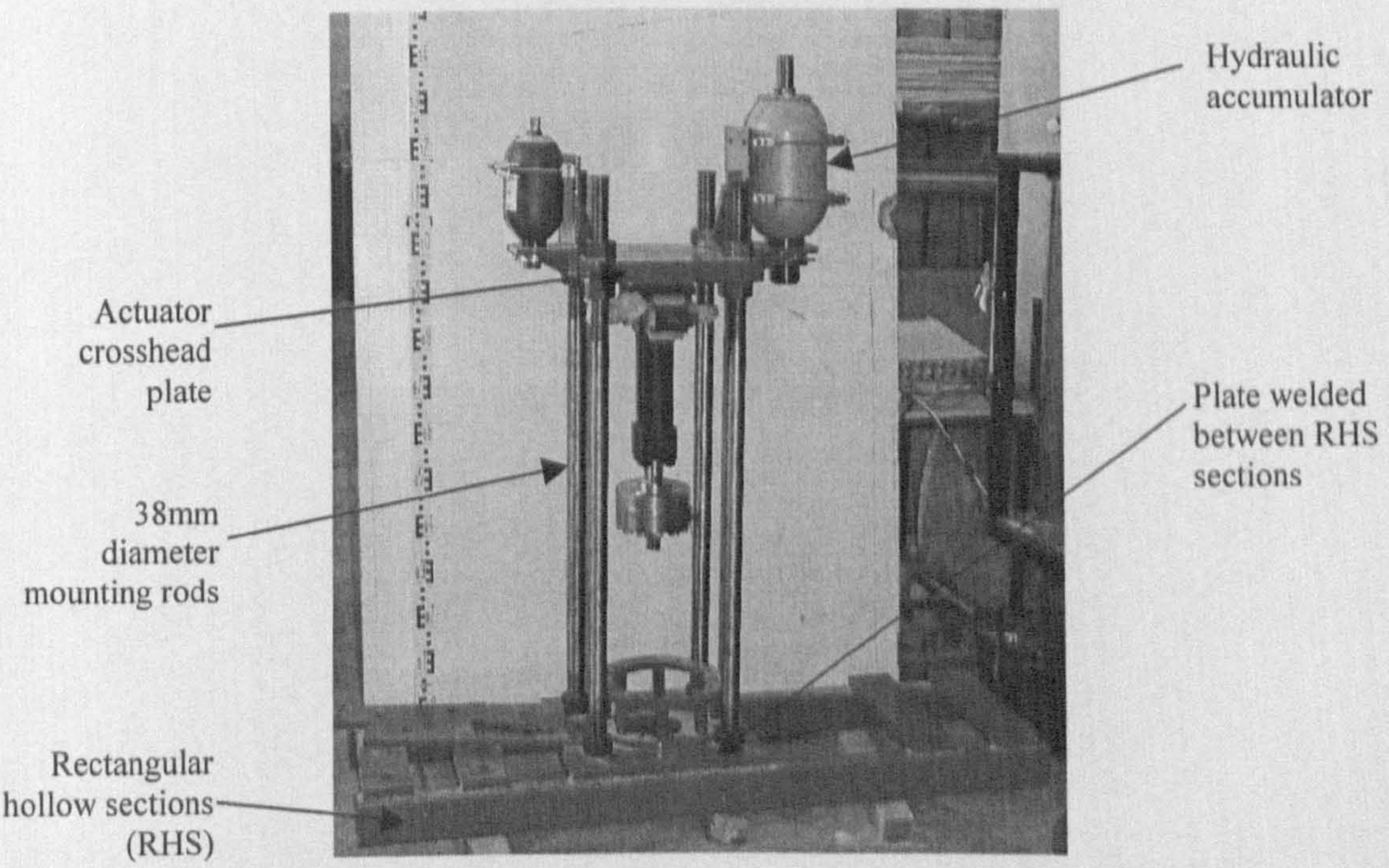

Figure 4.15, Hydraulic actuator mounted on loading the loading frame. Frame is shown during fabrication and prior to addition of hydraulic hoses.

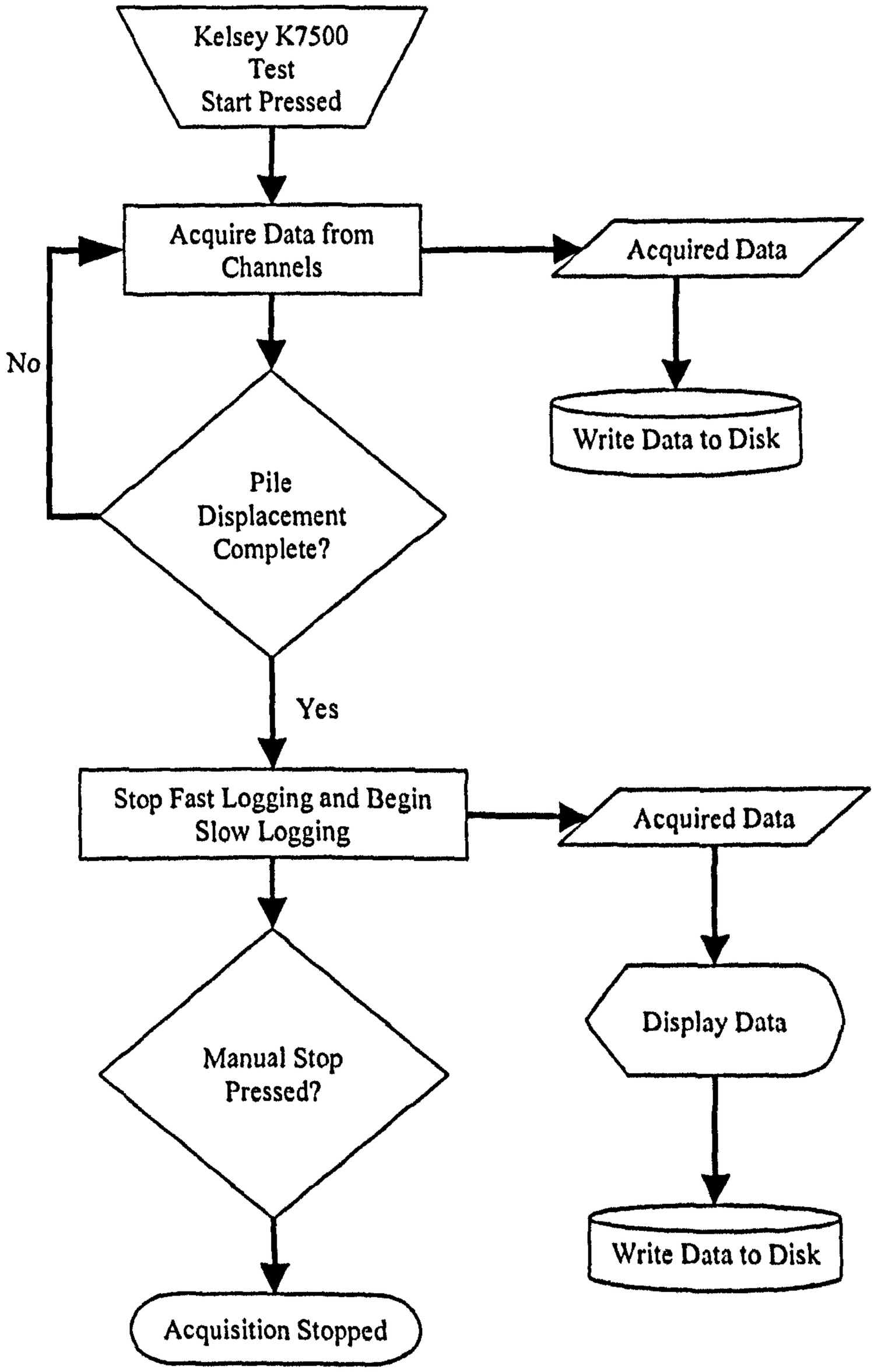

Figure 4.16, Flow chart showing CRP pile test control and acquisition.

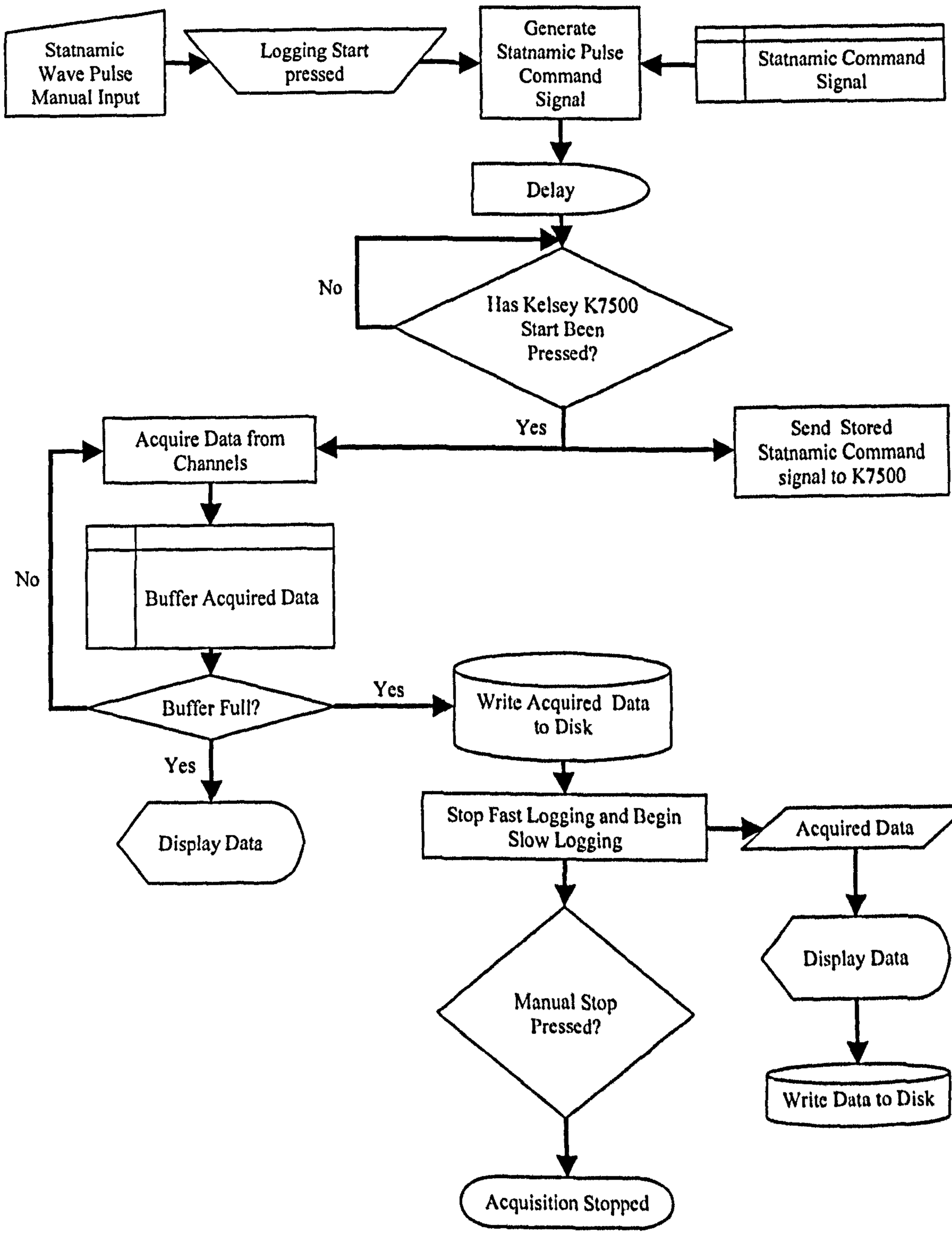

Figure 4.17, Flow chart of Statnamic pile test control and acquisition.

5.0 Results and Discussion of Model Pile Tests

5.1 Introduction

This chapter presents and discusses the results from model pile testing in the clay calibration chamber for both Constant Rate of Penetration tests (CRP) at varying rates and Statnamic (STN) type load pulses of different magnitudes.

The CRP tests were undertaken to determine how a pile's capacity varies with increasing rate of penetration or rate effects. Additionally, if a perfect CRP test was undertaken inertial effects are minimised, thus simplifying interpretation. From the CRP tests, it was possible to determine rate effect parameters that could be used to analyse the STN pulse loading.

Due to the long time periods involved with clay bed preparation, a suite of both CRP tests and STN tests were carried out consecutively in a bed. To aid comparison of the elevated rate tests, low rate CRP (0.01mm/s) tests were carried out at regular intervals. The low rate CRP tests at 0.01mm/s may be referred to as static tests. The rate chosen for these static tests was based upon guidance for prototype CRP testing of piles (ICE, 1997). Generally, a period of 24 hours was left between tests to allow bed excess pore pressures to return to their pre-test levels.

5.2 General information

5.2.1 Definition of reference terms

To aid understanding of the testing sequence a numbering system is used. For example:

BD3/7/CRP-0.01

This refers to the seventh test in Bed 3, which was a CRP tests at 0.01mm/s. For an STN pulse type load, the CRP will be replaced by STN followed by the target load.

As there were several transducers located in the clay bed at various heights and radial distances relative to the pile a system is required to define their position. The vertical position of the transducers below the top of the clay bed are referred to by upper, mid-height and lower. The positions associated with these classifications are shown in Table 5.1. Further details of the transducer positions during testing can be found in Appendix 3. To reference the vertical position of bed transducers relative to the pile tip position a z/R ratio is used. The z refers to the instrument's position behind the tip and the R is the pile radius (R=35mm). To denote positions below the tip the ratio is made negative. Additionally, the pore pressure transducers are referred to as PP 1 to 8 to aid quick reference.

The radial position of the transducers is defined by the ratio r/R, where r is the distance of the transducer from the pile centre line. Thus, $r/R = 1$ is a position at the pile's outer edge. The positions given for the transducers refers to their final positions found on bed strip down.

During this chapter, reference will be made to zones of the pile's load-penetration curves. These are broken into two predominant areas for all the measured components of the pile's capacity. The two zones are the elastic zone and the plastic zone as shown in Figure 5.1.

5.3 Constant Rate of Penetration tests (CRP)

5.3.1 Selection of pile ultimate load criteria

The point chosen for comparison between tests was taken as the point at which the pile penetration equalled 10% of the pile diameter ($0.1\,D_p$ or 7mm). This penetration dependent point was chosen because other definitions of ultimate pile capacity do not allow for the need to compare individual components of a pile's resistance. The choice of this point also allowed the pile penetration to be limited, thus increasing the number of tests in each individual bed.

5.3.2 Rate of penetration and system control

The Constant Rate of Penetration (CRP) pile tests were carried out at target velocities of 0.01mm/s to 500mm/s. The term "target" is used because it was very difficult to attain such speeds and keep the pile under control. For the lower rates, control was relatively simple with the gains of the servo-hydraulic loading system being manually adjusted during a test.

A pile penetration-time behaviour plot is shown (Figure 5.2) for a CRP test with a target velocity of 500mm/s. It is clear that the rate of change of penetration (velocity) of the pile varied considerably over the 7mm pile travel. The initial lag was due to the response of the actuator-pile-soil system and its inability to instantly achieve high velocity. The example given for Bed 4 (BD4/12/CRP-500) shows that the control of these high rate tests improved compared with earlier attempts as shown for Bed 3 (BD3/8/CRP-500). Due to the short duration of CRP tests and the limitations on total pile displacement, there were few opportunities to improve the system control at high rates.

One way to reduce the variation of velocity was to increase the pile displacement. This gave the control system time to reduce the feedback errors as shown in Figure 5.3. This is the same test as shown in Figure 5.2 (BD4/12/CRP-500) with the full displacement plotted. The corresponding velocity time history is also shown.

The problem with this behaviour is that the test did not have a constant velocity as desired. There were also inertial forces in the early stages. If pile failure was chosen for a displacement of 7mm, it can be seen that there was velocity variation over a large portion of the pile's displacement up to that point (Figures 5.2 & 5.3). This makes it difficult to assign a velocity to that portion of the test. For initial analysis three definitions were considered:

1. The average velocity over the complete penetration length.
2. The velocity at a pile penetration equal to $0.1\,D_p$.
3. The average velocity up to a penetration equal to $0.1\,D_p$.

As calculations were based on a pile penetration equivalent to 10% of the pile diameter, with interest in the behaviour up to this point, option 3 was considered the most relevant.

Additionally, the variation was undesirable in that it occurred in the pile's elastic behaviour or "Working zone" (Fleming *et al.,* 1992). This zone is the region of most interest to pile designers as few piles are taken to their ultimate load. This makes it difficult to assess the effect of pile displacement rate on the pile-soil stiffness in this zone.

Previous model pile studies of rate effects do not discuss the accuracy of penetration rate or definition of failure criteria. Generally, where such high constant penetration rates are required over small displacements, a drop hammer system is used rather than hydraulics. A similar hydraulic system was used by Litkouhi & Poskitt (1980) who claimed to control the velocity over the majority of the actuator stroke suggesting that similar problems were encountered at the start of the test. In the work by Eiksund & Nordal (1996), very high levels of control were achieved but their testing was undertaken in sands that showed little rate effect from 0.8 to 1800mm/s.

5.3.3 Model pile resistance

The construction of the pile loading system and model pile as discussed in Section 4.3 allowed measurement of several components of the pile's resistance to loading. This included the total resistance measured above the pile (pile head), the tip resistance and a portion of the skin resistance. Typical total load outputs from CRP tests at 0.01mm/s and 500mm/s can be seen in Figure 5.4. It can be seen that at 0.01mm/s, the pile had reached its ultimate capacity after 1mm of pile penetration with little appreciable increase in capacity with further penetration. This was equivalent to 3% of the pile diameter.

The shape of the load-penetration curve for the pile head loads at 500mm/s was far less typical. The peak behaviour between 2 to 3mm was probably influenced by the pile penetration rate lag problems as discussed in Section 5.3.2. The pile penetration rate in this region was much higher than that required due to the earlier lag which resulted in the increased pile resistance (Figure 5.2). From 6.5mm to 10mm, the velocity was

relatively constant (Figure 5.3 & 5.4) resulting in stable load readings. The CRP test at 500mm/s represented the greatest challenge regarding control of the applied load. At lower pile velocities, it was possible to achieve constant velocity at lower pile displacement. The choice of deformation equivalent to 10% of the pile diameter (7mm) as the point of test comparison was the minimum displacement at which the velocity was stable for all penetration rates.

The effect of varying the rate of pile penetration can be seen in Figure 5.5 for CRP tests in Bed 4. It is apparent that as the rate of pile penetration increased so did the total pile resistance. The inclusion of the 0.01mm/s CRP tests gave some indication of the variation in pile capacity due to increasing pile embedment, bed disturbance and proximity to the chamber base.

5.3.4 Model pile skin friction resistance

The pile skin friction load and shaft resistance were obtained in two ways. Measurements of load from the pile skin friction sleeve are referred to as measured skin friction loads. The derived skin friction loads were obtained by subtraction of the total pile load (pile head) from the tip load measurements. The pile skin measuring zone was 302mm in length and started 206mm above the pile tip (z=5.89 to 14.51R, Section 4.3.2). The measured and derived skin friction loads for CRP tests at 0.01mm/s are shown in Figure 5.6.

The measured skin friction load began with very low readings up to 0.4mm of pile penetration (Figure 5.6). This delay in measurement was greatest in Bed 3 and was thought to be due to play in the pile skin friction measuring system. Subsequently the pile was dismantled and re-built to remove the problem. As the skin friction measuring zone was 302mm in length, any play in this region affected the results for the pile's total resistance. This is illustrated by the point of maximum measured and derived skin resistance being coincident (Figure 5.6). This highlights the need for stiff measuring systems as discussed in Section 4.2.8. Where there was no delay, maximum shaft resistance was typically mobilised after 0.42mm (0.6% of the pile diameter). The measurements for post peak resistance tended to remain constant or reduce slightly with increasing pile penetration.

At elevated rates, low initial measured skin friction loads were also obtained (Figure 5.7). This delay differed in that there were increasing load readings from the beginning of the pile's movement rather than zero reading when play was considered an issue. The delay was thought to be due to load transfer occurring above the skin friction zone, which increased with increasing rate of penetration.

One noticeable difference between the measured skin friction load outputs at different rates was that at rates below 200mm/s the skin resistance generally displayed a peak followed by reduction of the skin load (Figure 5.8). At rates above this, the peak was reduced or not apparent and the skin resistance tended to increase with increasing penetration. There was a tendency for the velocity to gradually increase with penetration for the tests above 100mm/s, which may explain the variation. The CRP tests below this rate had constant velocities so the reduction must have been due to other factors.

To compare the measured skin friction with that derived by subtraction, the outputs were considered as average unit shaft resistance along the entire pile length and over the friction sleeve. Generally, the outputs from the measured shaft resistance were lower than the derived values by up to 20kN/m^2 for the lower rates (Figure 5.9). As the rates increased the difference reduced significantly with increased pile penetration. This suggests that more shaft load transfer was occurring in the upper portions of the pile for lower rate tests (<200mm/s). As the rate of pile penetration increased, the shaft resistance was mobilised throughout the pile length. Comparison of the derived and measured shaft shear resistance at a pile penetration equal to 0.1 D_p at varying rates is shown in Figure 5.9.

Assuming a linear variation in shaft shear resistance along the pile length and an in-situ undrained shear strength of 71kPa (Anderson *et al.*, 2003), the effect of rate on the shaft resistance adhesion factor (α_A), adopted for total stress pile design, can be found. The adhesion factor (Tomlinson, 2001) is used to relate pile ultimate unit shaft resistance to the average undrained shear strength of the soil over the pile length by:

$$q_s = \alpha_A \bar{c}_u \qquad (5.1)$$

Where

q_s = ultimate unit shaft resistance

α_A = adhesion factor

$\bar{c}_u$ = soil undrained shear strength

For low rate tests at 0.01mm/s, an adhesion factor of 0.46 was obtained with this value increasing to 1.56 at 400mm/s (Figure 5.10).

Further comparison is possible by using the shear resistance to calculate a coefficient of friction, which is used in effective stress design approaches (DOE, 1990):

$$\mu = \frac{\tau}{\sigma'_{rr}} \tag{5.2}$$

Where

μ = coefficient of friction

τ = pile shaft shear stress

σ'_{rr} = radial effective stress

The radial effective stress was assumed equal to the horizontal applied stress (280kPa) minus the pore pressure measured at the skin measuring point and the average within the bed. It is acknowledged that the pore pressure would vary over the length of the pile but, in the absence of further monitoring points this would seem the best approach. The angle of friction can be obtained from the equation above by:

$$\mu = \frac{\tau}{\sigma'_{rr}} = \tan\delta \tag{5.3}$$

Where

δ = angle of friction

The variation in friction coefficient followed a similar pattern to the pile shaft shear stress, as the effective radial stress did not vary significantly with increasing rate. For Bed 5, the derived friction coefficient increased from 0.187 for a penetration rate of 0.01mm/s to 0.405 at 500mm/s at 7mm pile penetration (Figure 5.11). This is equivalent to an increase of friction angle from 10.6° to 22.0° where the critical state friction angle from triaxial testing was 26.6° (Balderas-Meca, 2004). The difference in friction angle at peak friction coefficient and a pile penetration equal to $0.1\,D_p$ was generally of the order of 2 to 3° but, this would be influenced by the variation in velocity around the peak zone (Figure 5.7).

The friction angle noted at 0.01mm/s was very low, especially when compared with the residual friction angle of 20.9° quoted for the material by Rossato *et al.* (1992). They refer to the material as displaying transitional residual shear behaviour as defined by Lupini *et al.* (1981) from ring-shear testing of soils. This transitional mode lies part way between turbulent and sliding shearing modes (Figure 5.12), where the former is associated with low clay contents (low plasticity index, platy or rotund particles) and the latter with high plasticity (platy, low friction particles) index (DOE, 1990). The behaviour of material described as transitional is particularly sensitive to variation in clay fraction with friction angle increasing with reducing clay fraction (Skempton, 1985). The material used in this study had less clay fraction than that used by Rossato *et al.* (1992) at 38% compared with 48%, which would suggest a slightly higher residual shear angle. What has been noted is that the friction angle is dependent on the material against which the soil is sheared. Materials that would normally fail internally (soil-soil) in a turbulent (high residual strength) and transitional manner, fail partially in sliding (low residual strength) when sheared against smooth surfaces. This sliding shear against a smooth surface was referred to as S_1 and was assumed to be caused by separation of the more rotund particles from the smooth interface by orientated clay particles (Lupini *et al.* 1981). This is consistent with the relationship between clay fraction and residual friction coefficient (Figure 5.12) proposed by Lemos & Vaughan (2000).

It is considered relevant to consider the pile clay interface in the residual state prior to testing because of the disturbance caused during the pile installation phase (Section 4.3.4). The removal of the material during augering was achieved by screwing

in the auger and then pulling the auger vertically to remove the material without flighting of the auger. The upward shearing caused by this event would be reversed during penetration (up to 700mm) of the thin walled casing supporting the excavation. Once the pile was installed, the casing was removed vertically reversing the shear direction. It can be assumed this formed a shearing surface close to the casing as considerable resistance to casing removal was encountered.

Assuming residual shear strength had been reached then the KSS (μ=0.203, Clay Fraction=38%) material would be at the boundary between S_1 behaviour and transitional type shear for low rate tests (Figure 5.12). A typical residual shear angle for kaolin is given as 12.3° (Rossato *et al.* 1992) which compares to 11.5° for the angle of friction found from most of the CRP tests at 0.01mm/s for KSS. As the rate of penetration increased so did coefficient of friction (μ) apparently moving the shearing behaviour into the transitional mode (Figure 5.11 & 5.12).

The average surface roughness (R_A) of the pile used in this study was measured as 0.83μm. These values compare to those used by White (2002) and other model pile studies where values between 1-2μm have been used for piles installed in sand. Values of this order were considered low when compared with typical values of surface roughness found for offshore driven piles (10μm). To increase the surface roughness of the piles used in the DOE (1990) study the piles were shot blasted to increase roughness from 0.54μm to between 7 to 10μm. As the surface roughness approaches the dimensions of the sand particles in the clay the shearing resistance increases to levels associated with soil on soil shear (Lemos & Vaughan, 2000).

As discussed for the total pile resistance, it is apparent that both the measured and derived components of the pile's skin friction capacity are influenced by pile penetration rate.

5.3.5 Model pile tip resistance

The results of tip load measurements are presented in Figure 5.13. Unlike the skin friction resistance, the pile tip resistance increased with increasing penetration throughout CRP at 0.01mm/s. The rate of increase reduced between 1 to 2mm

penetration. The tip loads appear to increase with increasing rate of penetration but not to the same degree as noted for the other components of pile resistance.

Monitoring of the pile tip load cell showed residual loads after each test (Figure 5.14). The residual load increase, during an individual test varied anywhere from 0.3 to 1kN with the magnitude reducing on consolidation between tests. For some of the higher rate tests the magnitude of residual tip load actually reduced. This reduction is attributed to the rapid unloading seen at the end of the higher rate CRP tests, which is also seen in Figure 5.13 for the 500mm/s test. The rate of residual load increase observed (Figure 5.14) was far greater than that observed for jacked in place instrumented field piles observed by Cooke (1978). Residual loads are normally associated with driven and jacked in place piles rather than those installed by boring (Cooke, 1978). This would suggest that the residual tip loads were influenced by the proximity of the rigid chamber base, although the tests by Cooke (1978) were only carried out at low vertical stress levels.

The presence of these residual tip loads may have influenced the results of derived skin friction loads. Where skin loads were calculated by subtraction, they were based upon the tip load measured before the first test in a bed. The presence of residual tip loads would result in either upward movement of the pile or negative skin friction loads. Unfortunately, the skin friction measuring system was not designed to measure loads in the upward direction so the presence of negative skin friction could not be confirmed. The presence of such loads may explain the lags associated with the skin friction measuring sleeve. Additionally, subtraction of the total load from the tip residual loads lead to negative values of derived shaft resistance at the start of tests.

The measured residual tip loads may not have been directly caused by pile testing or installation but by the design of the loading system. It proved difficult to connect the hydraulic actuator to the pile without some pre-test loading or slight pulling of the pile, although care was taken to minimise disturbance.

The long term monitoring of the pile tip load during consolidation showed an initial increase in load of the order of 0.3kN in 2 days with a subsequent slight reduction in load prior to pile testing. As noted for the earth pressure cell in Section 4.2.7, there was

a slight fluctuation in the load readings during consolidation of the order of 0.05kN, which was considered negligible. The pattern of variation was on a 24-hour cycle as for the earth pressure cell.

5.3.6 Pile interface pore pressure behaviour

Measurements of pore pressure at the interface between the pile and the clay were undertaken directly under the tip and at the skin, 534mm above the tip (z=15.26R, Section 4.3). The pressures reported are excess pressures (ΔU) measured during and after loading events.

Comparison of pore pressures generated at the tip during different 0.01mm/s CRP tests carried out in Bed 3 can be seen in Figure 5.15. As the pile penetrated further into the bed, less excess pore pressure was generated. It should be noted that the 0.01mm/s tests were separated by various tests and periods of consolidation. This behaviour is consistent with triaxial testing of soils with increasing over consolidation ratio (OCR) Craig (1992). On final strip down of the clay bed, it was found that the state of the clay varied considerably in the zone directly under the pile tip. The moisture content directly below the tip and up to 20mm below was 4.5 to 6.5 % lower than the average for the undisturbed bed (Figure 5.16). Due to the proximity of the pile tip to the chamber base plate, it was not possible to take undisturbed samples or carry out Pilcon vane tests under the pile tip. Indicative measurements of the undrained shear strengths at the tip were derived from small hand vane and pocket penetrometer tests. For Beds 4 and 5 values of 180kPa and 200kPa were noted under the tip but there was considerable scatter in the results.

Results from excess pore pressure measurements at the skin position (Figure 5.17) during CRP at 0.01mm/s also show results associated with over consolidation with initial contraction followed by dilative behaviour. The magnitudes of excess pressure generated at the skin were relatively small (±10kPa) with little variation in response between the different tests. This would suggest that there was far less variation in soil void ratio associated with skin deformations than those associated with the tip. This is reinforced by the moisture contents measured close to the pile skin which although being lower than the undisturbed bed were not as low as at the tip (Figure 5.16). The average moisture content for clay in contact with the pile skin was between 1.5 to 2.5%

less. One bed was sampled along the pile skin for triaxial testing but this practice was not repeated as it led to sample tube deformation and scratching of the pile. Results from the triaxial testing showed higher undrained shear strength in the skin region than in the undisturbed zone. Peak pore pressure was reached at the skin after only 0.3mm penetration (Bed 3, Figure 5.17) in advance of maximum skin friction load at 0.4 to 0.6mm. Tip pore pressures typically followed similar magnitude-deflection behaviour as the measured tip loads.

As the rate of pile penetration increased there was a reduction in the measured excess pore pressures at the tip (Figure 5.18) over the duration of the test (<2kPa). Greater excess pressure was generated during the 10mm/s test (+10kPa). The response of the pore pressure transducers in their mountings was checked using water as the saturation fluid. Similar response times were obtained as Bond *et al.* (1991) as discussed in Section 4.2.8. As noted by Bond *et al.* (1991), the performance of a measuring device in the soil depends on the permeability and the compressibility of the soil. Using a similar arrangement as in this study, they calculated that 3 seconds were required for the system to register 95% of the true pore pressure in London Clay. This suggests that full pore pressure response would only be seen for the 0.01mm/s tests and not at rates above this.

Along with the short term logging during pile penetration, longer-term logging was normally undertaken after penetration had ceased at a reduced sampling rate. Typical results for a 0.01mm/s and a 50mm/s test can be seen in Figure 5.19. The change in test logging rate marked the maximum penetration achieved by the pile. The sampling rate was reduced as the pile was unloaded and the actuator disconnected. After the point of maximum penetration, the pile unloaded at a very slow rate (0.005mm/s) due to technical limitations of the equipment. The pile was usually disconnected from the pile within 1 to 2 minutes of reaching maximum penetration. After penetration, the excess pore pressure at the tip increased to a maximum for the higher rate test. This took between 20 to 26 minutes (Bed 4). The higher rates were associated with higher pore pressures and longer periods to reach a peak. The time to peak pore pressure varied from bed to bed with values for Bed 3 ranging from 3 to 8 minutes. This time would seem to be linked to the degree of bed disturbance and reduction in void ratio with increasing pile penetration. In Bed 3 the CRP tests were the first to be carried out whilst in Bed 4 CRP tests were carried out after Statnamic type testing. The excess pressures

generated during and after the tests then dissipated back to their pre-penetration values over a period up to 16 hours. Similar post drive increases in pore pressure were noticed by Bond & Jardine (1991) for a 102mm diameter model pile. The pile was driven up to 6m in London Clay and consequently the peak pore pressures were much greater.

The only variation from this typical behaviour for the tip pore pressure was encountered in Bed 3 for tests at 100mm/s and 500mm/s. Here the pore pressure reached peak after the test and then there was a sudden drop in pore pressure to the pre-test levels. This is thought to be due to sudden stress relief in the soil under the tip, movement of the pile or bleeding of the tip pore pressure to the skin zone. Neither the tip nor skin load monitoring recorded any variation coinciding with this event.

Long-term monitoring of the skin after elevated rate penetration showed a reduction in pressure during the test followed by a gradual increase to pre test levels (Figure 5.20). Again, the lowest pressure coincided with the maximum pile penetration with the largest reductions associated with the faster tests. In Figure 5.20, a sudden increase in pore pressure was noticed between 1 to 2 minutes. This was thought to be caused by the disconnection of the pile from the actuator. This did not adversely affect the rate of pore pressure recovery.

5.3.7 Clay bed pore pressure behaviour

Throughout the testing programme, pore pressure transducers were monitored at various positions within the clay bed. These were used to aid control of the consolidation process and give an insight into the effect of rapid loading on effective stresses.

A summary of the transducer positions for each test can be found in Table 5.1. Typically, the transducers were placed at three elevations; below or close to the pile tip (Lower, PP7 & PP8), close to the skin friction measuring zone (Mid-height, PP4 to 6) and 246-309mm below the bed upper surface (Upper, PP1 & PP2). The beds usually contained eight pressure transducers with two sets of three at the upper levels. These sets of three were placed at increasing radial distances from the installed pile. The positioning chosen in Bed 2 was designed to test the radius of influence of pile loading on pore pressure change. This resulted in transducers being placed up to $r = 10.02R$ away from the pile face (R=35mm, pile diameter). Excess pore pressures generated

during the tests were relatively small for transducers mounted at $6.85R$ and beyond. Thus, the maximum radial position for transducers was set at $5.29R$. The actual positions were set based on base plate access hole positions from the previous study.

Typical initial radial positions for the set of six transducers at bed mid-height and above were $2.14R$, $3.71R$ and $5.29R$. Initial radial positions are referred to as the transducers had a tendency to move away from their intended positions during consolidation. In the following discussion, final transducer positions are used.

Typical results for the transducers at various positions in a bed can be seen in Figure 5.21 during CRP at 0.01mm/s. Additionally, the different load components of the pile resistance are shown. Larger pore pressures were generated closer (PP1, 15.4kPa at $1.43R$) to the pile than further away (PP2, 9.8kPa at $2.86R$). The bed pressures also remained positive throughout the test whereas the skin pressure became negative after 1 to 2mm of pile penetration (Figure 5.17). The pore pressure at PP1 (Figure 5.21) was also less "Brittle" than the skin readings shown in Figure 5.17 with a gradual reduction post-peak pressure. Peak pore pressure was reached at the skin after only 0.343mm penetration (maximum skin friction load at 0.558mm), whereas the closest bed transducer (PP1) reached peak at 0.724mm (Figure 5.21). The difference between pore pressures at PP1 and PP2 is a reflection of how close PP1 was to the pile (15mm). For the mid-height transducers, the results from PP4 ($2.37R$) are similar to PP2 ($2.86R$). This suggests that the greatest pore pressures increase occurred between 1 to $2.37R$ from the pile but the effects are still apparent at $5.29R$. No results are presented for the upper level PP3 because the porous stone in front of the transducer was found to be detached during bed strip down.

The profile of the mid-height transducers response with penetration (PP4, PP5 & PP6) was very similar to the profile of the pile resistance during penetration. It may be noted that the upper and mid-height transducers indicated relatively uniform pore pressure generation over the pile's skin friction measuring zone. The test shown was the second test carried out in Bed 3.

Relatively large pore pressures were generated in advance of the pile tip with the magnitude reducing on moving radially away from the pile during 0.01mm/s CRP (Figure 5.21).

During analysis of results, it was noticed that there was considerable variation in the pressures of the top and side chamber total cell pressures during CRP tests at rates above 0.01mm/s (Figure 5.22). The variation took the form of a reduction in top cell pressure for the majority of the pile penetration with negative peaks of up to –52kPa for CRP at 500mm/s. The side pressure reduced initially by up to –15kPa followed by a positive increase part way through penetration, the lowest pressures occurring at maximum pile load application. It was assumed that these relatively large variations were caused by upward deflection of the chamber top plate during pile loading. As this deflection occurred very rapidly, the chamber's pressure supply system could not accommodate such a rapid change in pressure. The positive end of test cell pressures suggests that some inflow of water had occurred to equalise the pressure drop. The reduced variation for the side cell pressure is assumed to be due to the greater volume of water behind this membrane. Results from the 0.01mm/s CRP tests did not show any penetration or load induced cell pressure variation during testing.

The variation in cell pressure was not noticed until the end of the testing programme so, it was not possible to verify the assumption of chamber top plate deflection. Calculations suggest that a volume change of 3.6ml would be sufficient to cause the measured pressure drop to occur. This corresponds to an upward deflection of 0.011mm at the centre of the chamber top end plate. To remove the problem in future it is suggested that both top and bottom end plates are restrained against vertical movement. Although, if the calculated required volume changes are correct, the restraining system would have to be of a high stiffness. This could be achieved by preloading hydraulic jacks between the restraint system and the end plates. Attempts to calculate the system deflection by considering the loading frame and chamber top plate as structural steel elements suggested a central deflection of 0.25mm (85ml volume change). This would result in a much greater pressure drop than encountered, but this may be offset by the pressure increase associated with additional pile penetration.

The effect of the cell pressure variation on the upper most transducers during a 50mm/s CRP test can be seen in Figure 5.23. The transducers located closest to the pile (PP1, 1.43 R) showed very little response to the variation in either top or side cell pressure, but influence was seen with increased radial distance (PP2, 2.86R). Increasing the CRP penetration rate to 500mm/s caused pressures at PP1 to reduce to -5kPa and PP2 to reduce to –90kPa (Figure 5.22).

The magnitude of the pore pressures generated by the pile close to the tip would appear to have been masked by this cell pressure change. Although the shape of the pore pressure curves close to the tip is similar to that for cell pressure, the pore pressure magnitudes are much greater. This suggests that negative pore pressures are generated in advance of the pile tip at 50mm/s and above (Figure 5.22 & 5.23).

Pore pressures measured in advance of the pile seemed to be heavily influenced by both rate and vertical position relative to the pile. For Bed 3, the transducers were located in advance of the tip. For tests at 10mm/s (Figure 5.24) and 50mm/s (Figure 5.23), (z =-1.68 to –1.46 R & z =-1.00 to –0.77 R, respectively) PP7 remained positive with a peak pore pressure of 260kPa for the lower rate test. For the higher rate, the peak pore pressure reduced to 130kPa even though the pile tip was closer (Figure 5.23). For PP8 the pressure fluctuated from –25kPa to a final value close to +50kPa during the 10mm/s test, whereas during the 50mm/s test the pressure reduced to –55kPa only returning to pre-test levels at the end of penetration. The reduction in pressure for PP8 during the lower rate test could be explained by the cell pressure change, but the increases in pressure towards the end of the test cannot.

The general trend for the pore pressures at PP7 was reduction in pressure from high positive pressures (260kPa, 10mm/s, z =-1.68 to –1.46 R) to very low pore pressures (-170kPa, 500mm/s, z =0.06 to 0.34) with increasing rate and proximity to the pile tip (Figures 5.22 & 5.24). It is acknowledged that this low pressure was probably only indicative because unless very high degrees of saturation were achieved, cavitation would have occurred below –100kPa. The corresponding reduction in cell pressure was only 65kPa so, this does not seem to fully explain the low pressures. Behaviour similar to this was noted for high rate CRP testing in sands by Eiksund & Nordal (1996). At 800mm/s, they noted pressures down to –33kPa in advance of the pile tip. As their

loading was produced by a remotely mounted hydraulic actuator, there is no question of the chamber top plate having deflected under loading. The chamber used consisted of a cube with a rigid base and flexible top membrane. Horizontal pressure was applied via air filled membranes but these were not on all faces of the cube. During this study, the cell pressures were not monitored (Eiksund, 2003).

For PP8 the lowest pressures were encountered during the 50mm/s (-25kPa) test with a gradual move back to positive pressures for the 200mm/s and 500mm/s tests. This occurred when the cell pressure variations were at their greatest. This behaviour was probably caused by the increasing proximity to the pile tip and differs from PP7 due to the increased radial distance. Again, this is consistent with Eiksund & Nordal (1996) findings for transducers mounted just above the pile tip. This would suggest that below rates of 100mm/s pore pressure behaviour in advance of the pile is typically positive but then becomes negative at 100mm/s and above. The magnitude of these pressures was masked by the cell pressure variations and the changing z/R ratio.

Long term monitoring of the transducers after a 50mm/s test is shown in Figure 5.25. At the end of penetration, the excess pressure at PP2 rapidly reduced to that for PP1 followed by an increase to 10kPa in less than a minute. Prior to this PP1 had begun to dissipate and had reached pre test pore pressures in less than 3 minutes. This suggests lower permeability or preferential drainage close to the pile. The dissipation of pressure further away takes much longer with pre-test levels reached in excess of 300 minutes. Similar results were obtained for the mid-height transducers.

The long term increase in the bed pore pressure close to the pile tip (PP7 & PP8, Figure 5.25) after high rate CRP was much greater than that measured at the pile tip (Figure 5.19). Peak pressures close to the tip were reached after 1 minute rather than 35 minutes at the tip. As discussed in Section 5.3.6, the sudden reduction in pore pressure sometimes associated with the post peak pile tip pore pressure measurements was not apparent in the lower bed pressure transducers.

5.3.8 Pile and clay bed inertial behaviour

It was initially envisaged that CRP testing would result in no significant acceleration of the pile or clay bed. However, due to the problems of velocity control and system inertia, relatively large fluctuations of velocity did occur as discussed in Section 5.3.2. The highest accelerations occurred for the higher rate tests. Although the accelerations were high, the actual corresponding inertial forces generated due to the pile weight were relatively small because the pile only weighed 19kg. At the peak pile resistance the inertial load was 3.36kN, which was 14.6% of the total pile resistance (pile head load) at the corresponding displacement. The inertial load was only –0.21kN at a deflection corresponding to 10% pile diameter. Although there was an inertial component during the early stages of the CRP tests, inertia will be disregarded in further analysis, as the magnitudes were small at $0.1\,D_p$. The accelerations measured by accelerometers mounted in the clay bed were very small and do not warrant further discussion at this stage.

5.3.9 Boundary measurements

In an attempt to check the influence of the rigid base of the chamber on pile resistance, an earth pressure cell was installed below the pile in Bed 5 (Section 4.2.8). The increase in pressure at the cell base plate with the approach of the pile tip during various CRP tests at 0.01mm/s is shown in Figure 5.26. Although there was an increase in the total stress measured at the base, there were no obvious corresponding effect on pile tip load measurements during penetration. At 0.01mm/s, the peak increase in total stress coincided with the maximum pile penetration followed by rapid reduction to approximately 30% (not shown) of the peak stress during penetration. Further reduction in stress was consistent with the reduction in residual pile tip loads (Section 5.3.5).

For pile tests at elevated rates shown in Figure 5.27, there was no obvious relationship between the rate of penetration and the increase in total stress. The total stress increased with increasing pile penetration irrespective of the penetration rate and generally the base stress was higher for rates above 0.01mm/s. This would suggest that there was a rate effect but it was being masked by the greater influence of the tip to base separation. In addition, there was an apparent rapid increase in the transmission of load from the tip to the base on increasing the rate above 0.01mm/s (Figure 5.27). Above 0.01mm/s the

tip to base separation would appear to have greater influence than pile penetration rate. This phenomenon could influence the choice of full scale pile installation or testing methods where sensitive buried infrastructure is present.

Although variation of the cell membrane pressures were recorded during elevated rate testing, no obvious influence on the stress at the base of the chamber was recorded.

5.3.10 Bed material disturbance due to testing

After completion of testing, the beds were stripped down and sampled for moisture content and shear strength determination (Section 4.7.2). It is apparent from Figure 5.16 that reduction of moisture content was associated with the pile, especially at the tip. As discussed in Section 5.3.6, the moisture content at the tip was of the order of 4.5% to 6.5% lower than the average for the bed. Lower moisture contents were also associated with the skin zone. The reduction in moisture content near the pile top is thought to be due to the proximity of the upper bed filter membrane. The pile may have also been acting as a drainage flow path. To further understand the influence of pile testing on the moisture content variation it would be necessary to create a bed, install the pile and then allow a suitable period of consolidation with no tests prior to strip down. There seemed to be little pile influence on moisture content above 3.5 to 4 R from the pile. Due to the limited separation between the pile tip and the chamber end plate, it is difficult to comment on the extent of disturbance in this zone.

The Pilcon hand vane used to measure undrained shear strength was not sensitive enough to determine variation throughout an individual bed. It's use was also limited to 3.5 R from the pile due to it's size. A pocket penetrometer or small hand vane may have given a better indication of the radial variation of strength. As noted in Section 5.3.6 the indicative shear strengths measured at the tip (180-200kPa, SD 21kPa) were considerably higher than the undisturbed regions of the bed (53kPa, SD 5kPa) but, considerable scatter in results was encountered.

5.4 Models for rate effects

5.4.1 Low rate benchmark resistance

The variation in total pile resistance with rate and penetration depth is shown in Figure 5.5. It can be seen that CRP tests at 0.01mm/s were carried out at the beginning and end of the sequence. This was done to allow determination of a low rate benchmark to which all other test results could be compared. Ideally, to compare a high rate test with a low rate one, slow tests would have been carried out before and after the fast test. This was not possible because of the limited travel of the pile and the need to maximise the number of tests from each bed.

The determination of such a benchmark was required because of several factors that affected the comparison of consecutive tests. The increase in pile resistance with increasing depth of penetration could be allowed for when comparing between tests. The assessment of other factors such as re-consolidation and hardening of the clay was more difficult.

To define the low rate benchmark, the resistance of the pile was found at penetration equivalent to 10% of the pile diameter (0.1 D_p) for each CRP test at 0.01mm/s over the cumulative pile penetration. A linear increase in the benchmark pile resistance was assumed between the points. This was then used to determine the equivalent low rate pile resistance for normalisation of the increased rate CRP tests. The variation of low rate benchmark with increasing penetration was found to follow a power law for Beds 3 and 4, but this did not fit the results for Bed 5 (Figure 5.29). Additional data is required to test the validity of this approach at lower penetrations especially in the first 40mm. For this study a linear relationship was used between points.

5.4.2 Determination of rate effects

The term rate effect has been used to describe the ratio of pile resistance at an elevated rate (R_d) to that at a lower rate (R_s, low rate boundary).

Due to the previously mentioned variation in velocity around the peak loads, the rate effects were only considered at a pile penetration of 0.1 D_p. This was done for all the

individual components of measured pile capacity. The rate effects for the total pile resistance in Beds 3 to 5, referred to as the kinematic resistance ratio, are shown in Figure 5.28. The kinematic resistance ratio for Bed 5 was consistently lower than that for the other two beds. Problems were encountered with Bed 5 that led to chamber strip down and membrane replacement (Section 4.2.6). Additionally, the effective stress state throughout testing was lower than the other beds.

What appears to have the greatest effect on the rate effect is the choice of the function for the static (low rate) benchmark values. The difference in this function for the various beds can be seen in Figure 5.29. The function varies considerably up to 40mm of cumulative pile penetration. For instance in Bed 3 the first test was a 10mm/s CRP test prior to a CRP test at 0.01mm/s. The rate effect for the 10mm/s test was negative where tests at further cumulative pile penetration were all positive. This would suggest that there was an alteration in the shear plane during increased pile penetration. For low plasticity clays (KSS is classified as CL) sheared against smooth surfaces, Lemos & Vaughan (2000) showed that a considerable reduction in friction coefficient may occur in the first 20mm of shearing followed by a rapid increase to initial levels by 100mm of penetration. Accepting the explanation for S_1 shearing discussed in Section 5.3.4, Lemos & Vaughan (2000) suggested that this behaviour was due to the sand particles disrupting (ploughing) the clay layer at the interface based on electron micrographs at various stages of shearing. This would initially reduce the shearing resistance. As more disruption occurs, the effect of shearing against sand begins to dominate and shear resistance increases.

The variation in results for the initial low rate "static" benchmark for Bed 5 would then be explained by the amount of prior disturbance to the interface between the pile and the clay rather than the bed effective stress. Due to the suggested sensitivity of the friction coefficient to the initial cumulative pile displacement, it would seem that the interface in Bed 5 had not undergone as much shearing as the previous tests during pile installation. This assumes that an oriented shear plane was formed during the pile installation as discussed in Section 4.3.4. At the time of testing, the low shear resistances encountered in Bed 5 were attributed to lower effective stress caused by membrane leaks, which resulted in the bed having to be stripped down.

On carrying out low rate tests after cell re-assembly, the low rate benchmark function was found to higher in Bed 5 than in the previous beds. This is thought to be due to a loss of system control at the end of the last test prior to strip down resulting in extraction of the pile by 12mm. The pile was re-driven this amount prior to the 0.01mm/s test. This reversal and re-drive would have caused considerable disruption (ploughing) at the pile interface and would place the pile at a theoretically deeper penetration based upon the variation in interface friction ratio suggested by Lemos & Vaughan (2000).

The results from Bed 5 have been used in the analysis as measured friction results were only obtained for Beds 4 and 5, but it is acknowledged they will introduce considerable scatter.

5.4.3 Selection of the rate law and parameters

The rate effect relationship for shear resistance generally takes the form of a power law (Gibson & Coyle, 1968, Lithkouhi & Poskitt, 1980 & Randolph & Deeks, 1992) or a logarithmic law (Dayal & Allen, 1975 & Triantafyllidis, 2001), as discussed in Section 2.4. Initial trials of a logarithmic relationship showed better degrees of fit for individual beds. When the results from the three beds were combined, it was found that a power law gave a better fit. The final form of the rate law was chosen in conjunction with results from triaxial testing of the KSS material (Balderas-Meca, 2004) to allow direct comparison of rate parameters from model pile and element tests. The final choice was based upon Randolph & Deeks (1992) modification of the power law suggested by Gibson & Coyle (1968):

$$\tau_d = \tau_s\left[1+\alpha\left(\frac{\Delta v}{v_0}\right)^{\beta}\right] \tag{5.4}$$

Where

τ_d = resistance to shear at elevated rates

τ_s = resistance to shear at low rates (0.01-0.1mm/s)

α & β = damping constants

Δv = relative velocity of the pile and the soil

v_0 = reference velocity (1m/s)

This equation was further modified by Hyde *et al.* (2000), as proposed by Randolph & Deeks (1992):

$$\frac{\tau_d}{\tau_s} - 1 = \alpha\left(\frac{\Delta v}{v_0}\right)^{\beta} - \alpha\left(10^{-6}\right)^{\beta} \qquad (5.5)$$

such that the dynamic resistance equals the static resistance at the "static" velocity. In the case of this study, the static resistance has been defined at $1x10^{-5}$m/s rather than $1x10^{-6}$m/s as suggested by Hyde *et al.* (2000).

The rate law defined by Equation 5.5 was then used in non-linear least squares curve fitting to determine the rate parameters for the various components of pile resistance.

5.4.4 Validity of the rate law

The rate law used above was initially derived from results of high-speed triaxial testing (Gibson & Coyle, 1968) and was later applied to piles and objects penetrating soil at elevated rates. It was suggested by Randolph & Deeks (1992) that this "viscous" damping model was only suitable for rate effects associated with a pile's skin resistance during plastic deformation rather than the pile's tip resistance.

The best agreement with the adopted rate law was for the total pile resistance (R_d/R_s) as shown in Figure 5.30. It is acknowledged that there is considerable scatter in the data and that a significant amount of data lies outside the 95% confidence limits. The data that lies outside the confidence limits is associated predominantly with Beds 3 and 5. As discussed in Section 5.4.1, the scatter is attributed to the definition of the static benchmark values. The data which lies above the 95% confidence limit, is associated with the early tests in Bed 3. For Bed 3, no low rate tests were carried out between 15 and 77mm penetration although it is acknowledged that the rate of increase of low rate capacity is at its greatest up to 40mm penetration. The results for Bed 5 show the

lowest rate effects as would be anticipated based upon the comments for Section 5.4.1. The derived damping coefficients are shown in Table 5.2.

The results for the measured skin friction loads and shaft resistance had considerable scatter because results were only available for Beds 3 and 5 which were associated with low rate benchmark problems, as discussed above. As considerable scatter occurs for the measurements that are not dependent on pile tip resistance, it is difficult to attribute the scatter for the shaft results to determination of tip load. Results from the pile tip show a low degree of scatter but have a low degree of fit to the rate law suggesting that this approach is not valid for the tip measurements. The rate effect for the tip was considerably lower than that for both the pile total resistance and the shaft resistance as shown in Figure 5.31.

5.5 Rapid load testing

5.5.1 Statnamic (STN) simulation

The Statnamic pulse loads were usually carried out in sequence with target loads of 10, 15, 20, 25 and 30kN. To produce the Statnamic (STN) type pulse, an ideal pulse was sent to the hydraulic controller linked to the hydraulic actuator, which was used to load the pile. Again, the use of 25kN refers to the target load rather than that actually achieved during the test. In the example shown in Figure 5.32, the applied load only reached around 20kN but this was predominantly due to yielding of the soil rather than poor system performance. Where it is necessary to refer to the load reached, the target load is followed by the actual peak load in parentheses. The form of the target Statnamic curve was similar to field results and published information on the Statnamic test. In all cases the duration of the pulse was maintained constant along with the coordinates of the turning points. The only variation was the magnitude of the loads, which were proportionally factored up at each turning point to reach the required peak load.

For the CRP tests it was necessary to increase the gain for servo control. In the case of the pulse loading, it was necessary to reduce the gain for better control of the actuator. The result of this attenuation can be seen as a lag in the load increase at the start of the loading. The amount of attenuation needed to be increased with increasing rate of load change (target load) so, the lower target loads displayed much better response.

Typical measured and calculated behaviour is shown for a 25kN STN pulse in Figure 5.32. Values for velocity and acceleration were determined by differentiating the displacement-time history. In Bed 5, the pile accelerations were measured directly.

5.5.2 Model pile resistance

The total pile resistance measured at the pile head for different pulse loads can be seen in Figure 5.33. There was minimal permanent displacement of the pile for pulse loading of 10 & 15kN. Larger permanent displacements were measured at 20kN (18.3kN) and above. The ultimate capacity of the pile from CRP tests at 0.01mm/s carried out before and after the STN pulse loads was 14kN. As the pulse target load increased there was a resulting increase in permanent pile penetration with a 30kN (21.5kN) pulse being associated with a pile deflection equivalent to 10% pile diameter. All calculations for the STN results have been corrected for pile inertia.

Comparison of elastic stiffness for STN and CRP at 0.01mm/s showed no significant difference up to 60% of the ultimate static load (Figure 5.34). Although it should be noted that at these load levels the displacements were less than 0.1mm and the readings susceptible to noise and the influence of the logging system resolution. As with the CRP tests any stiffness measurements were also influenced by the system response and in the STN case the shape of the pulse load.

It is of interest to note that the load displacement behaviour for both the STN and the 0.01mm/s CRP loading were very similar in the elastic or working zone (Figure 5.34). Especially given that there were no performance problems associated with the 0.01mm/s CRP tests and that the pile velocities associated with the STN tests were higher. This would suggest that the elastic behaviour at the beginning of a rapid load test is governed by strain level rather than strain rate (velocity). At a certain point, the CRP loading became less stiff (exploded in Figure 5.34) than the STN load until abruptly yielding where maximum skin friction resistance was mobilised. The points where the stiffness deviated seems to lie consistently between 0.1-0.18mm penetration or 0.58-0.62 times the ultimate low rate pile resistance. This result was confirmed with or without the correction for pile inertia. This suggests that the STN test results accurately predict the

low rate CRP test outcome for 60% of the elastic pile response without correction for rate effects or inertia.

Although mention has been made of correction for the pile's inertia the required corrections were minimal. As the pile only had a total mass of 19kg, it is not surprising that there was little alteration of the original pulse load. The mass of the pile appears low but it is actually heavier than an equivalent solid reinforced concrete pile (9.4kg).

5.5.3 Model pile skin resistance

As for the higher rate CRP testing, the measured skin friction resistance lagged behind that of the derived resistance up to the point of maximum STN pulse load, after which it was the same as the derived resistance. Again, this suggests that load transfer was occurring above the skin friction sleeve or that the load was transferred to the soil by another mechanism rather than purely shaft shearing.

The variation in friction coefficient from derived shaft resistance can be seen in Figure 5.35 for a 30kN STN pulse. The friction coefficient varied from 0.118 to 0.346 for STN pulse loads from 10kN to 30kN respectively (Figure 5.36). This is equivalent to an increase of friction angle from 6.7° to 19.1° where the critical state friction angle from triaxial testing is 26.6°. The higher magnitude STN pulses gave lower friction coefficient values than during high velocity CRP testing. This was because the velocities encountered during STN testing were less than the typical maximum values for high rate CRP tests (Figure 5.32). The highest velocity during STN testing was 284.2mm/s for the 30kN pulses compared to velocities of up to 440mm/s during CRP testing.

Comparison of the derived STN coefficient of friction with both high and low rate CRP tests again showed an increase in stiffness in the elastic zone (Figure 5.35) above 50% of the ultimate static pile resistance. As the velocities are typically higher in the CRP tests, this would suggest the increased stiffness was not purely velocity dependent. Again, it is difficult to separate soil-pile behaviour and system performance in this region of loading.

5.5.4 Model pile tip resistance

The tip loads measured during STN pulses carried out in Bed 5 can be seen in Figure 5.37. It can be seen that up to a third of the applied total load during a 10kN pulse reached the tip (Figure 5.37). Results from the measured skin friction loads for the 10kN pulse showed that very little load transfer was occurring for the skin friction measuring zone. This would suggest either that the skin friction sleeve had an initial "Dead zone" where readings were minimal until a certain load/displacement was reached or that skin load transfer occurred in some other manner rather than shear.

As for the CRP testing, the residual tip loads continued to exist throughout STN pulse loading. The variation of the residual tip loads measured after each test in Bed 3 can be seen in Figure 5.14. The STN tests did not seem to be associated with the rate of increase of residual loads seen for the CRP testing. The test results for the STN loading are more likely to be influenced by test mode (Load Control) and equipment performance. For example, the rapid unloading seen at the end of STN pulses often lead to short duration tensile loads as the system tried to follow the command signal (Figure 5.37 & 5.38). The trend seen during CRP testing for the residual load to increase continued for CRP tests carried out after STN tests (Figure 5.14). These residual loads were measured approximately 3 hours after the loading events. The variation between the load at the start of a STN pulse and that at the end (prior to disconnection) increased with increasing STN load from 0kN at 10kN to 2.56kN at 30kN. This highlights the influence of time and handling on the residual load. In turn this may have ramifications on the use and timing of cycled STN loads on a single pile at field scale, especially where direct comparison is undertaken with CRP testing.

5.5.5 Pile interface pore pressure behaviour

The pore pressures generated during STN pulse loading varied from CRP testing in that no significant change in either the tip or skin pressures were measured during the Statnamic event. The skin did show slight positive pressure (+1kPa) with a reduction to negative pressures (-2.5kPa) after loading.

Longer term monitoring of the tip showed a pressure increase after loading to a value dependent on the magnitude of the pulse load. For the 30kN pulse a maximum peak

pressure of 26.6kPa was reached 21 minutes after commencing loading. The time taken to reach peak load was also linked to the peak load magnitude, increasing from 7 minutes at 10kN up to 21 minutes for the 30kN pulse. The long term skin pore pressure monitoring showed an increase from the negative test pore pressures back to pre-test levels. This took between 76 to 157 minutes.

5.5.6 Clay bed pore pressure behaviour

During the pulse loading, the bed pore pressures appeared to be strongly influenced by the variation in chamber confining pressure. The upper units (PP1 & PP2) typically displayed large negative pressures throughout the STN pulse loading with magnitudes of up to –43kPa for a 30kN pulse, which was of similar order of magnitude as the reduction in top membrane pressure. After the pulse event, there was a tendency for positive pressure to develop but this was probably due to the chamber pressure system attempting to accommodate the pressure drop (Figure 5.38 & 5.39). Although this behaviour is linked to chamber deformation, Moller & Bergdahl (1981) showed very similar behaviour for drop hammer tests on piles installed in sand at varying densities. Their chamber consisted of rigid boundaries with pressure application via a mobile top plate. The pile was loaded using a drop hammer but it is not clear if this was mounted remotely from the chamber. The readings were obtained from pressure transducers mounted 1.5 R (10mm from pile face) from the pile.

For the mid-height transducers, negative pressures were initially encountered up to the point of peak pulse load. At this point, a sudden increase in pressure occurred (75-125ms) up to 30kPa (Figure 5.38). Again, this behaviour may be attributed to the variation in cell pressure as seen in Figure 5.39.

Although the upper and mid-height transducers seem to be heavily influenced by the cell pressure variation it was far less apparent for pressures monitored by the lower transducers (PP7 & PP8). In Bed 5, these transducers registered large positive pore pressures approximately 10ms after peak pulse load. Pressures for the transducer located closest to the pile showed increases in pressure up to +211kPa (Figure 5.39). During STN pulses in this bed, the transducers were just above the pile tip (z =1.22 to 1.35 R). An increase of only 5kPa was noted in Bed 4 where these transducers were located in advance of the pile (z =-0.88 to –0.44 R). Additionally, transducers at distances

$>1.85R$ above the tip showed only small short term positive responses. Thus, large positive pore pressures occurred above the pile tip during STN pulses but these were localised.

Long term monitoring of the bed transducers showed a rapid return to pre-test levels (2 minutes) for the upper transducers, with a more gradual dissipation for the mid-height transducers (10 minutes). The large test pressures generated close to the tip dissipated over a period of 3 to 4 hours.

5.5.7 Pile and clay bed inertial behaviour

The measured pile acceleration from Bed 5 where an accelerometer was installed in the pile is shown in Figure 5.32. The small variation in acceleration at 50ms was associated with the initiation of STN loading. The load began to increase with very little displacement and velocity until approximately 60ms where it increased notably causing the variation in acceleration up to 80ms. The peak positive accelerations were associated with the rapid increase in load and velocity towards peak velocity where the acceleration reduced to zero. The pile then underwent rapid unloading and reduction in velocity resulting in negative accelerations. The sign of both the velocity and acceleration is defined as positive in the downward direction. The large variations in acceleration at the end of the test (130 to 160ms) were associated with the pile loading system trying to slow down the unloading to avoid tension. This resulted in the pile having upward components of velocity. The acceleration trace minus the initial and post test perturbations was similar to that for a prototype test (Figure 5.32). The magnitude of the peak pile acceleration increased with increasing STN pulse load (± 32 m/s^2 at 30kN).

The vertical accelerations in the bed were usually monitored by two accelerometers (Section 4.2.8) mounted at typical radial positions of $3.00R$ and $6.63R$ but at different heights in different beds. The exception to this was Bed 5 where one of the accelerometers was mounted in the pile. For Bed 3, the bed accelerometers were mounted at their highest levels above the pile tip (z=7.95 to $8.29R$) as shown in Figure 5.40a & b. As can be seen, the accelerations measured were very noisy with large accelerations apparent prior to the STN pulse.

Based upon the apparently noisy data, a cut off filter at 1000Hz was activated as part of the Kistler accelerometer conditioning equipment. Cut off at 1kHz was chosen based upon frequency analysis of the accelerometer time histories using a fast Fourier transform. Minimal frequency content was identified above 600Hz prior to filter activation. Unfortunately, repeat testing was not undertaken with filtered acceleration outputs from transducers installed at the higher level.

The remaining inertial bed data was acquired with the accelerometers mounted below the pile tip (z =-1.01 to –0.83 R). The data for these points varies from that above in that the accelerations noted further away from the pile exceeded those closer to the pile (Figure 5.40c & d). The measured accelerations further from the pile also remained predominantly positive whilst those closer were mainly negative. As for the upper accelerometers, the accelerations did not return to low values after the pulse event. This was initially thought to be a baseline shift sometimes associated with the permanent movement of the accelerometer during the pulse event. It would appear that the accelerometers were influenced by something other than acceleration. Based on the sealing arrangements of the accelerometers with their bases exposed to the clay bed, it is possible that the large pressures near the tip during the pulse loads were affecting the accelerometer readings. The measured acceleration was then a superposition of the actual acceleration measured on that induced by pressure change. This would also explain a slow reduction of the accelerometer zero error after a pulse event related to pile tip load reduction. The accelerometers used in this study had base sensitivities of 0.1m/s^2 at 250μstrain. The effect of pressure on the accelerometer readings was not checked during this study as it was deemed inappropriate to induce potentially damaging loads on the units. It is recommended for further studies that the units be completely sealed in a pressure rated enclosure.

The bed accelerometers were intended to give information about the inertial soil resistance to Statnamic load and to help plan the transducer deployment during the full scale pile study. In view of this, it was decided to proceed with accelerometer analysis for transducers in the upper positions where the maximum variation of pressure was only a quarter of that near the pile tip.

To aid the positioning of radial accelerometers in the field, the variation of vertical acceleration with radial distance from the pile was investigated. As only two accelerometers were available, the pile was used as the initial acceleration source. It was found that the data adequately fitted a two parameter exponential decay of the form:

$$\frac{\ddot{x}_l}{\ddot{x}_p} = 1.257e^{-0.226R} \qquad (5.6)$$

Where

$\ddot{x}_l$ = the local bed acceleration

$\ddot{x}_p$ = the peak pile acceleration

R = the pile radius

From this it was found that very little useful information would be obtained by exceeding a radial distance of 15R with accelerometer installation. It is acknowledged that this relationship is based on limited noisy measurements but this was considered adequate for positioning purposes.

5.5.8 Boundary measurements

As for the CRP tests in Bed 5, an earth pressure cell mounted at the base of the chamber directly below the pile was monitored during pulse loading. The measured earth pressure at the chamber base can be seen in Figure 5.41 for pulse loads compared with low rate CRP tests. Pulse loads from 10 to 15kN were associated with low permanent deflection and showed very similar behaviour throughout. The earth pressures associated with the pulse loads from 10 to 20kN did not exceed those recorded for the low rate CRP tests. As base separation reduced and STN pulse loads increased, the measured base pressures exceeded the pressures associated with the low rate CRP tests. As increasing pile tip loads as well as reducing base separation were occurring together, it is difficult to comment on the influence of pulse loads on the base pressure increase.

5.5.9 Initial prediction of equivalent static pile behaviour from rapid load testing

A prediction was made of the static pile capacity from the pulse load testing results using the rate model and parameters discussed in Section 5.4. Predictions were made for the static equivalent total pile capacity and the shaft resistance using the parameters presented in Table 5.2 with Equation 5.7. The results have been corrected for pile inertia but no attempt has been made to incorporate soil inertia.

$$F_{static} = \frac{F_{STN} - Ma}{1 + \alpha(v)^{\beta} - \alpha(10^{-5})^{\beta}} \tag{5.7}$$

Where

F_{static} = the derived static pile resistance

F_{STN} = the total measured Statnamic load

α & β = damping coefficients

M = pile mass

a = pile acceleration

v = pile velocity

The results for derivation of the total static pile load from a 30kN pulse load can be seen in Figure 5.42. Also presented is a static derivation based upon parameters deduced from high speed triaxial testing of the KSS material (Balderas-Meca, 2004). The rate parameters used for this were α=0.77 and β=0.2. In the case presented (Bed 4, 30kN), the derived static resistance in the elastic zone is very similar to that for the measured static (CRP at 0.01mm/s) up to approximately 8kN (57% ultimate measured static capacity). From this load onwards, the derived static resistance slightly under predicts the measured pile stiffness (exploded in Figure 5.42). This is similar to the load at which the pulse loads exceeded the measured static as discussed in Section 5.5.2. This under prediction was found in the 30kN pulse for all test beds. On reducing the magnitude of the pulse load, the under prediction also reduced such that the derived and static resistance where equal throughout the elastic zone for pulses of 20kN and below. This was to be expected as the lower the STN pulse the lower the pile velocity.

Comparison with the values of α=1.0 and β=0.2 suggested by Randolph & Deeks (1992), shows a better prediction than the parameters derived from triaxial testing but also under predicts in the elastic zone.

The predicted static pile resistance in the plastic zone gradually increased with increasing pile penetration as seen in the measured CRP tests. On reaching maximum penetration associated with STN unloading, the predicted ultimate static load increased very rapidly (spiked). This was caused by rapid unloading, as it was more difficult to control the hydraulic loading system during this portion of the test. The peak load corresponded to a point of very low velocity and thus little rate dependent component of load was removed.

For the equivalent static pile response, derived from the 30kN pulse load, the maximum deviation from the measured static resistance was +4.5% to –12.3%. Comparison was made with the 30kN pulse load, as this was the test located closest to a 0.01mm/s CRP test where significant permanent pile penetration occurred. For the majority of the plastic zone, the static equivalent pile resistance was over predicted by up to 17.2% using the parameters derived from triaxial testing. The static equivalent resistance was also deduced for the lower magnitude pulses with derived load-displacement curves very similar to those derived from the 30kN tests. For the 10kN and 15kN pulses, the derived static load remained within the elastic zone of the pile with no apparent yield.

The same prediction of static behaviour was also undertaken for the derived shaft resistance. As shown in Figure 5.43, the derived static shaft resistance-penetration curves are of a very similar form to the total load curves. What differs is that the derived static shaft resistance does not follow the gradual reduction in resistance noted for the measured shaft resistance from the 0.01mm/s CRP tests.

Transducer Positions	*Range of Typical Positions*		
	Vertical Position (mm)*	*Radial Position (r/R)*	*Position Relative to Pile Tip (z/R)*
Upper (PP1-3)	246 to 309	1.43 to 4.59	10.66 to 16.49
Mid-height (PP4-6)	508 to 536	2.06 to 5.06	4.57 to 8.70
Lower (PP7-8)	741 to 768	1.94 to 5.14	-1.29 to 2.72

**Defined below clay bed upper surface.*

Table 5.1, Typical clay bed transducer positions.

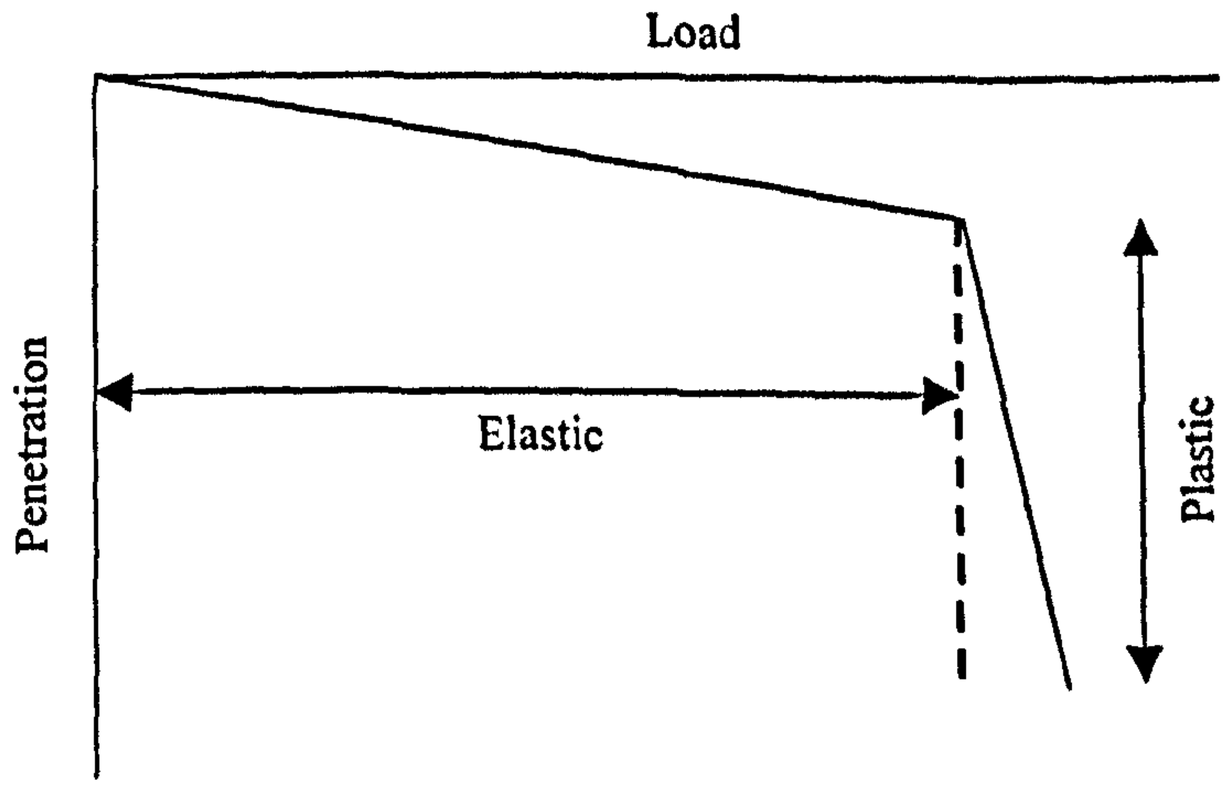

Figure 5.1, Definitions of zones of pile behaviour.

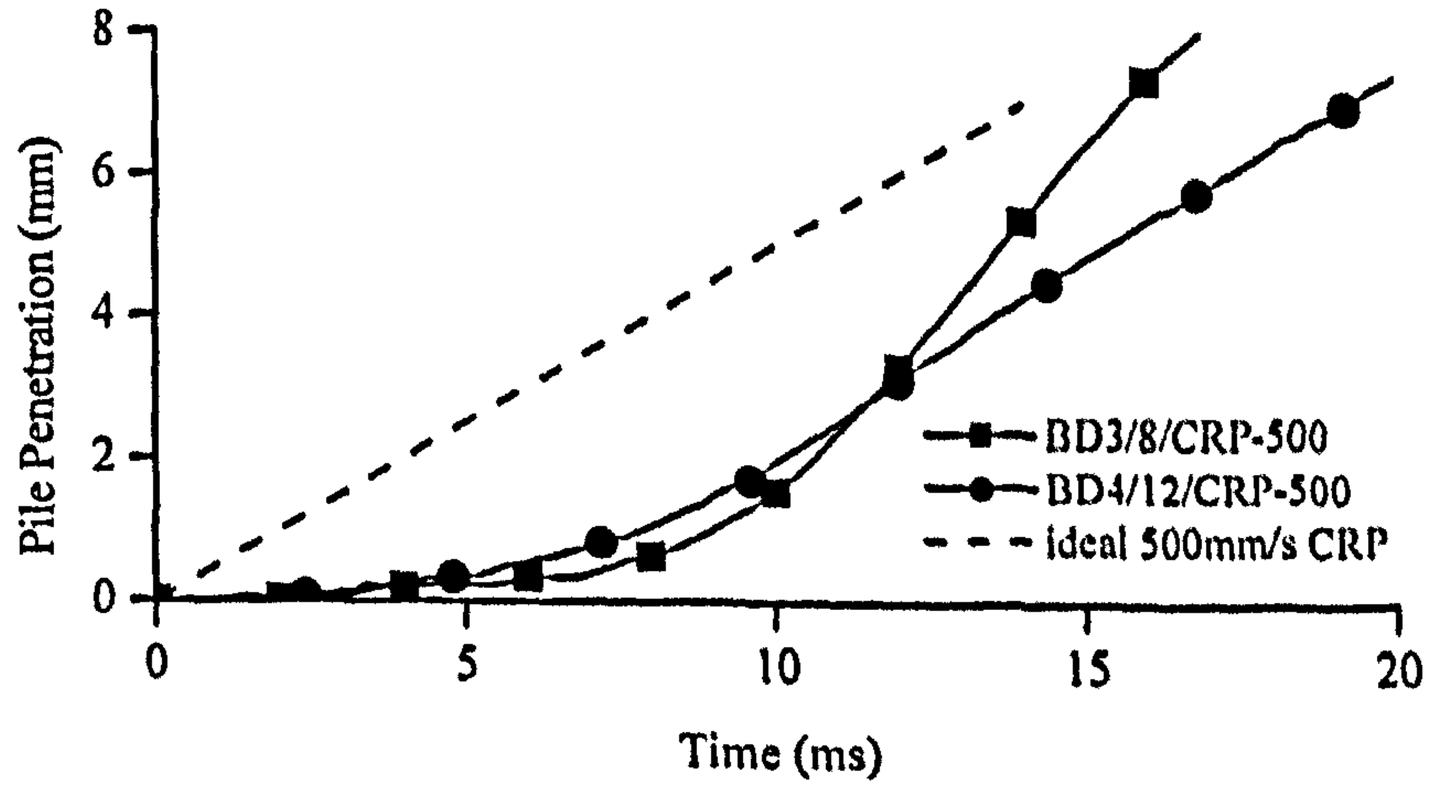

Figure 5.2, Comparison of rate of change of pile penetration during a 500mm/s CRP test.

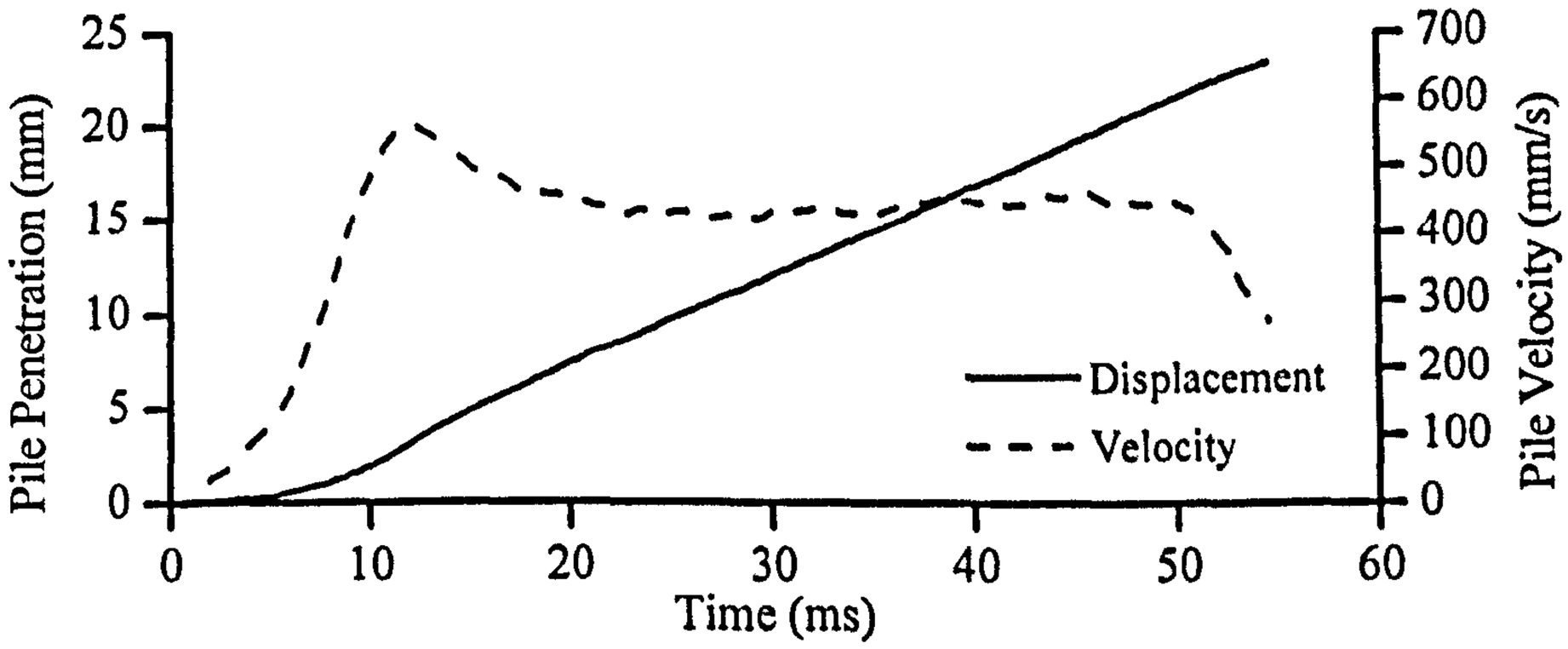

Figure 5.3, Comparison of pile velocity and penetration during CRP at 500mm/s (BD4/12/CRP-500).

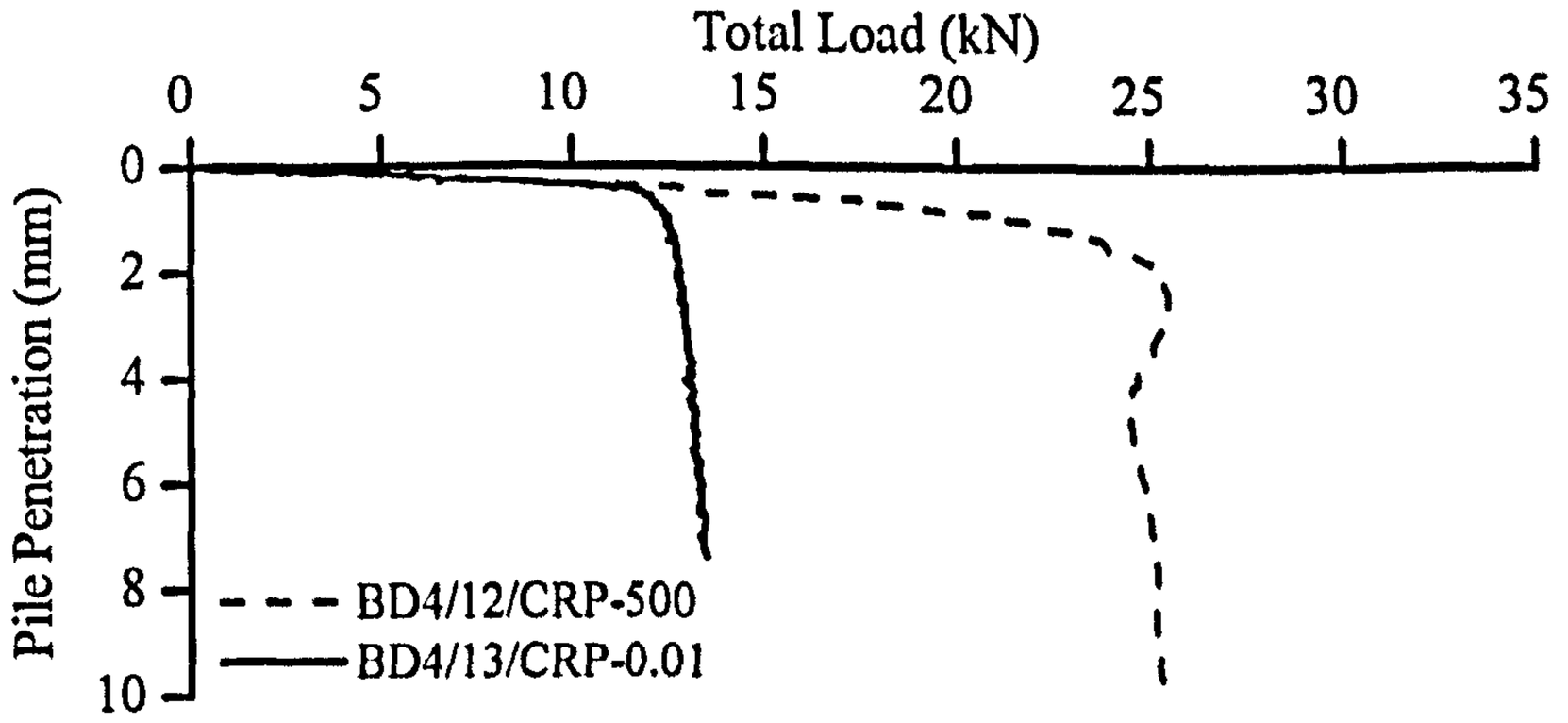

Figure 5.4, Total pile resistance at 0.01mm/s & 500mm/s during CRP testing.

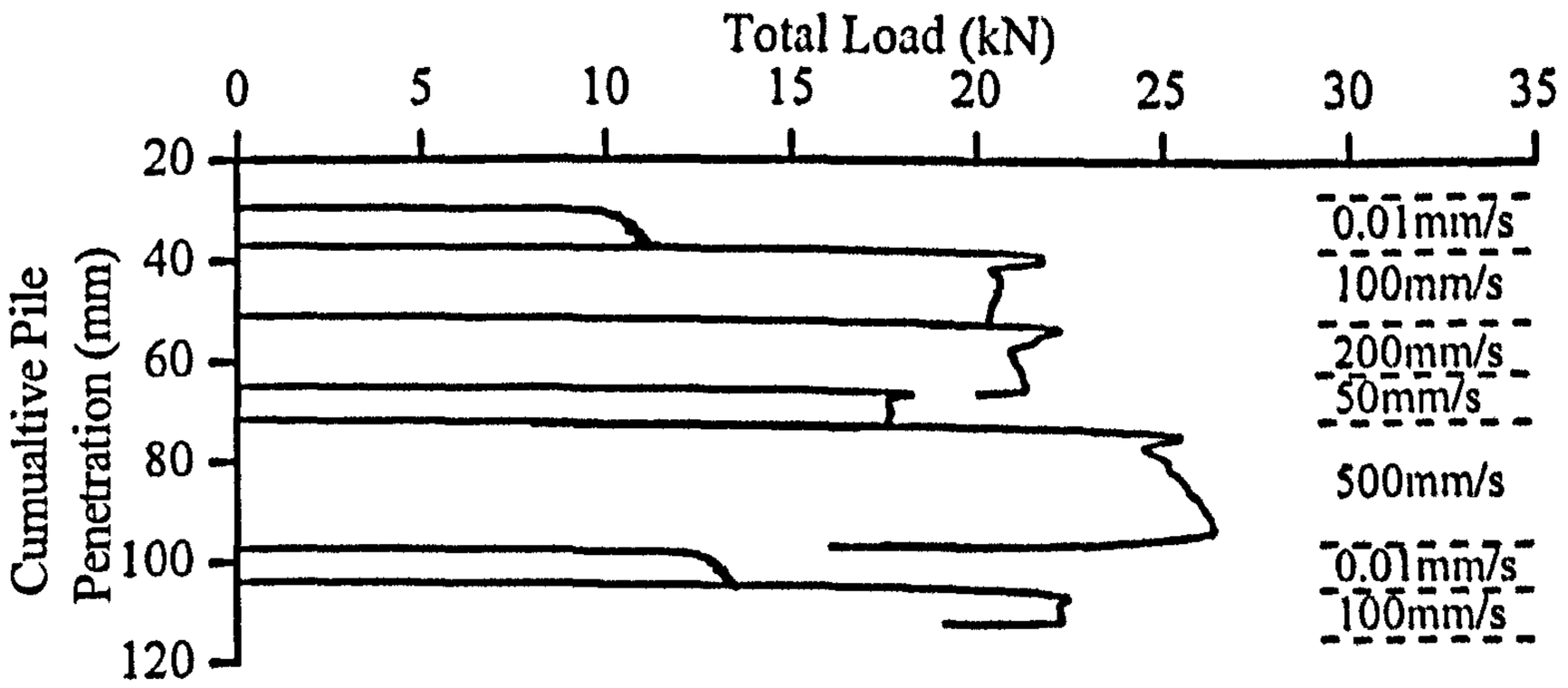

Figure 5.5, Consecutive CRP tests at different rates in Bed 4.

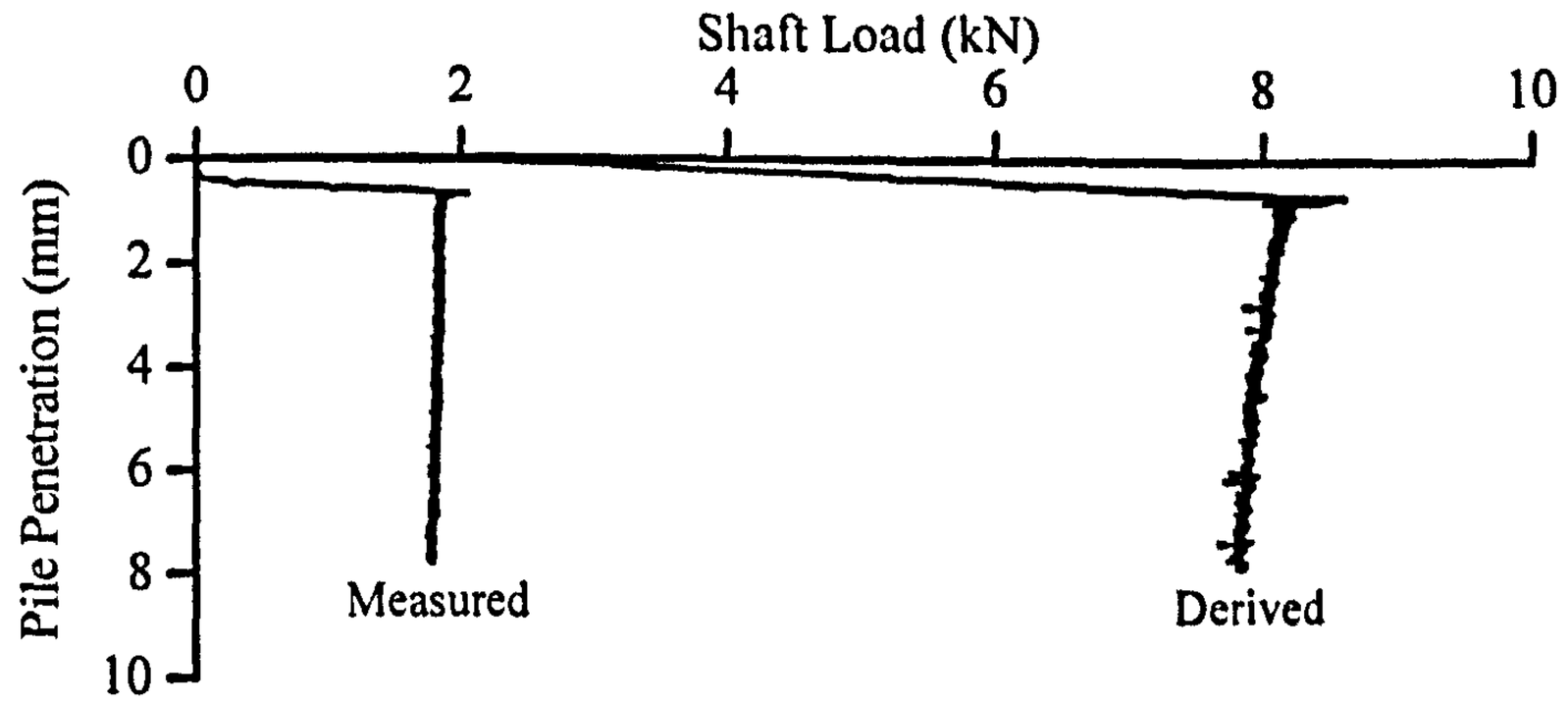

Figure 5.6, Measured and derived shaft loads for 0.01mm/s CRP (BD3/17/CRP-0.01).

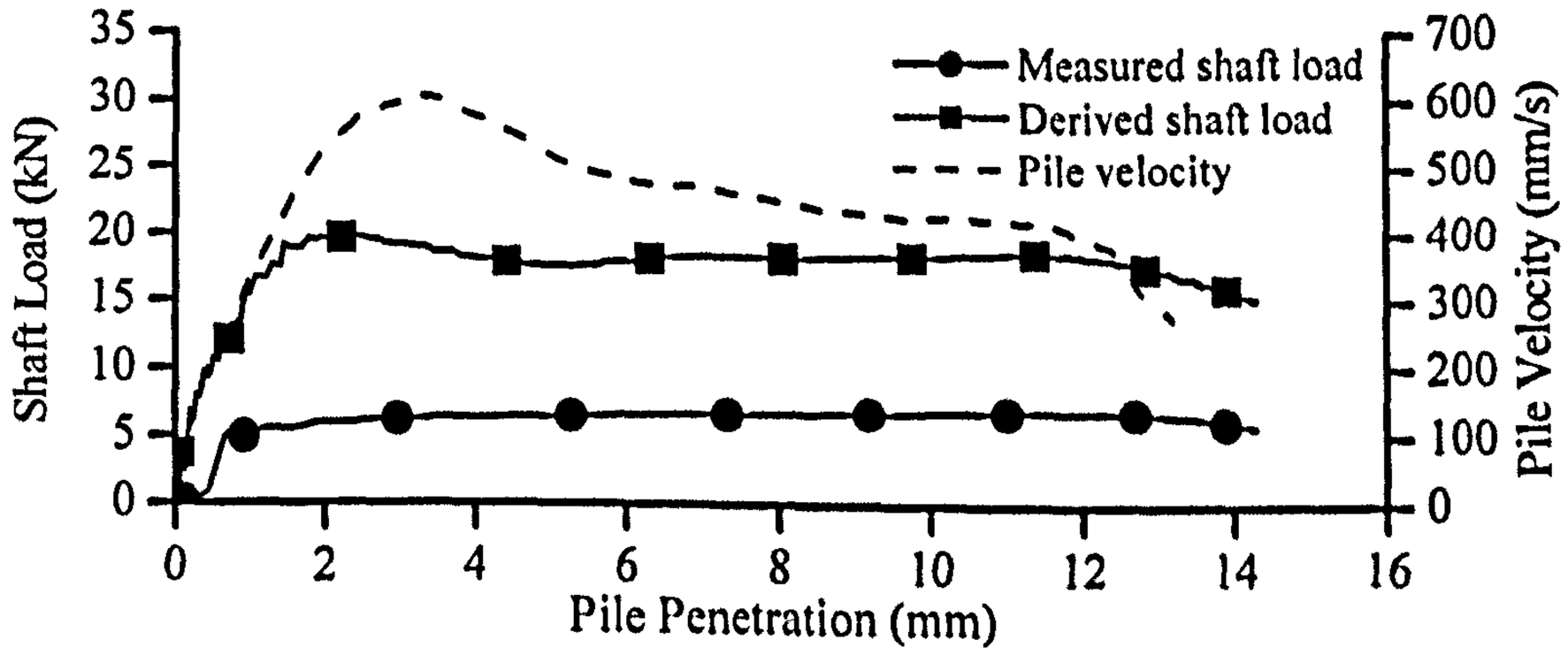

Figure 5.7, Effect of velocity variation on shaft load for 500mm/s CRP (BD5/9/CRP-500).

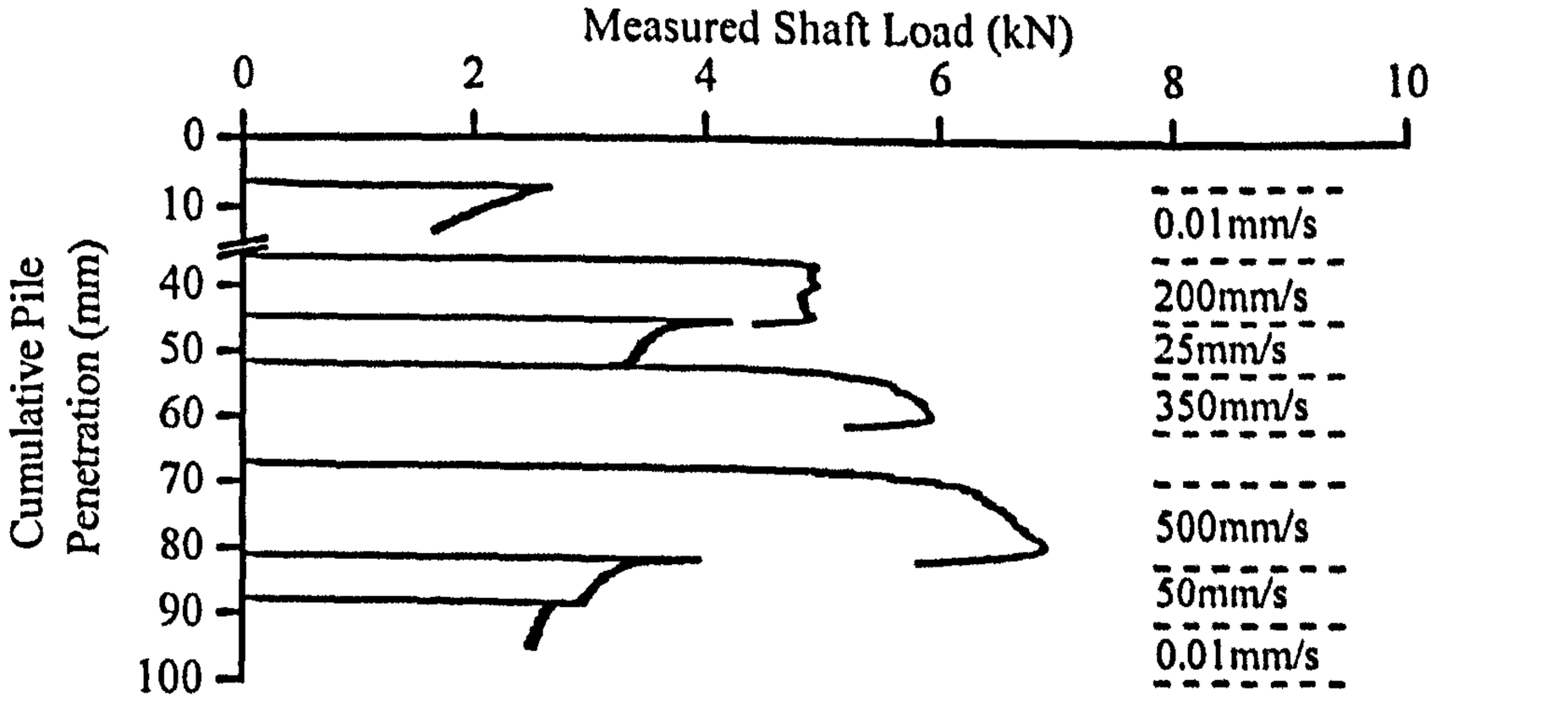

Figure 5.8, Measured shaft friction load for consecutive CRP tests in Bed 5.

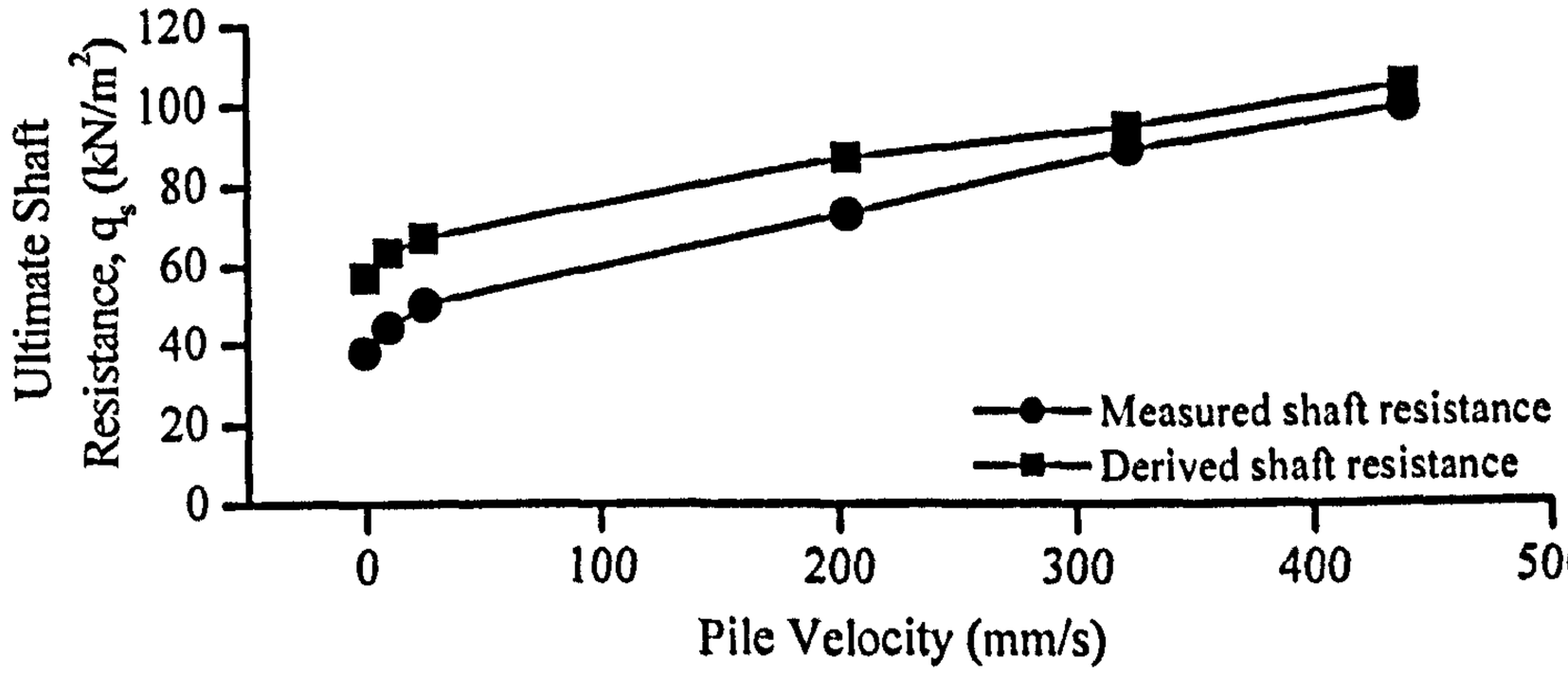

Figure 5.9, Comparison of measured and derived ultimate shaft resistance for CRP at different rates (Bed 5).

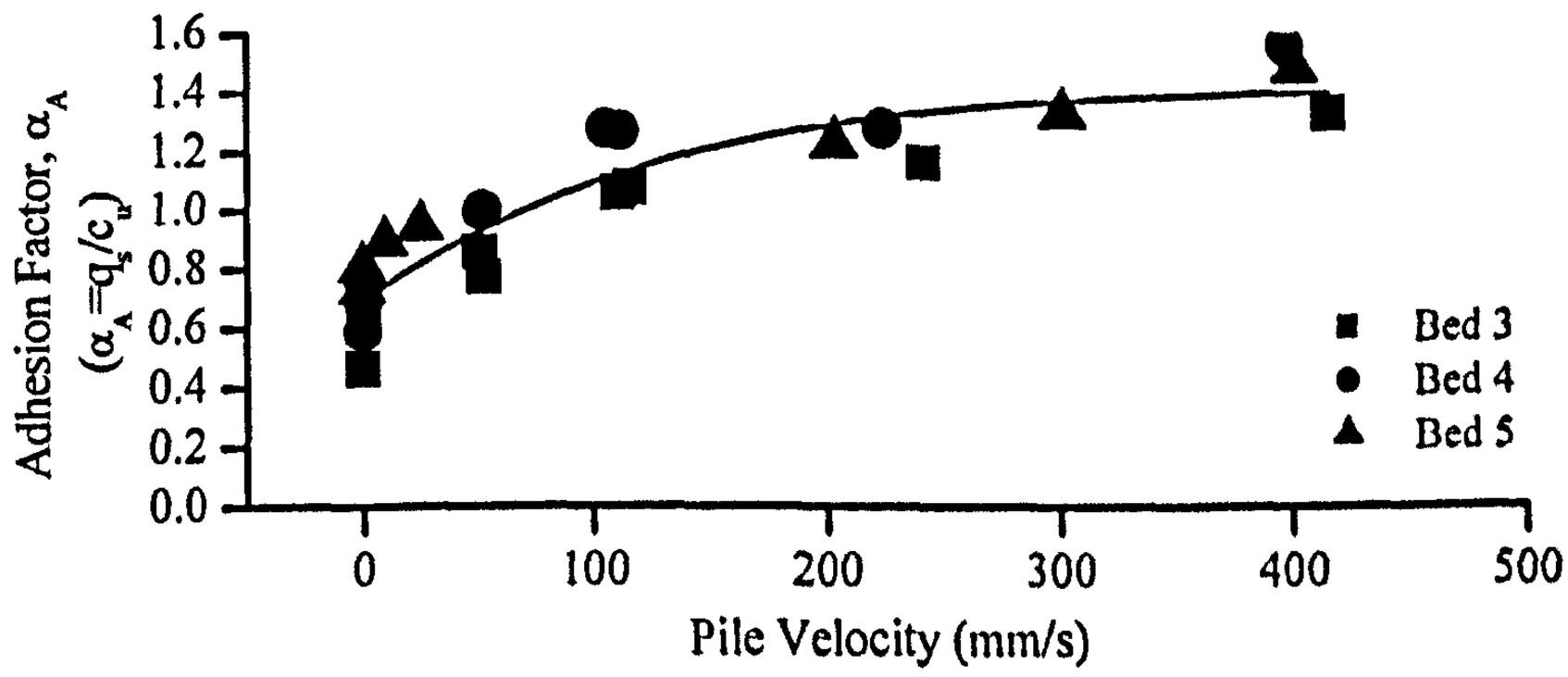

Figure 5.10, Variation of shaft adhesion factor with increasing velocity.

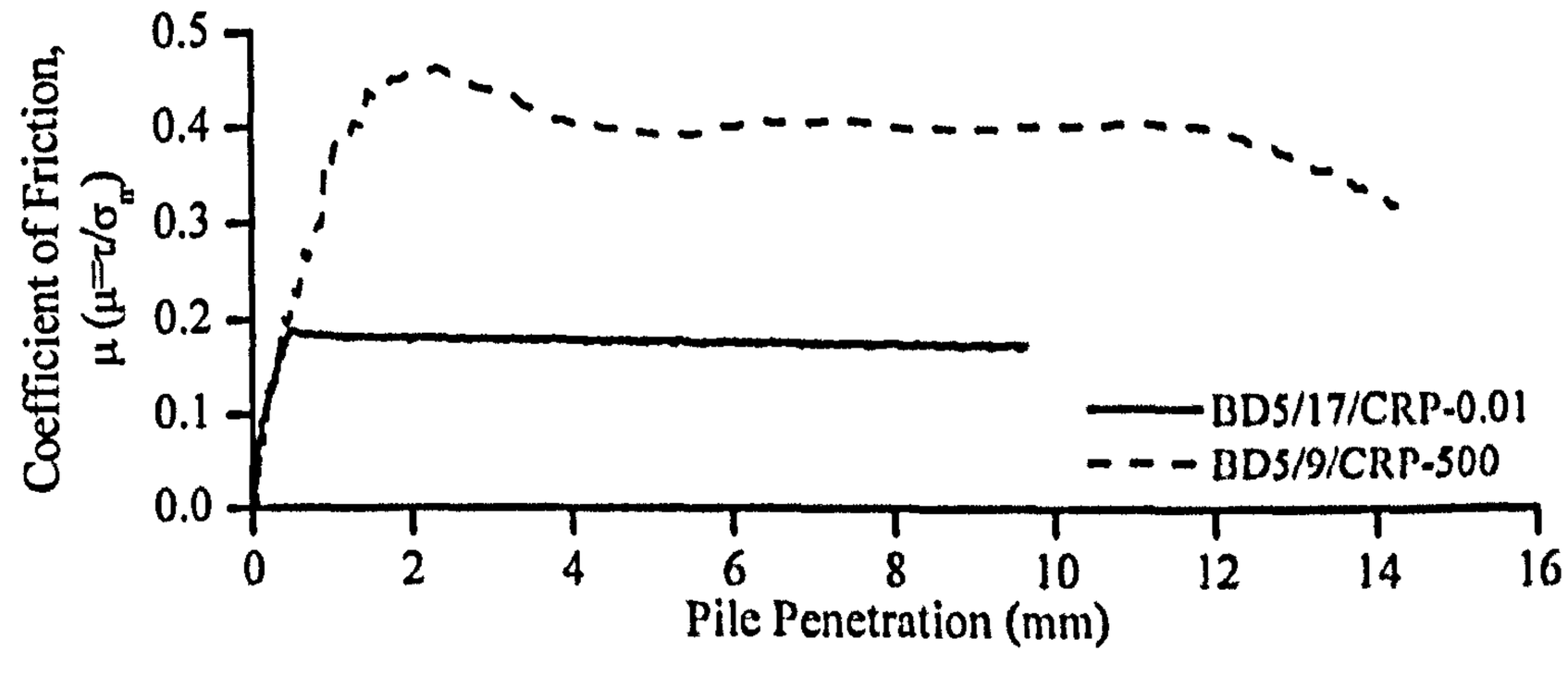

Figure 5.11, Coefficient of friction during CRP at 0.01mm/s & 500mm/s.

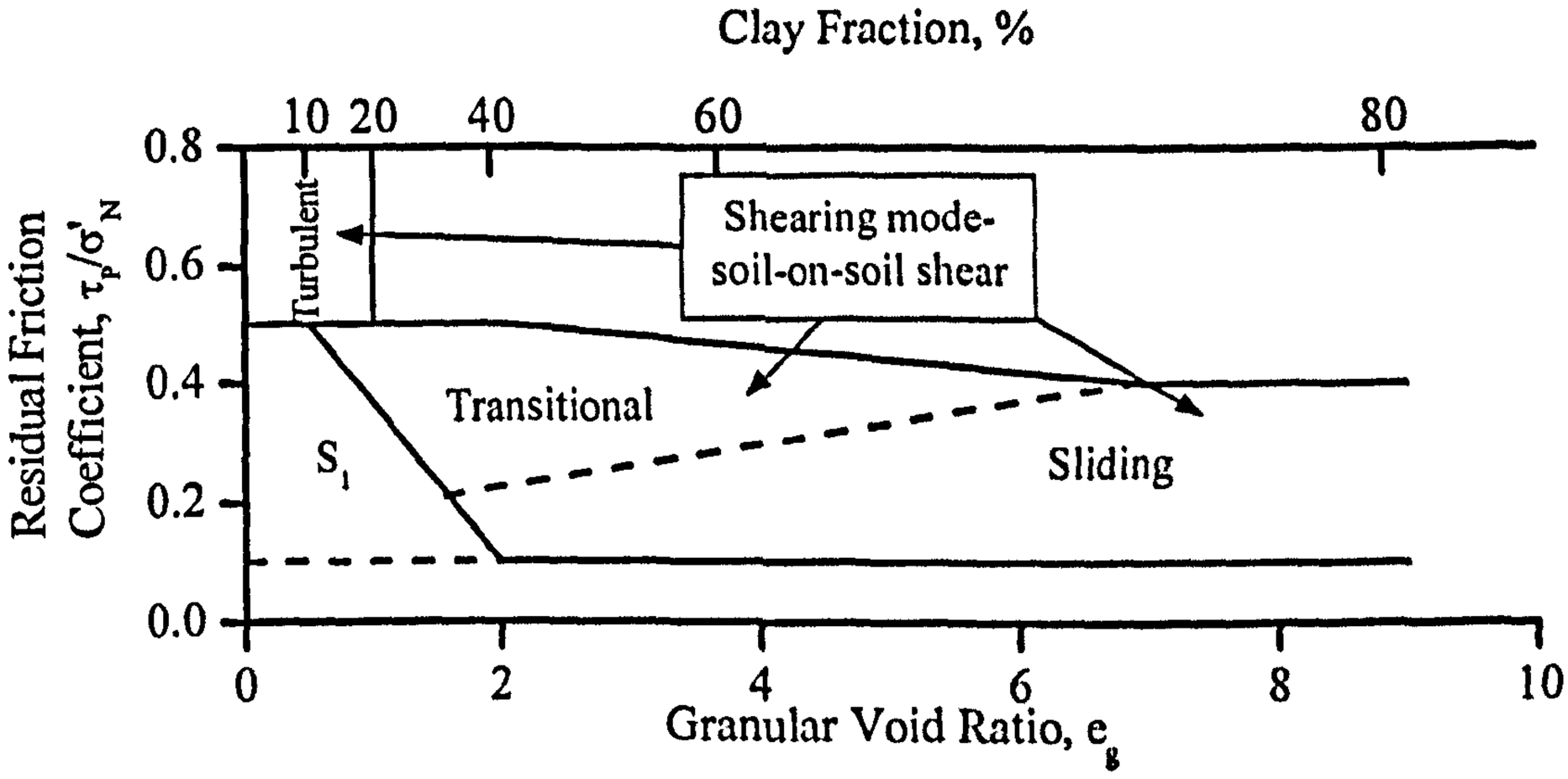

Figure 5.12, Possible interface shear by sliding in clays (Lemos & Vaughan, 2000).

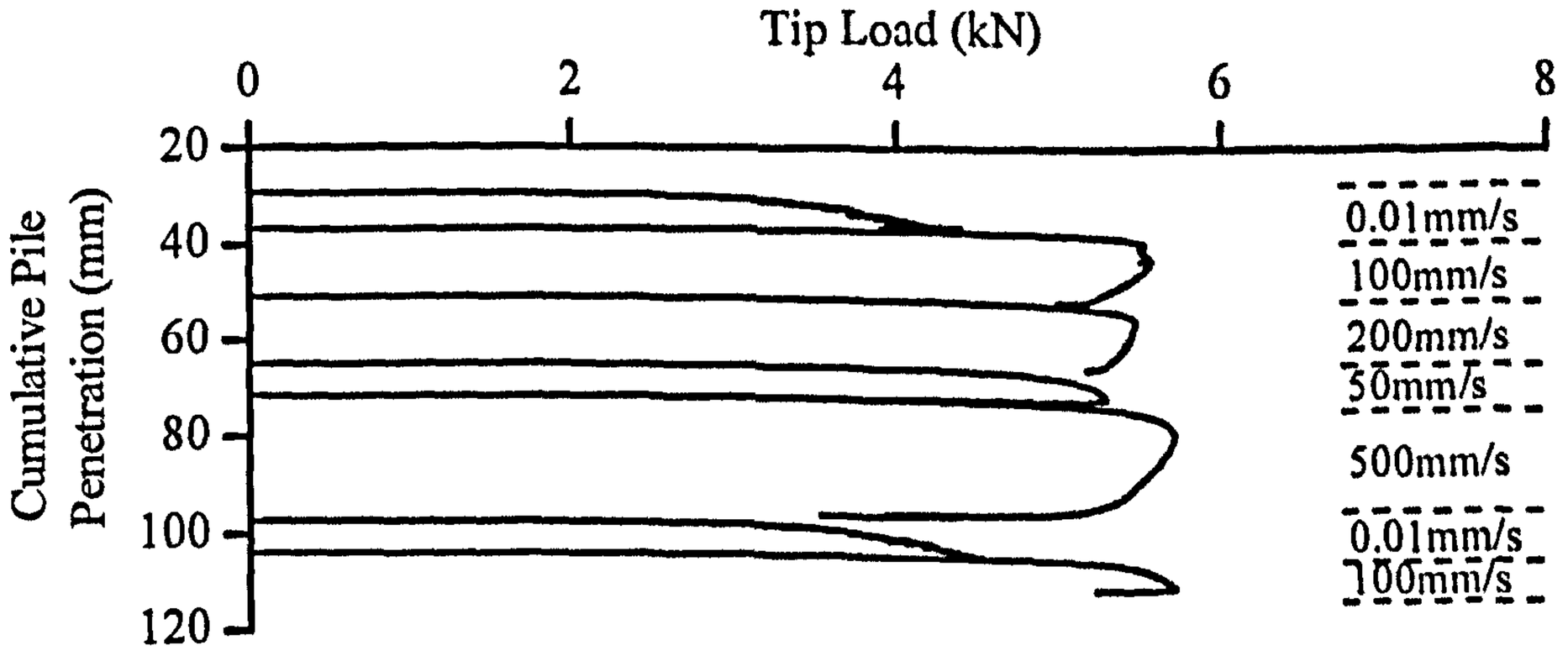

Figure 5.13, Measured tip loads for consecutive CRP tests in Bed 4.

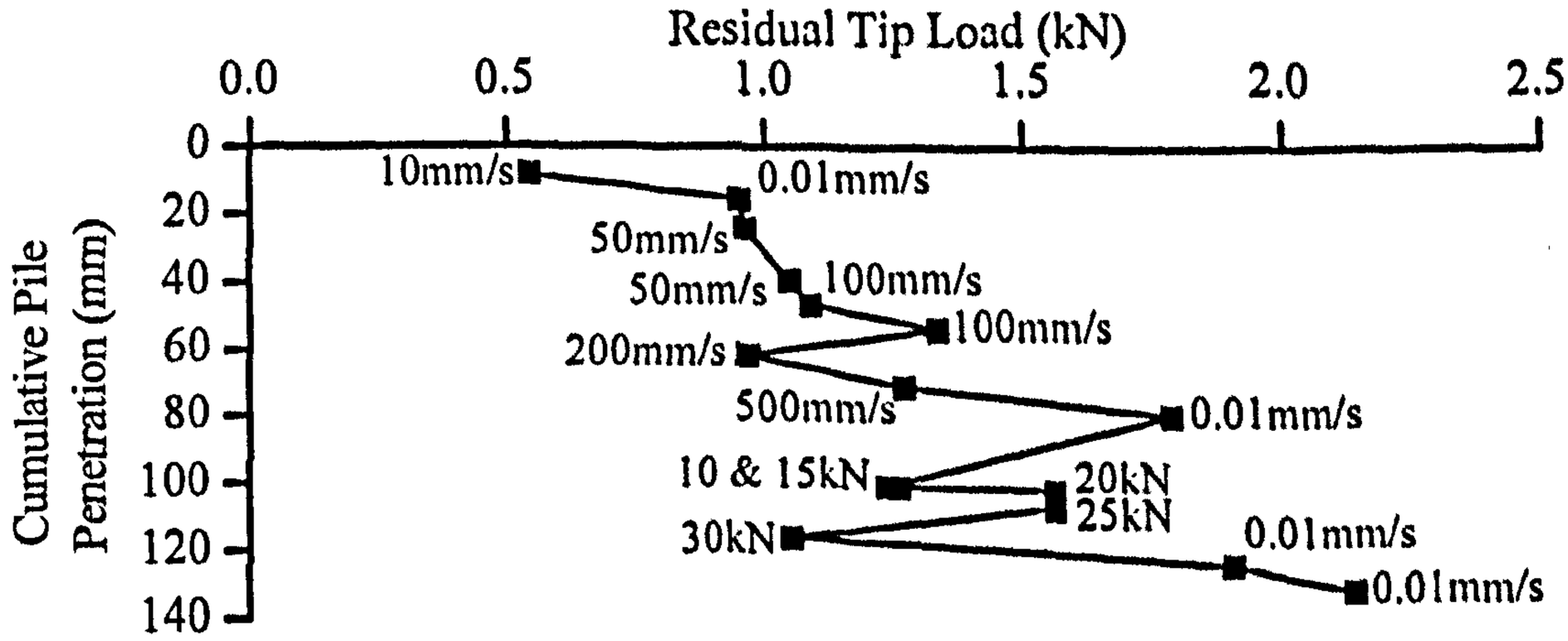

Figure 5.14, Measured residual tip loads with increasing penetration. Measured after each test (Bed 3).

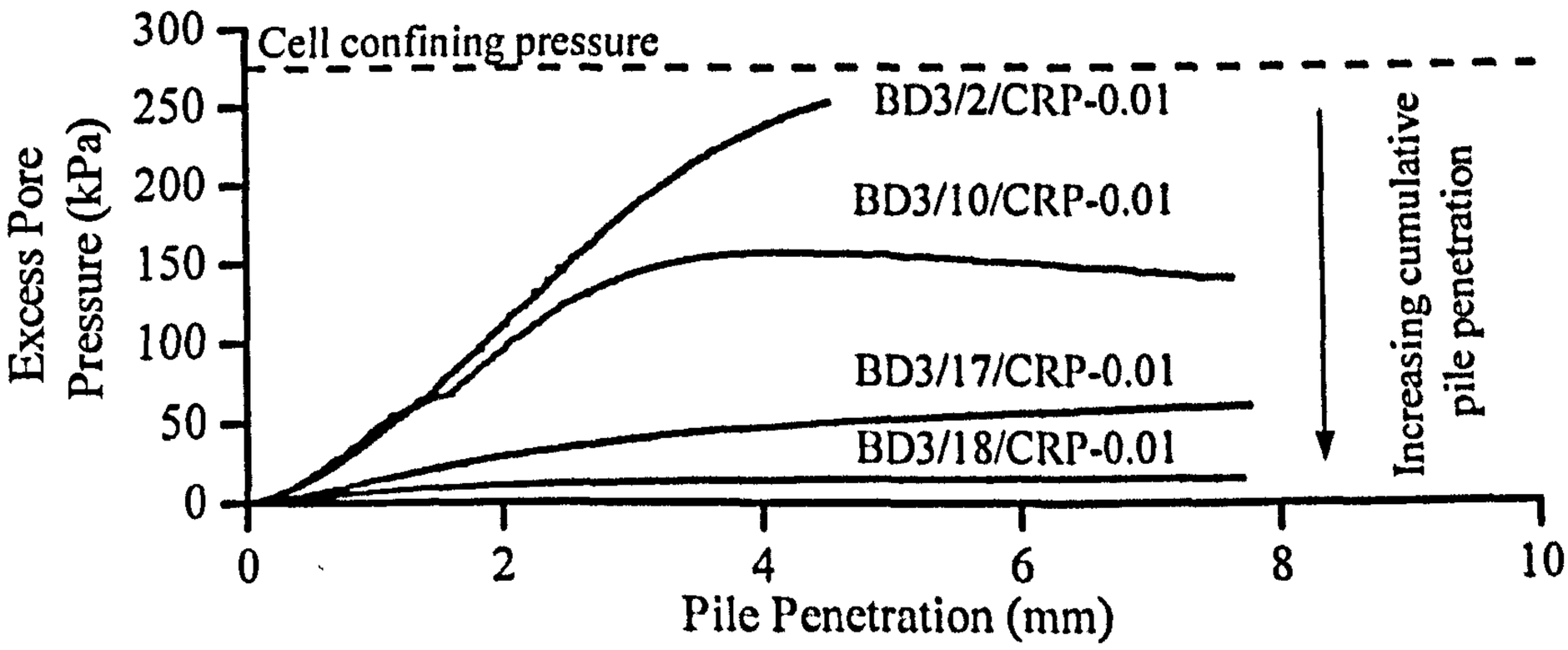

Figure 5.15, Variation in excess tip pore pressure with increasing pile penetration for CRP at 0.01mm/s.

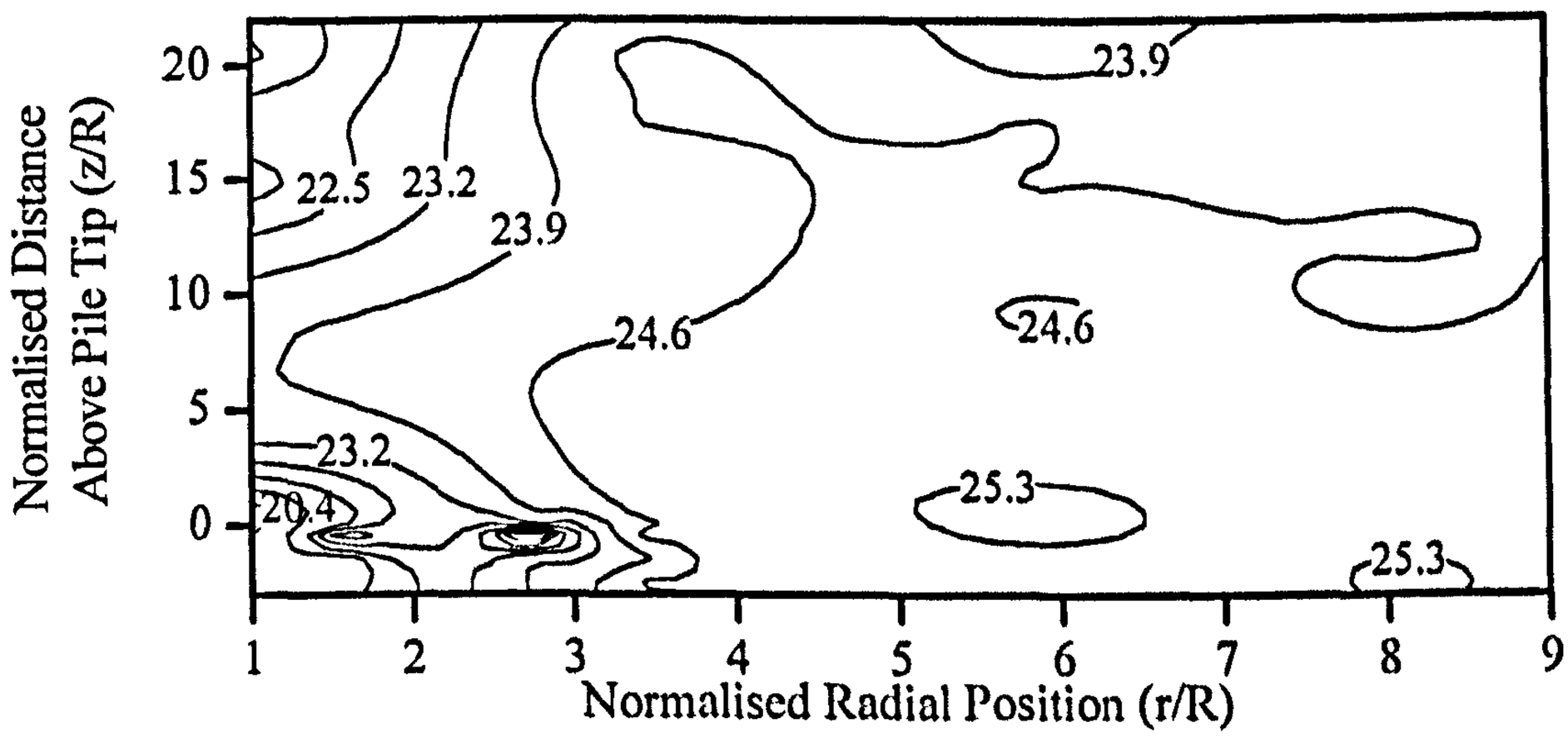

Figure 5.16, Clay bed moisture content distribution after testing (Bed 5).

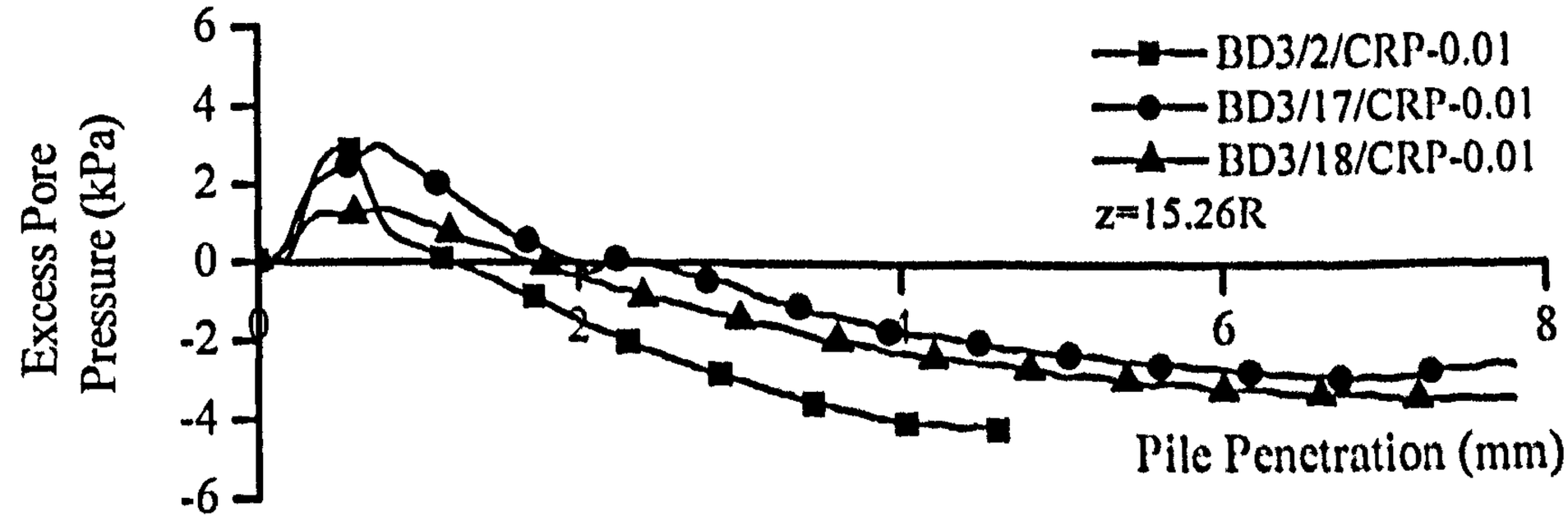

Figure 5.17, Variation in excess pile skin pore pressure for CRP at 0.01mm/s.

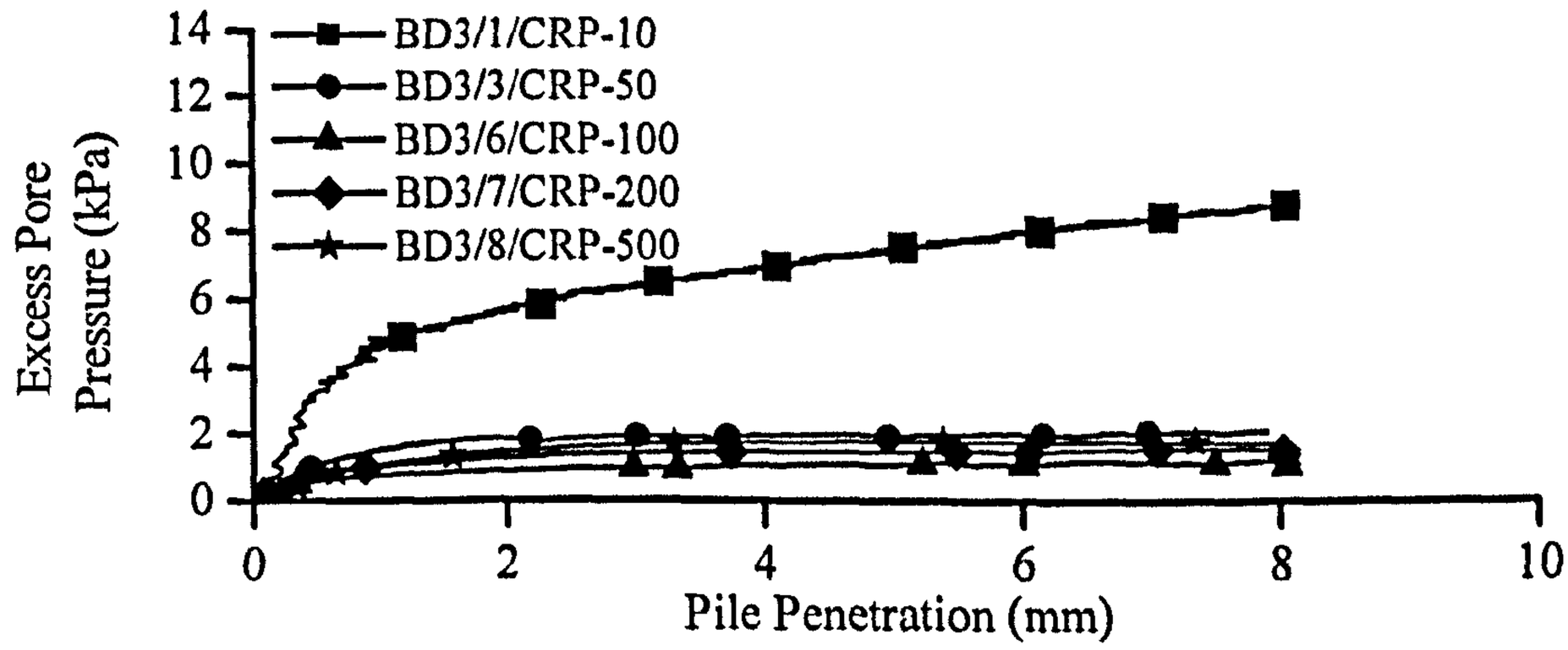

Figure 5.18, Effect of increasing pile velocity on pile tip excess pore pressure.

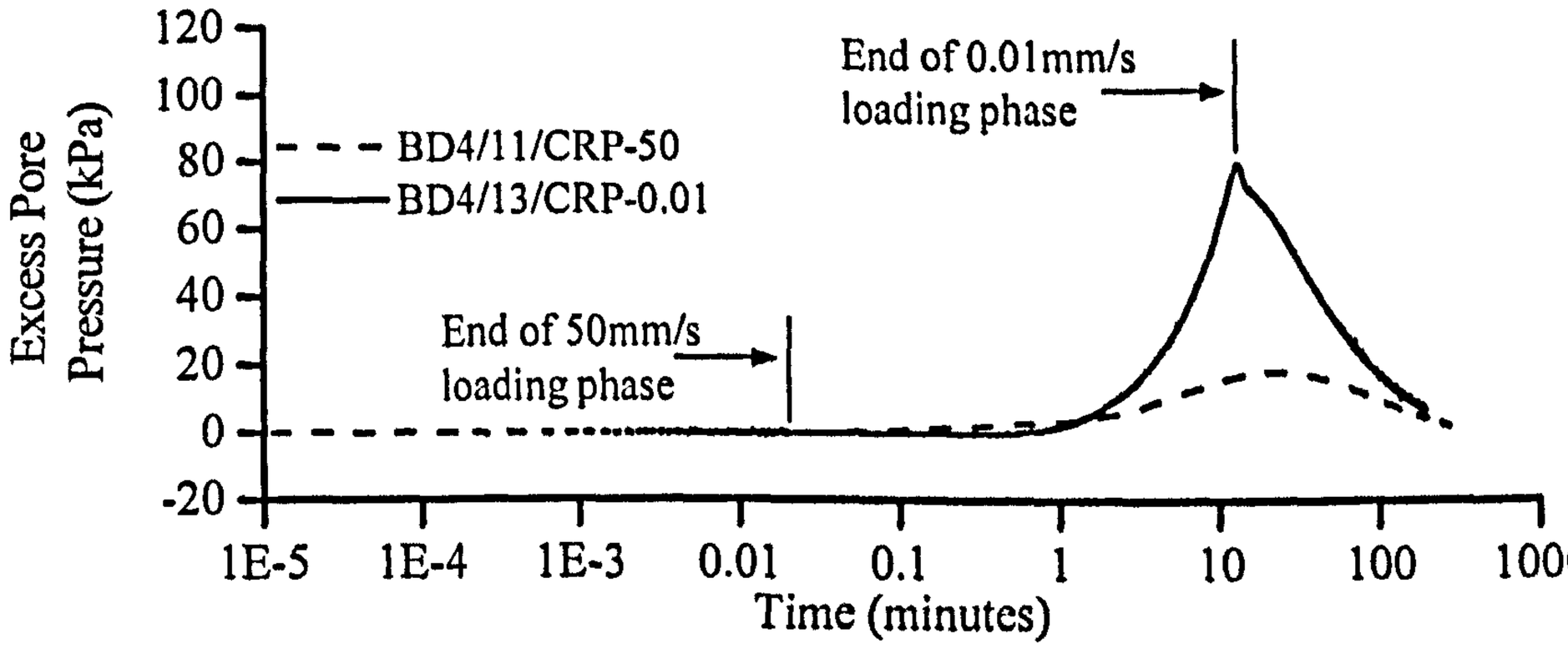

Figure 5.19, Long term monitoring of pile tip excess pore pressure for CRP tests at 0.01mm/s & 50mm/s.

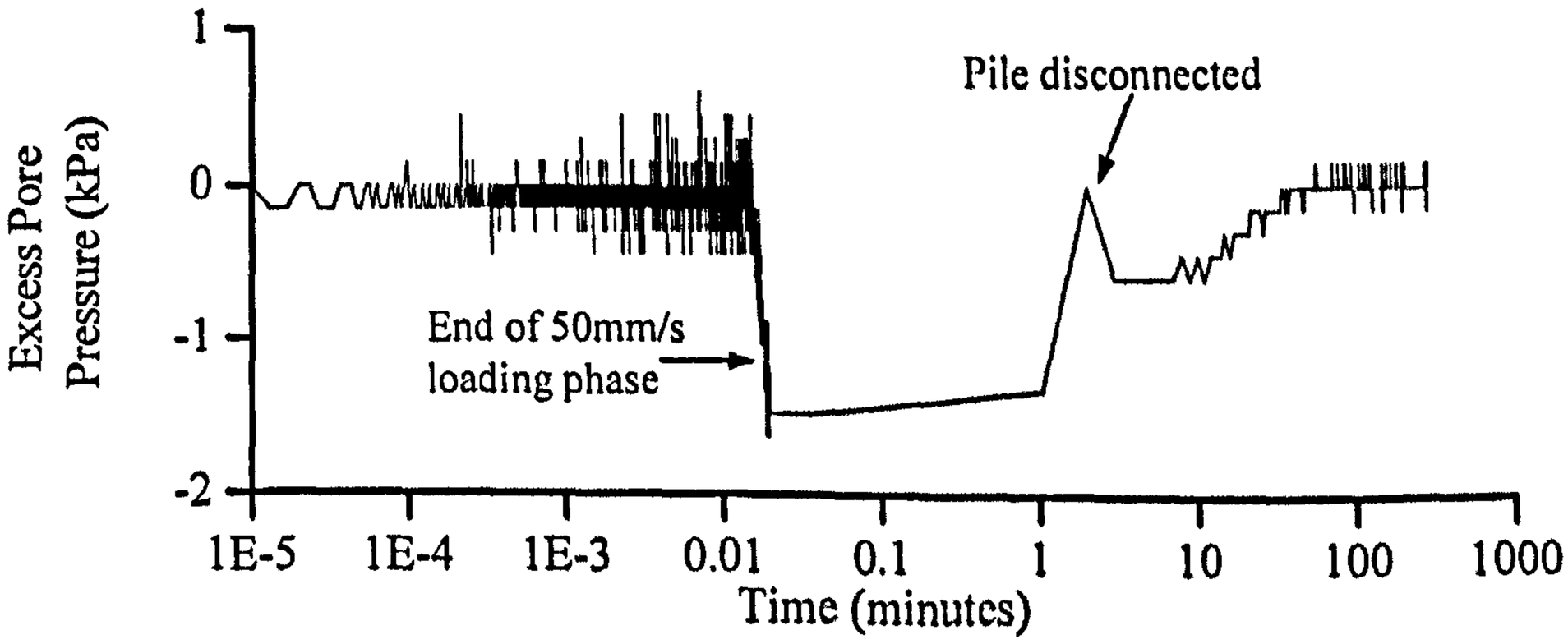

Figure 5.20, Long term monitoring of pile skin excess pore pressure for CRP at 50mm/s (Bed 4).

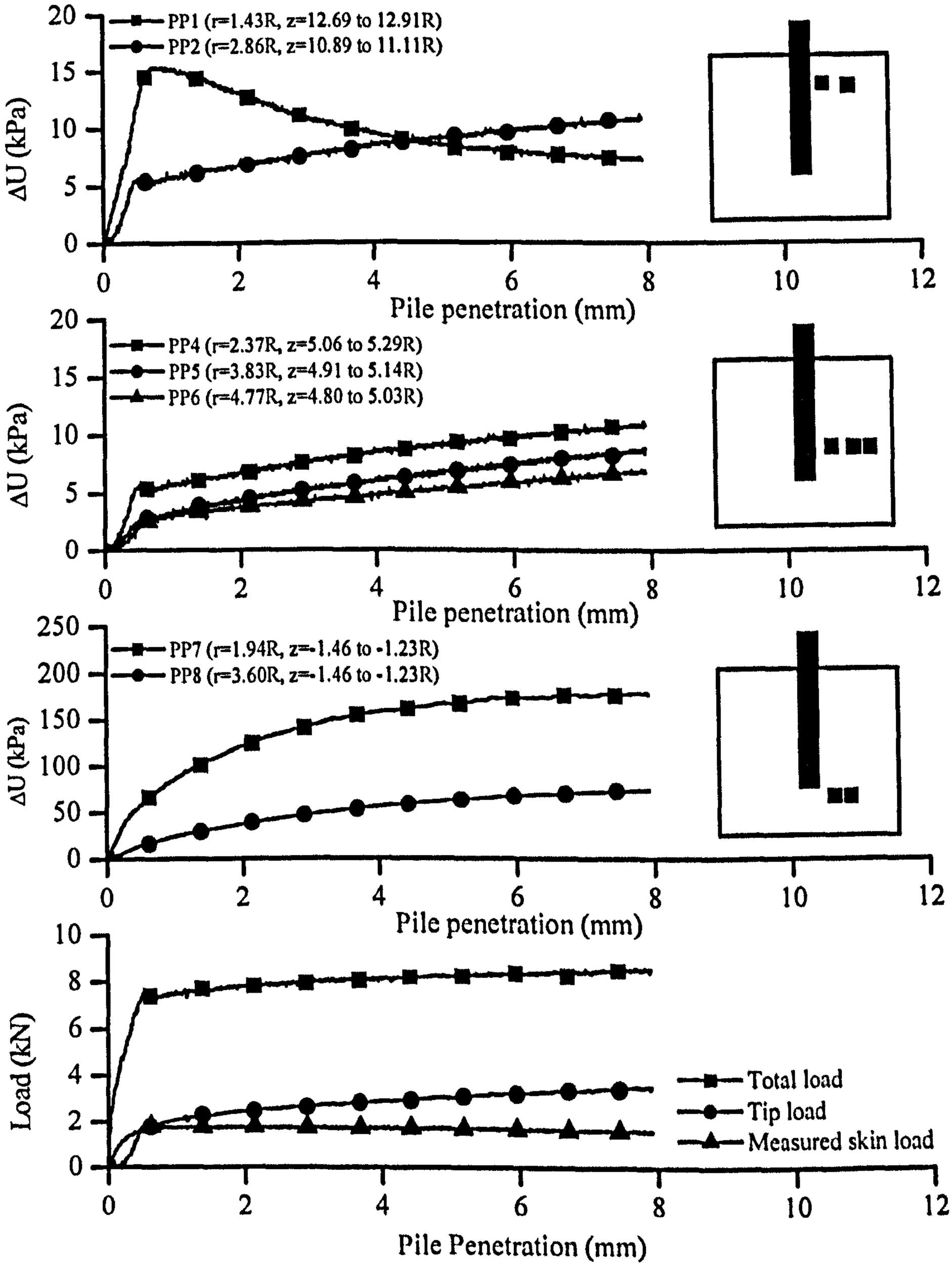

Figure 5.21, Comparison of bed pore pressure behaviour during CRP at 0.01mm/s with pile loads shown for reference (BD3/2/CRP-0.01). Inset schematics show approximate transducer positions relative to the model pile.

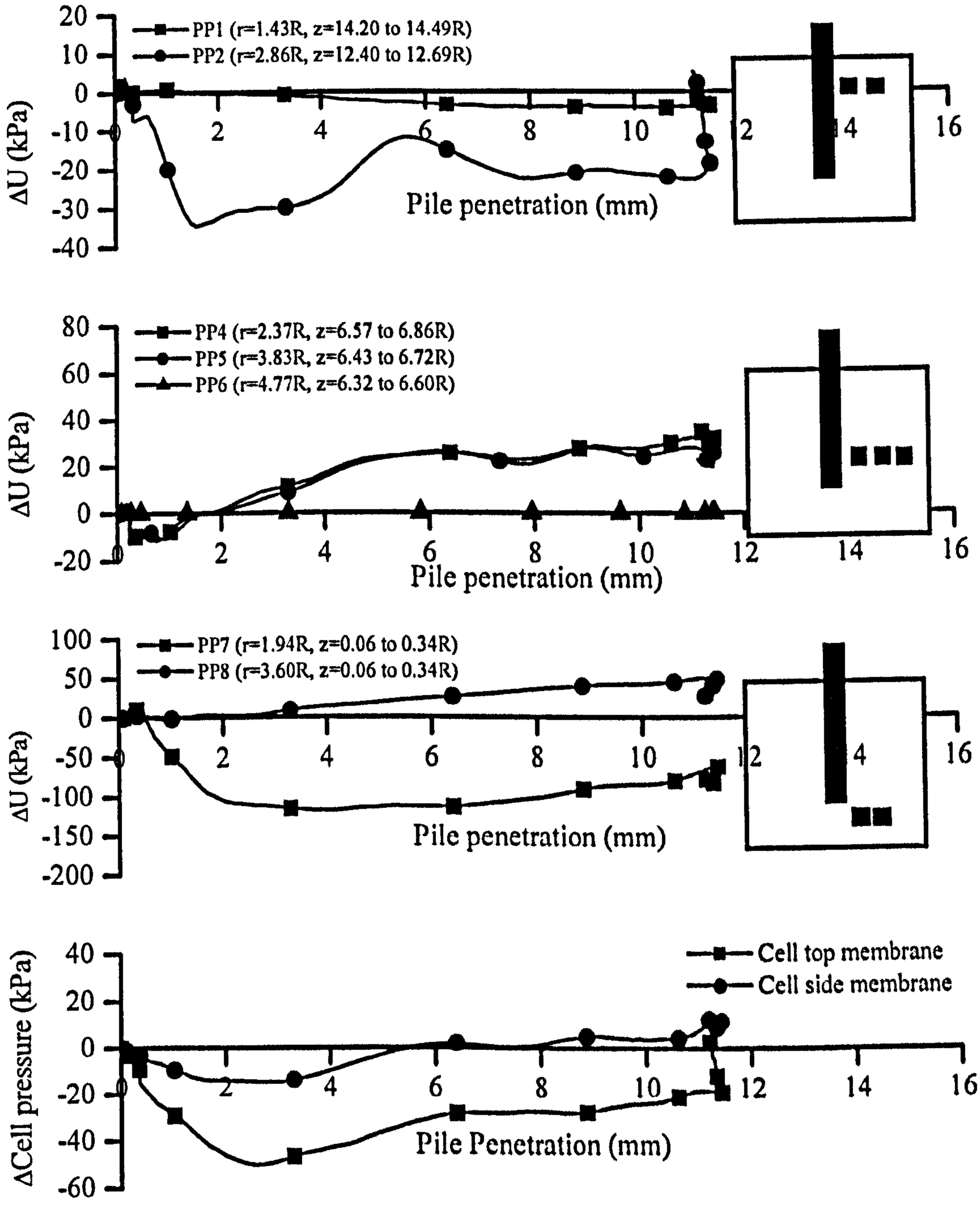

Figure 5.22, Comparison of bed pore pressure behaviour during CRP at 500mm/s with cell pressure change shown for reference (BD3/8/CRP-500).

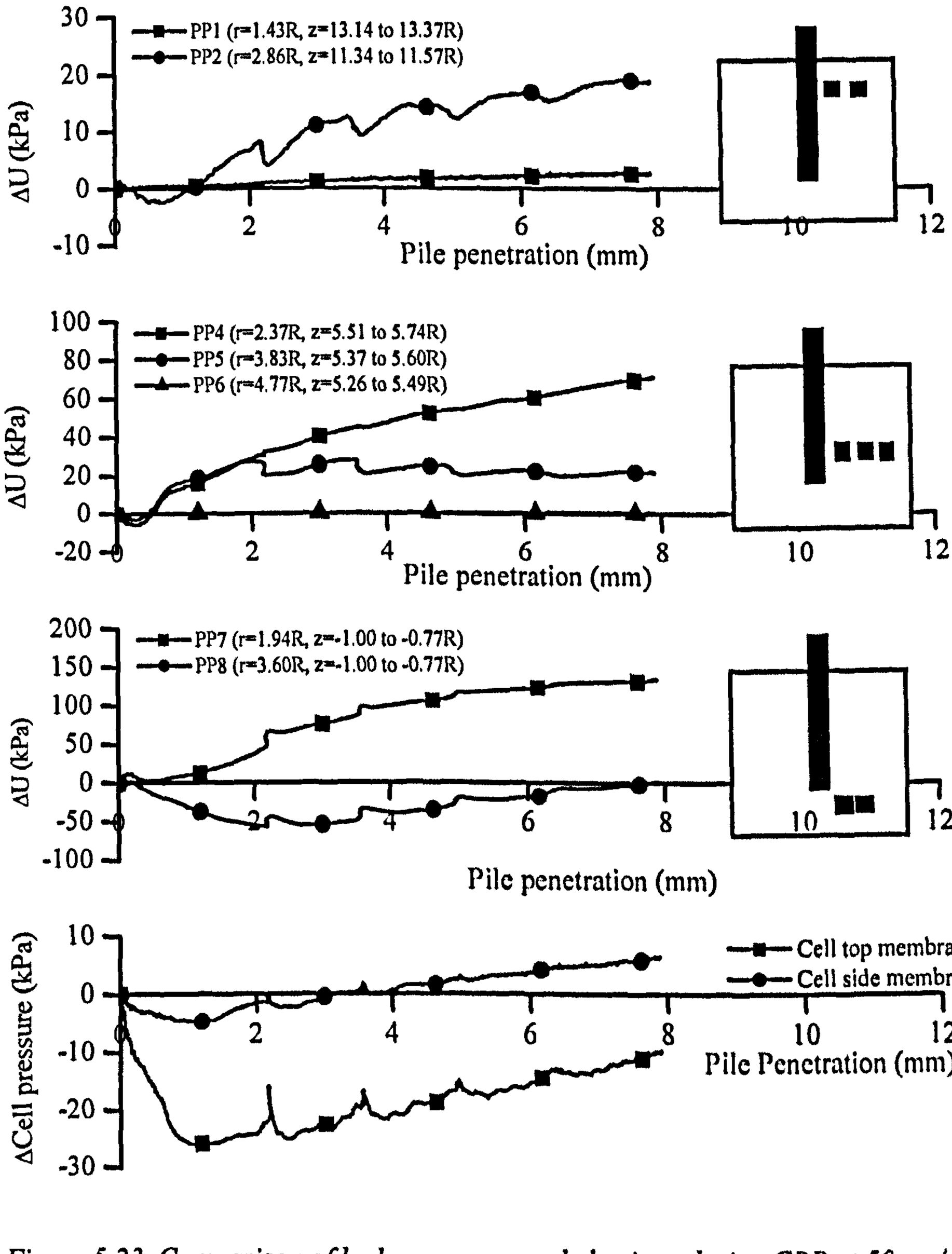

Figure 5.23, Comparison of bed pore pressure behaviour during CRP at 50mm/s with cell pressure change shown for reference (BD3/3/CRP-50).

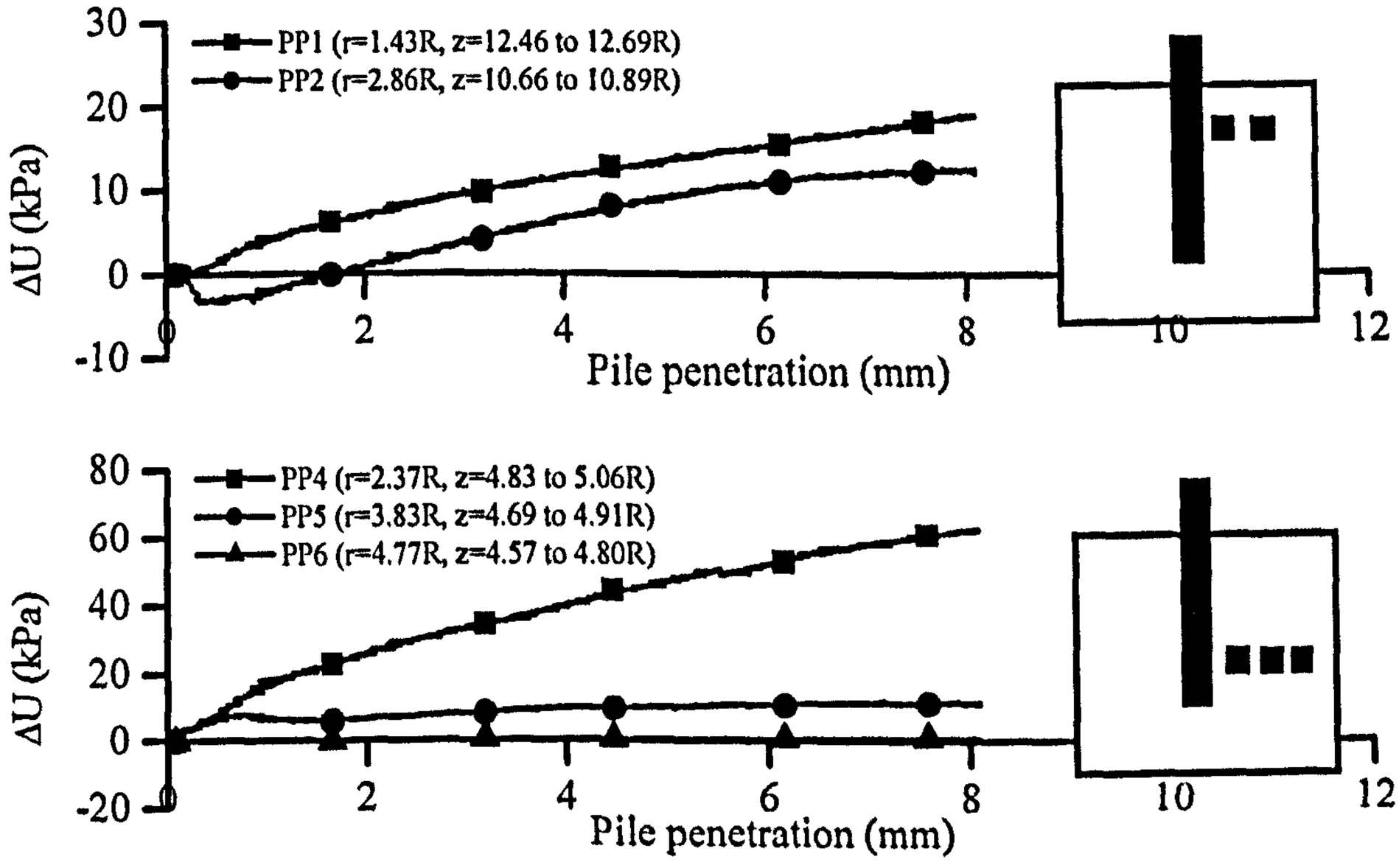

Figure 5.24, Comparison of bed pore pressure behaviour during CRP at 10mm/s with cell pressure change shown for reference (BD3/3/CRP-10).

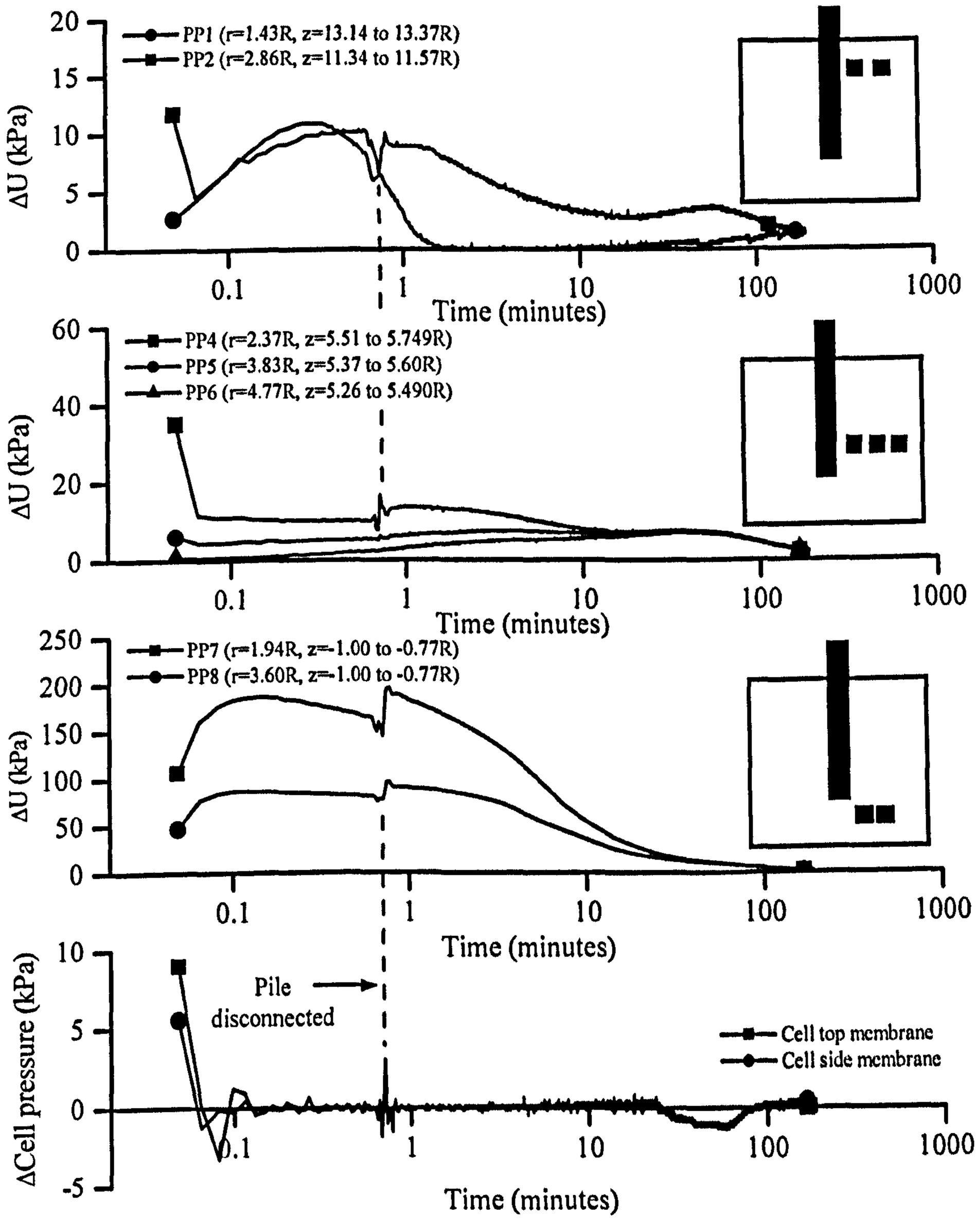

Figure 5.25, Long term monitoring of bed pore pressures after CRP at 50mm/s with cell readings shown for reference (BD3/3/CRP-50).

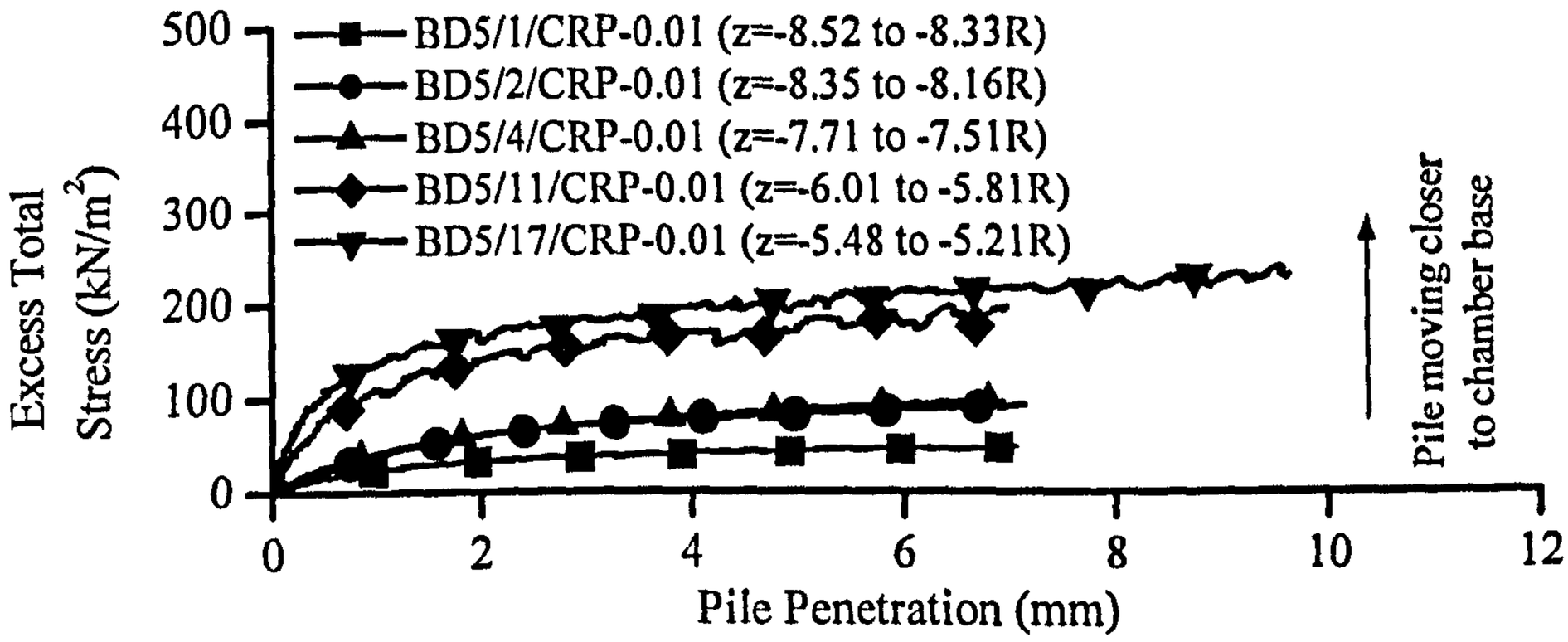

Figure 5.26, Increase in total stress at the chamber base during CRP testing at 0.01mm/s (Bed5).

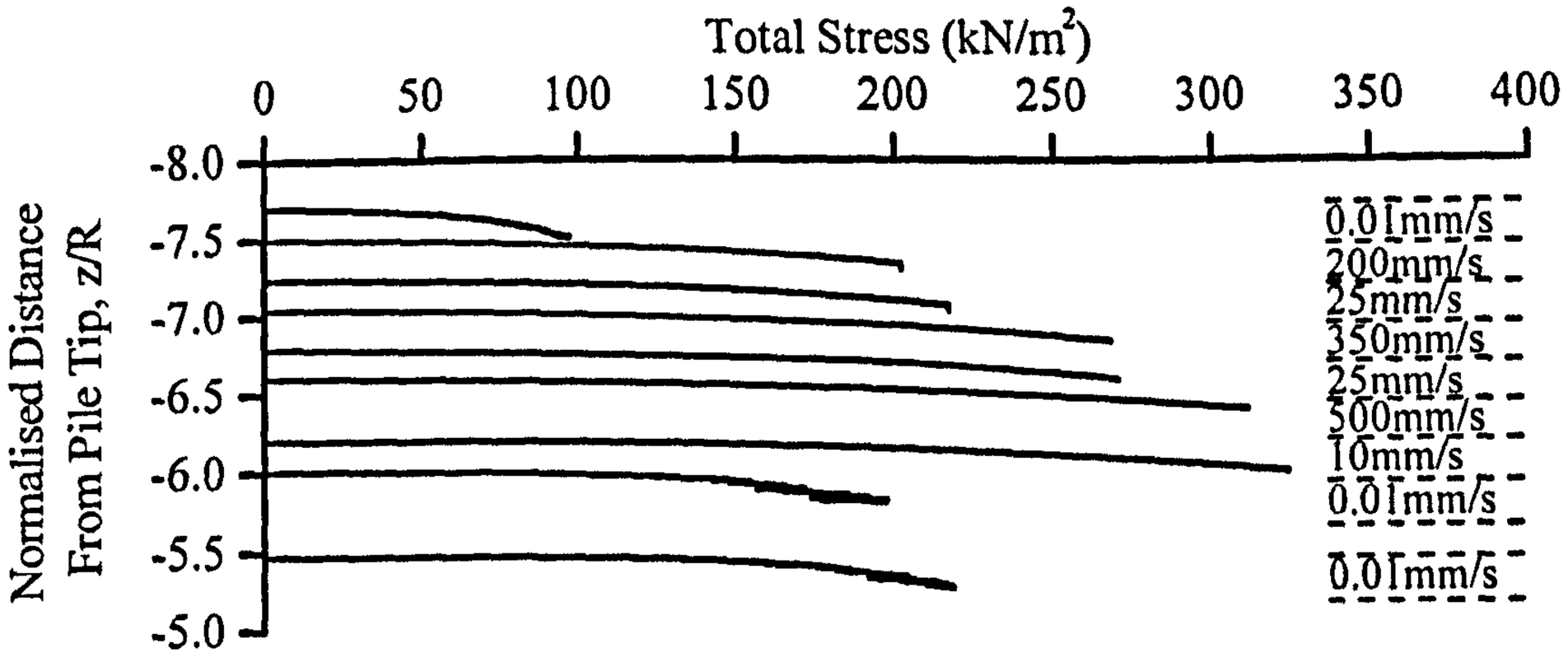

Figure 5.27, Total stress increase measured at the chamber base during CRP testing (Bed 5).

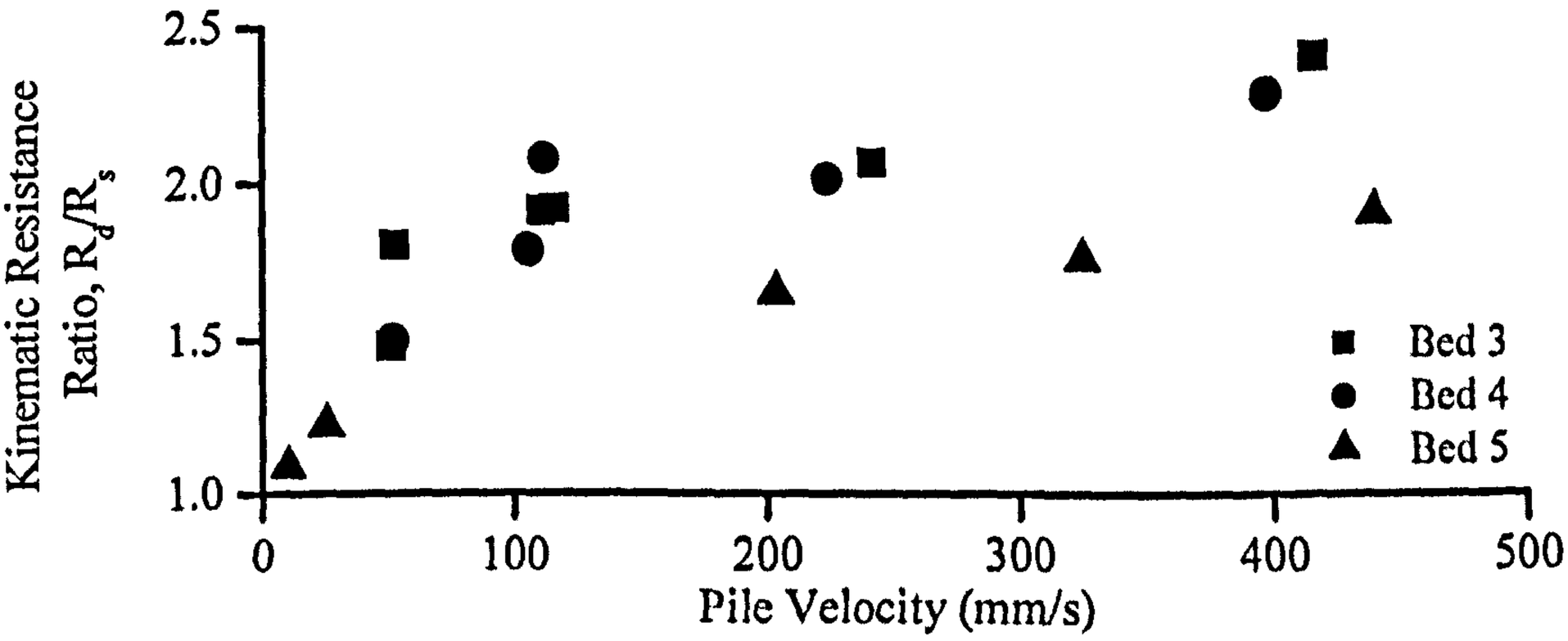

Figure 5.28, Kinematic resistance ratio for total pile resistance.

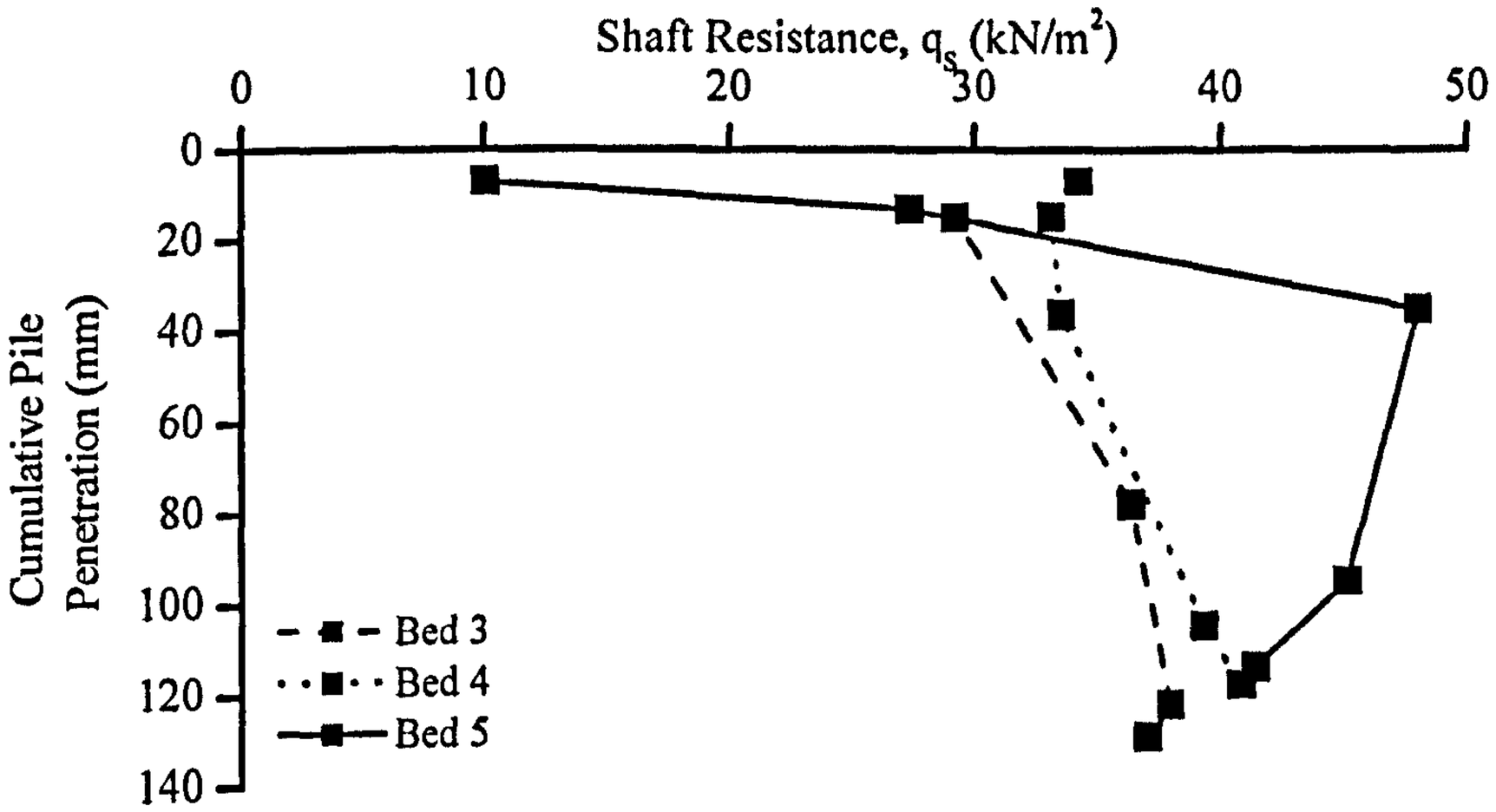

Figure 5.29, Low rate benchmark definition for derived shaft resistance from CRP at 0.01mm/s.

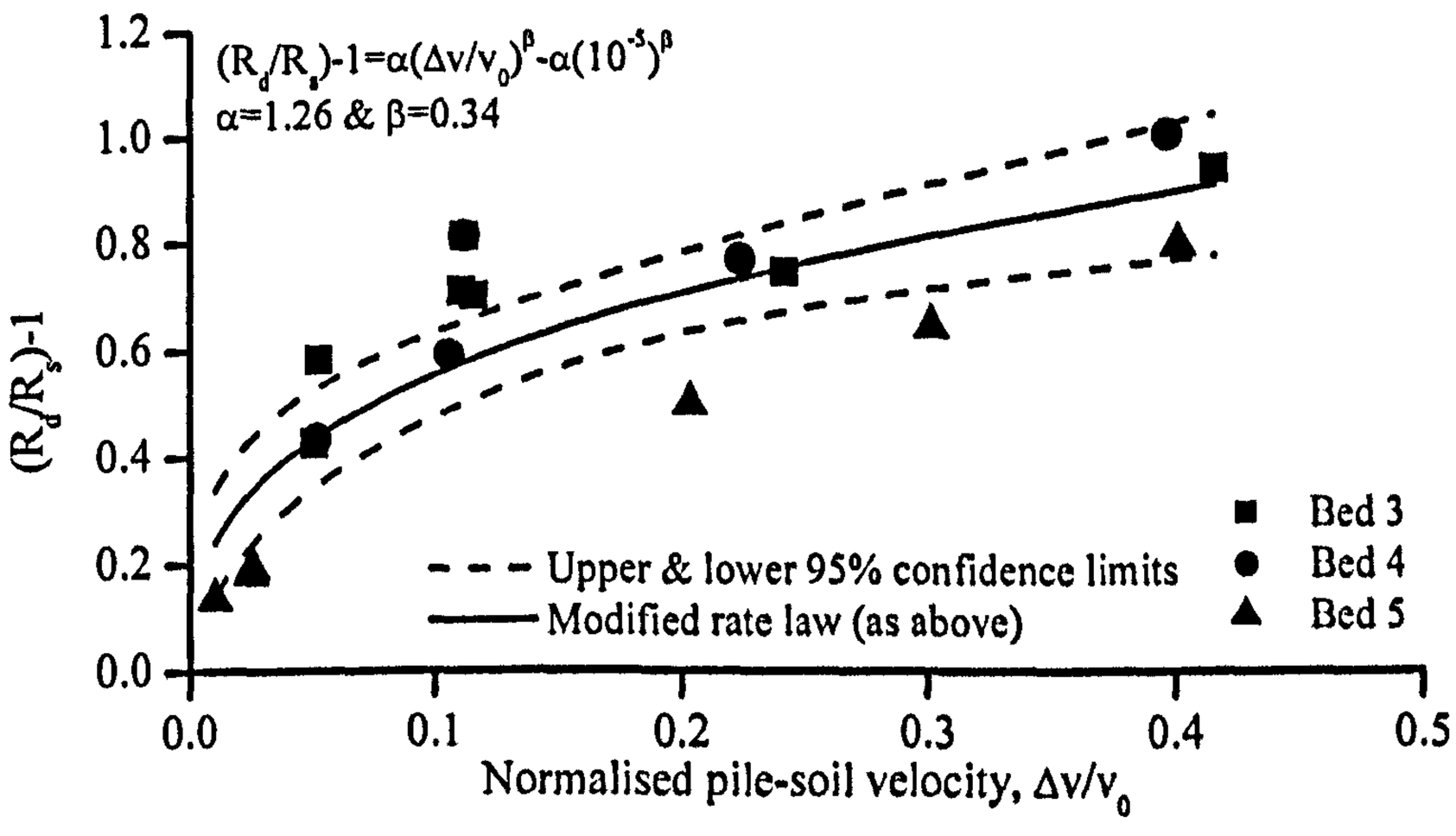

Figure 5.30, Application of modified rate law to total pile resistance to obtain rate parameters.

Relationship	*Damping Coefficient* α	*Range**	*Damping Coefficient* β	*Range**
$\frac{R_d}{R_s}-1$	1.26	1.05-1.56	0.34	0.19-0.48
$\frac{\tau_d}{\tau_s}-1$	2.00	1.51-2.69	0.40	0.21-0.60

**Defined based upon 95% confidence limits.*

Table 5.2, Damping coefficients for modified Randolph & Deeks (1992) rate law.

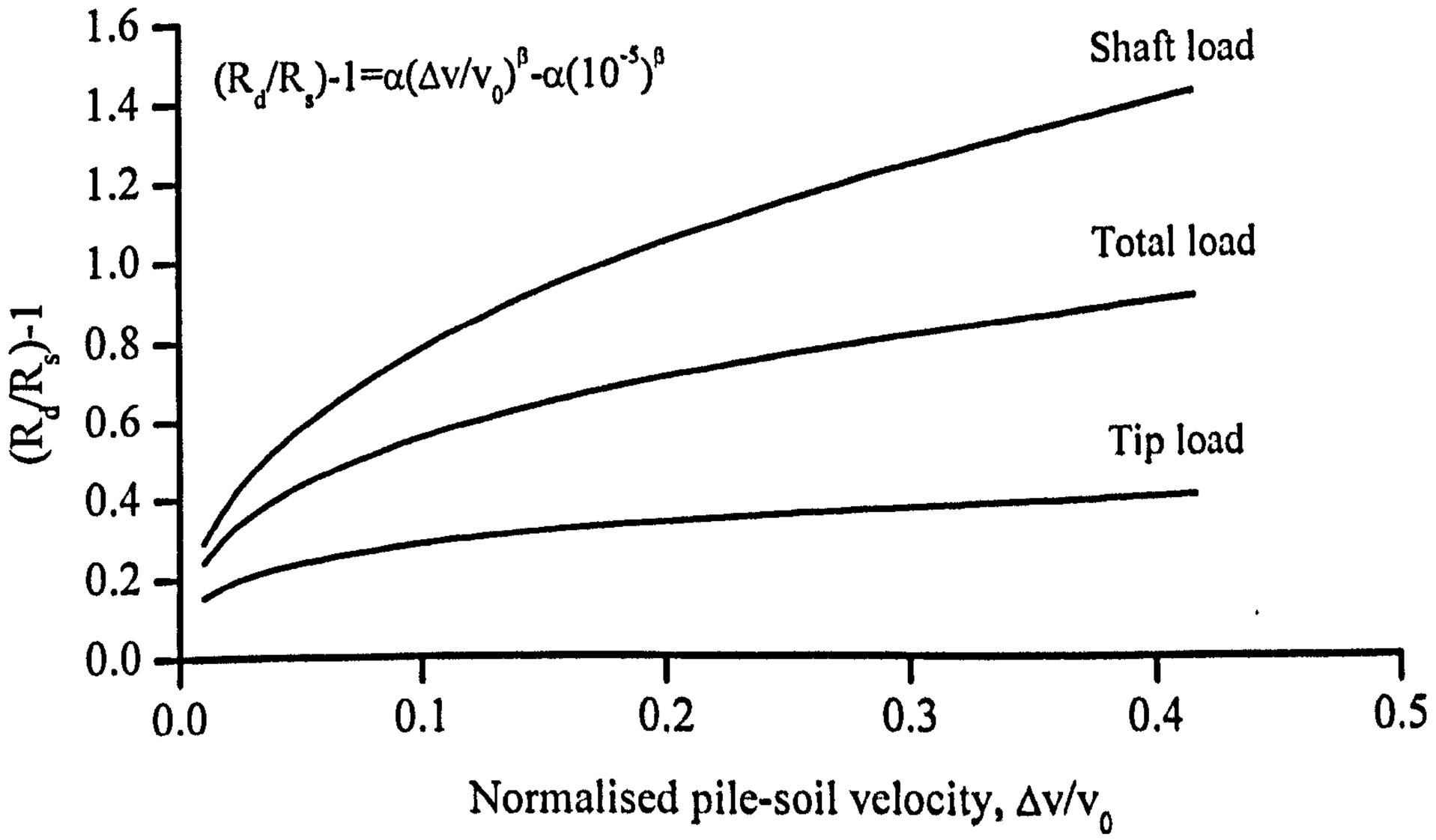

Figure 5.31, Rate effects comparison for load components of pile resistance.

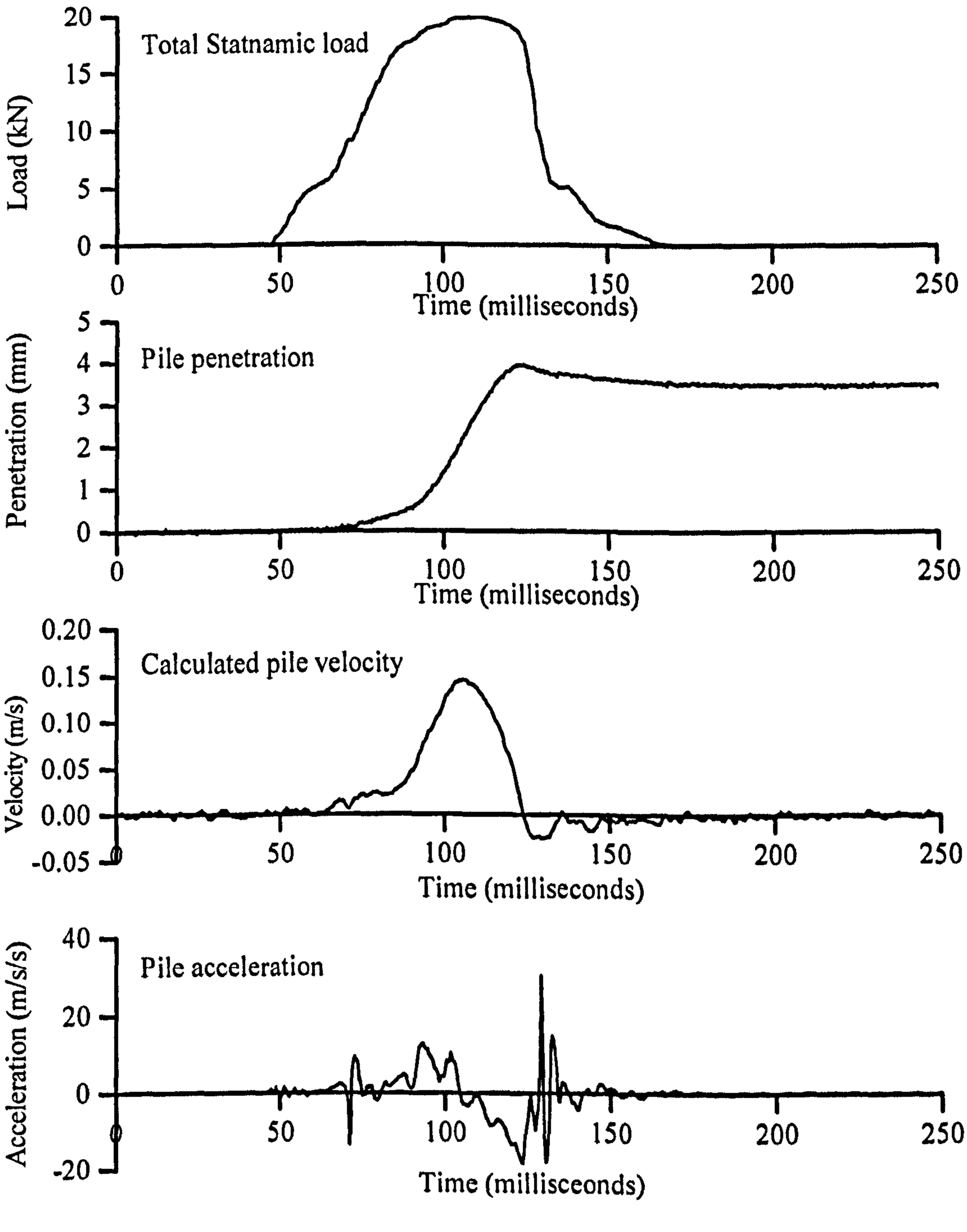

Figure 5.32, Typical measured and calculated components of a 25kN Statnamic load pulse (BD5/15/STN-25kN).

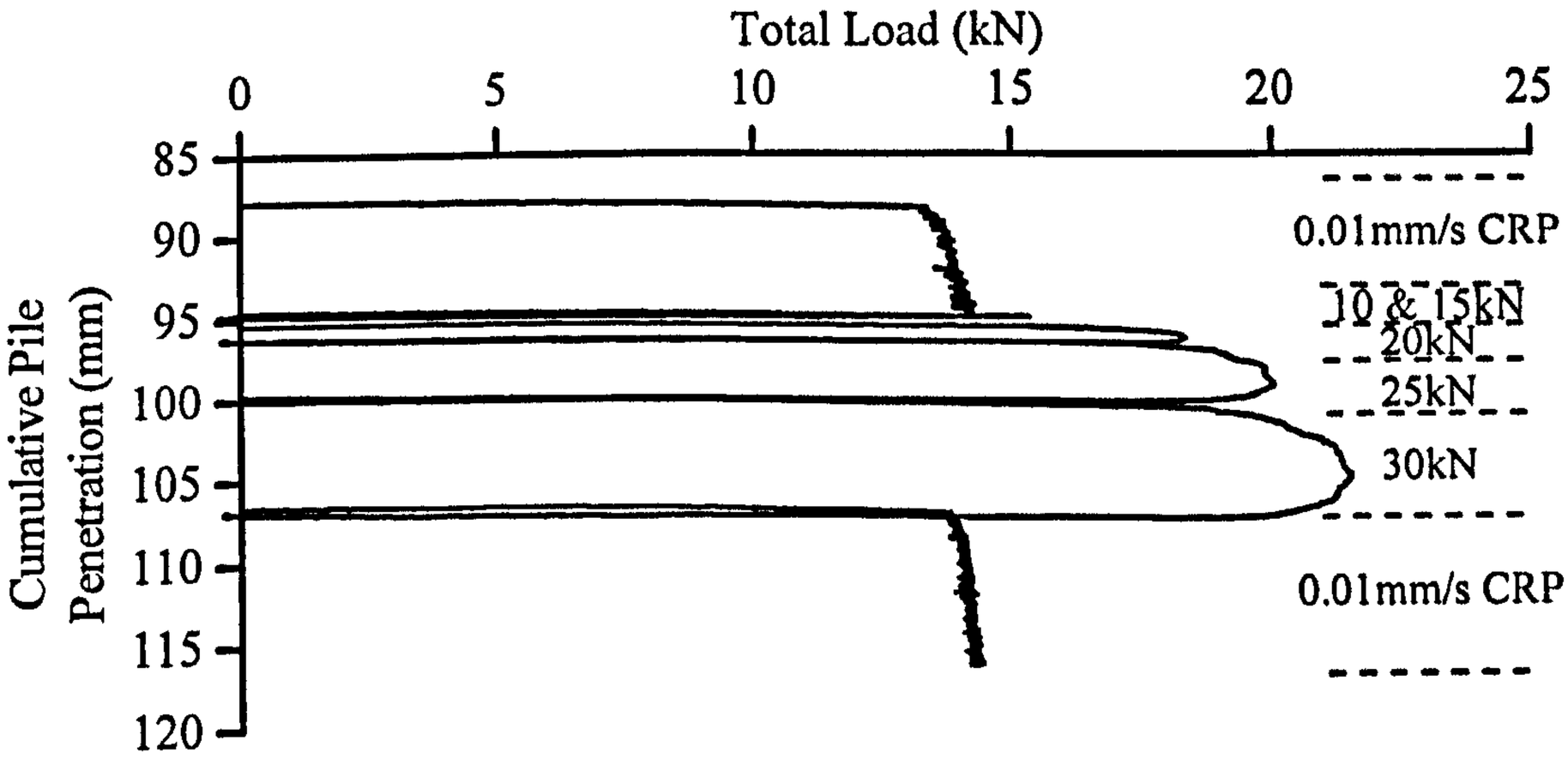

Figure 5.33, Total load measurements during Statnamic pulse loading at various target magnitudes compared with CRP at 0.01mm/s (Bed 5).

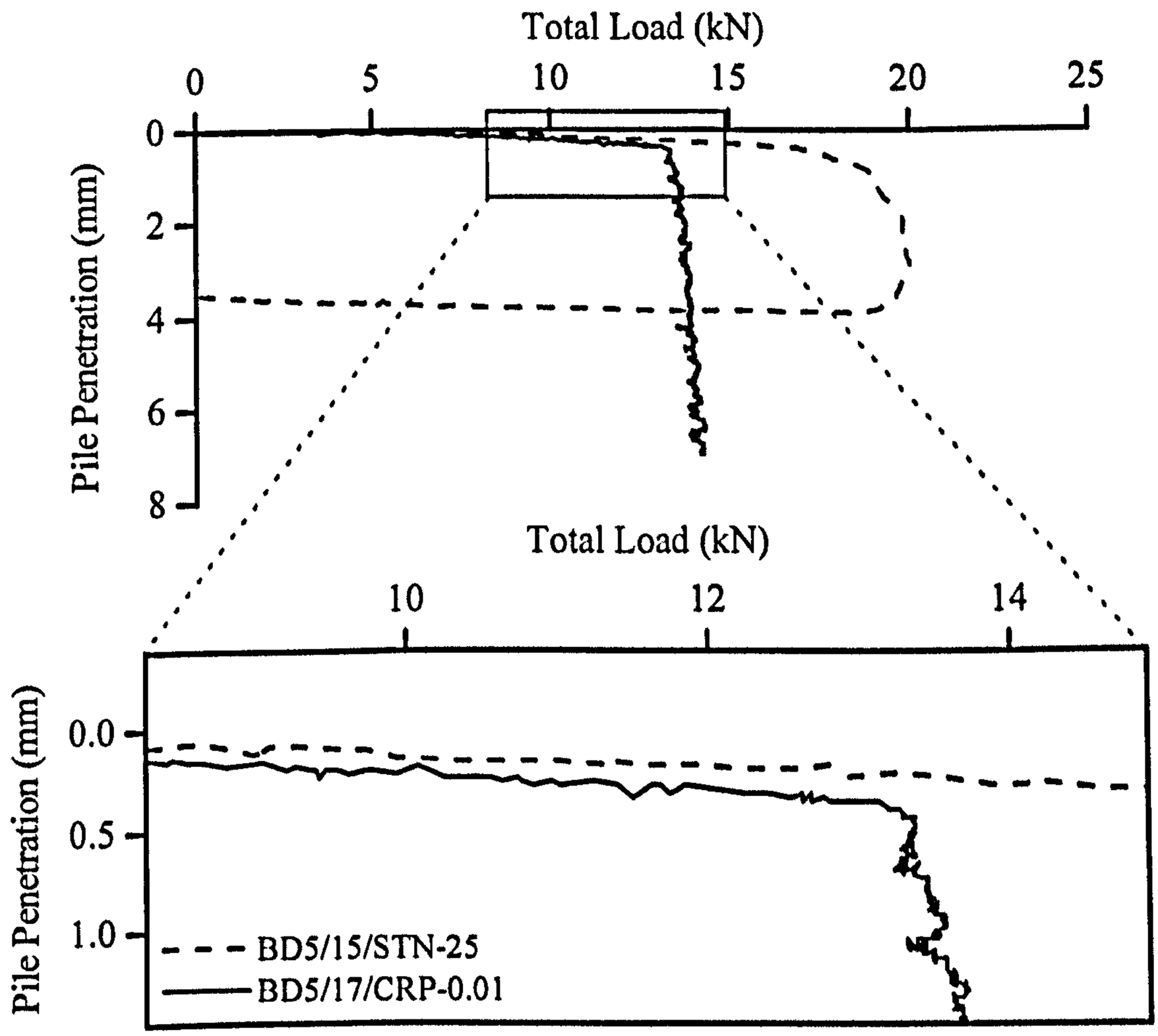

Figure 5.34, 25kN Statnamic total load corrected for inertia compared with 0.01mm/s CRP. Zone of interest exploded.

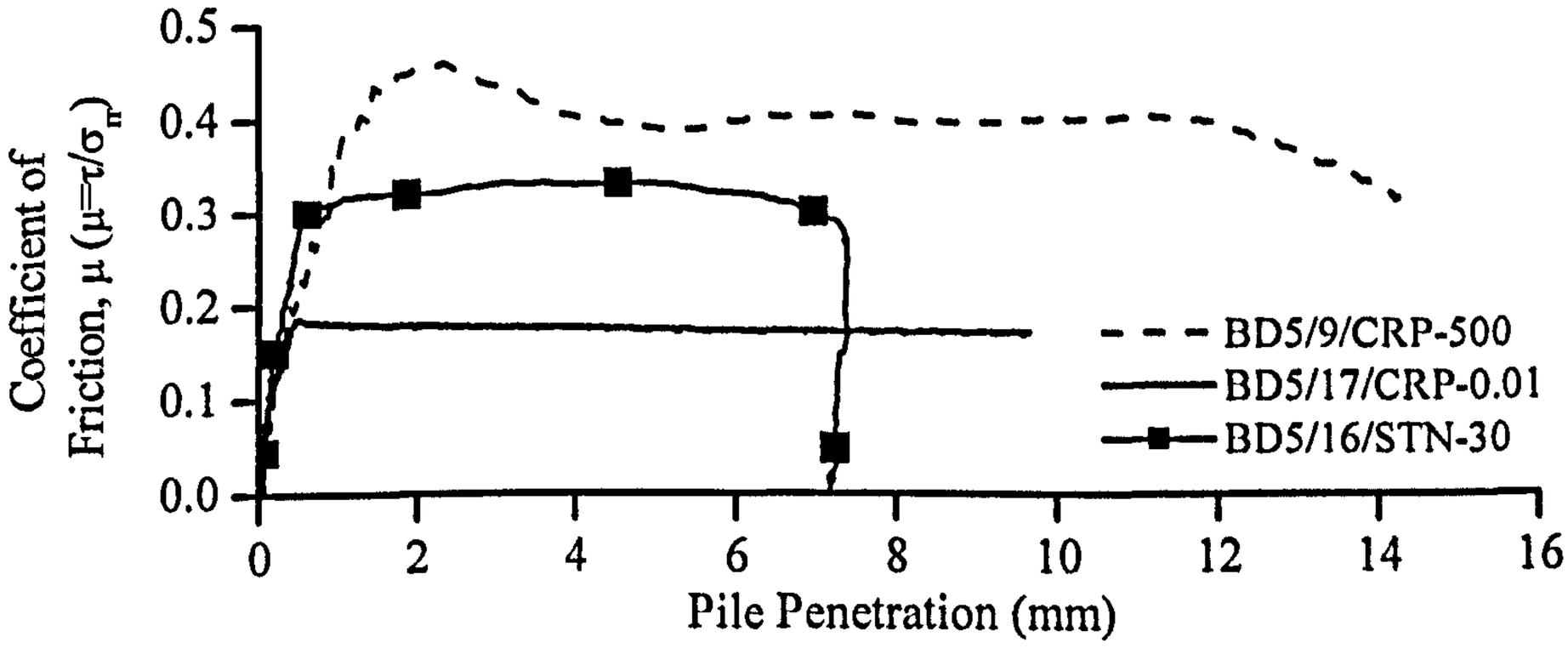

Figure 5.35, Coefficient of friction obtained from Statnamic testing compared with CRP tests at 0.01mm/s & 500mm/s.

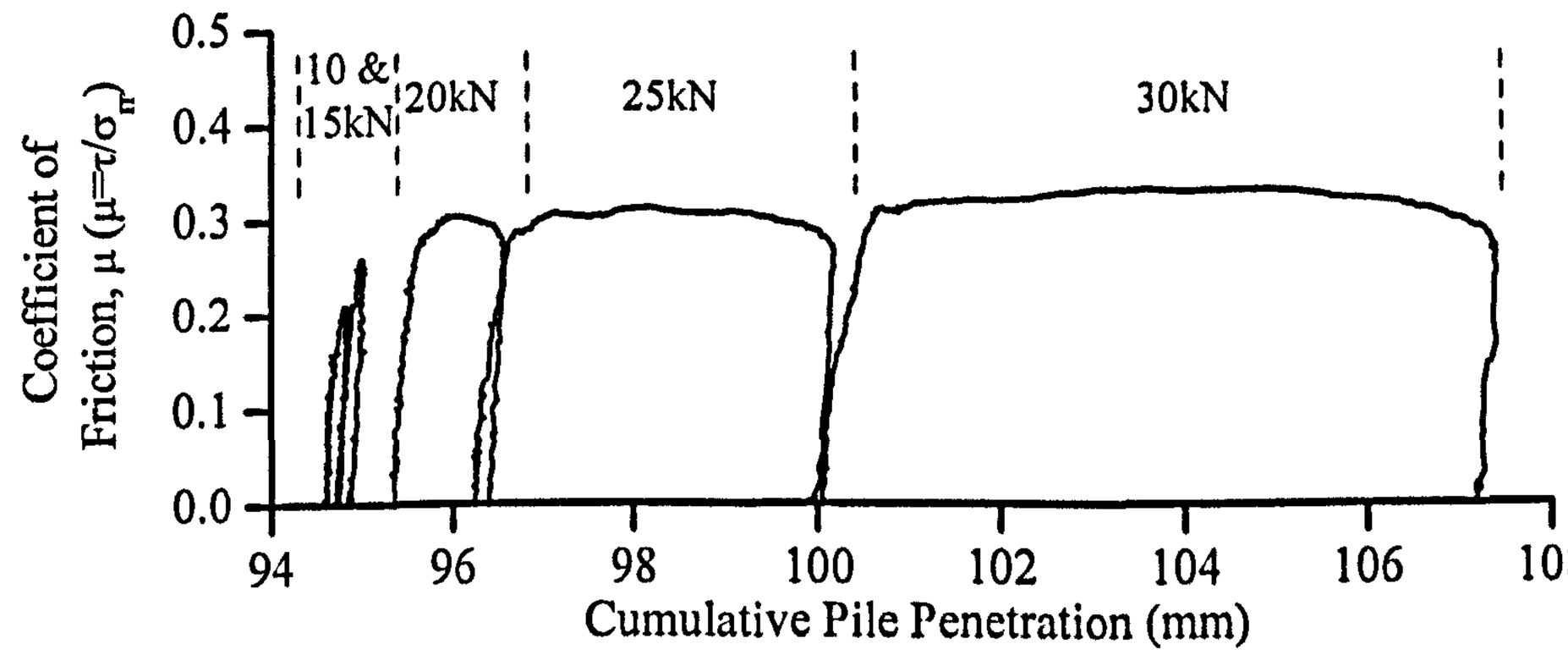

Figure 5.36, Coefficient of friction for Statnamic pulse loading (Bed 5).

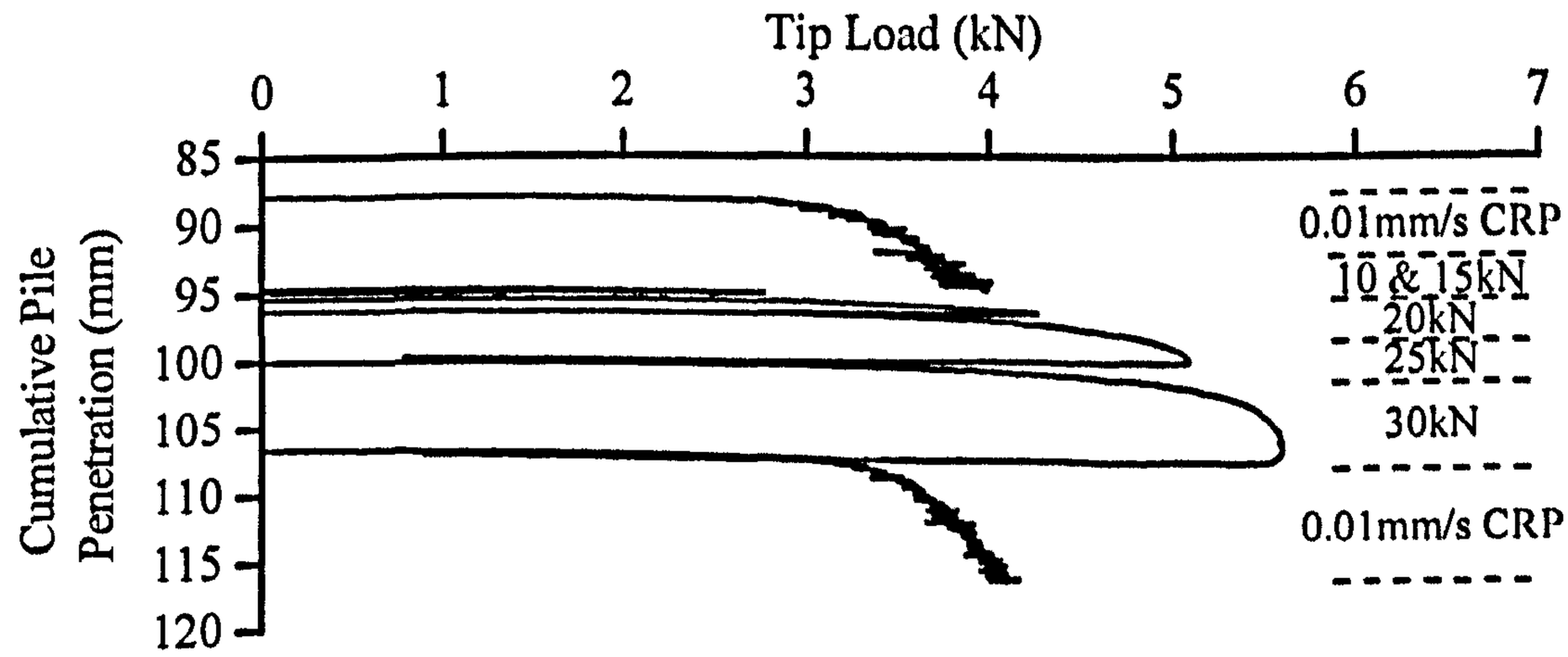

Figure 5.37, Pile tip load measurements during Statnamic pulse loading at different target magnitudes compared with CRP at 0.01mm/s (Bed 5).

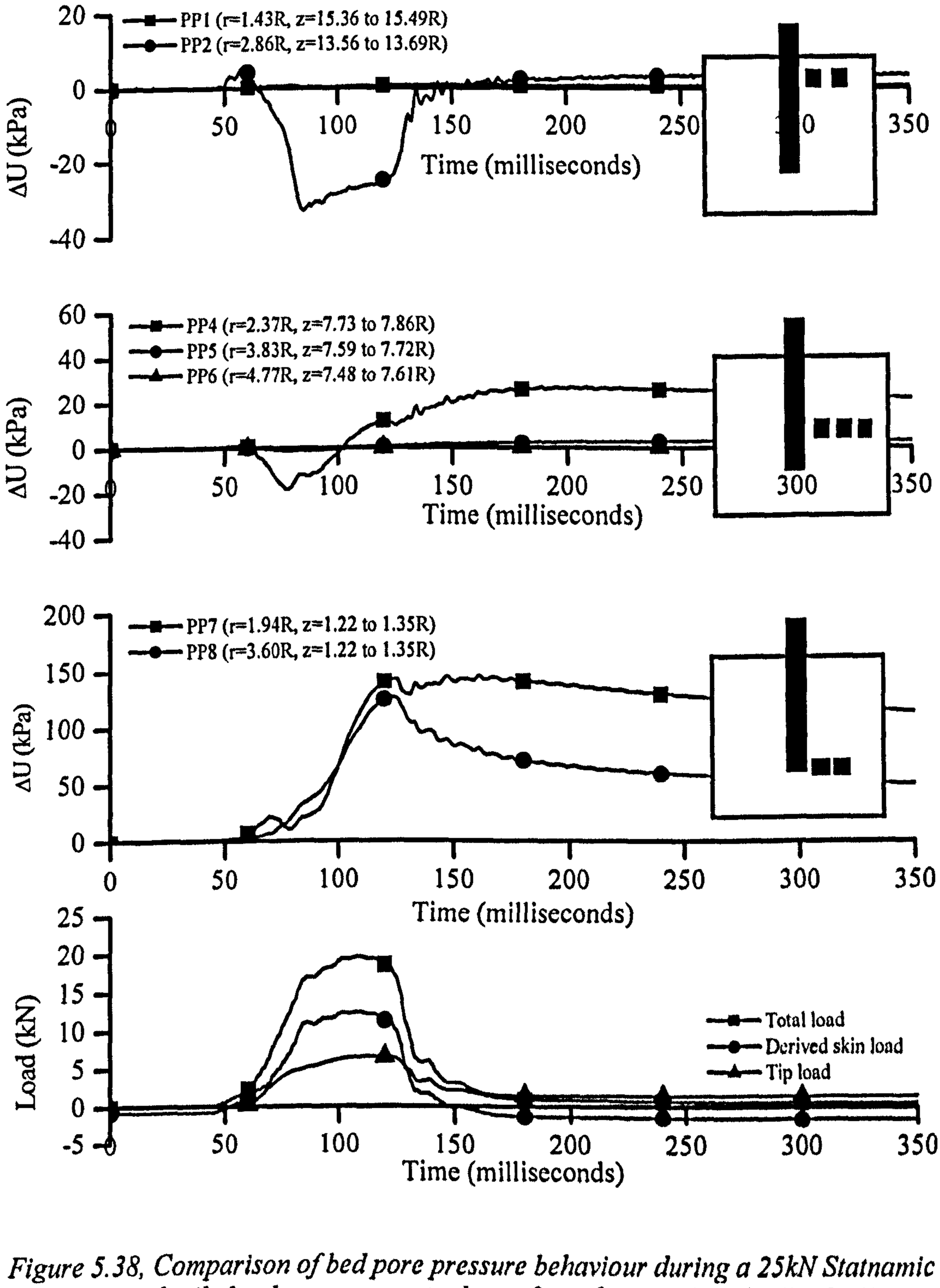

Figure 5.38, Comparison of bed pore pressure behaviour during a 25kN Statnamic pulse with pile load measurements shown for reference (BD5/16/STN-25).

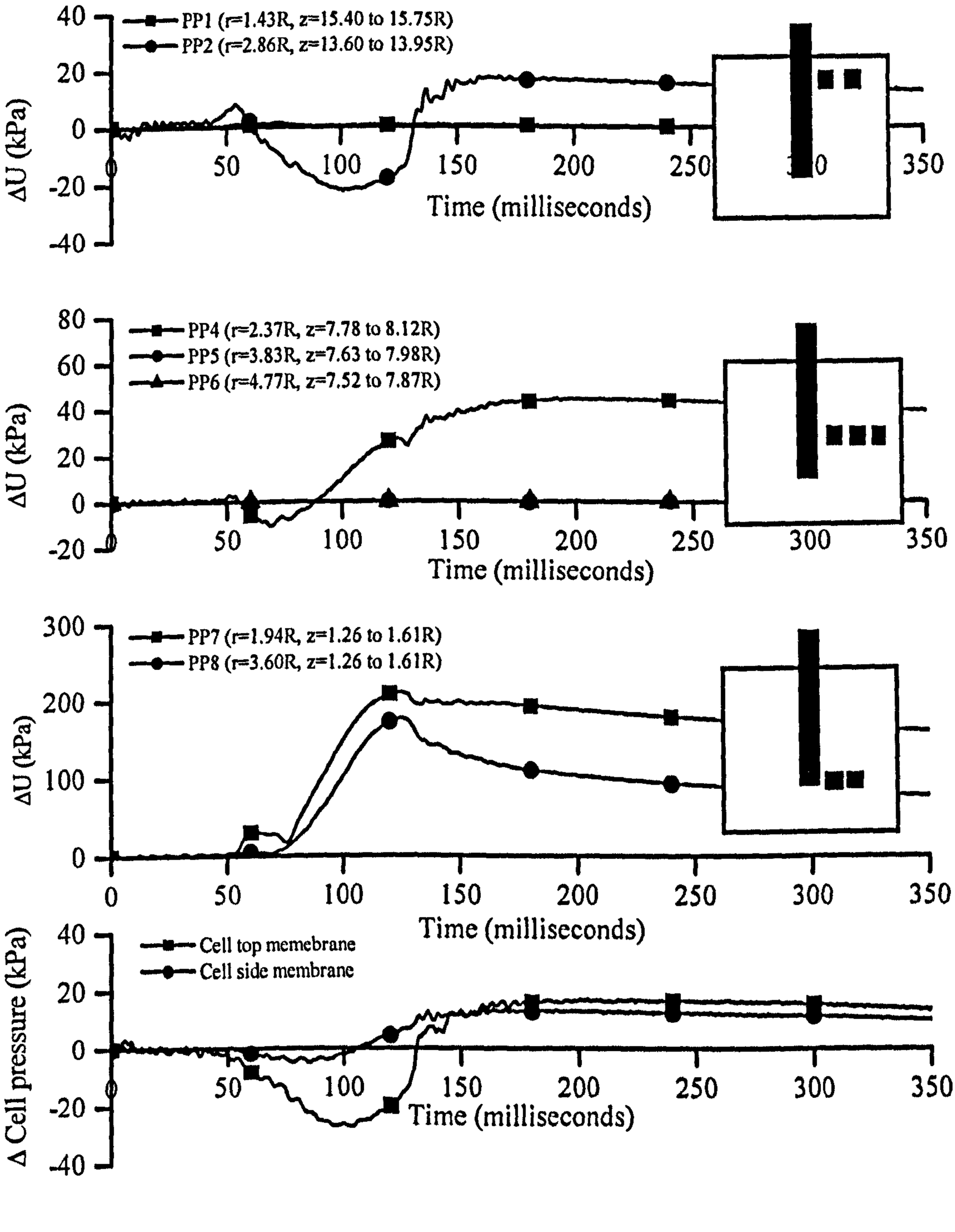

Figure 5.39, Comparison of bed pore pressure behaviour during a 30kN Statnamic pulse with cell pressure change shown for reference (BD5/6/STN-30).

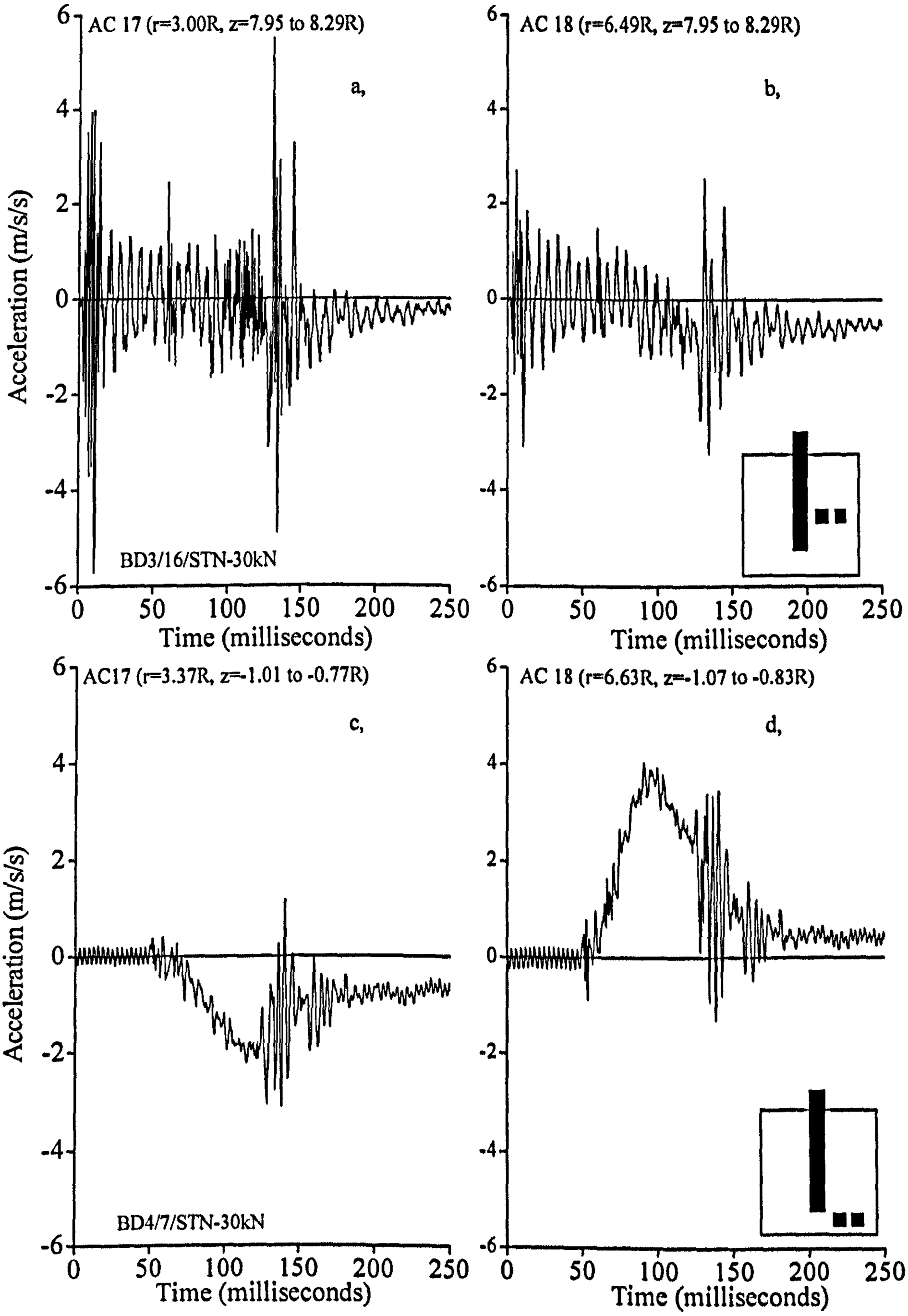

Figure 5.40, Comparison of measured bed accelerations during 30kN Statnamic pulse loads (Beds 3 & 4).

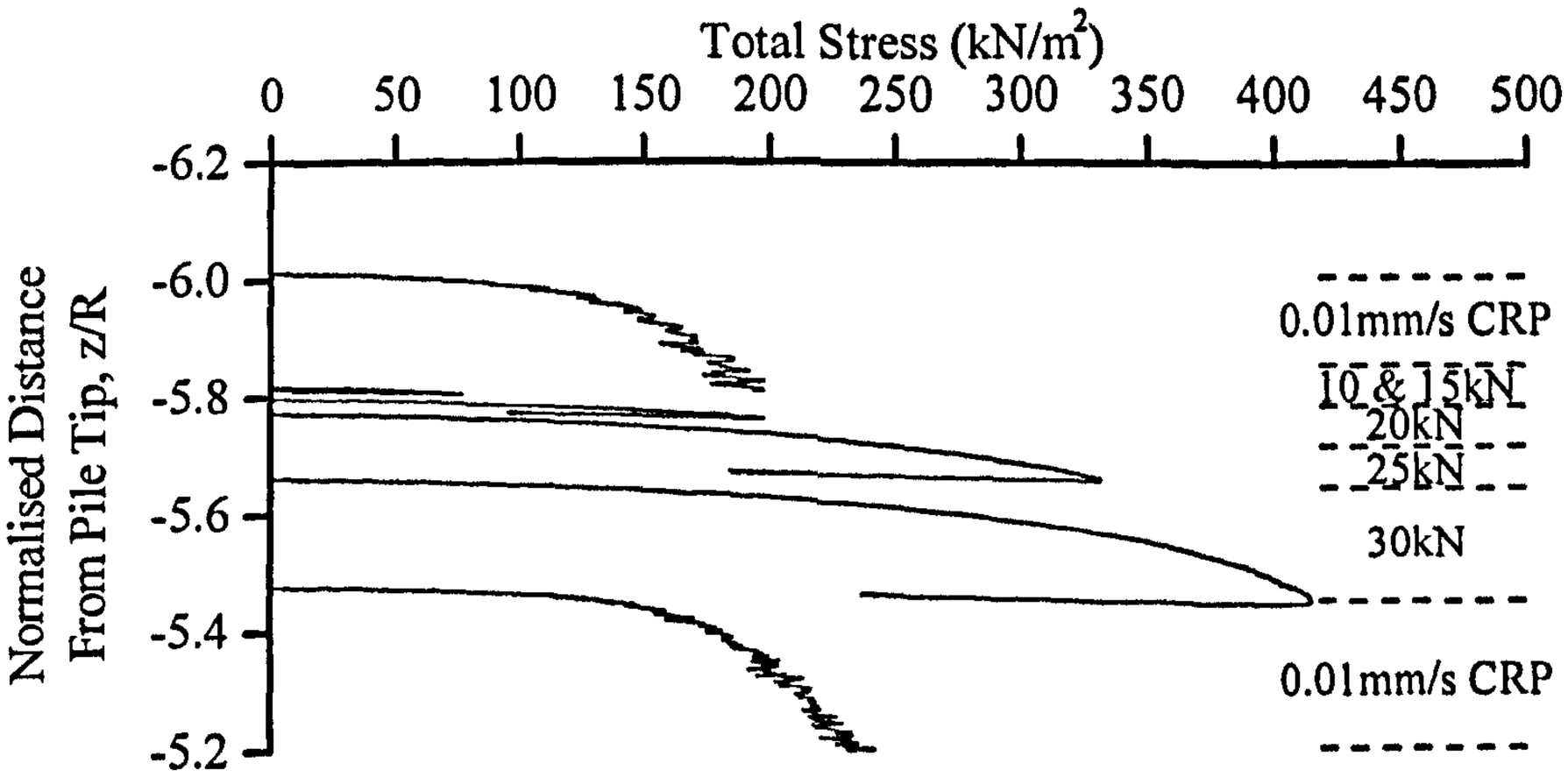

Figure 5.41, Comparison of total stress measured at the chamber base during Statnamic loading with CRP at 0.01mm/s (Bed 5).

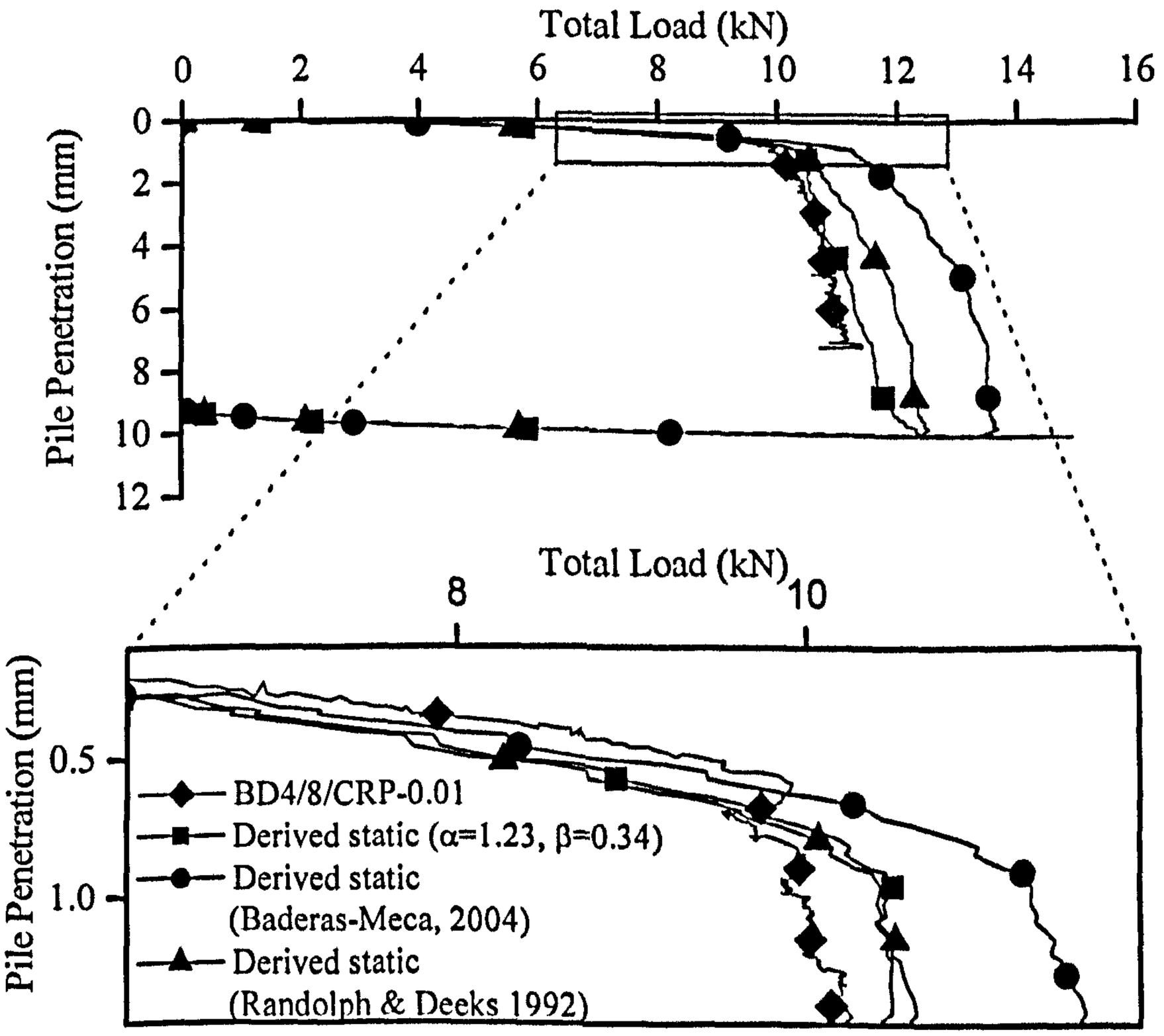

Figure 5.42, Static equivalent total load derived from a 30kN Statnamic pulse using various rate parameters (BD4/7/STN-30kN). Zone of interest exploded.

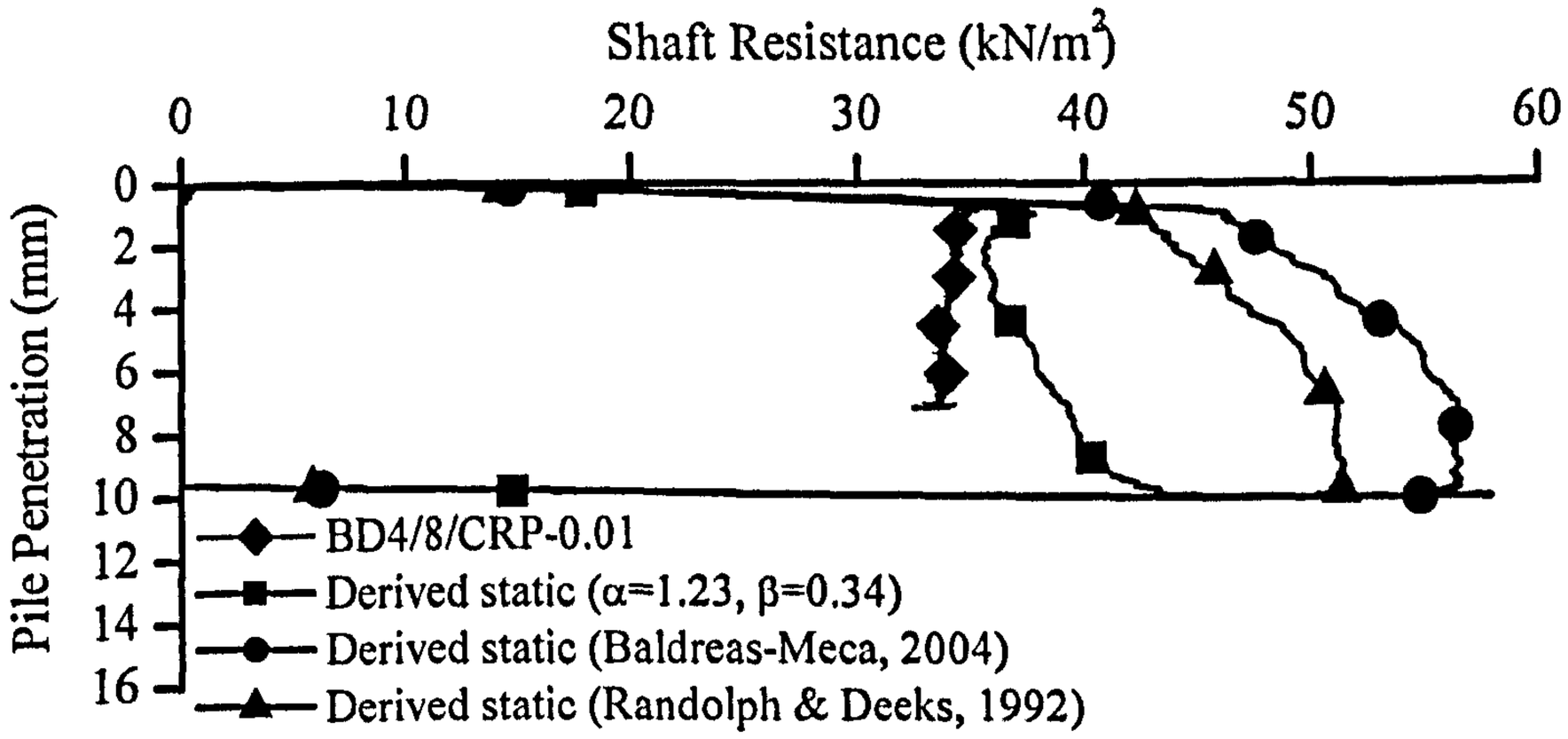

Figure 5.43, Static equivalent shaft resistance from derived shaft resistance for a 30kN STN pulse using various rate parameters (BD4/7/STN-30kN).

6.0 Results and discussion of the Statnamic Field Study

6.1 Introduction

One of the original objectives of the research project was to measure the success of improved Statnamic test analysis found from model pile testing by undertaking a class A prediction (Lambe, 1973), using Statnamic test data of the static pile behaviour of a full scale pile. Additional funding was provided by EPSRC to set up a field test site. This facility was provided by the Expanded Piling Company Limited (EPCL) at their head office near Grimsby where two test piles and associated anchor piles were installed. The site was underlain by a glacially derived till which is a frequently encountered foundation material in the UK, both onshore and offshore.

6.2 Site characterisation

6.2.1 Site location and description

The Grimsby research site formed part of The Expanded Piling Company Limited's (EPCL) Cheapside head office, Waltham, Grimsby, OS Grid Reference (527814, 401664). The location of the compound is shown in Figures 6.1 & 6.2. A more detailed location plan of the area used for research can be found in Figures 6.3 & 6.4.

The site is presently used as the head office and plant yard of a major piling contractor. Previously the site was used for agricultural purposes. The site was generally of constant elevation (15mAOD) with some paved areas. The majority of unpaved areas are for the storage of equipment and steel reinforcement. Located approximately 50m to the west of the site was an area used for research by EPCL. The site was located 900m north of the nearest watercourse and 7.5km southwest of the nearest coastline.

Prior to commencing the study the research site (Figure 6.2) was used as a storage area for reinforcement. The area was cleared and covered with a compacted hardcore platform to allow piling operations. The research site was initially used by EPCL to

investigate the set-up of precast driven piles (Bell, 2001). The site was also used for research during the 1960's, but the exact location of the installed piles is unclear (Taylor, 1966 & James, 1967). A description based upon site features would place them within 200m of the current research site.

6.2.2 Pre-existing ground investigation

Prior to intrusive ground investigation a review of the existing literature was undertaken. Based upon EPCL records and a borehole log from the British Geological Survey (BGS), the site was underlain by glacial till from ground level to approximately 28m. The borehole recorded nearest to the site and held by the BGS was at Cheapside Farm (OS Grid Reference: 527930, 401710), 100m north of the site. This borehole was typical of those in the area, which were undertaken for drinking water wells, and revealed little information. The chalk bedrock was encountered at 28.65m below ground level (BGL) and the water encountered rose to 10.67m.

The geological maps and memoirs for the region describe the till of North East Lincolnshire as stiff to firm, greyish to dark brown, predominantly silty clay with a variety of boulders, cobbles and pebble sized units (Berridge & Pattison, 1994 & Williamson, 1983). It is described as cohesive, overconsolidated, but may also be soft and weathered (reddish brown) with grey joint surfaces. Minor beds of sand and gravel may occur within and under the till (Bell, 2001). The till is referred to as a lodgement till based upon the mode of glacial formation (Trenter, 1999).

The lodgement tills usually have consistent grain-size and uniform matrix composition. They are generally over consolidated (OCR 2-5) with high bulk densities, penetration resistance and seismic velocity. They also have much lower permeability relative to other tills (Trenter, 1999). The lodgement tills associated with the research site are described as matrix dominant (Weltman & Healy, 1978). Description of the soil encountered by Taylor (1966) is shown in Table 6.1.

6.2.3 Ground investigation (2002-2003)

The ground investigation for this study consisted of boreholes and cone penetration testing (CPT) undertaken at different times throughout the project to suit the needs of

the research. As well as ground investigation specific to the research, EPCL also undertook boreholes and CPT investigation approximately 50m to the east of the research site for in-house research purposes.

Two boreholes (BH), boreholes 1 & 2, were undertaken by cable percussive methods with soil samples recovered in 100mm diameter plastic tubes (U100). These were sealed with wax on site and transported back to the university where they were sealed in plastic bags and stored in a high humidity room prior to testing. In BH1, alternate U100 sampling and standard penetration testing (SPT) was undertaken to 20.35m below ground level (BGL). On completion of the borehole, a standpipe piezometer was installed with its tip at 12.9mBGL. Although no water seepage was noticed during the boring of BH1, slight seepage was seen in BH2 consistent with the level of a thin sand lens. The second borehole (BH2) was undertaken to recover samples for high speed triaxial testing (Balderas-Meca, 2004). The logs for the boreholes can be found in Appendix 4. A description of the soil encountered is shown in Table 6.2 with summarised in-situ borehole tests shown on Figure 6.5.

Cone penetration testing (CPT) in several different forms was undertaken at the site. The majority of testing included cone face monitored excess pore pressure (PCPT). For PCPT tests, a standard cone was driven to approximately 2.5m and then withdrawn (pre-drilling). The hole was then filled with water and the complete test driven down the same hole using a piezocone. This was done because on the first PCPT the very stiff upper layers compressed the cone tip filter ring resulting in a loss of saturation. The data from the pre-drilled hole and the piezo drive were then linked to form one CPT trace.

Additionally seismic CPT (SCPT) (Lunne *et al.*, 1997) and PCPT at elevated rates were also undertaken. Seismic CPTs were used to derive seismic velocity using a surface to downhole technique where the source was fixed at the ground surface and the detectors were advanced into the ground behind a standard cone assembly. The source comprised a 2.6m long timber railway sleeper, restrained under a 20 tonne crawler hybrid CPT truck (Brouwer, 2002), with metal plates at each end that were struck with a sledgehammer. This was offset 1.2m from the line of CPT penetration. The seismic detectors were three component geophones mounted 1m apart in the string behind a standard CPT cone. The geophones were advanced in 1m increments with the first

readings taken when the upper geophone was 1mBGL. Prior to undertaking the seismic readings, a standard CPT was advanced (pre-drilled) to the 20mBGL to check for obstructions. Seismic readings were taken at 1m intervals down the pre-drilled hole to 20mBGL (Ricketts, 2002). The deduced seismic shear wave velocity profile for the site is shown in Figure 6.5. The L and R notation refer to the side of the sleeper that was struck at each level. This process was undertaken to allow phase reversal during seismograph interpretation to allow easier identification of shear wave arrival.

The magnitude of average S wave velocities derived from the seismic CPT testing varied from 210m/s to 380m/s with the profile of velocities mimicking the CPT cone resistance. The highest peak velocities were noted for the zone of high cone resistance between 1.8 to 4.0mBGL.

An innovative use of the PCPT method was attempted by carrying out tests at elevated rates above the standard penetration rate of 20mm/s. These tests were undertaken to investigate the potential for obtaining rate effects parameters from in-situ testing. As introduced in Section 4.0, to obtain the rate parameters, highly specialised laboratory equipment is required. The high rate CPT tests were carried out using standard un-modified PCPT equipment. The rates were achieved by adjusting the CPT truck engine revs and by putting the truck gearbox into high and low ratios. Stable penetration rates of 40, 50, 100 and 140mm/s were achieved by this method. The higher rate tests were carried out between 5 to 11mBGL as the standard rate cone resistance profile was most predictable between these depths. The position of the three high rate CPTs is shown in Figure 6.4, next to a standard rate test used as a control.

There was little apparent change in the cone resistance (q_c) with penetration rate. This is consistent with the findings of the model pile tip rate study (Section 5.4.4). Comparison of the elevated rate test (PCPT4(H)) with the control test (PCPT7) at standard penetration rate (20mm/s) is shown in Figure 6.6. Only the sleeve friction resistance is shown due to the low cone rate effects. The difference in the rate effect for the two components is apparent from the calculated friction ratio ($R_f = (f_s/q_c)100$). This ratio is comparable through the standard rate portion of both tests but increases during the higher rates. The measured sleeve friction appears to be enhanced for all of

the rates above 20mm/s with the rate effect increasing with increasing rate of penetration. Analysis of the effect of rate on CPT pore pressure is limited by the cone encountering harder layers or obstructions. However, the pore pressure did tend to display step increases in pressure with increasing loading rate.

The results of the high rate CPT testing show that it is possible to use CPT to assess the potential for rate effects. Although, analysis to derive rate parameters is complicated due to the "noise" associated with natural ground conditions (Figure 6.7). As can be seen in Figure 6.7, there is considerable scatter in the data that resulted in a poor fit to the rate analysis. The rate parameters derived from the CPT data were α=2.79 and β=0.41. The alpha value lies outside the range of values derived from model testing (Section 5.4.4) whereas the beta value compares well with that derived from the model pile's skin friction sleeve (β=0.40). It is difficult to make further comparisons with the model testing when the low rate tests used for CPT (20mm/s) were so much faster than during the modelling (0.01mm/s). Lower rates were not used due to time and equipment limitations. The use of lower rate CPT tests with more individual tests per site may prove an adequate method of assessing in-situ rate parameters. Further testing is required to verify these conclusions.

6.2.4 Laboratory soil testing

Laboratory testing associated with this project was designed to allow classification of the soil encountered and provide parameters for pile design and instrumentation. Additionally, test results from the EPCL research site and the investigations from the 1960's are presented. Further details of soil properties can be found in Balderas-Meca (2004). Additional test results from the EPCL research site and the investigations from the 1960's are presented.

All laboratory testing was carried out in accordance with BS1377 (1990). The only variation from standard testing methods was in the determination of undrained shear strength from triaxial testing.

To determine undrained shear strength 100mm diameter samples, 200mm in length were prepared from U100 samples retained within wax sealed plastic liners stored as

described earlier. This diameter was chosen over 38mm samples to reduce the influence of macro-structure and any larger hard particles within the clay matrix (McKinlay *et al.*, 1974). To maximise the results obtained from each sample, a multistage testing approach was followed as described by Anderson (1974). Lubricated end platens were not used in this investigation. Results obtained by Taylor (1966), who tested sets of 38mm samples at each depth, are also presented. Additionally, during site sampling, a limited number of shear strength determinations were made using a small hand shear vane (Torvane). The shear strength variation with depth is shown in Figure 6.10. No attempt has been made to allow for the variation in shear strength between 38mm and 100mm sample diameter samples due to fissuring of the Grimsby Clay, as undertaken by Bell (2001).

The variation of undrained shear strength with depth is similar to the profile observed during in-situ SPT and CPT testing (Figure 6.10) with firm to stiff (<100kPa) clay down to approximately 1.8m BGL. This was followed by a zone from 1.8m to 5m of material that had previously been exposed to a weathering environment. The undrained shear strength in this zone peaked at 2.3m depth (280kPa) reducing to approximately 100kPa at 5m depth. The undrained shear strength remained between 80 to 100kPa between 5 to 10m depth and then increased to 180kPa at 17mBGL. Results from the previous study compare well with those obtained in the recent investigation.

Results from undrained shear strength testing and from previous studies were compared with the measured cone resistance to allow estimation of the undrained shear strength at levels where soil samples were unavailable. The relationship between measured cone resistance and undrained shear strength (c_u) can be expressed by Equation 6.1.

$$q_c = c_u N_k \tag{6.1}$$

where

q_c = measured cone resistance

N_k = cone factor

From Figure 6.9 it can be seen that the cone factor lies between 15 to 20 with an average value of 16. A similar operation was carried out for the SPT N value, with the relationship varying from c_u=3.5N to 16N. This range is similar to that found by (Weltman & Healy, 1978), who recommended that a low factor of 2.5 to 3.5 should be used for estimates of shear strength in glacial till.

Index properties for the Grimsby Clay material are shown in Table 6.3. The KSS index properties tend to the upper range of Atterberg limits and clay fraction values for Grimsby clay. The activity of the KSS material falls within the range of that for Grimsby Clay. The range of values for the Atterberg limits are similar to the typical results presented by Mckinlay *et al.*, (1974) for Glasgow lodgement till (w_L=28%, w_P=16%, I_p=12%). The laboratory test results were also combined with the in-situ tests to produce site information. The variation of dynamic shear modulus derived from the seismic CPT testing and the bulk density (from Equation 6.2) is shown in Figure 6.10.

Where the shear modulus G was obtained from the expression:

$$G = \rho V_s^2 \tag{6.2}$$

Where

ρ = soil density (saturated)

V_s = shear wave velocity

The particle size distribution (PSD) for the Grimsby Clay can be seen in Figure 6.11. Sampling for this test was limited to the upper levels due to the need for undisturbed samples for the soil element study (Balderas-Meca, 2004). Also shown is the particle size distribution for KSS model soil used in the laboratory study. The KSS material is generally finer than the Grimsby Clay and lacks the coarser sand and gravel components. If greater similarity between the materials were required, a reduction in the medium sand content and an increase in the medium silt content would be required for

the KSS. For true comparison, further PSD determinations would be required at depth for the Grimsby Clay.

6.3 Test piles and instrumentation

6.3.1 Pile types and installation

Two different piles were installed at the Grimsby test site. The first was a pre-cast concrete driven pile installed by EPCL to investigate the set-up of precast driven piles (Bell, 2001). The second was a cast in-situ auger bored pile designed and installed specifically for this study (Figure 6.12).

The pre-cast concrete pile was 13.5m long (non-segmental) with a 275mm by 275mm square cross section. It was initially driven to 12.5mBGL (14/06/01) using a Junttan PM20 pile driving rig with a 5 tonne hammer falling through 400mm. From the results of ground investigation Bell (2001) calculated that the pile would have an ultimate capacity of 1186kN. This was based upon the following total stress calculation:

$$Q_b = N_c c_{u(base)} A_{base} = 9.0 \times 113 \times 0.076 = 77kN \tag{6.3}$$

$$Q_s = ((\alpha_A c_u)_{(0.5to6.5m)} + (\alpha_A c_u)_{(6.5to12.5m)}) A_{shaft} = ((0.78 \times 110) \times 6.6) + ((0.95 \times 87) \times 6.6) = 1109kN \tag{6.4}$$

Where

Q_b = pile ultimate base resistance

N_c = bearing capacity factor

c_u = undrained shear strength

A_{base} = pile base area

Q_s = pile ultimate shaft resistance

α_A = adhesion factor

A_{shaft} = pile shaft area

The value for α_A was obtained from values suggested by Weltman & Healy (1978), based upon undrained shear strength results.

During the installation of the driven pile, dynamic pile testing was also undertaken. Results from this test and subsequent re-strike dynamic tests of the pile are given in Table 6.4.

The dynamic tests show an increase in pile capacity with time. On completion of the dynamic testing programme, the pile was loaded statically using standard Maintained Load Test (MLT) procedure (ICE, 1997). Reaction for the static tests was provided by EPCL reaction beams and three 600mm diameter auger-bored reaction piles (11.5m deep) arranged in a triangular pattern (Figure 6.4). The results show that the dynamic assessment of static pile capacity underestimated the statically determined capacity by 7%.

The auger bored cast in-situ pile was installed using a Soilmec RT3 rotary auger rig mounted on an NCK Ajax crane. The 600mm nominal diameter pile bore was advanced to 12.06mBGL and left unsupported. After excavation, a steel casing of 610mm outer diameter and 8mm wall thickness was advanced to 1.8mBGL with 480mm left above ground level (Figure 6.12). The quality and cleanliness of the bore was inspected visually with the aid of a lamp lowered from the surface. A tip load cell was installed at the base of the bore and the instrumented reinforcing cage lowered to just above the tip load cell. The main reinforcement consisted of six 12m long T16 bars with horizontal reinforcement consisting of a single helical running up the main reinforcement. The helical reinforcement consisted of a T12 bar spaced at 300mm centres. The pile reinforcement was initially tied together and then spot welded at connections. This minimised flexure of the cage during craneage and thus reduced the risk of instrumentation damage. Minimum cover to the reinforcement was maintained at 75mm by the use of plastic spacers. The pile concrete consisted of a C35 mix with 10mm aggregate. This was poured over the back of a shovel to reduce segregation. The use of a tremie pipe or vibrating pokers was avoided to reduce the chance of instrumentation damage. The concrete had a 28 day strength of 36N/mm^2 and an average density of 2.345Mg/m^3. The concrete was poured within 6 hours of finishing excavation up to the top of the steel casing.

During the field study, only very simple total stress design calculations of pile capacity were undertaken for selection of pile length. The pile's installed length was determined such that the anticipated pile resistance during high rate testing would not exceed the Statnamic testing device capacity. Rigorous analysis of pile capacity was avoided to retain the integrity of the class A prediction.

6.3.2 Test pile instrumentation

Pile instrumentation consisted of three main elements; a pile tip load cell, strain gauged reinforcement and embedded accelerometers (Figure 6.12). The majority of the instrumentation was designed and fabricated at the university.

The pile tip load cell consisted of an upper and lower plate separated by strain gauged load columns (Figure 6.13a). A similar design was successfully used by Whitaker (1964) and Whitaker & Cooke (1966). Their systems were made up of between 8 to 24 individual load columns. More recently Delpak *et al.*, (1998) used a similar arrangement but with six load sensing columns. One problem with using so many load columns is the problem of load focus and eccentricity resulting in single columns attracting significantly larger loads than their neighbours (Omer, 2002). To reduce this, the load cell used in this study only had three columns (Figure 6.13 & 6.14). The upper and lower load cell plates were fabricated from 40mm thick mild steel plate, 500mm in diameter.

The load cell was designed to carry loads of up to 600kN, with each individual load column calibrated against a 2000kN compression load column (ISO376:1999E) using a 1000kN ESH universal testing machine. Each load column consisted of a cylinder 210mm in length with an outer diameter of 43.74mm and a wall thickness of 18.74mm and was calibrated and monitored individually so that any eccentricity of loading could be assessed. The cylinders were machined from 17-4 ph grade stainless steel, which was chosen for its high strength and low hysteresis.

To monitor the loads, each load cell was fitted with 10 strain gauges. The main monitoring set consisted of eight gauges mounted at the mid-height of the columns in sets of two, mounted diametrically opposite each other. Each set consisted of one vertical gauge and one mounted horizontally. These sets of eight were wired to give a

full Wheatstone bridge arrangement. Each individual load column had one independent full bridge arrangement. The remaining two gauges on each column were aligned diametrically opposite just above the main set of gauges. These gauges were wired in a half bridge arrangement with two high precision completion resistors mounted in a watertight junction box bolted to the base of the load cell. The inclusion of the completion resistors allowed the set of two strain gauges to be monitored as a full bridge. The completion resistors were added close to the gauges rather than at the surface monitoring point to avoid the addition of resistance due to long lead wires. The set of two gauges were designed as a back up system to the main set. Again, this set was monitored as an individual channel. Thus, each load column had two channels for monitoring making six channels for the tip load cell.

The bonded foil strain gauges used for the load columns were 350Ω foil gauges (Kyowa, KFG-5-350-C1-11). Generally, vibrating wire strain gauges are used for long term site use as they are less affected by long term burial and long lead wire lengths. These types of gauges were not used in this study as it is unclear how a rapid load pile test would affect the readings of a vibrating device (Dunnicliffe & Green, 1988). The gauges were bonded to the load columns using a bakeable adhesive and then coated with resin and wax as described for the model pile strain gauges in Section 4.3.5.

The load columns were hollow to allow a threaded steel rod (M20) to pass up their centre for clamping the top load cell plate to the bottom one. To further protect the load columns, a thin walled stainless steel cylinder surrounded them (Figure 6.13b). This slotted into O-ring sealed retaining rings bolted to the top and bottom load cell plates. Each protective cylinder contained silica gel crystals (desiccant) to reduce moisture condensation. The cable outlet from the protective cylinders passed through watertight cable glands (Figure 6.14a). Each load column had a watertight junction box bolted to the cell base plate into which two leads from each column fed. This box was designed to allow easy connection of the column to the long lead wires that connected the load cell to the surface monitoring point. Cable outlet from the load cell to the surface was via two lengths of 1½" BSPT galvanised steel water pipe cast within the concrete of the pile. This was surrounded by PVC water pipe to de-bond it from the concrete.

It was necessary to incorporate an inflatable packer between the top and bottom plates of the load cell to allow the load cell to be cast in the pile bore (Figure 6.13a & 6.14b). This was inflated with water prior to pouring concrete and left pressurised for 24 hours after concreting. The packer was inflated against a 6mm thick polypropylene cylinder bolted to the cell base plate. Four lifting eyes were incorporated in the top cell plate to lower the cell to the base of the pile bore.

For measurement of strain within the concrete and to deduce pile load transfer characteristics, strain gauged reinforcement bars were fixed to the horizontal helical reinforcement of the pile. This type of strain installation is often referred to as a "Sister bar". As well as the sister bar reinforcement, two embedded gauges were cast directly into the concrete (Figure 6.12).

The sister bars consisted of 1m lengths of standard T12 reinforcing bar with a 50mm section turned down at the mid-point. The reduction in diameter due to turning was kept to a minimum whilst creating a smooth surface for strain gauge application. Single strain gauges of the same type as used in the tip load cell were fixed to the reinforcement bar. These were then wired to the full length of lead wire and protected. Gauge protection consisted of two coats of polyurethane followed by a layer of Teflon tape. This was followed by a coating of an epoxy resin, which when dry was wrapped with a layer of adhesive aluminium foil tape. To this was applied another coating of epoxy resin. Generally, 24 hours was left between each protective coat for curing. The final coating consisted of covering the central zone with a 150mm long length of adhesive lined shrink fit. This was heated with hot air to seal the strain gauge arrangement. Additionally, this coating acts to debond the gauged length from the concrete (Dunnicliffe & Green, 1988).

The sister bar reinforcement was tied to the main reinforcement in sets of three (120° apart) at five different levels as shown in Figure 6.12. The wiring was then run up the outside of the reinforcing cage to the surface. The lower level was chosen to be as close to the pile tip load cell as possible to aid load comparison and, the upper set was located within the zone of the outer steel casing. The outer steel casing was designed as a friction reducer such that compression in this zone would be due to the applied load

with minimal load transfer to the surrounding soil. This aids analysis of the strain gauge readings.

As well as the sister bar reinforcement, two embedment gauges were cast directly in the concrete. These were referred to as plastic encased gauges by Dunnicliffe & Green (1988) because they consisted of a standard foil gauge hermetically sealed between plastic plates (Kyowa, KM-120-120-H2-11). These units are susceptible to large zero drift due to creep of the plastic plates. Although they are only recommended for short term use, they were incorporated for redundancy, which was justified by their relatively low cost. These units were mounted in the region of the steel casing towards the top of the pile.

As only single gauges were mounted on the strain sister bars, quarter bridge wiring arrangements were employed. These were wired using three-wire screened leads to minimise the effect of temperature change and, subsequent resistance change on the long lead wires. Where full bridge circuits were used, the lead wires consisted of twin twisted pair individually shielded wires. For the quarter bridge arrangements the wires were twisted and overall shielded. For all instrumentation, no connections were made until the logging unit.

Two accelerometers were cast in the pile. These were sealed in waterproof protective stainless steel housings and wired to the pile reinforcement at two levels. Again, the protective housings contained a chemical desiccant. These units were incorporated to allow comparison of the calculated accelerations at the pile top with those measured at depth. The units used were those previously used for the laboratory study as described in Section 4.2.8.

All of the instrumentation cabling exited the pile approximately 100mm below its top. These were then run into the ground, into two 60mm internal diameter steel pipes that were placed between 100 and 300mm below ground level. These fed back to the instrumentation hut (Soudain, 2002) approximately 15m away from the pile (Figure 6.3).

6.3.3 Soil instrumentation

As well as instrumenting the pile, the ground surrounding the pile was instrumented with accelerometers. These were placed at two depths with three accelerometers at each depth at various spacings away from the pile (Figures 6.4 & 6.12). The units were placed in similar protective housing as those used in the pile. They were Kistler ceramic shear type 8774A50. These units were installed at 4mBGL and 8mBGL at varying radial distances away from the pile (Table 6.5). The depth was designed to correspond to the initial depth of the accelerometers cast in the pile.

The soil accelerometers were installed using the standard cone penetration testing (CPT) truck on completion of seismic CPT. To place the accelerometers a hollow casing of 36mm internal diameter with a sacrificial tip was pushed to the required depth. The accelerometer in its protective casing was lowered down the casing until contact could be heard with the tip. The casing was then withdrawn as a grout consisting of a cement/bentonite mix was poured down the casing. The cabling was then run in 50mm diameter tubing, buried below ground level, back to the main pile cable ducts. This system of installation worked very well and allowed six accelerometers to be placed in seven hours.

6.3.4 Data acquisition

All the cabling from the pile and soil instrumentation was fed back to the instrumentation hut. Here the excitation and conditioning of the signals was carried out using the system as discussed in Section 4.5 with minimal modification. Additional high speed cards were added to the Fylde unit along with type FE-376-IP (ICP amplifier) for conditioning of the additional accelerometers. This proved more cost effective than adding channels to the Kistler conditioner. The accelerometer outputs were all filtered using a 1kHz low pass filter, as for the model testing.

Due to the distance of the instrumentation hut from the EPCL main buildings and the high volume of vehicle movements, it was considered impractical to run mains power cables across the site. Power for the hut and instrumentation was provided by petrol driven generators. Unfortunately, these may be unreliable and do not provide a constant power source. To solve this problem, the generator output was plugged into a Belden

Universal Power supply (UPS), which provided a regulated safe voltage as well as battery back up to the system. Such a system is advised during the logging of short duration test events and where sensitive equipment is used on site.

Data acquisition was also carried out with the same system described for model testing. The LabVIEW program for model Statnamic logging was simplified and the static pile testing was logged using the slow logging program used for model pile tests.

6.4 Pile testing and interpretation of results

The programme of loading undertaken on the two piles included Statnamic and static testing and is outlined in Table 6.6. Although both piles were tested the majority of this section will be concerned with testing of the auger bored pile unless otherwise stated.

6.4.1 Statnamic testing

Statnamic testing was carried out using a 3MN tripod rig with a hydraulic catch mechanism provided by PMC limited (PMC, 2003), as shown in Figures 6.15 & 6.16. The rig was transported to site on the back of a standard artic flat bed trailer and unloaded using a 70 tonne mobile crane. On the first day of testing, the pre-cast driven pile was subjected to three Statnamic loading events of 1000, 1250 and 1500kN before the Statnamic rig was moved over to the auger bored pile. The auger bored pile was then tested at 1000kN. The auger bored pile was left overnight before further loading was undertaken at 1500, 2000, 2500 and 3000kN. A repeat test at 1500kN was carried out after the 2000kN load cycle as the first 1500kN test exceeded the target load. The loads quoted for Statnamic loading are the target maximum loads required rather than the actual loads achieved.

The STN testing was carried out over two days as shown in Table 6.6. It is acknowledged that for comparison of STN tests and comparison of cycles with subsequent static tests this approach was not ideal. Rapid re-cycling of the pile under STN testing would have led to an increase in pore pressure around the pile and subsequent reduction in effective stress. The approach was adopted to obtain the greatest amount of test data in the shortest period and minimise financial penalties on the contractor supplying the equipment.

The measured load and displacement along with the calculated velocity and acceleration from the 3000kN test on the auger bored pile can be seen in Figure 6.17. The main difference between these prototype results and those obtained from the model tests is in the measured displacement. The maximum measured displacement was of the order of 10.8mm but reduced to a residual displacement of 4.4mm. This suggests that either the pile resistance was still within the elastic zone or the soil/pile was undergoing considerable elastic deformation. The peak calculated pile velocity for the test was 467mm/s which was approximately twice that found for the model Statnamic tests, although the peak velocity was of similar magnitude to those achieved during high rate model CRP testing.

The velocity and acceleration shown were obtained by differentiation of the displacement-time history. To calculate the acceleration, the calculated velocity was smoothed by five point adjacent averaging. The minimal smoothing was not the result of high quality data sampling but was enforced by the relatively low logging rate of one sample per millisecond associated with the STN equipment. This resulted in the loss of peak acceleration values as can be seen by comparing the calculated acceleration with that measured by an accelerometer cast in the pile (Figure 6.18). The measured accelerations are less noisy than those calculated and show greater peak accelerations. The high rate of change of measured acceleration highlights the need for high logging rates. As the number of logging points is spread further apart during the rapid changes in acceleration, the use of smoothing by adjacent point averaging should be minimised to avoid peak clipping. Similarly, the velocity calculated from the displacement time history is far noisier than that calculated from acceleration readings. This may prove significant for static pile capacity derivation from STN tests. The slight increase in pile velocity calculated from the measured accelerations after the STN event is due to a zero shift on the accelerometer. This can easily be corrected by doing a "baseline" correction. Logging of the pile instrumentation was carried out at 0.5 millisecond intervals.

The logging rates used during the laboratory testing were as high as every 0.25 millisecond. This was possible as the logging was initiated by a triggering signal so that the duration of logging was carefully controlled. Due to time limitations and the risk of using triggering signals on noisy field sites, this approach was not used. Instead, the

logging was manually started and allowed to run for thirty seconds within which time the STN test occurred. Thus, the logging system limited the logging rate due to logging card buffer size. Synchronisation of the PMC STN logging system and the pile instrumentation was achieved by logging a triggering pulse generated by the STN logging system.

Typical load–displacement results from the repeated STN testing of the auger bored pile can be seen in Figure 6.19. Each new test has been reset to zero displacement due to problems associated with determining the final pile level based upon the STN displacement readings. At the end of some of the tests, there was a tendency for an apparent rapid increase in pile settlement (Figure 6.20). This is thought to be due to either surface ground waves from the pile disturbing the laser reference beam (Figure 6.15b) or movement of the STN piston/load cell arrangement on the head of the pile (Figure 6.15a). The latter would seem the most likely and suggests the need to rigidly connect the STN device to the pile but this could raise technical issues. Mounting of an accelerometer at the head of the pile could be used as a check of the optical displacement measuring system used with the STN test. It would also be a better source of acceleration readings and potentially velocity calculations for STN analysis. Ideally, the displacement measuring system should be connected to the pile.

To back check the actual pile displacements, results from the two accelerometers mounted in the pile were integrated to find the pile's displacement at 4m and 8m below ground level (Figure 6.21). The accelerometer-derived displacements do not display any significant post test displacement fluctuation as seen in Figure 6.20. They also show significantly less displacement than at the head of the pile. It is difficult to speculate on the cause of this additional movement without having accelerometer based displacement measurements at the pile head. The results from the embedded accelerometers do confirm that rigid body assumptions are valid between the two measuring points due to the very similar displacements.

Calculation of the pile ultimate capacity based upon the methodology used by Bell (2001) in Section 6.3.1 would suggest a static skin capacity of 1539kN and a tip capacity of 266kN (total of 1805kN). Although this value has been exceeded during the repeated STN tests shown in Figure 6.19, it is difficult to assess whether the pile

capacity was fully mobilised i.e. moving from elastic behaviour to plastic behaviour. With hindsight, the STN load should have been taken higher or the pile designed with less capacity. The load applied to the pile was the maximum achievable with the STN device used. Where STN is used in a commercial environment, the magnitude of each load cycle should be chosen after inspection of the previous test. Additionally, the maximum test load should be chosen such that there is sufficient excess load above the equivalent static capacity.

6.4.2 Constant Rate of Penetration (CRP) testing

Constant Rate of Penetration (CRP) testing was carried out after the Statnamic testing (Table 6.6). This form of testing was undertaken to allow comparison with the CRP test used during model testing. The static CRP test was undertaken by PMC limited as per the guidance in ICE (1997) at a rate of 0.01mm/s, as used during the model testing. Load was applied to the pile using a hydraulic jack with load readings monitored by a load cell. Readings of pile displacement were made by four LVDT's placed upon the pile head. These were mounted on magnetic stands in pairs on two arrangements of scaffold driven into the ground (reference beams) to allow remote measuring of settlement. Pressure was provided to the hydraulic jack from a compressor via an air-hydraulic interface. Control of the penetration rate was achieved by monitoring a computer display of penetration rate and manually adjusting a relief valve on the pressure application system. Reaction for the jack was provided by reaction beams running over the test pile anchored to three 600mm diameter auger bored piles installed to 11.5m deep. Further detail of the reaction system is given by Bell (2001).

Logging of the applied loads and pile displacement was carried out at 12 second intervals. To aid synchronisation of the pile instrumentation readings, an additional LVDT was placed upon the pile head and logged by the instrumentation used during the STN testing.

The load displacement readings for the auger bored pile during the CRP test are shown in Figure 6.22. The test was terminated at 26.78mm displacement or approximately 5% of the pile diameter to allow further penetration of the pile to occur in subsequent testing whilst avoiding damage to the pile instrumentation wiring. The pile appeared to behave elastically up to approximately 1600kN and then displayed plastic behaviour.

Unlike the model testing where no appreciable increase in pile capacity was noted after a displacement equivalent to 3% of the pile diameter, the full scale pile capacity increased at a rate of 125kN per mm of penetration. The final load measured at 26.78mm was 2205kN.

6.4.3 Maintained Load Testing (MLT)

Finally, a Maintained Load Test (MLT) was carried out by PMC using the same equipment and arrangement as for the CRP testing. Again, testing was undertaken according to ICE (1997) for a proof load test, followed by an extended proof load test. The design verification load chosen was 900kN with a specified working load of 900kN. The maximum load applied during the proof load test was 1350kN and the maximum load applied to the pile during the extended load test was 1800kN. The load displacement readings are shown in Figure 6.22.

6.4.4 Comparison of pile load test results

Comparison of the results from the different tests is shown in Figure 6.22. The behaviour of the pile for all three tests is very similar in the elastic zone up to 1000kN, which may be taken as approximately 50% of the ultimate CRP static pile capacity. After this point, the STN stiffness increases over the low rate tests. The MLT and CRP tests had similar stiffness up to 1350kN at which point the MLT results display abrupt yield. Significant plunging of the pile during MLT testing was encountered at a load of 1800kN. Yield of the pile during CRP testing commenced at a similar load to that in the MLT test but was more gradual up to approximately 1900kN. Yield in the STN test was not apparent until very close to the peak STN load of 3071kN.

Displacements achieved during the MLT and CRP tests were limited to 23.05mm and 26.78mm respectively. In comparison, the STN test only achieved a maximum displacement of 10.96mm but 28% more load was applied than during the CRP test. Maximum STN displacement was achieved at 2456kN. Residual displacements at the end of the tests for the CRP and MLT tests were 22.22 and 19.46mm respectively. This is 84% of the maximum displacement whereas the residual displacement during the STN test was only 32% of the maximum displacement. This, along with the shape of the STN load-displacement curve would suggest that the STN results reflect the pile-soil elastic behaviour rather than the mobilised plastic behaviour.

The difference in the ultimate capacities suggested by the MLT and CRP tests is likely to be due to the difference in rate between the two tests. This difference will also be influenced by the test history of the pile. To compare CRP and MLT it is common practice to ignore the load hold periods during MLT tests. This method of comparison is not considered reliable, as there is apparently little control over the rate of load increase between load hold increments for this type of test.

6.4.5 Pile instrumentation results

To analyse the results from the embedded sister bars it was necessary to determine the stiffness (modulus) of the pile. This is often undertaken by the testing of concrete cylinders under laboratory conditions to BS 1881-121 (1983), but this method does not allow for the presence of reinforcing steel in the pile. Additionally, concrete quality may vary throughout the pile and thus stiffness determinations should be based upon in-situ pile behaviour.

The pile stiffness was determined by considering the average strain in the uppermost sister bars (Level 1, Figure 6.12) which were located at 0.75mBGL, within the sleeved section of the auger bored pile. As the elastic modulus of concrete is not a constant and varies with imposed load, the MLT test strains at each increasing load increment were used to find the modulus. The tangent modulus was calculated using the Equation suggested by Delpak *et al,* (1998):

$$E_{ct} = \frac{P_h - E_s A_{s1} \varepsilon_1}{\varepsilon_1 A_{c1}} \tag{6.5}$$

Where

E_{ct} = tangent modulus of concrete (kN/mm^2)

P_h = pile head load (kN)

E_s = Young's modulus of steel (taken as 200kN/mm^2)

A_{s1} = cross-sectional area of steel at level 1 (mm^2)

ε_1 = strain in the concrete at level 1 (microstrain)

A_{c1} = cross-sectional area of the concrete at level 1

The variation of tangent modulus with strain can be seen in Figure 6.23 with modulus varying from approximately 28kN/mm^2 to 24kN/mm^2 with increasing strain. The average stiffness obtained from laboratory testing of concrete cylinders to BS1881-121 (1983) gave stiffness values of 31.37kN/mm^2 (concrete cube strength, f_{cu} =44kN/mm^2). Where Delpak *et al*, (1998) used a non-linear representation of tangent modulus-strain relationship a linear approach was found to be adequate in this case. This was then used to find the axial force at the different levels in the pile by using Equation 6.6.

$$P_i = \varepsilon_i \{[-21961\varepsilon_i + 27.963]A_{ci} + E_s A_{si}\} \quad (6.6)$$

Where

P_i = axial force at the level of interest

Note subscript i denotes the level at which the results are calculated.

The pile stiffness calculated from the MLT test was then used to consider load transfer in both CRP and STN testing. The apparently noisy data seen in Figure 6.24 was apparent in the strain measurements for the upper strain monitoring levels only. On moving down the pile the amount of noise reduced. This was possibly due to the presence of electrical generators and hydraulic power packs close to the pile during testing.

Calculated axial loads in the pile during MLT testing can be seen in Figure 6.25. It is apparent that very little load transfer (reduction in axial load) is occurring between Level 1 and Level 2 (Figure 6.25b) due to the presence of the friction reducing casing. As the applied load increased above 1125kN, transfer occurred but this is was to be expected as the Level 2 monitoring point was located 1m below the cased section (Figure 6.25a). Full mobilisation of the skin resistance along the length of the pile would appear to occur between 1350kN and 1575kN, based upon the convergence of calculated shaft resistance (Figure 6.25c) and the significant increase in load at level 5 (Figure 6.25b). The calculated maximum shaft resistance was found to be between 67 to

83kN/m^2 depending on the level considered. The higher reading was associated with a zone of lower undrained shear strength and cone penetration/skin resistance between 6 to 8m BGL. The increase in axial force measured by the strain gauges at level 5 for applied loads of 1575kN and 1800kN, combined with little apparent increase in load measured by the tip load cell, generated an anomalously large skin friction close to the pile tip. Although Delpak *et al*, (1998) observed a similar effect, it is thought that the effect is due to failure of the pile tip load cell rather than representing a real phenomenon.

The results from the sister bars during CRP testing were considered at similar loads as the increments used in the MLT testing (Figure 6.26). Again, similar load transfer behaviour is noted for Levels 1 and 2. Load transfer to the ground along the complete length of the pile appears to occur between 1350kN and 1575kN (Figure 6.26b). The reduced rate of convergence observed for the calculated shaft resistances (Figure 6.26c) suggest that ultimate shaft resistance has not been achieved. The maximum calculated shaft resistances during CRP testing were found to be between 92 and 104kN/m^2, which is approximately 20% greater than during MLT. This difference may be a result of the different testing methodology but it will also be influenced by the increasing cumulative pile displacement in moving from CRP to MLT.

Due to the nature of the STN test, it is not straightforward to compare like for like load transfer with static tests. Figure 6.27 shows the load transfer results for a 2000kN STN test considered at load increments similar to those used during MLT testing. Considerable load transfer is occurring between Levels 1 & 2 at loads as low as 450kN, which is not apparent in the static tests until loads as high as 1125kN. One feature that was noted in all of the STN test cycles was the presence of considerable strain variation over the three sister bars located at Levels 1 and 2. Below these levels, the strains were of similar magnitude in each of the three bars. The high load transfer between levels 1 and 2 results in the lower levels displaying relatively low axial loads. For example, the 2000kN pulse reached a maximum load of 2048kN. The axial loads derived for levels 2, 3 & 4 at peak STN load are similar to those measured for a load increment of 1575kN in both the CRP test and the MLT. Thus, for a STN load of 2048kN the load transfer for the majority of the pile is similar to that for static tests at 1575kN. Loads for the STN tests at Level 5 are more like those found during an 1125kN static increment.

Considering the pile shaft resistance during the 2000kN STN test, it can be seen that the shaft resistance between Level 2 and 3 are converging at approximately 70kN/m^2 whilst the lower shaft resistance is increasing up to 88kN/m^2. These values are similar to those obtained during MLT testing and would suggest that the maximum shaft resistance had not been reached. As discussed in Section 6.4.4 this would suggest that the pile was still operating in the elastic zone and the rate dependant enhancement of skin resistance associated with plastic behaviour was not a major factor. The shaft loads obtained during the 3000kN STN cycle (3071kN peak load) are shown in Figure 6.28. In contrast to the 2000kN STN, the shaft resistance varies from 96 to 130kN/m^2 at peak STN load. This is 34% higher than the MLT results and 20% greater than the CRP values. The results also contrast with the static results in that the greatest shaft resistances are obtained between Levels 4 and 5 rather than 3 and 4. The high load transfer noted during STN tests between levels 1 and 2 may be enhanced due to the ground conditions at this level. The undrained shear strength, cone/skin resistance and seismic velocities were all at their greatest in this zone.

One objection to the use of STN testing over other pile testing methods was that the stress in the upper portion of a pile was considerably greater. This increased stress resulted in increased strains as can be seen in Figure 6.24. It is clear from Figures 6.22 & 6.24 that the increase in strain is proportional to the increase in pile head load and thus applied stress. There were no visible signs of damage to the pile due to these increased stresses.

Results for shaft load transfer generally show a very large increase in shaft resistance between the lowest sister bar position and the pile tip load cell. This is thought to be due to failure of the pile tip load cell. Problems were encountered during installation that resulted in the load cell central cable pipe work rising as the concrete was poured into the pile shaft. It is unclear what caused this and how it affected the load cell. During the STN testing, the tip load cell appeared to work but the results shown in Figure 6.29 indicate that columns 2 and 3 carried lower loads during the STN loading. This was thought to be due to eccentric loading of the three columns. Pile tip loads used for the STN load transfer calculations were based upon the average of the three columns. On returning to site to carry out the static testing, large zero load shifts were noted on all

the three columns. On analysing the results, it was found that only the backup gauges on one of the columns were giving sensible stable results. This column load was taken as an average reading for each of the three columns and used for load transfer calculations. This assumption does not allow for any eccentricity in the load cell.

Even when the load cell appeared to be working satisfactorily during STN testing the measured loads would appear to be conservative based upon the calculated shaft resistance results.

6.4.6 Soil inertial behaviour

During the STN testing of the auger bored pile, the accelerometers installed in the pile and the surrounding ground were monitored. Typical accelerations monitored in the pile compared with those received at the buried transducers can be seen in Figure 6.30. In contrast to the recorded accelerations recorded during model testing, the soil accelerations follow the pile accelerations with diminished magnitude and a small phase shift. This goes some way to confirming that the model test accelerometers with their exposed surfaces were affected by pressure during testing as discussed in Section 5.5.7.

In order to consider the dissipation of acceleration away from the pile, the accelerations were compared for the greatest positive acceleration. To aid comparison, the pile accelerometer at the relevant depth was used as the initial acceleration source. The dissipation of acceleration for transducers mounted at 8mBGL is shown in Figure 6.31. It is clear that the accelerations have decayed rapidly by 3R and have fallen below 10% of the pile's acceleration by 6R. Similar results were obtained for the transducers installed at 4mBGL.

To allow calculation of soil inertia the decay was expressed as a two parameter exponential decay as suggested in Section 5.5.7:

$$\frac{\ddot{x}_I}{\ddot{x}_p} = 3e^{-1.103(r/R)} \tag{6.7}$$

Where

$\ddot{x}_l$ = local bed acceleration

$\ddot{x}_p$ = peak pile acceleration

r = radial position of accelerometer

R = pile radius

Some delay was noted between the first arrival times of the ground accelerometers and those mounted in the pile, with the arrival time increasing with increasing distance from the pile. For example, the delay to the first ground accelerometer was generally of the order of 1 millisecond increasing to 10 milliseconds for those furthest away.

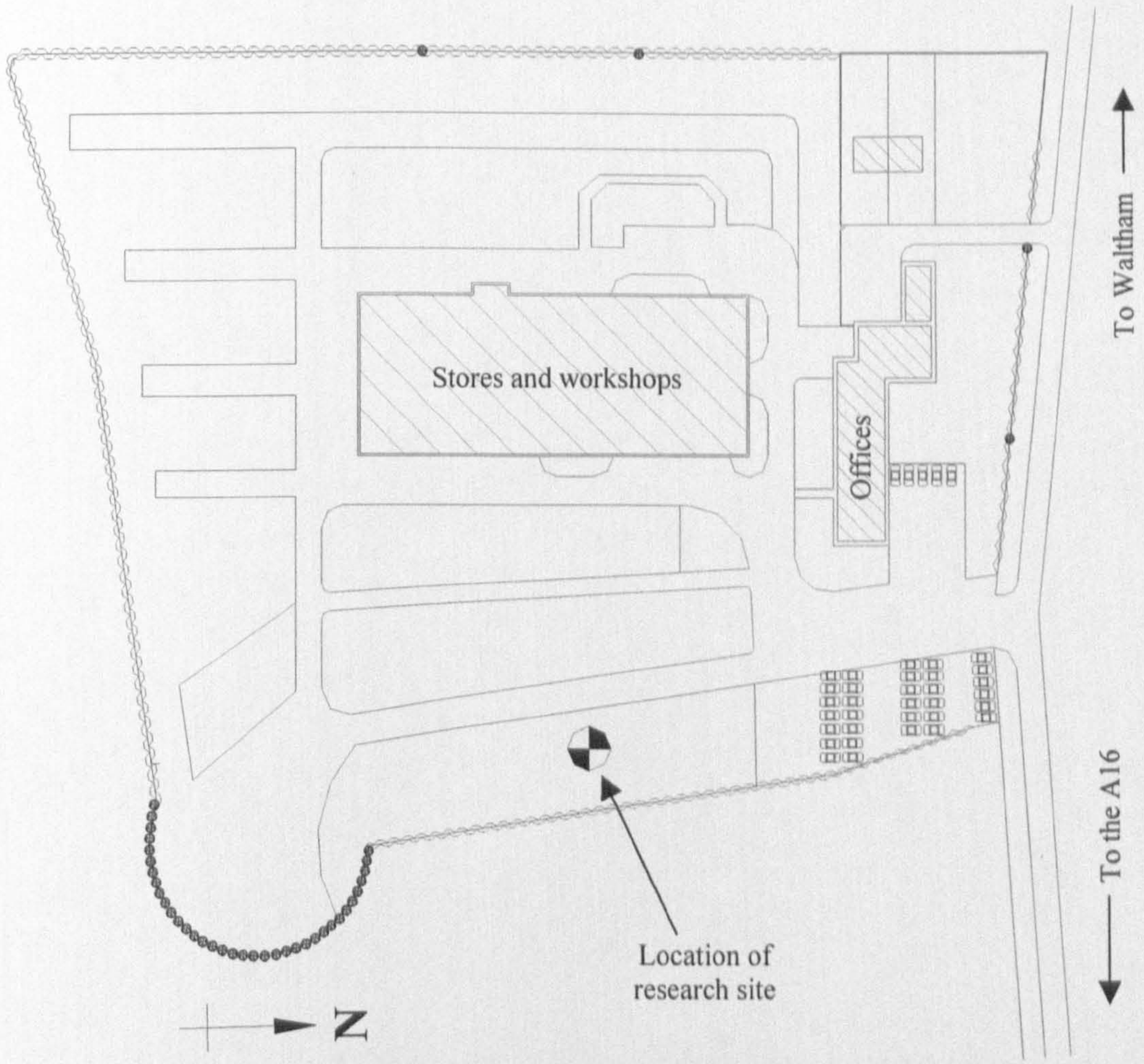

Figure 6.1, Layout of Expanded Piling Limited Grimsby Depot showing research site location. Plan provided by EPCL.

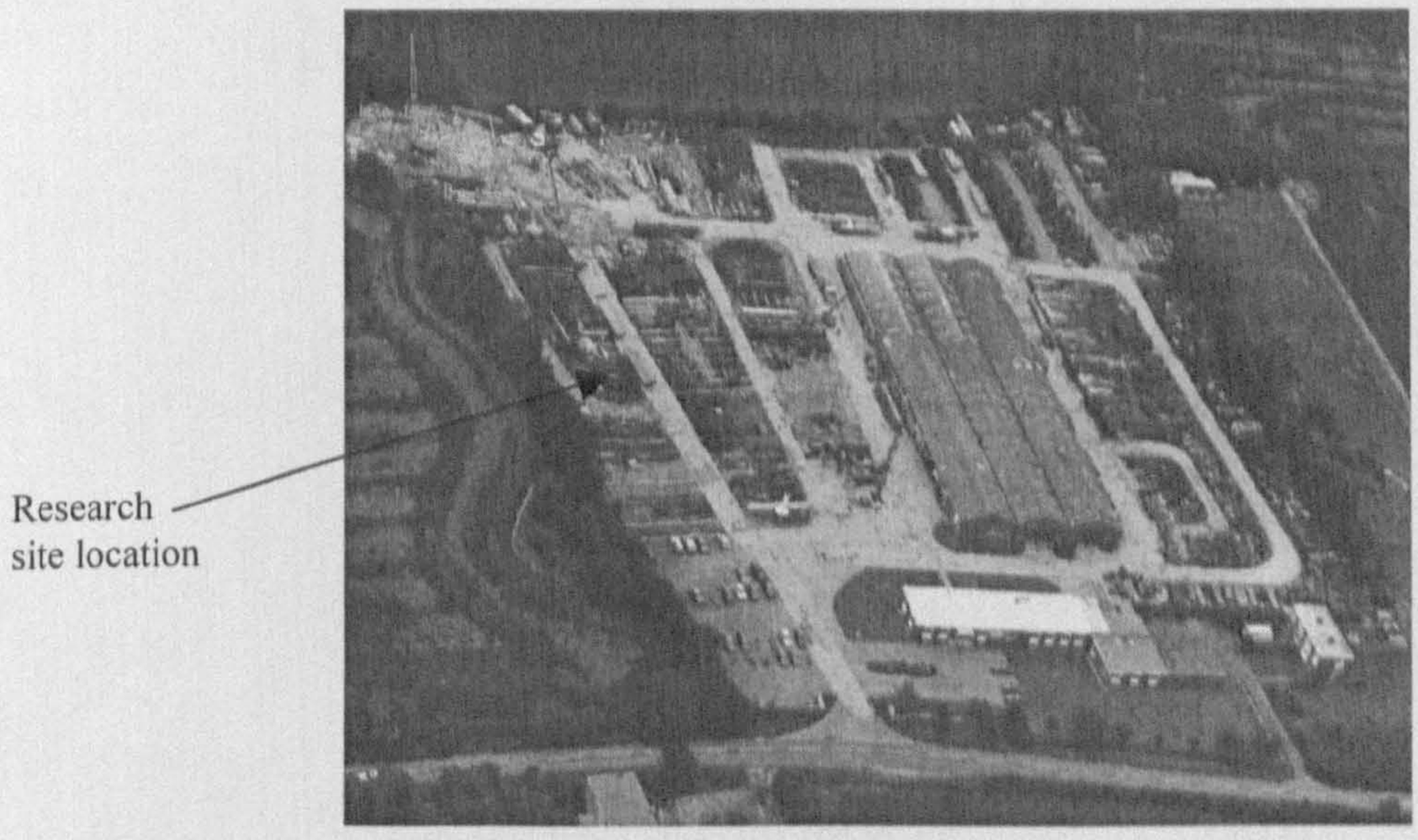

Figure 6.2, Aerial photograph of EPCL depot. Photograph provided by EPCL.

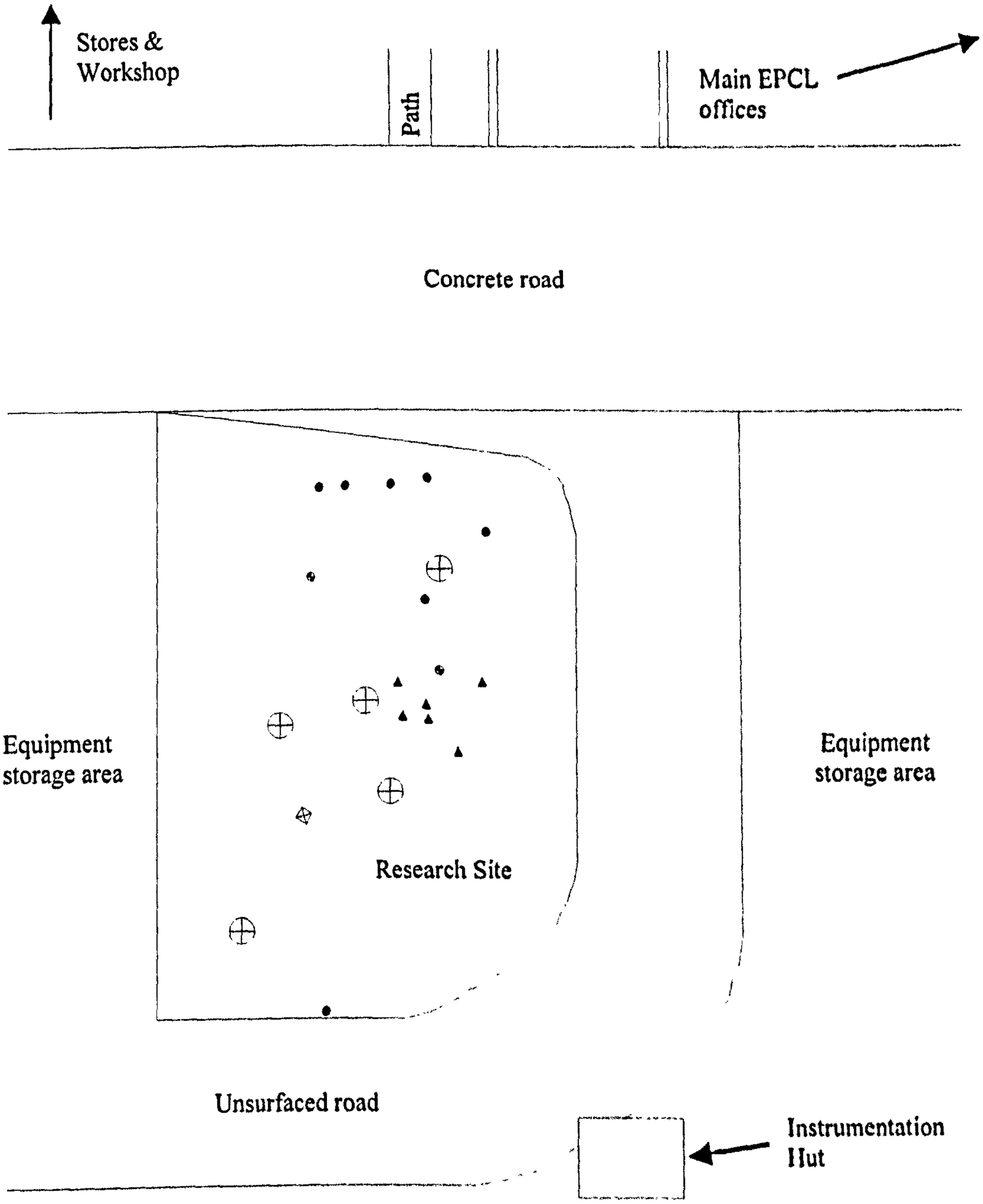

Figure 6.3, Location plan of Grimsby research site.

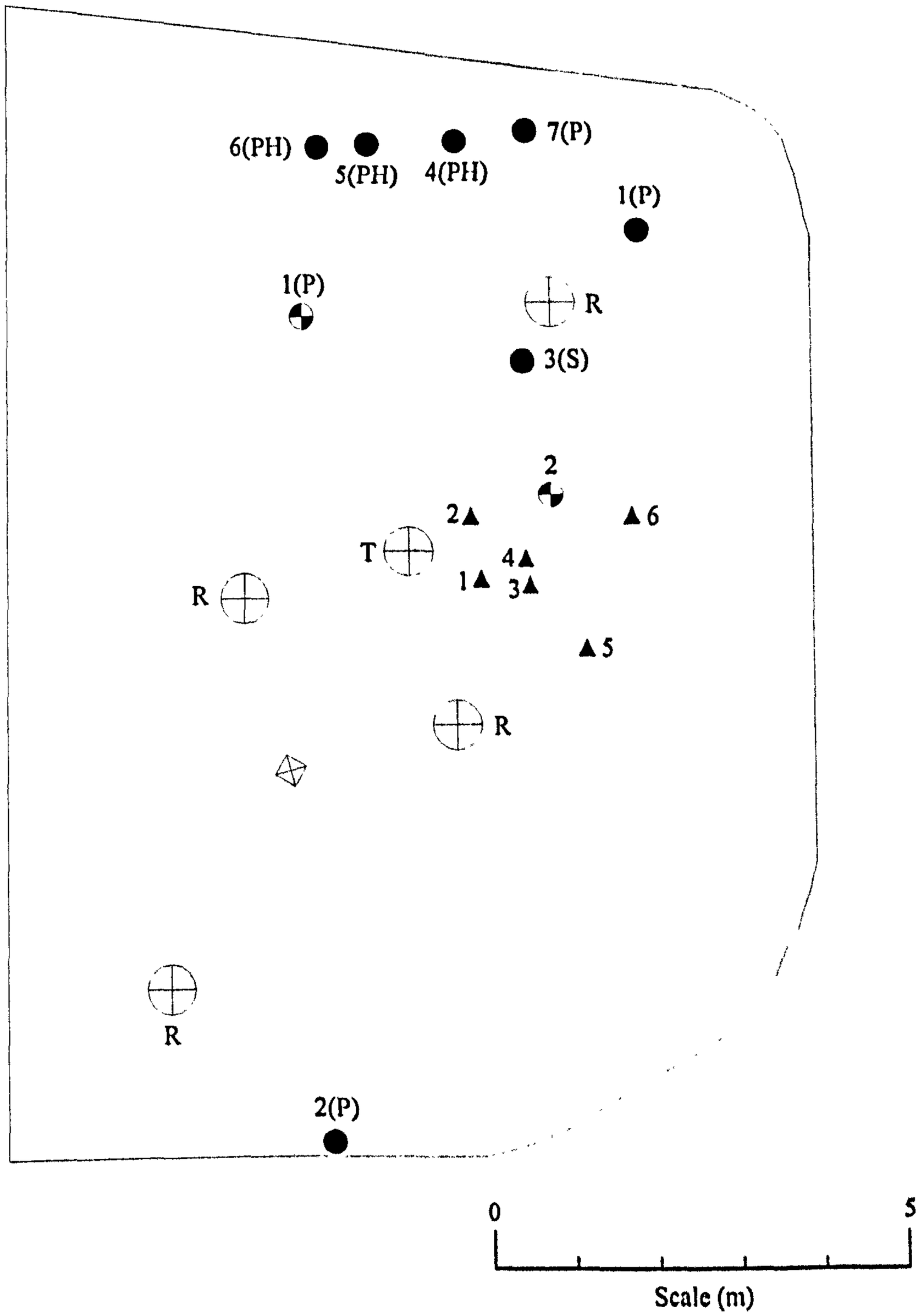

Figure 6.4, Detailed plan of Grimsby research site showing test and installation positions.

Depth BGL (m)*	*Soil Description*
0 to 0.6	Topsoil
0.6 to 1.5	Medium Stiff, Light Brown CLAY with gravel.
1.5 to 10.0	Very Stiff to Firm, Dark Brown, gravely CLAY, gravel medium to coarse with occasional cobbles. At 4.5m Thin beds of silty sand.

**BGL-Below Ground Level.*

Table 6.1, Description of soil encountered by Taylor (1966).

Depth BGL (m)*	*Soil Description*
0 to 0.3	Firm to Stiff, slightly sandy, mottled orange Brown CLAY with occasional black organic fragments.
0.3 to 2.4	Firm to Very Stiff, slightly gravely, light orangey Brown CLAY with occasional black organic fragments and extremely close spaced thin lamina of silt, gravel fine to medium, rounded to sub-rounded.
2.4 to 20.35	Firm to Very Stiff, greyish brown to dark brown CLAY with occasional coarse gravel and rare cobbles, gravel fine to medium, rounded to sub-rounded. At 4.2m Firm to Stiff. At 9.2m Thin lens of Fine, silty Brown SAND (BH2 only) 10.45m becoming Stiff.

* *BGL-Below Ground Level.*

Table 6.2, Description of encountered soil based upon boreholes 1 & 2.

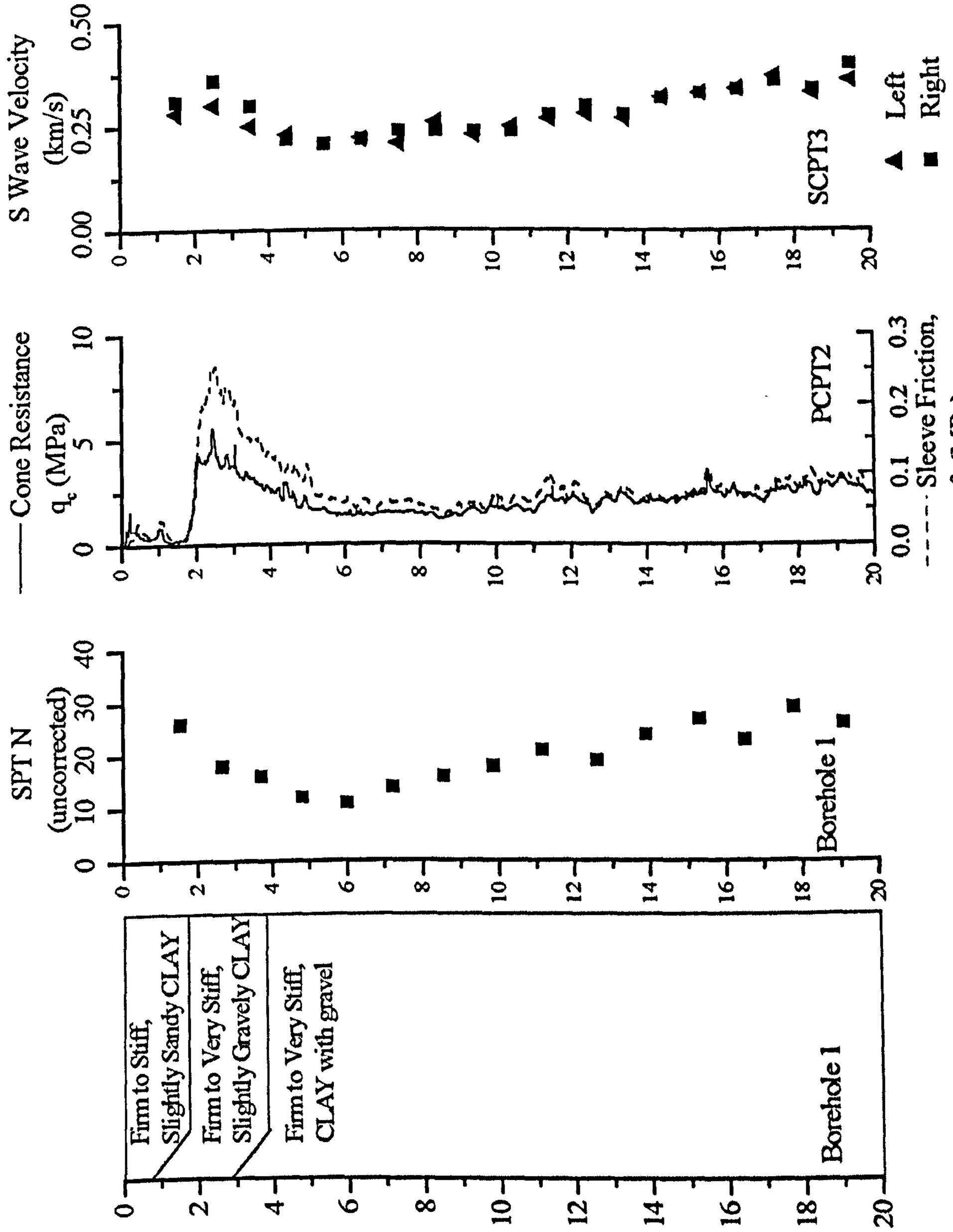

Figure 6.5, Ground investigation information from borehole and CPT investigations.

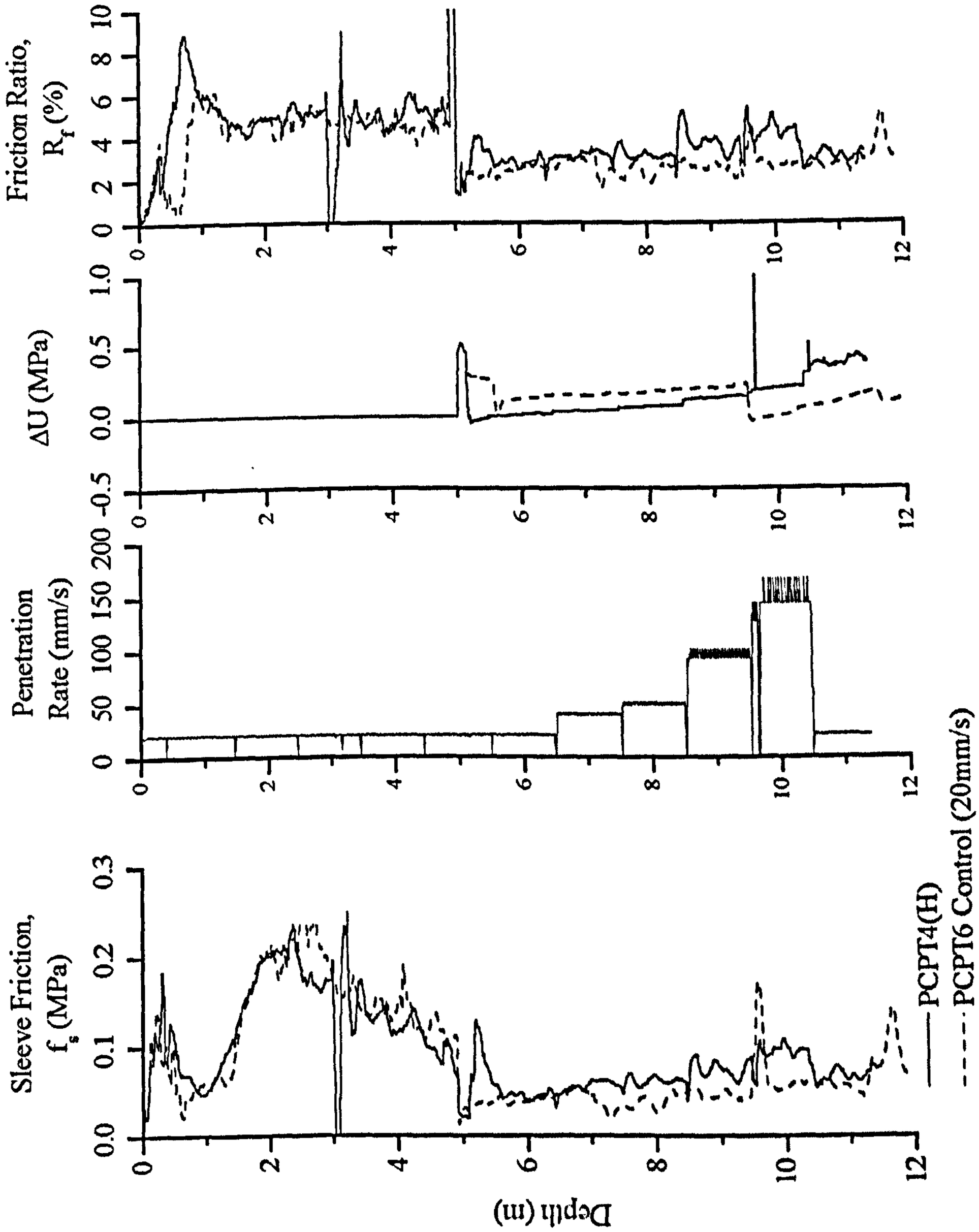

Figure 6.6, Comparison of standard rate PCPT testing (20mm/s) with a test undertaken at elevated rates.

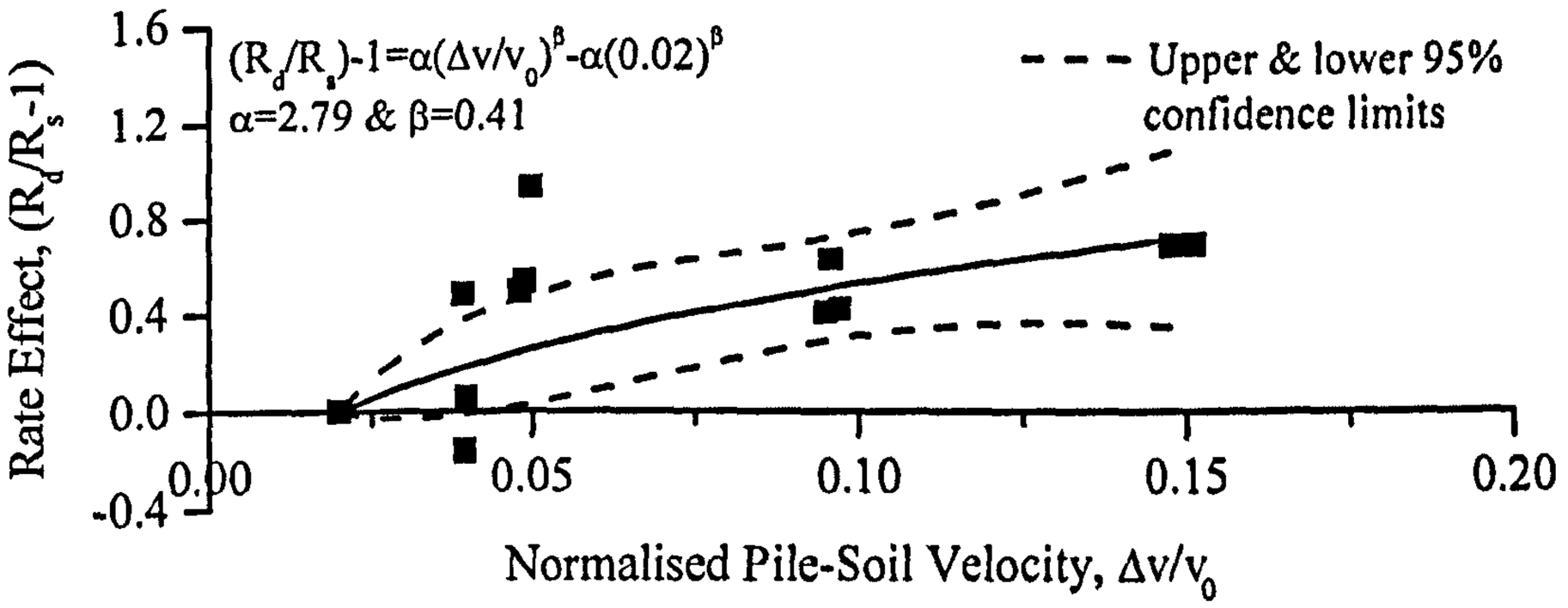

Figure 6.7, Application of rate law to CPT skin friction resistance to obtain rate parameters.

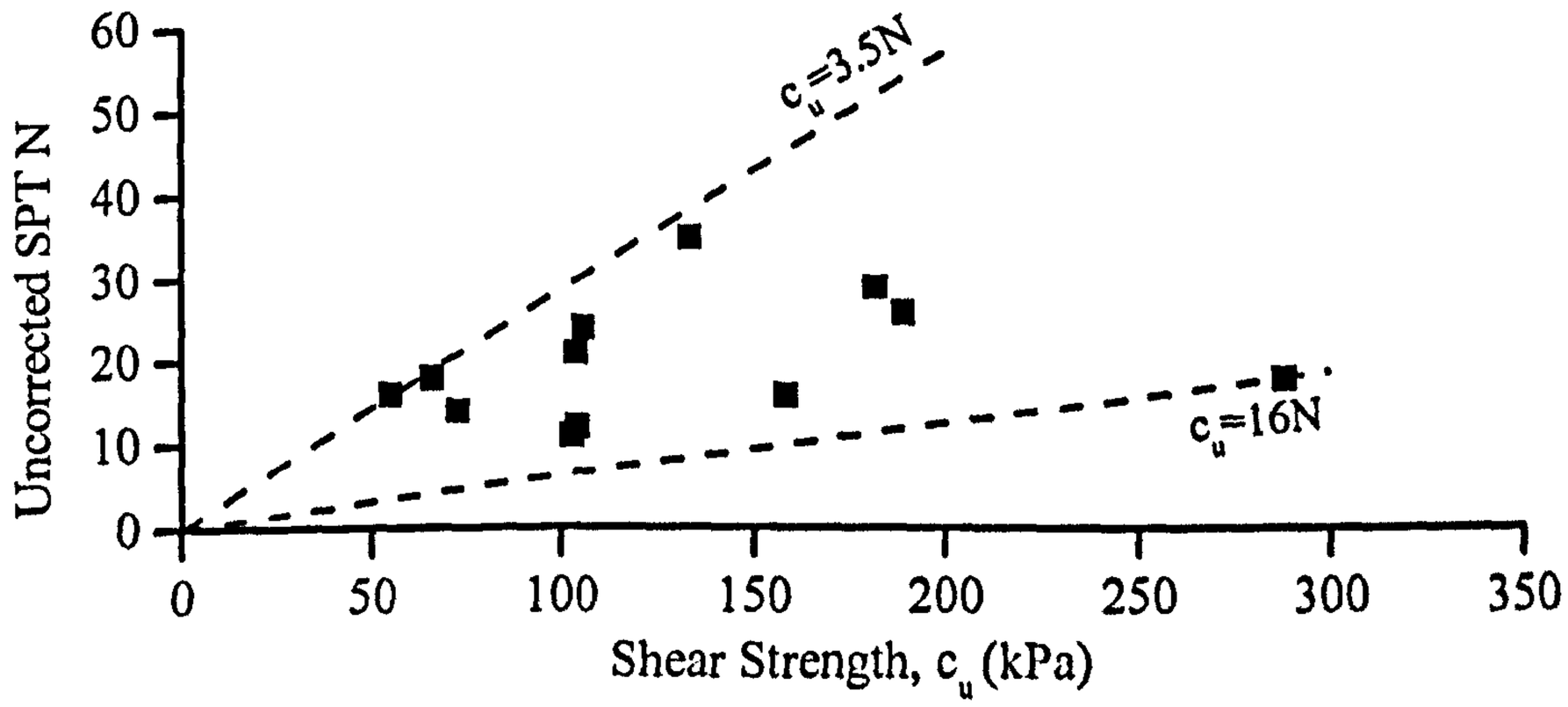

Figure 6.8, Relationship between SPT N value and undrained shear strength.

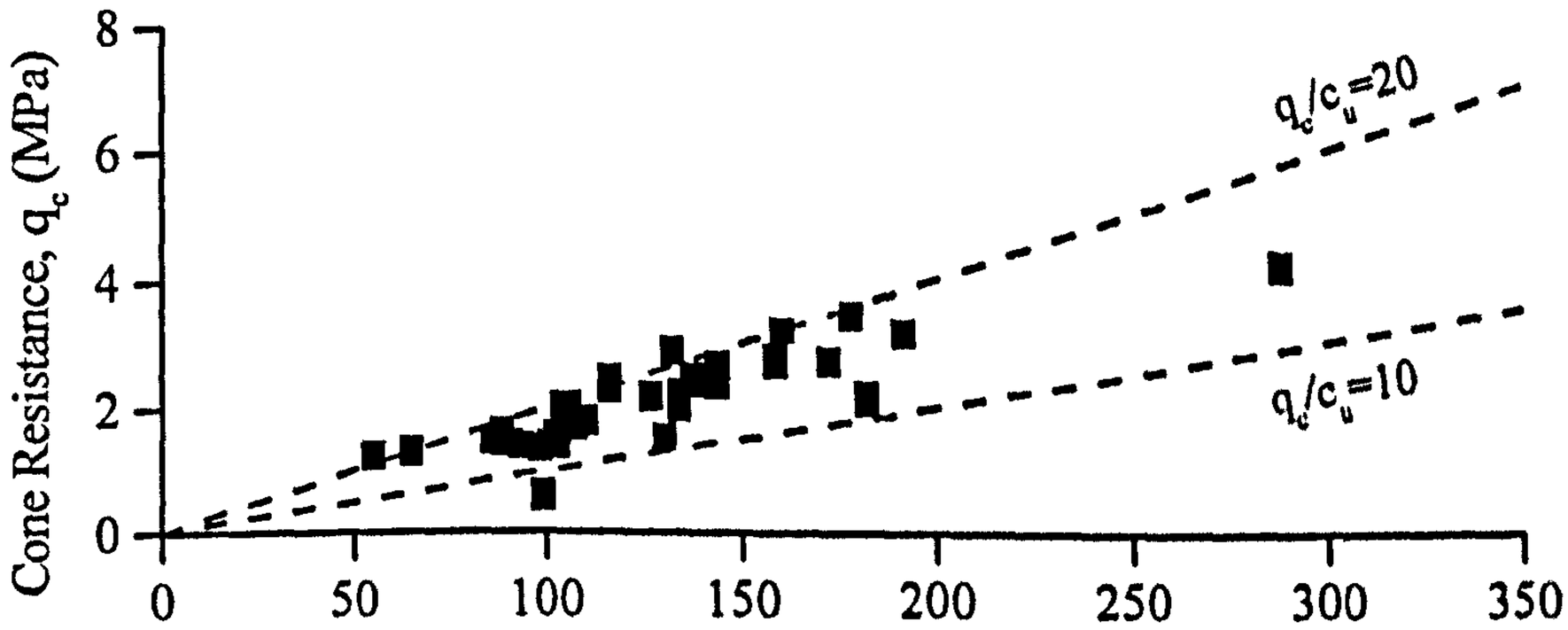

Figure 6.9, Relationship between CPT cone resistance and undrained shear

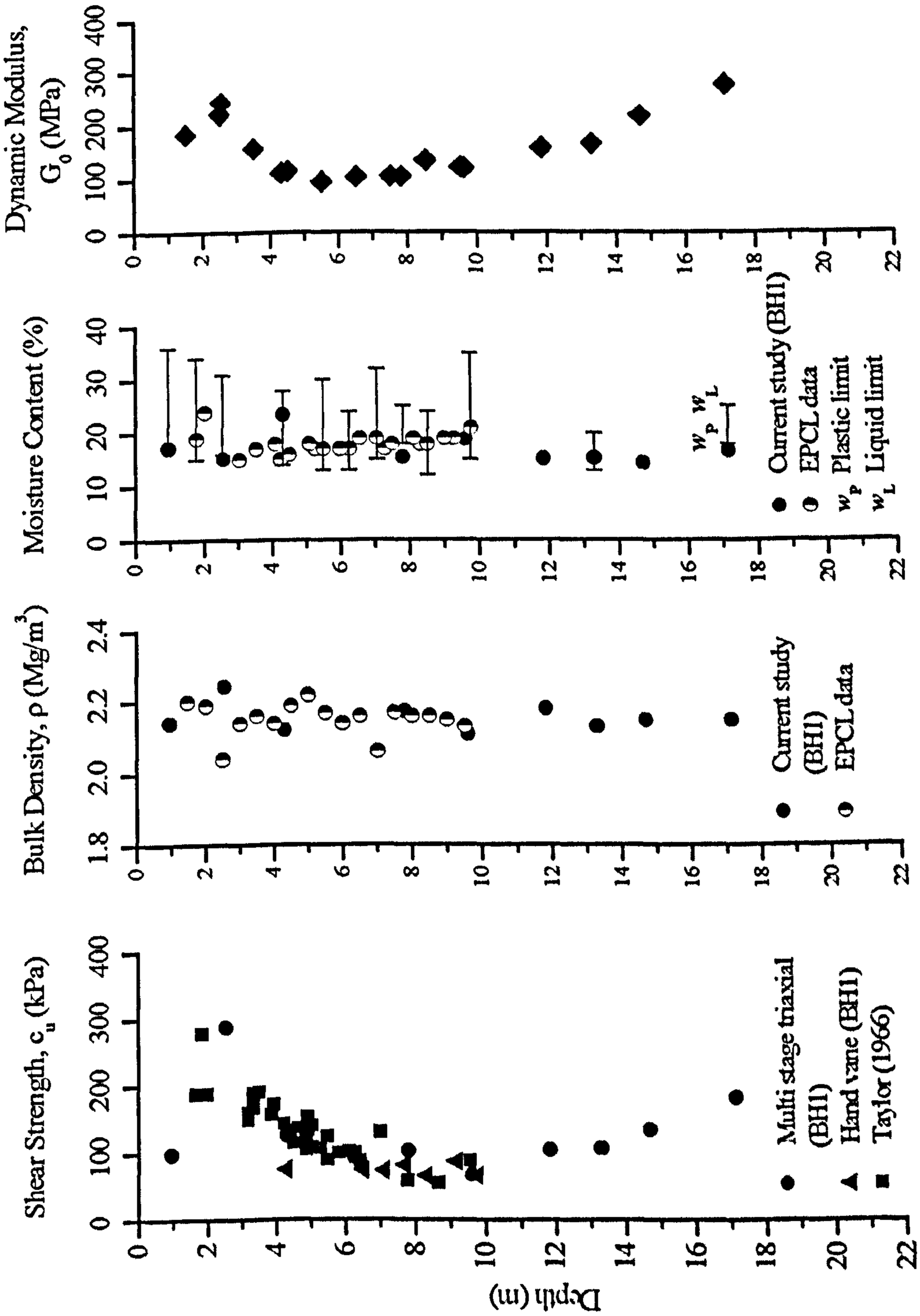

Figure 6.10, Laboratory and in-situ test results from current research compared with those from other studies.

Property	*Symbol*	*Value*
Liquid limit	w_L	20-36%
Plastic limit	w_P	12-18%
Plasticity index	I_P	7-20%
Specific gravity of solids	G_s	2.69
Clay fraction (%<2μm)	*CF*	20-38%
Activity	*A*	0.35-1.07
Coefficient of vertical permeability at void ratios of 0.40 to 0.42	k_v	$3.64\text{-}4.85\text{x}10^{-11}$
Slope of consolidation line	λ	0.03-0.04
Slope of critical state line	M	1.07 $\phi'=27.0°$

Table 6.3, Summary of strength and undrained properties for the Grimsby Clay (Balderas-Meca, 2004).

Test type	*Time after installation (Days)*	*Ultimate pile capacity (kN)*
Dynamic	0	825
Dynamic	32	1100
Dynamic	63	1185
Static (MLT)*	70	1268#

**MLT-Maintained Load Test, #Average of Chin-Kondner and Decourt extrapolations.*

Table 6.4, Increase in ultimate load capacity of the driven pile with time (Bell, 2001).

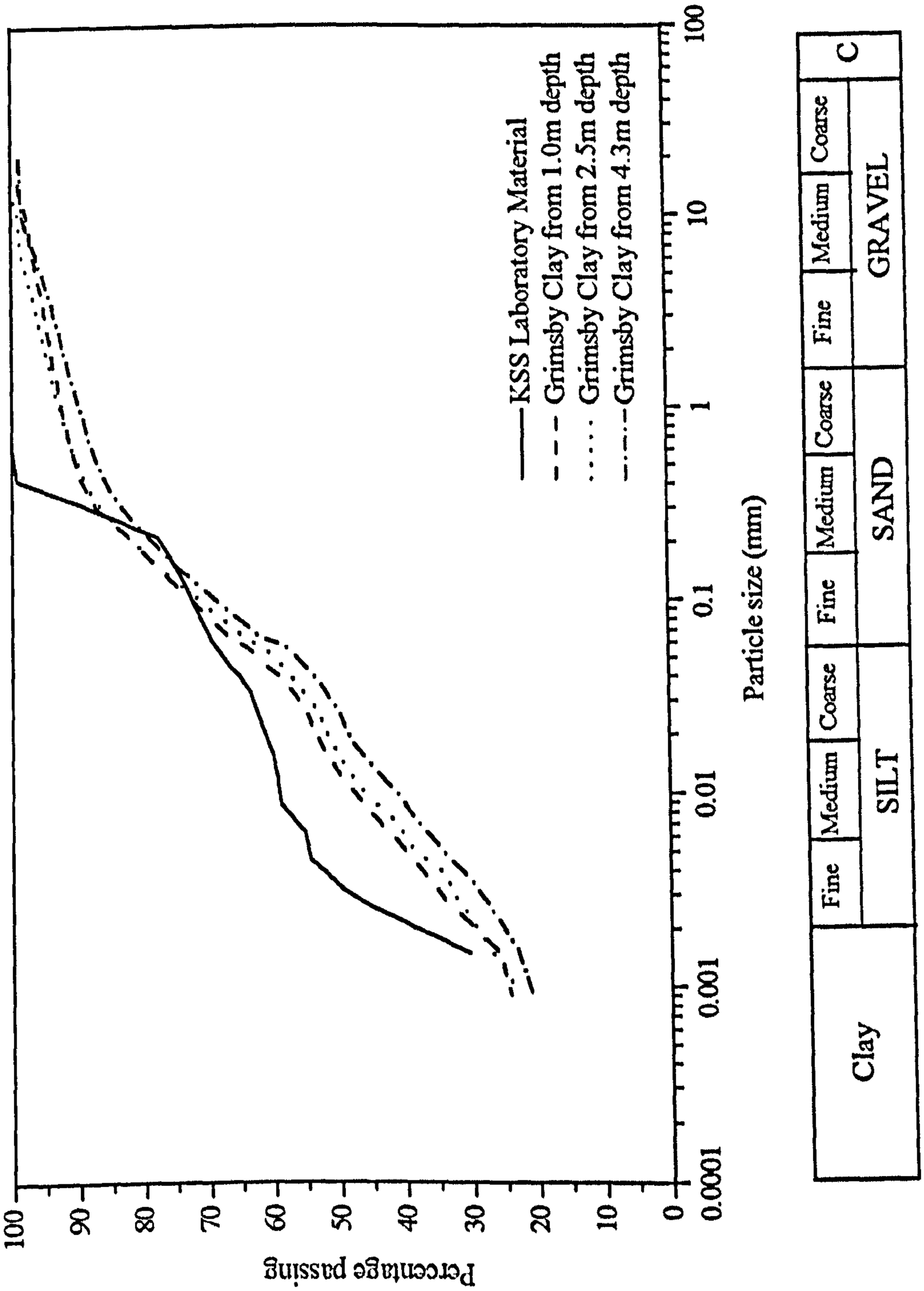

Figure 6.11, Particle size distribution for Grimsby Clay compared with laboratory model soil (KSS).

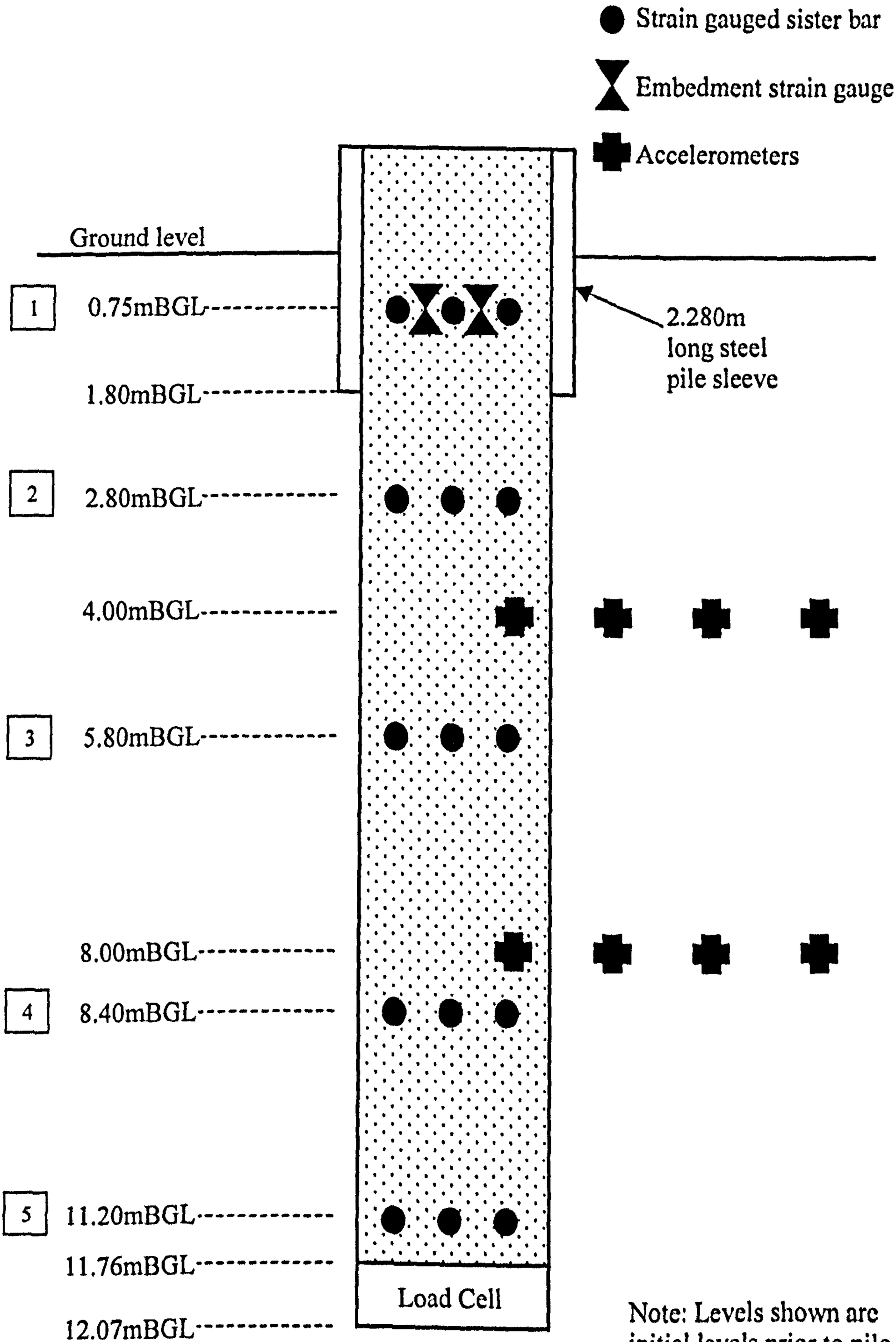

Note: Levels shown are initial levels prior to pile testing.

Figure 6.12, Schematic of 600mm diameter auger bored pile and associated instrumentation locations (not to scale).

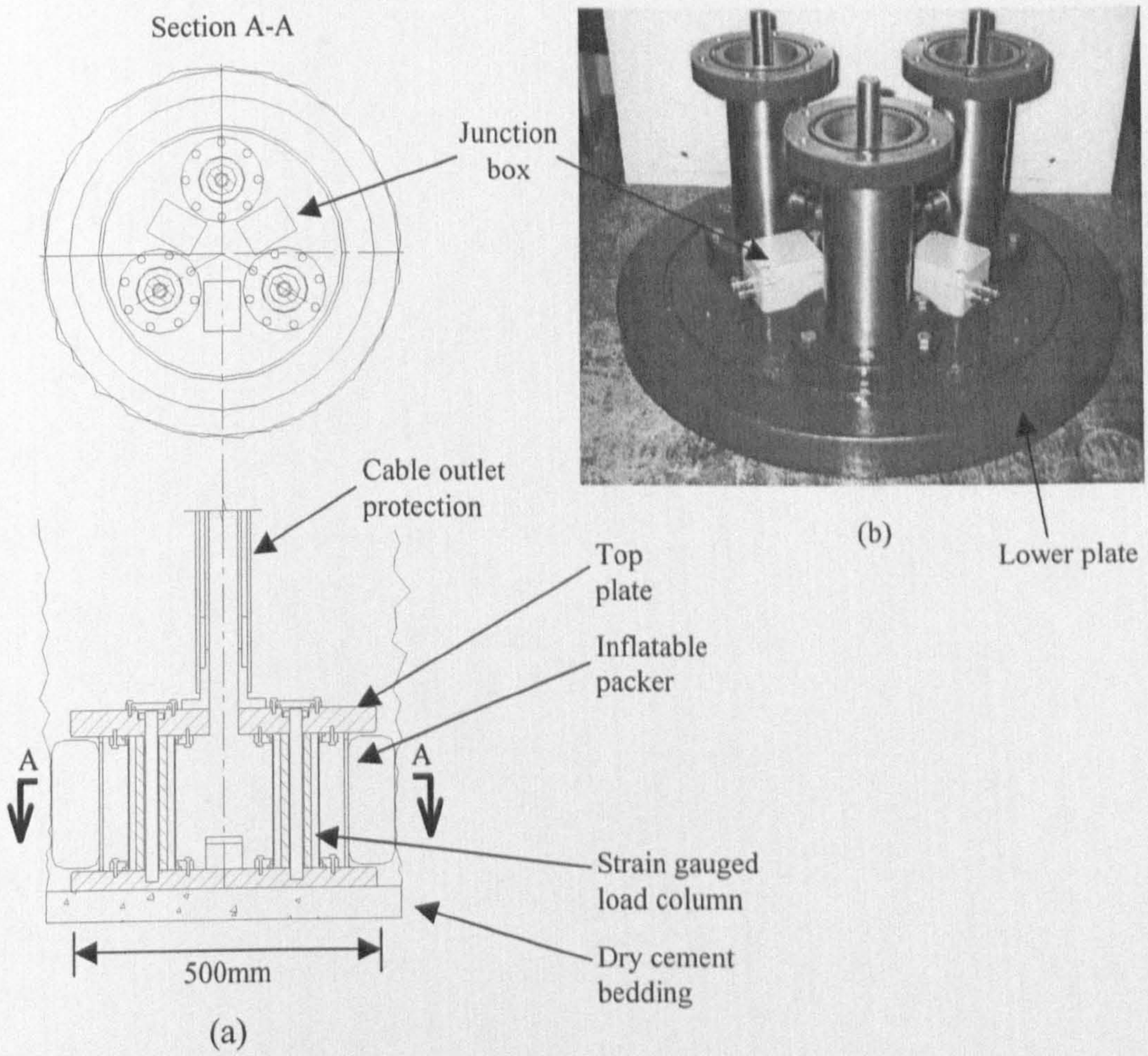

Figure 6.13, Pile tip load cell details: (a) As installed, (b) Showing protective cylinders with o-ring sealed retaining rings bolted to lower plate.

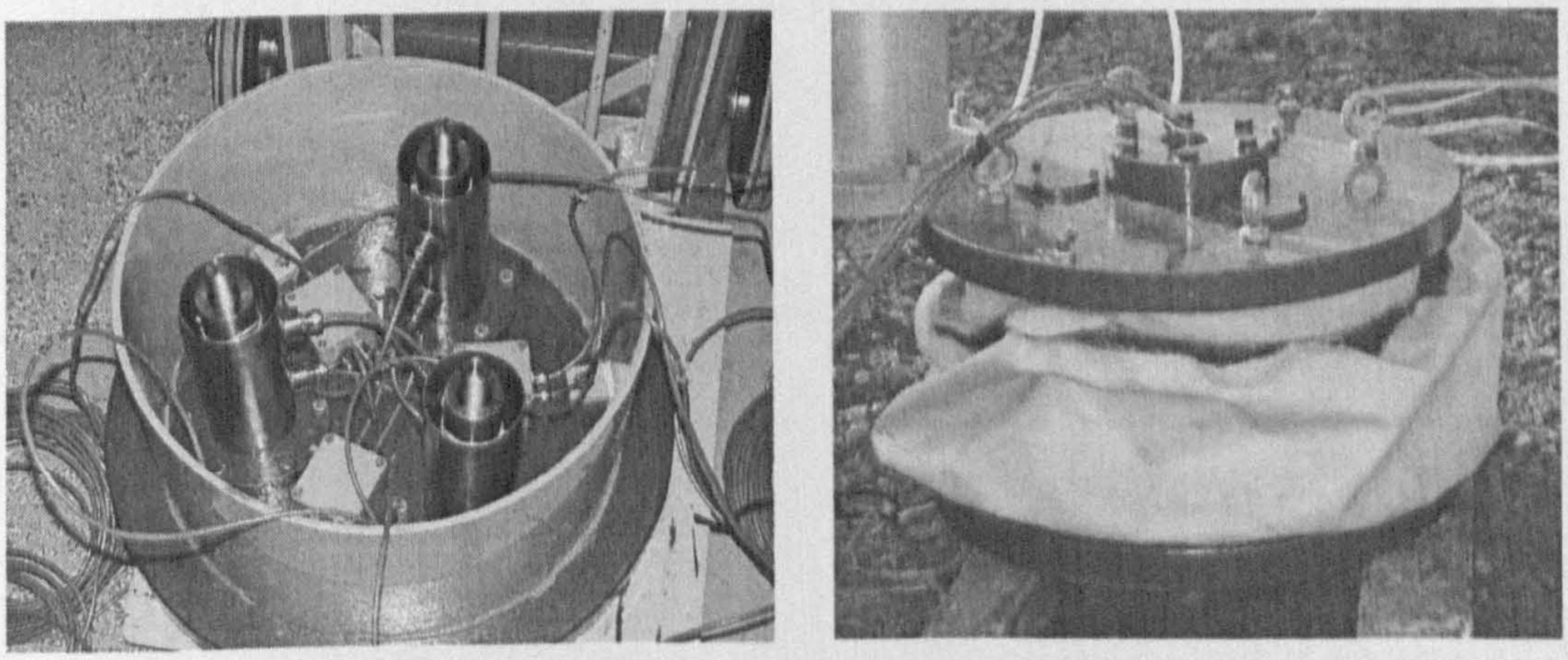

Figure 6.14, Pile tip load cell details: (a) Load columns installed and wired. (b) Packer and top plate in place awaiting installation.

Location	*Instrument Type*	*Depth (mBGL)*	*Radial position**	*Channel*
Bored pile	Tip load cell	11.77-12.07		19 to 24
	Accelerometer 1	4.00		33
	Accelerometer 2	8.00		34
	Sister bars Level 1	0.75		1 to 3
	Sister bars Level 2	2.80		4 to 6
	Sister bars Level 3	5.80		7 to 9
	Sister bars Level 4	8.40		10 to 12
	Sister bars Level 5	11.20		13 to 15
	Embedded gauge 1	0.75		16
	Embedded gauge 2	0.75		17
Soil	Accelerometer 1	4.00	3.046R	27
	Accelerometer 2	8.00	2.890R	28
	Accelerometer 3	4.00	5.037R	29
	Accelerometer 4	8.00	4.700R	30
	Accelerometer 5	4.00	8.150R	31
	Accelerometer 6	8.00	9.123R	32

**Defined from pile axis in terms of pile radius R (=300mm)*

Table 6.5, Summary of the instrumentation installed in the auger bored pile and the surrounding soil.

Dates	*Test type*	*Pile type*	*Comments*
14/01/03	Statnamic	Pre-cast & Auger bored	Precast loading: 1000, 1250 & 1500kN Auger bored loading: 1000kN
15/01/03	Statnamic	Auger bored	Auger bored pile tested at 1500, 2000, 1500, 2500, 3000kN
06/02/03	CRP static	Auger bored	Maximum displacement of 26.78mm
10-11/02/03	MLT static	Auger bored	Maximum displacement of 23.05mm
21/02/03	CRP static	Pre-cast	Maximum displacement of 30.42mm
24-25/02/03	MLT static	Pre-cast	Maximum displacement of 32.99mm

Table 6.6, Summary of the field pile testing programme.

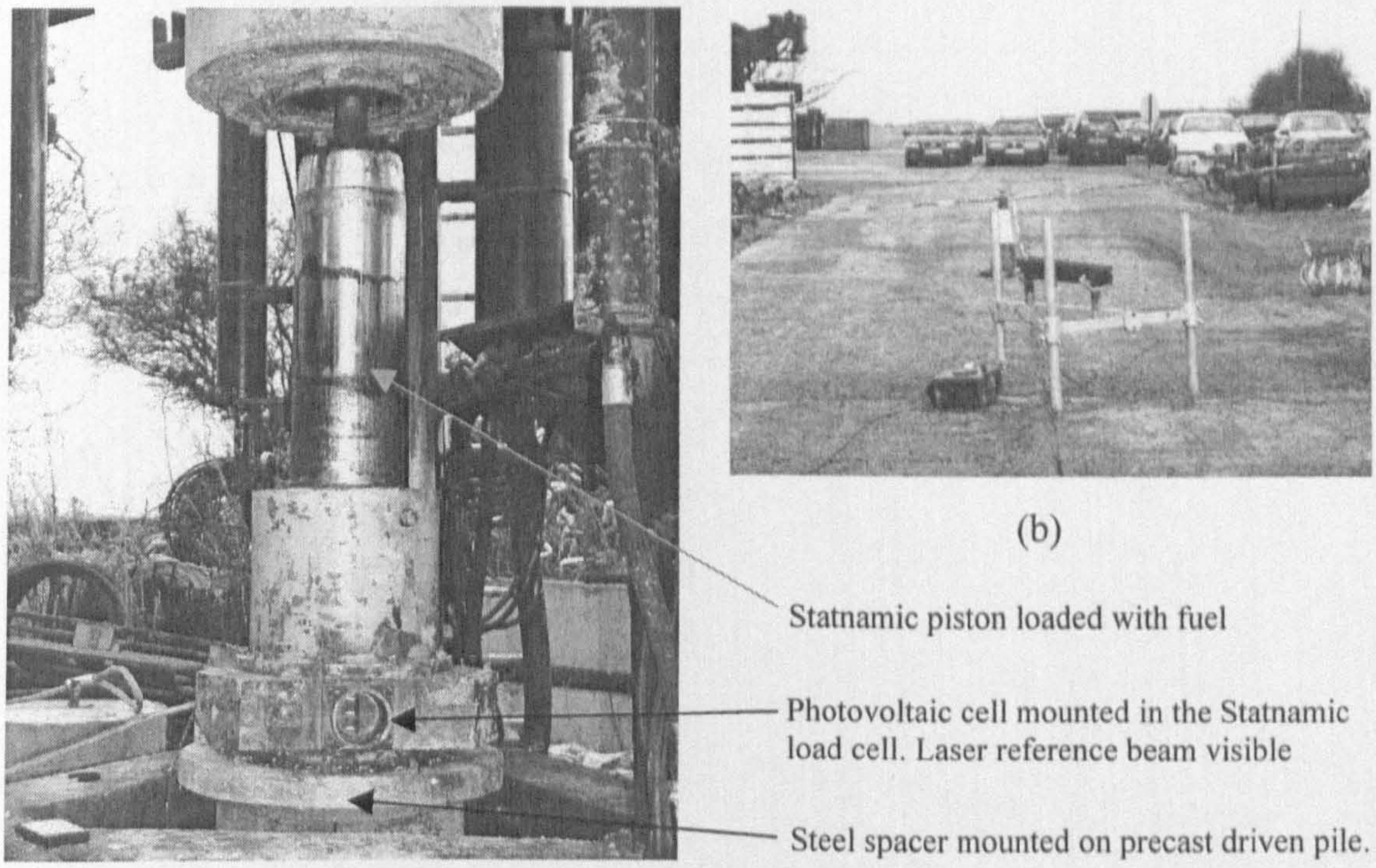

(a) (b)

Figure 6.15, Components of Statnamic device: (a) Statnamic piston mounted on the precast driven pile. (b) Laser reference device for displacement measurement.

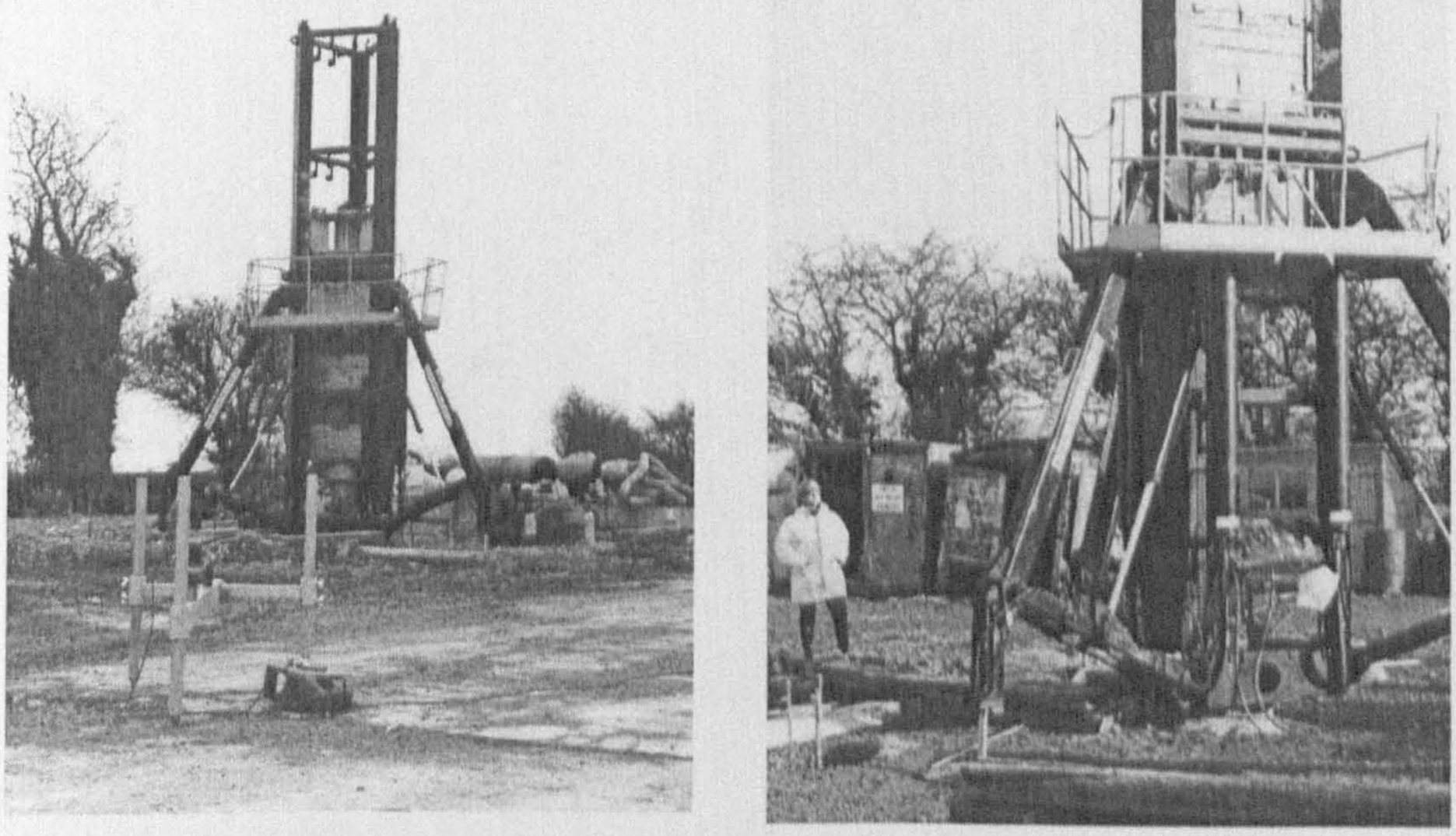

(a) (b)

Figure 6.16, Statnamic device testing the instrumented auger bored pile. (a) Laser reference beam generator in foreground. (b) Weight pack raised for fuelling.

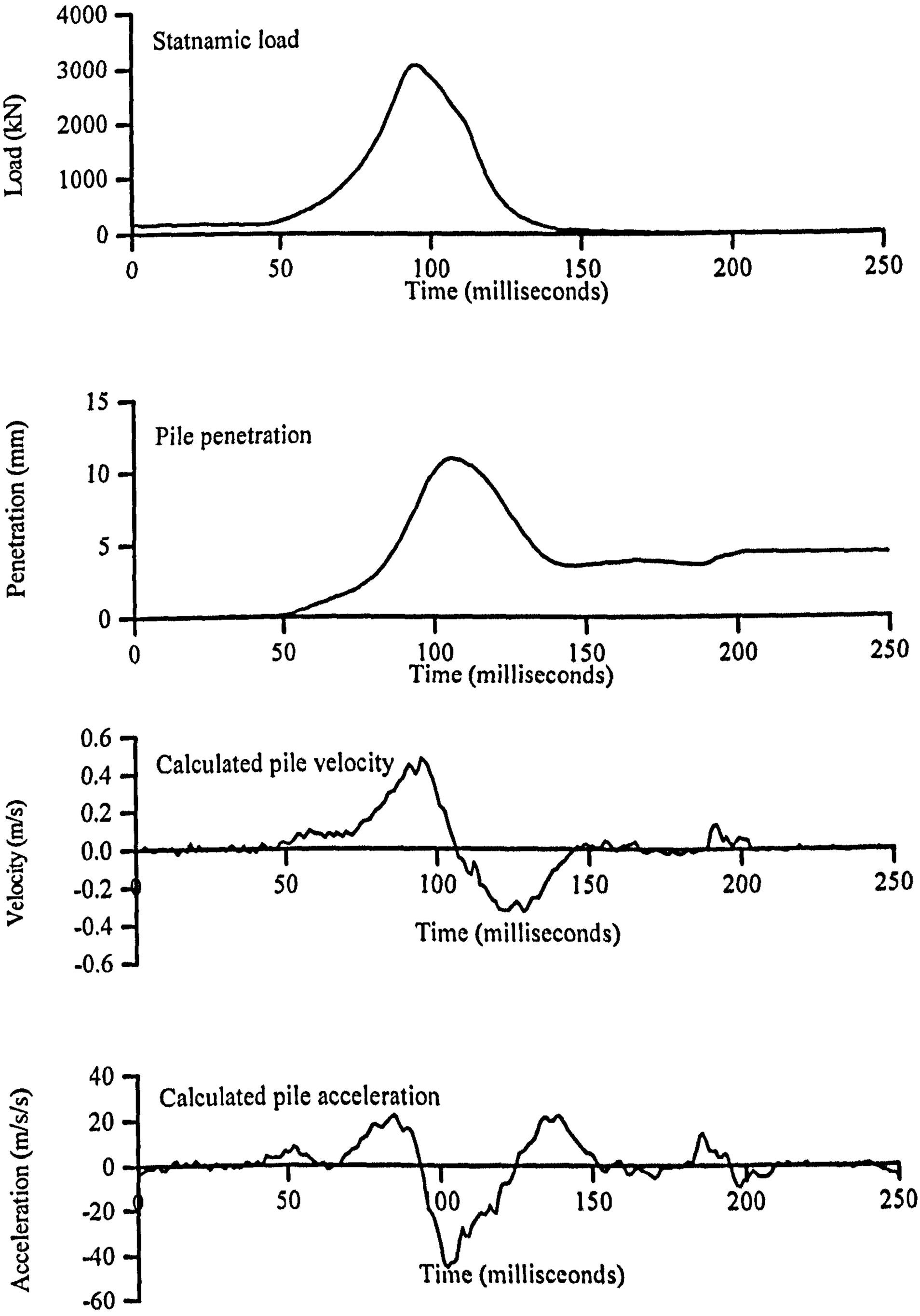

Figure 6.17, Measured and calculated results from full scale testing of the Grimsby auger bored pile during a 3000kN Statnamic test.

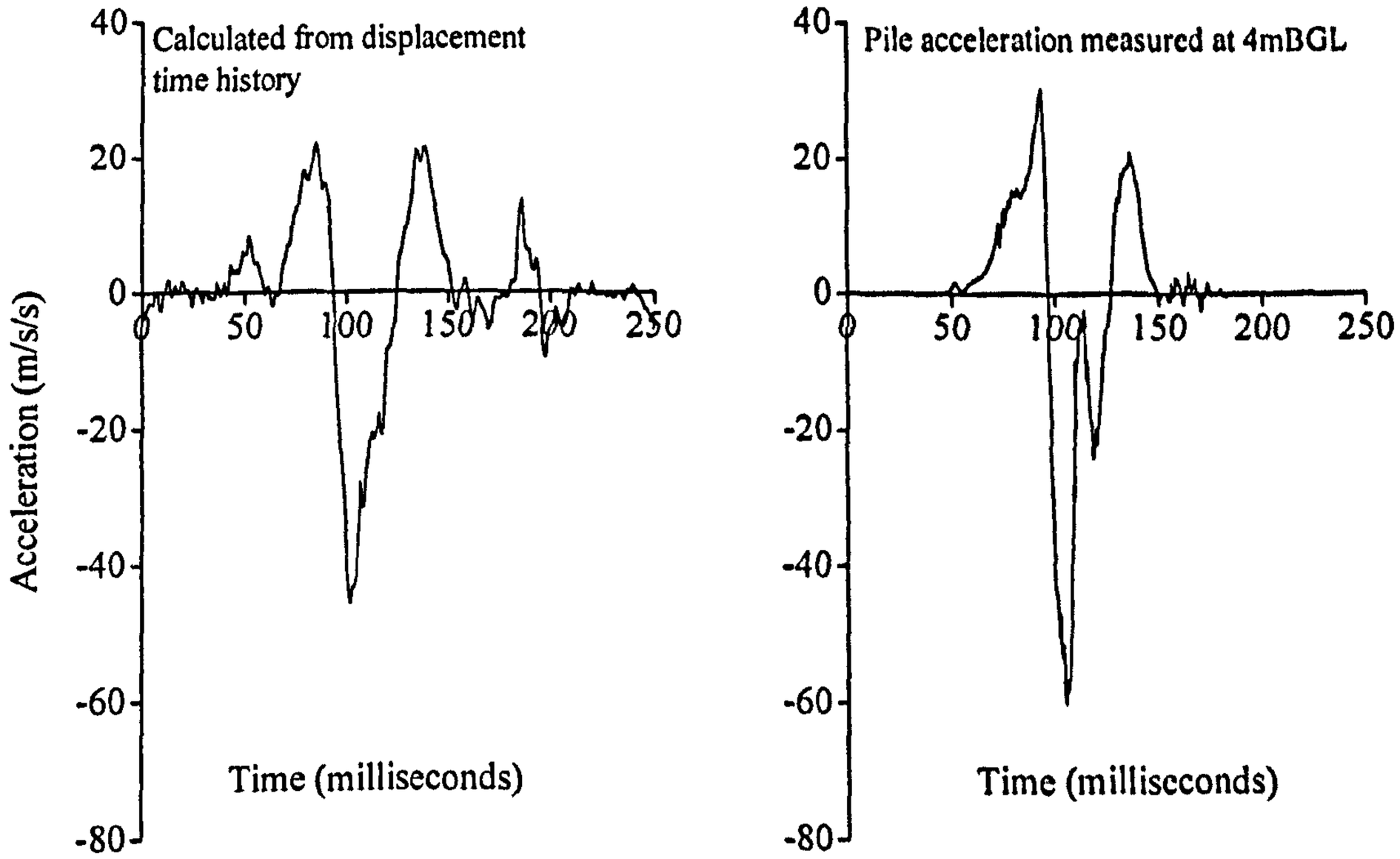

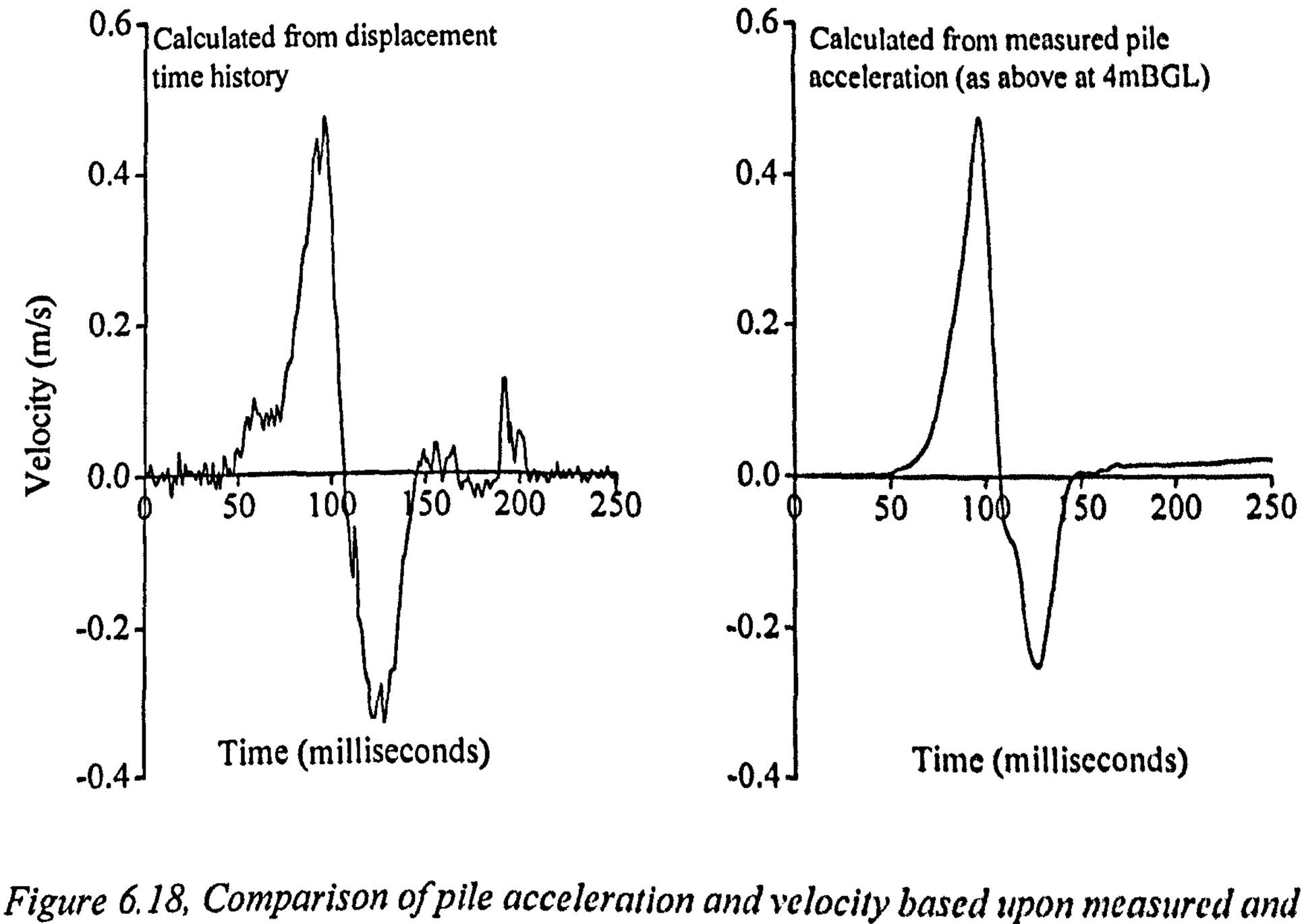

Figure 6.18, Comparison of pile acceleration and velocity based upon measured and calculated readings from a 3000kN STN test.

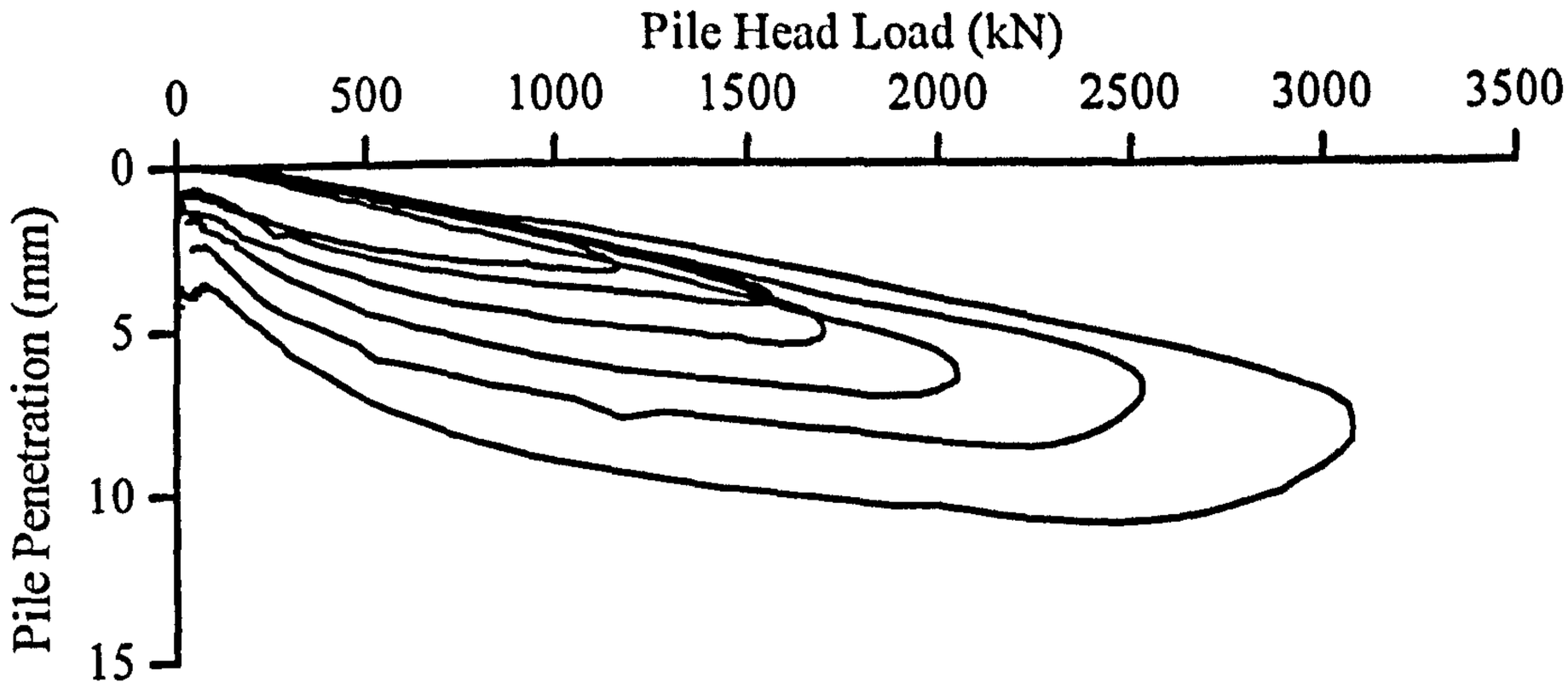

Figure 6.19, Measurements of pile load – displacement behaviour during cycles of increasing Statnamic loading for the auger bored pile.

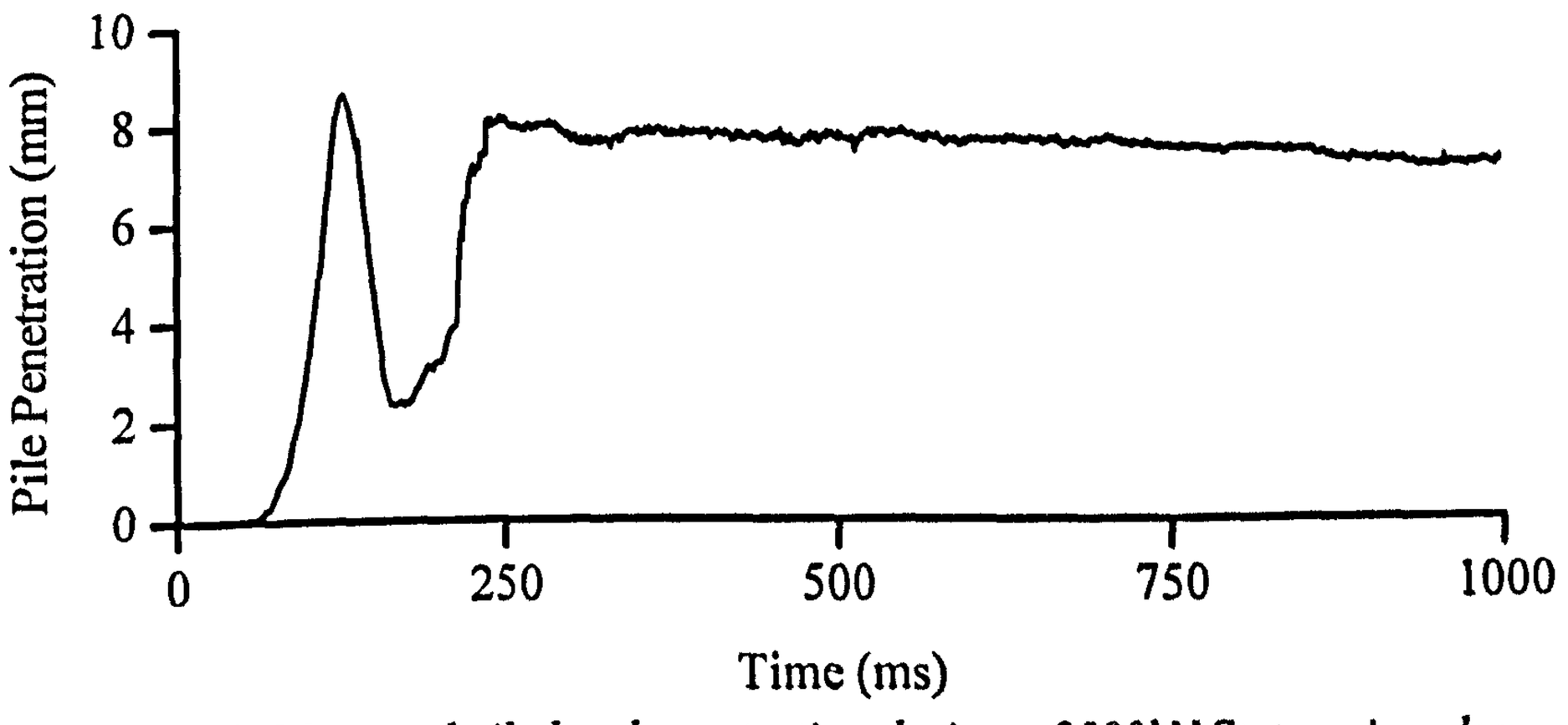

Figure 6.20, Measured pile head penetration during a 2500kN Statnamic pulse.

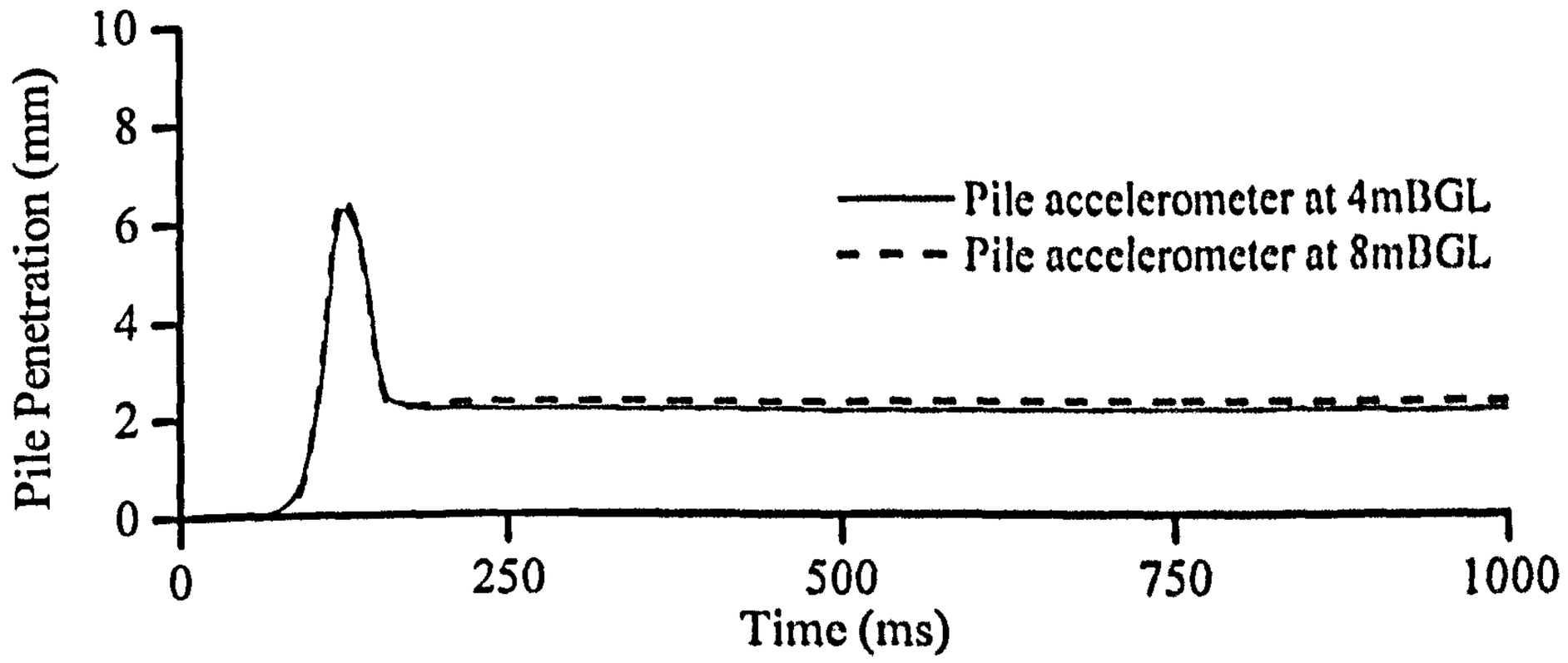

Figure 6.21, Calculated pile penetration from accelerometer measurements during a 2500kN Statnamic tests.

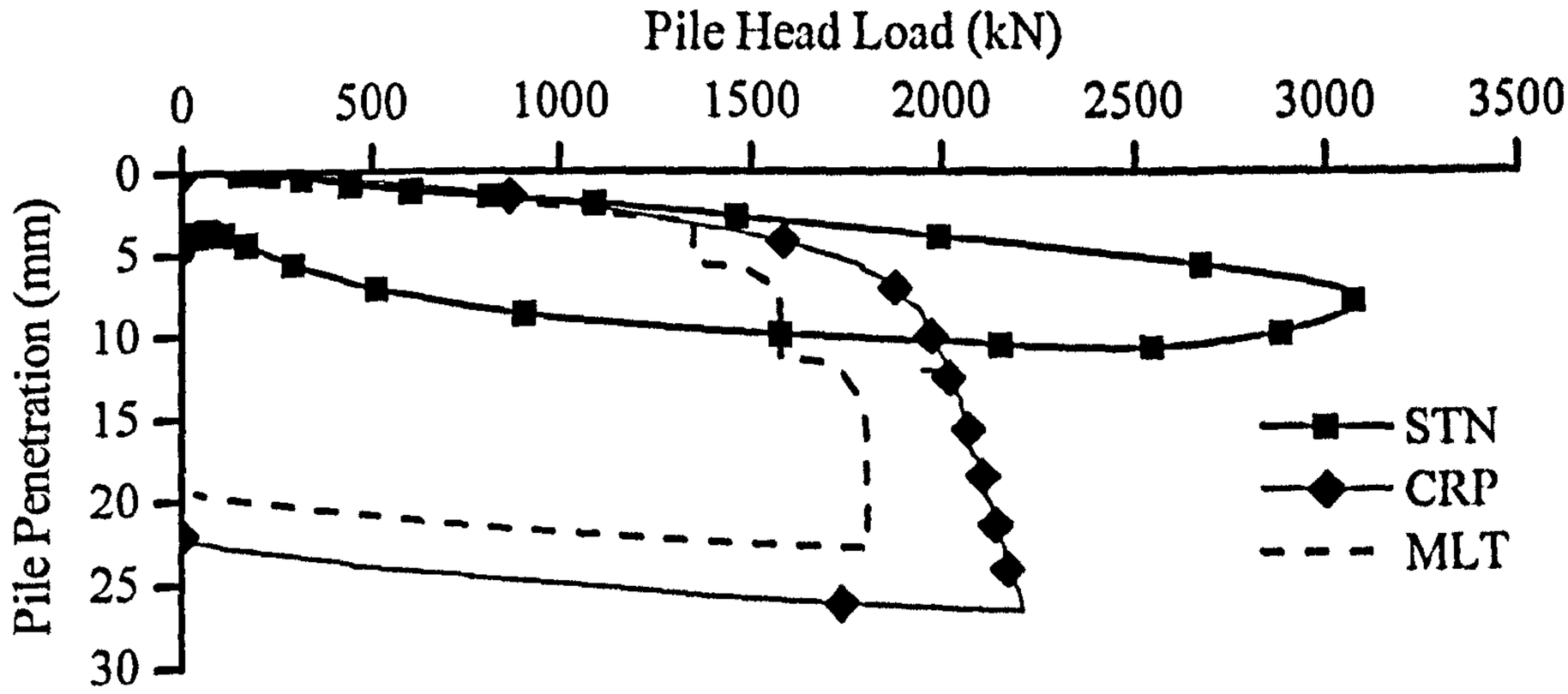

Figure 6.22, Comparison of pile load – displacement behaviour for different pile testing methods (Brown, 2003).

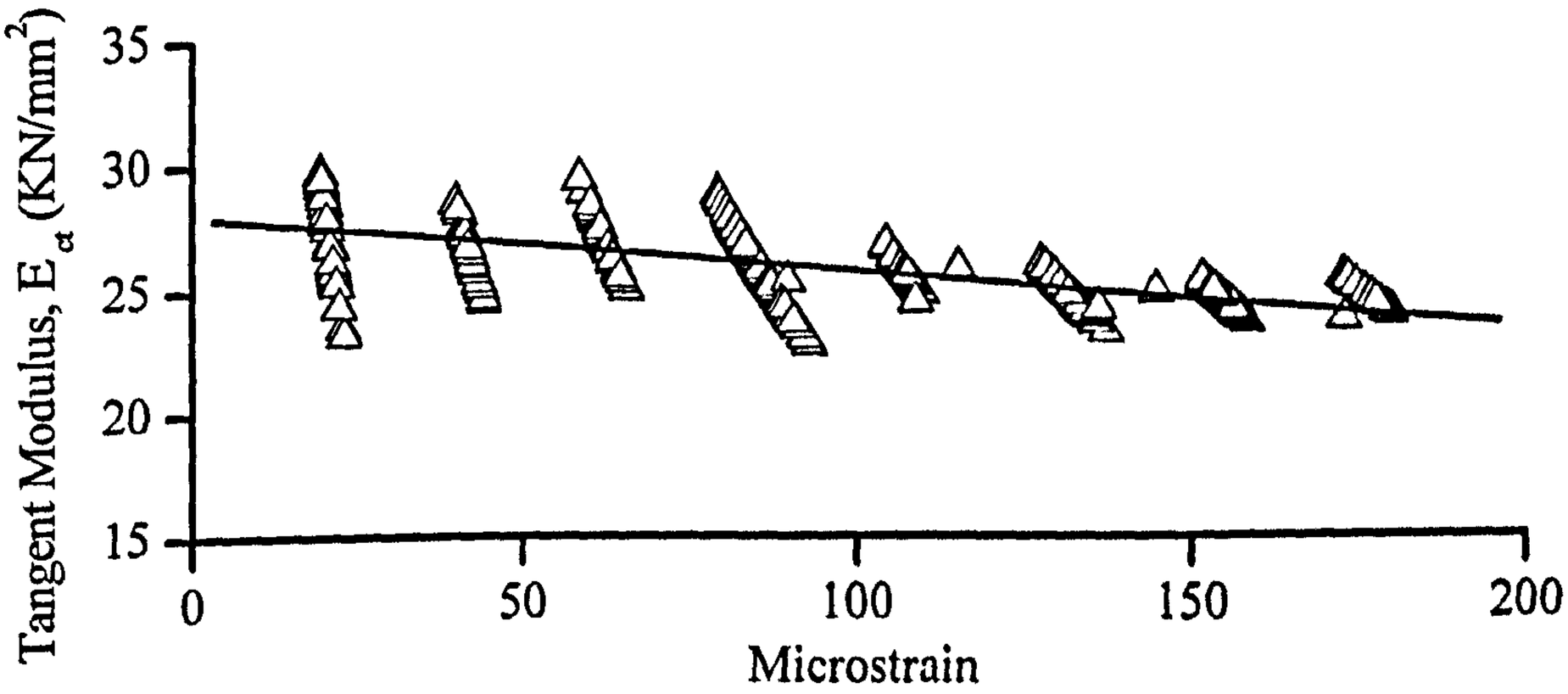

Figure 6.23, Variation of concrete tangent modulus with strain at level 1 during the MLT test.

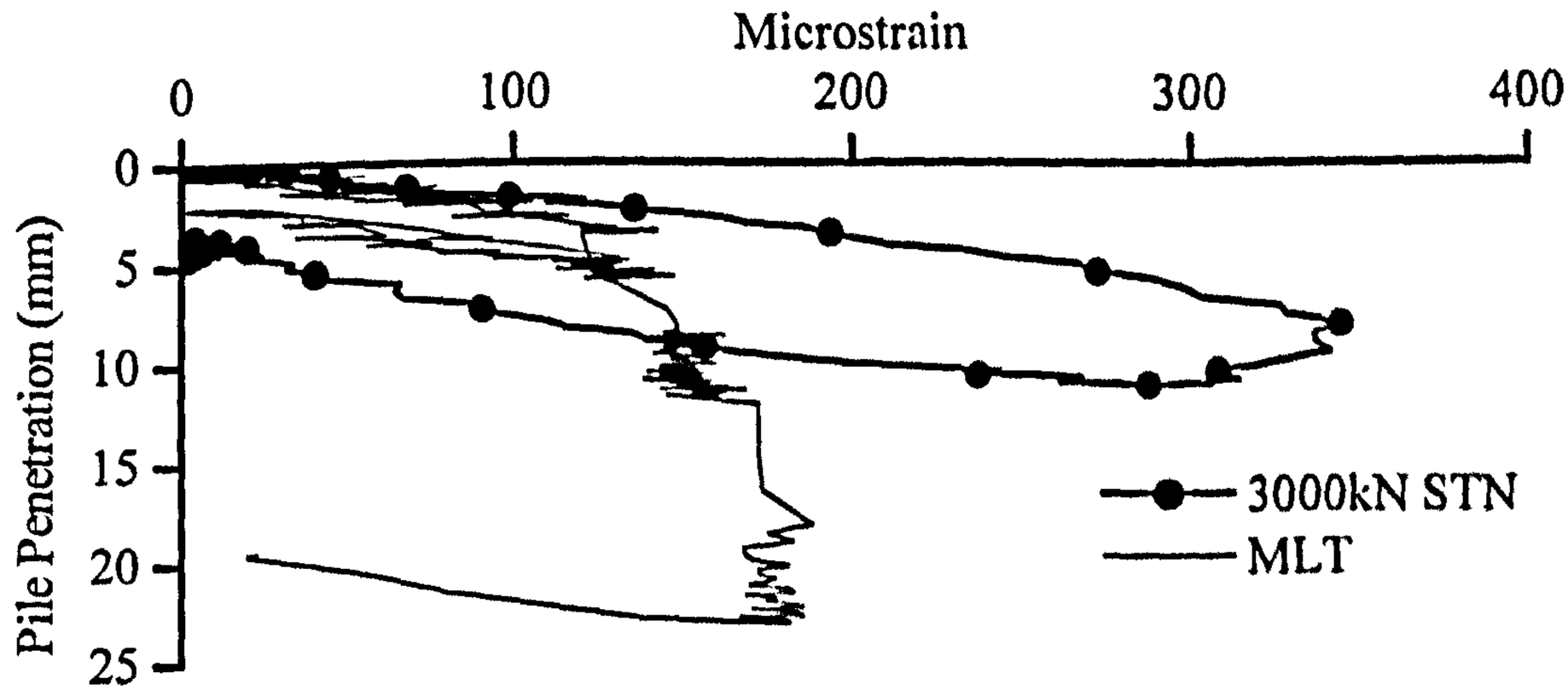

Figure 6.24, Strain measured by sister bar reinforcement at level 1 during Statnamic and MLT testing.

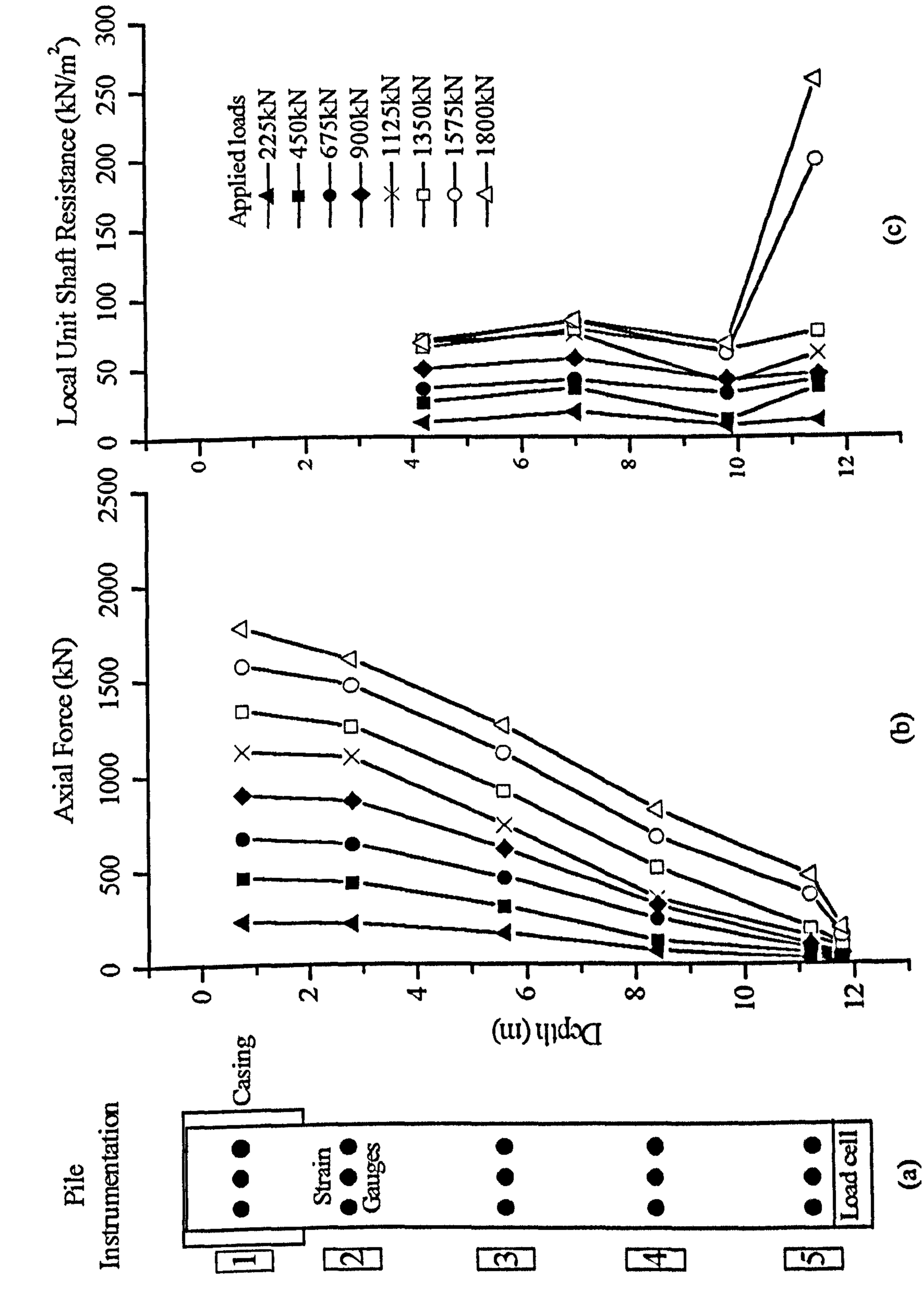

Figure 6.25, Axial loads and shaft resistances derived from pile instrumentation during MLT testing of the auger bored pile.

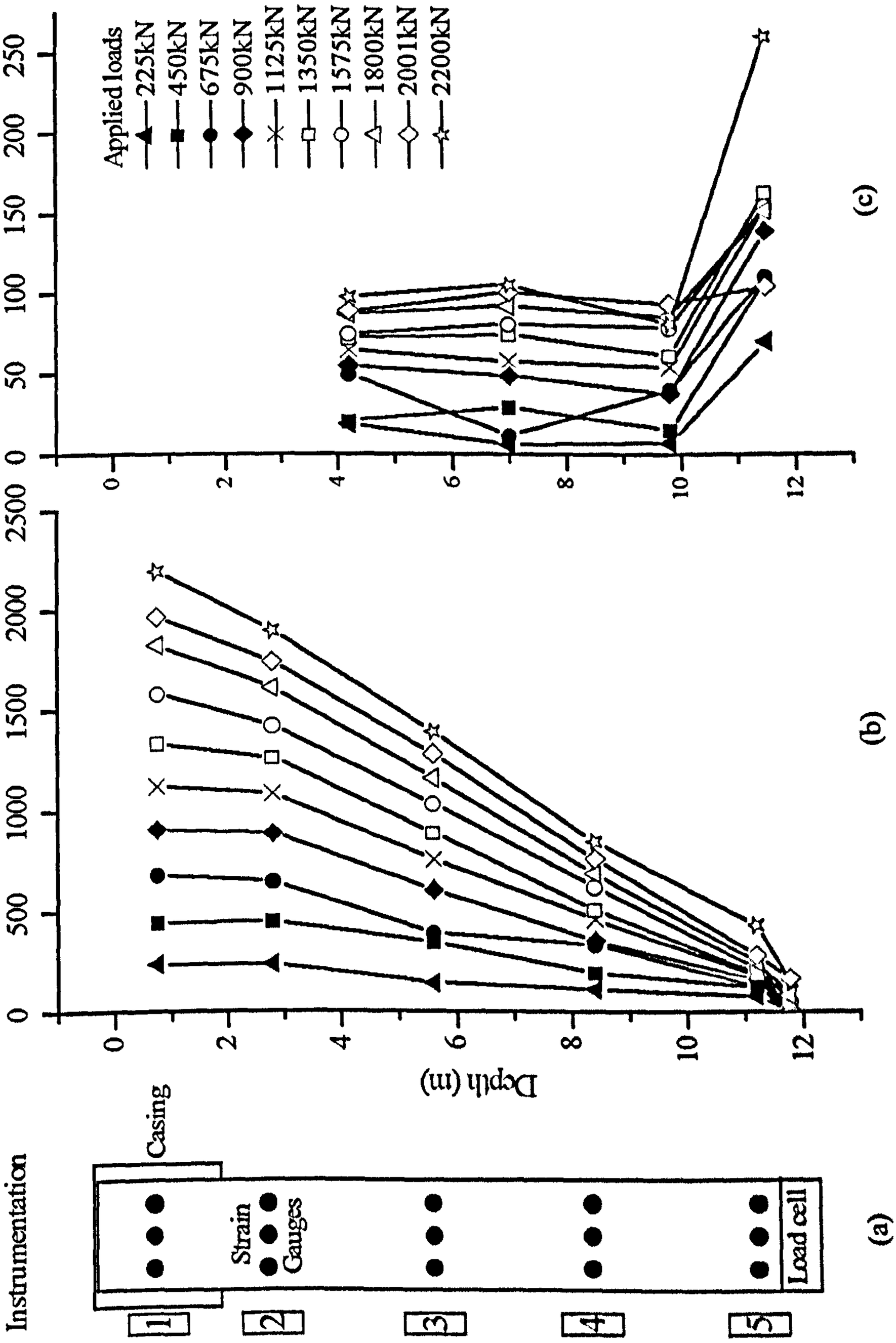

Figure 6.26, Axial loads and shaft resistances derived from pile instrumentation during CRP testing of the auger bored pile.

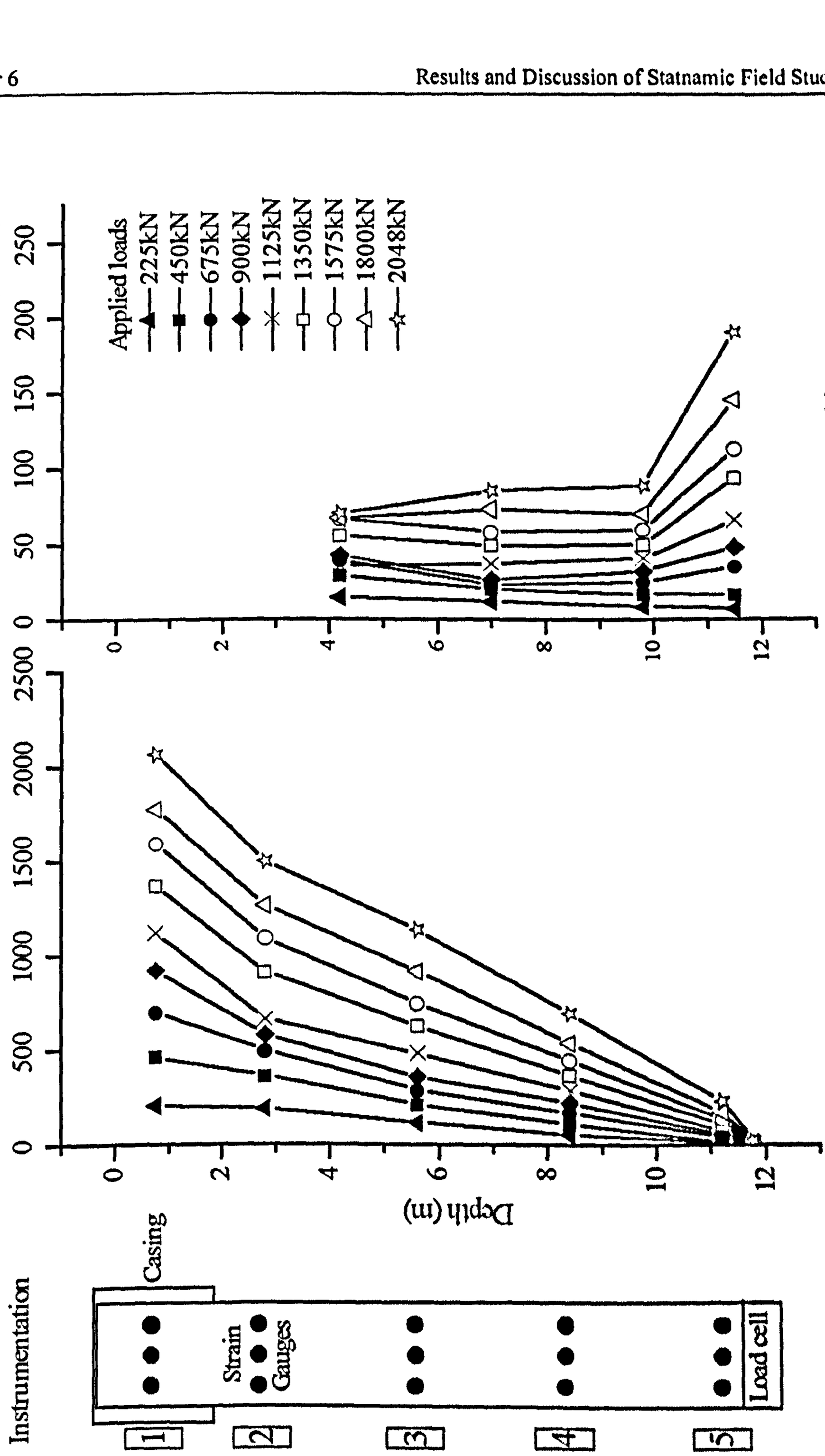

Figure 6.27, Axial loads and shaft resistances derived from pile instrumentation during a 2000kN Statnamic test on the auger bored pile.

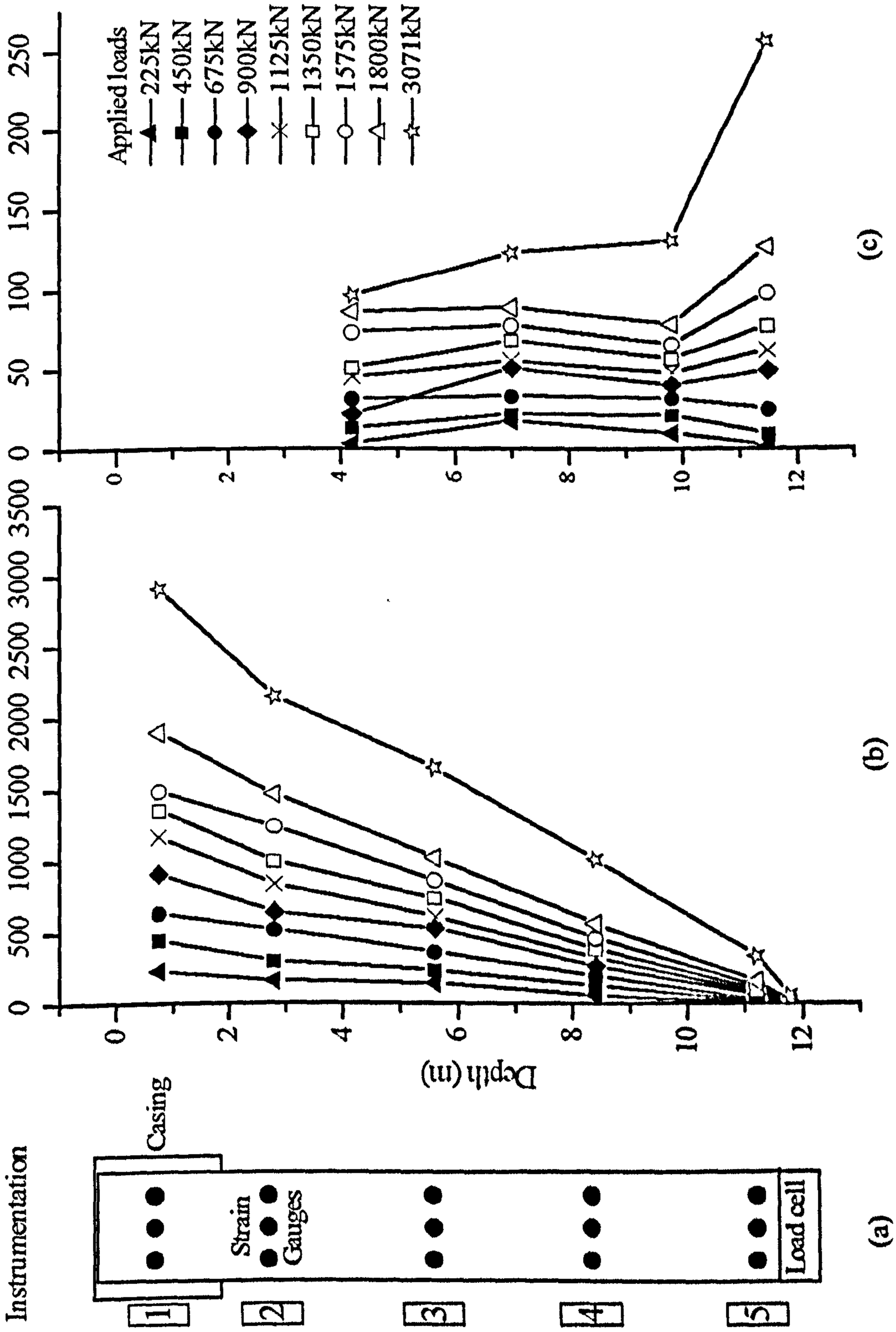

Figure 6.28, Axial loads and shaft resistances derived from pile instrumentation during a 3000kN Statnamic test on the auger bored pile.

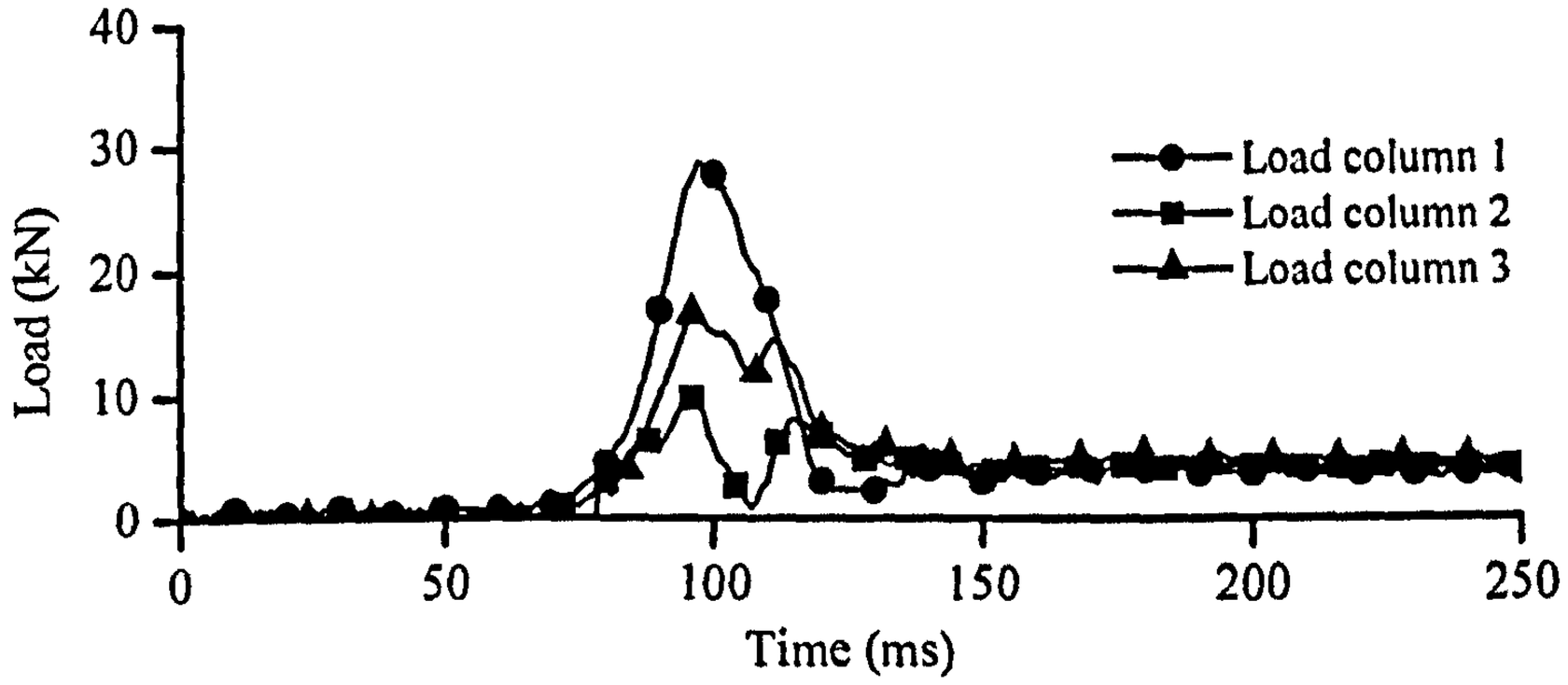

Figure 6.29, Tip load cell column readings during a 3000kN Statnamic test.

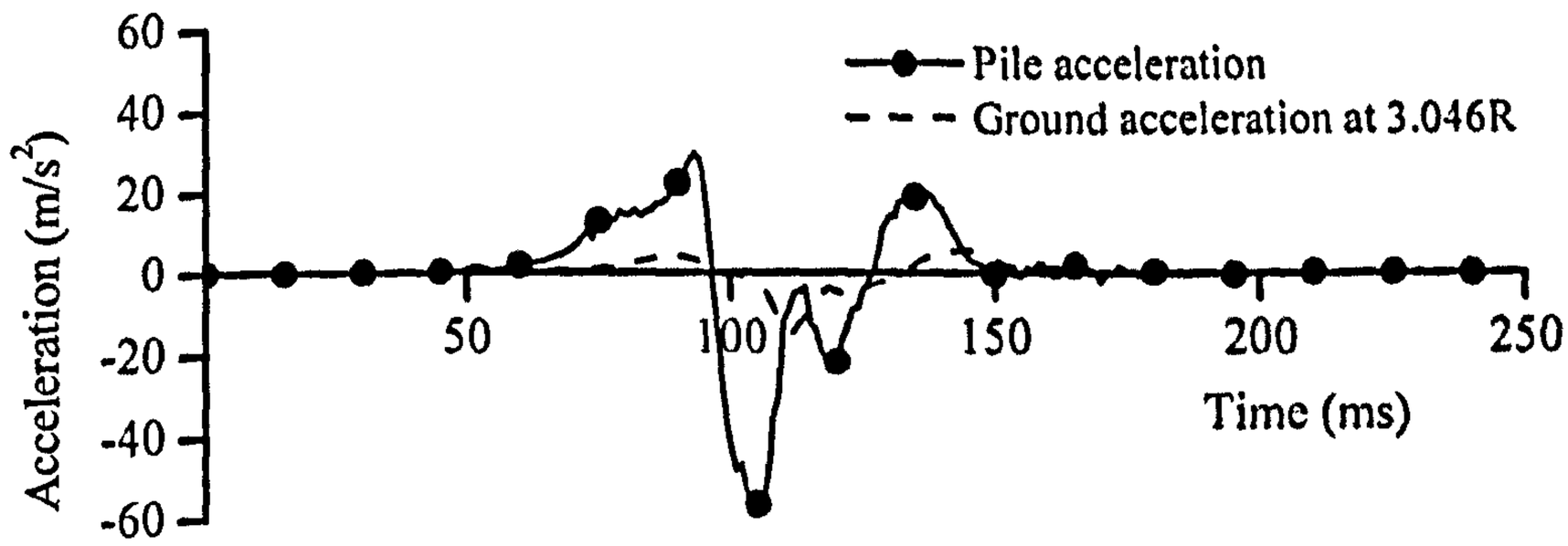

Figure 6.30, Comparison of measured pile acceleration with ground acceleration at 3.046R during a 3000kN Statnamic test.

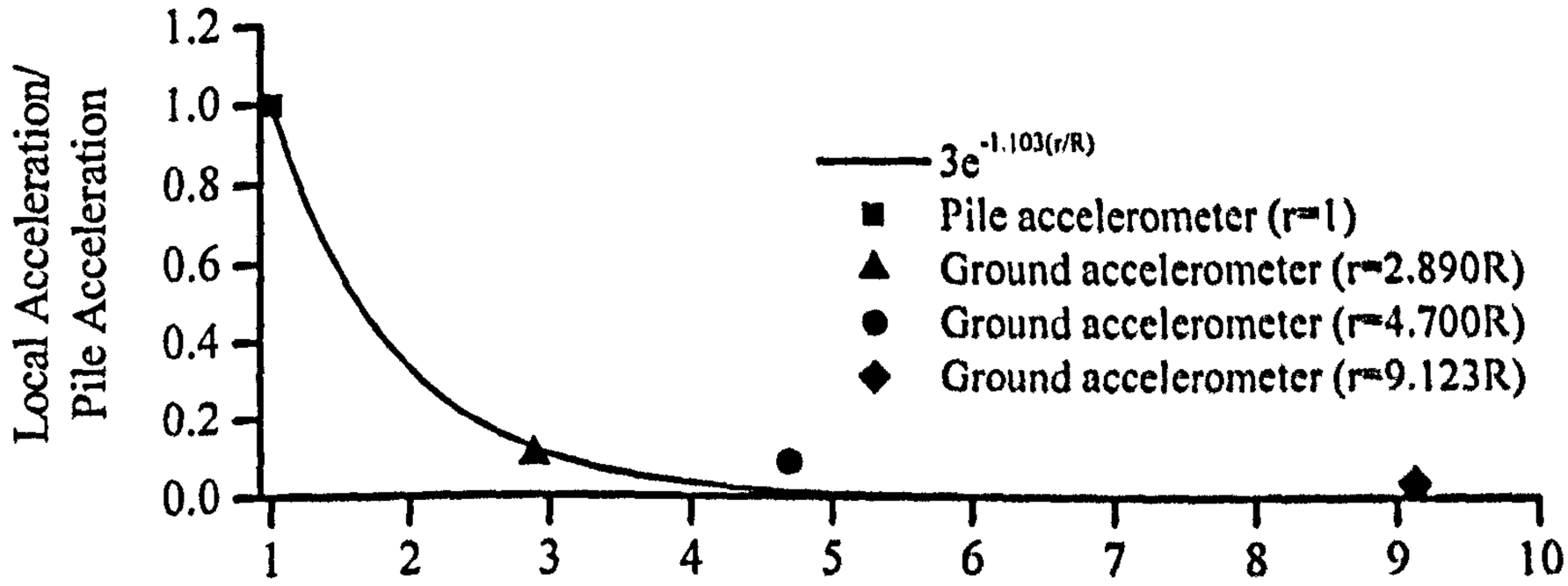

Figure 6.31, Dissipation of ground accelerations on moving radially away from the pile during a 3000kN Statnamic test.

7.0 Prediction of Static Pile Behaviour

7.1 Class A prediction

One of the original project aims was to undertake a class A prediction of the static capacity of a pile installed in clay soil from the results of a Statnamic (STN) test. A class A prediction is one that is made before an event, based purely on existing data and information (Lambe, 1973). In this case, the "static" pile capacity was predicted before the CRP and MLT static tests by interpreting Statnamic test results using a model developed from laboratory model pile testing (Section 5.5.9). Before carrying out the static pile testing, copies of the class A prediction were forwarded to Professor Malcolm Bolton (Cambridge University) to allow third party verification of the prediction. The class A prediction was based upon the results of prototype STN testing of the auger bored pile installed at the Grimsby test facility (Section 6.3 & 6.4). Copies of the submitted class A prediction documents are contained in Appendix 5.

7.1.1 Class A prediction method

The derivation of static pile capacity from STN load measurements was undertaken using Equation 7.1 applied throughout the elastic and plastic zones of the pile's load-displacement behaviour. This equation was introduced in Section 5.5.9.

$$F_{static} = \frac{F_{STN} - Ma}{1 + \alpha(v)^{\beta} - \alpha\left(10^{-5}\right)^{\beta}} \tag{7.1}$$

Where

F_{static} = derived static pile resistance

F_{STN} = total measured Statnamic load

α & β = damping coefficients determined from the laboratory tests

M = pile mass

a = pile acceleration

v = pile velocity

The values of the damping coefficients used were α=1.22 and β=0.32 which were taken directly from the model pile testing. The validity of applying the coefficients derived from the model testing in the KSS material to full scale testing in glacial clay was confirmed by high speed triaxial testing in both materials (Balderas-Meca, 2004). Balderas-Meca (2004) found that both KSS and the Grimsby clay had very similar damping coefficients. From high speed triaxial testing the rate parameters of KSS were α=0.77 and β=0.20 and for the Grimsby clay α=0.78 and β=0.21.

Due to the uncertainties over whether or not the pile load-displacement behaviour had moved from the elastic to plastic behaviour during the STN testing, the 3000kN load cycle was chosen for the prediction (Section 6.4.5).

7.1.2 Form of prediction

The static pile capacity prediction was split into two parts to aid checking of the prediction when the results were available. Firstly, prediction of the static load-displacement characteristics or stiffness in the elastic zone (Figure 7.1a) was presented. The predicted stiffness is also summarised in Table 7.1. The second component of the prediction was to calculate a value for the ultimate pile resistance. It was difficult to predict the ultimate static capacity, as it was unclear if the full shaft and end bearing capacities of the pile were reached at the STN device's maximum capacity of 3000kN. Examination of the STN load displacement curve, corrected for inertia, suggested that the ultimate load might have been reached at the maximum value of $F_{STN} - Ma$ (Figure 7.1b). Based upon this, the pile displacement was obtained at the maximum load on the curve of $F_{STN} - Ma$ versus displacement. The corresponding load was then corrected for damping and is presented in Figure 7.1b and Table 7.1 as the predicted ultimate static pile capacity. In both cases, the results were compared with the Unloading Point Method (UPM) of analysis (Figure 7.1c) discussed in Section 2.2.4.

7.1.3 Prediction results

The results obtained from the CRP and MLT tests compared with the predicted static equivalents are shown in Figures 7.2a to c, Tables 7.3 & 7.4 and Brown (2003). It can be seen from Figure 6.22 that for approximately 50% of the elastic pile behaviour, the

static pile stiffness is similar to that found for the uncorrected STN results. This was also found for the comparison of the model pile testing results (Section 5.5.2). Application of the rate effect (Equation 7.1) correction in this zone results in an under prediction of stiffness (Figures 7.2a to c). This is also true for the UPM. The predicted stiffness was only 60% of that actually achieved in the CRP test. Comparison of the predicted and measured pile stiffness is summarised in Table 7.3. It was encouraging to note however that the shape of the predicted static load displacement curve was closer to the CRP test than the UPM curve.

Confidence in the prediction of the ultimate static pile capacity from the STN results was not particularly high as, it was unclear from the 3000kN STN results if the pile had begun to display plastic behaviour. Examination of the CRP test results in Figure 6.22 show that the pile capacity after an initial yield at about 1800kN continued to increase up to 27mm of pile head displacement. However, the prediction of ultimate pile capacity coincides with this yield point

The predicted ultimate static capacity of 1746kN (at 8.85mm displacement) is only 10% less than the measured CRP load of 1946kN. In comparison, the UPM over predicts the ultimate pile capacity by 17% (Figure 7.2b) and up to 23% if the analysis is extended past the peak STN load (Figure 7.2c). The point where yield occurs is not clearly defined by the UPM.

Although the class A prediction was made for the CRP test, it is interesting to also compare it with the MLT data, particularly as the maintained load test is the preferred method of testing piles in the UK. The maximum predicted load of 1746kN compares well with the load of 1800kN at which plunging of the pile occurred (Figure 6.22).

All the figures and tables presented in this section are those that were originally submitted for the class A prediction and have only been reformatted to suit this thesis.

7.1.4 Improvements to the prediction

The results presented suggest that the prediction method used is adequate for the pile's behaviour post yield, but under predicted the elastic stiffness. The difference in the model and field pile response was assumed to be mainly due to the sensitivity of the

adopted prediction method to velocity. Maximum pile velocities encountered during the model tests were 240mm/s whereas the field velocities were double this during a 3000kN pulse at 480mm/s. This assumption was tested by halving the field measured pile velocity in the analysis (Equation 7.1). Although this improved the prediction of ultimate static pile resistance (Figure 7.3, class A prediction, velocity at 50%), there was still considerable under prediction of stiffness in the elastic zone.

Based upon the results of the static pile tests and the class A prediction, the parameters used for the rate analysis (Equation 7.1) were altered to achieve a closer prediction of the static pile behaviour (class C1). Lambe (1973) defines a class C1 prediction as a prediction carried out after the event where the test results are available. By adjusting the α & β parameters from α=1.22 and β=0.32, as used for the class A prediction to α=1.05 and β=0.4 the prediction of ultimate pile capacity was improved (Figure 7.4). The value for class C1 β is similar to 0.41 found from the high rate field CPT testing as discussed in Section 6.2.3. The new α value is the same as that derived at the lower confidence limit from the model pile testing while the β value tends to its upper confidence limit of 0.48. Adjustment of these parameters has no significant effect on the prediction of the static pile elastic behaviour.

As well as the class C1 prediction of the rate parameters, Figure 7.4 also refers to a modified class A prediction. This modified result is based upon the use of the embedded pile accelerometers (4 & 8mBGL) to calculate pile velocity and acceleration, which was then used as average pile velocity in Equation 7.1. This approach is similar to the Modified Unloading Point Method (M-UPM) as proposed by Mullins *et al.*, (2002). Only the embedded accelerometers were used in the calculations. In the original method proposed by Mullins *et al.*, (2002), this approach should be based upon a tip and head accelerometer (Section 2.2.4). The shape of the modified class A prediction shows little evidence of pile yield and, in that respect has more in common with the UPM results discussed earlier. It may be that this method is more applicable where instrumentation is placed at the pile tip and head but for this case with instrumentation at mid-height of the pile, the prediction was worse (Figure 7.4).

It is interesting to note that the initial class A predicted ultimate static pile capacity lies between that of the measured CRP and the MLT results. This may be due to the original rate taken for the model CRP testing of 0.01mm/s. As noted by Steenfelt *et al.* (1981) it is important to take account of scaling effects with regard to excess pore pressure generated during pile loading. Assuming that the KSS is similar to the Grimsby clay in terms of the coefficient of consolidation the scaling factor for pore pressure dissipation time is $1 : N_s^2$ (Taylor, 1995). Where N_s is the ratio of the controlling linear dimensions of the field pile to the model pile. In this case, the important dimension is the pile radius or diameter, which is 70mm (D_{model}) in the model and 600mm (D_{field}) in the field. The scaling factor N_s is thus given by:

$$N_s = \frac{D_{field}}{D_{model}} = \frac{600}{70} = 8.57 \qquad (7.2)$$

Based upon the discussion above:

$$\frac{t_{field}}{t_{model}} = N_s^{\,2} \Rightarrow t_{model} = \frac{t_{field}}{8.57^2} = \frac{6000}{8.57^2} = 82 \text{ seconds} \qquad (7.3)$$

Where

t_{field} = time to ultimate pile resistance for the field pile (penetration equal to 10% pile diameter).

t_{model} = time to ultimate pile resistance for the model pile.

Thus, the model CRP test should have been completed in 82 seconds rather than the 700 seconds it took at 0.01mm/s. This is equivalent to increasing the rate to 0.086mm/s. This would then result in a slight reduction in the rate effect and make the prediction closer to the measured CRP results. Variation of the low rate model pile tests for comparison with either MLT or CRP should be considered for future studies.

7.2 An improved model for Statnamic analysis

7.2.1 Proposed skin friction model

The derivation of static pile response from Statnamic loading using Equation 7.1 and parameters discussed in Section 5.4.4 appears to be valid in the pile yield zone. As discussed in Sections 5.5.2 & 6.4.1, comparison of pulse loads with measured low rate CRP test data suggests that little or no modification of the pulse load results are required for the initial portion of the elastic response (50% of ultimate resistance). Randolph & Deeks (1992) suggested that a different model should be applied in the zone of elastic behaviour from that in the plastic zone.

The description in this section lends much of its content to the work performed by Randolph & Deeks (1992) regarding the behaviour of piles during dynamic events. The authors proposed a new elasto-dynamic model (Fleming *et al.*, 1992) for the shaft response of a pile as described by Figure 7.5a. Initially, the behaviour of a pile subjected to a dynamic event is controlled by radial dissipation of the energy travelling down the pile to the soil. This is enhanced by the increased stiffness of the soil during a dynamic event because of its inertia. The energy dissipation to the surrounding soil is referred to as inertial or radiation damping (Randolph & Simons, 1986). This portion of the capacity is described by the lower part of Figure 7.5a with a spring (dynamic elastic behaviour) and dashpot (inertial or radial damping) in parallel. Although the term is referred to as being inertial, the dashpot resistance is velocity dependent with the force per unit length of pile shaft represented by Equations 7.4 & 7.5.

$$F_{d,elastic} = K_{shaft}x + C_{shaft}\dot{x} \tag{7.4}$$

Where

$K_{shaft} = 2.9G$ and $C_{shaft} = 2\pi R\sqrt{G\rho}$, thus:

$$F_{d,elastic} = 2.9Gx + 2\pi R\sqrt{G\rho}\dot{x} \tag{7.5}$$

Where

x & $\dot{x}$ = displacement and velocity, respectively

G = shear Modulus

ρ = soil density (saturated)

R = pile radius

It should be noted that this derivation differs from those discussed in Section 2.2.3 in that the spring constant (K_{shaft}) is not that associated with the static pile resistance but is enhanced due to inertial damping.

At some point, the pile reaches a displacement that is equivalent to the ultimate static capacity where plastic behaviour is initiated. At this point, the pile begins to slide relative to the soil and visco-plastic behaviour takes over based upon the rate law described in Section 5.4.3. This is represented by the upper portion of Figure 7.5a with a plastic slider and viscous dashpot in parallel. This behaviour is limited to the soil directly adjacent to the pile.

The suggestion by Randolph & Simons (1986) that the soil stiffness in the elastic zone is twice that during static loading was not observed during this study for model or prototype STN loading. A closer representation of Statnamic displacement dependant resistance might be given by Randolph & Deeks (1992) equation for static shear stress:

$$\tau_{shaft} = \frac{Gx}{\zeta R} \tag{7.6}$$

Where

ζ = a dimensionless parameter that describes the ratio of local pile movement, normalised by the pile radius, to the local soil shear strain (typically 3 to 5 (Randolph, 1983) and taken here as 4). Taking the pile radius from the model study as 0.035m, the static shaft shear resistance per unit length is given by:

$$\tau_{shaft} = 7.14Gx \tag{7.7}$$

The stiffness term K_{shaft} in Equation 7.4 has been recognised as being frequency dependant (Makris & Gazetas, 1993, Badoni & Makris, 1997) and thus is not appropriate for rapid loading. Equation 7.7 is a more realistic representation of actual displacement dependant shear resistance and it is proposed therefore to incorporate it as the first term in Equation 7.4

This frequency dependency of the elastic stiffness is shown in Equation 7.8 (Makris & Gazetas, 1993, Badoni & Makris, 1997):

$$K_{shaft} = 0.6E_u\left(1+\frac{1}{2}\sqrt{a_0}\right) \tag{7.8}$$

Where

E_u = Young's modulus of the soil during undrained loading

a_0 = dimensionless frequency = $\omega R/V_s$

R = pile radius

V_s = S-wave velocity in the soil = $\sqrt{G/\rho}$

ω = circular frequency of oscillation (angular velocity)

Based upon a frequency analysis of the pile accelerometer and load components, the predominant frequencies associated with the STN pulse event were less than 100Hz, which compares to 1kHz and above for dynamic loading (Randolph & Simons, 1986). This results in a dimensionless frequency (a_0) value of 0.09 as opposed to 2 to 3 for dynamic events. This increases the multiplier in Equation 7.7 from 7.14 (static) to 9.41 (pulse), which is less than 13.2 (dynamic) obtained from Equation 7.5.

In order to understand the influence of the velocity dependent component in Equation 7.5, it is necessary to look in more detail at the derivation proposed by

(Randolph & Simons, 1986). The shear stress mobilised by a pile of radius R, subject to a periodic axial vibration $x = x_0 \sin \omega t$ was presented as:

$$\tau_{d,elastic} = \frac{Gx_0}{2\pi R}[S_{w1}(a_0)\sin \omega t + S_{w2}(a_0)\cos \omega t] \quad (7.9)$$

Where

x_0 = amplitude of vibration

S_{w1} & S_{w2} = stiffness coefficients (Figure 7.6) that are a function of the non-dimensional frequency a_0 introduced above (Randolph & Simons, 1986, El Naggar & Novak, 1994 & Danziger *et al.*, 1999).

From Figure 7.6 it can be seen that S_{w1} (in phase stiffness) varies considerably at low values of a_0 like those associated with STN loading. This confirms the frequency dependant definition of the inertial damping stiffness used in Equation 7.8, whereas for a_0 associated with dynamic events, the value of S_{w1} is relatively constant at 2.9 (Equation 7.5). The out of phase stiffness S_{w2} is proportional to the frequency and was represented by $S_{w2}/a_0 = 2\pi$ (Danziger *et al.*, 1999). This then modifies Equation 7.9 to:

$$\tau_{d,elastic} = \frac{Gx_0}{2\pi R}[S_{w1}\sin \omega t + 2\pi a_0 \cos \omega t] \quad (7.10)$$

Substituting

$$a_0 = \frac{\omega R}{V_s},\ x = x_0 \sin \omega t \ \ \& \ \ \dot{x} = x_0 \omega \cos \omega t$$

Gives

$$\tau_{d,elastic} = \frac{1}{2\pi R}\left[GS_{w1}x + \frac{2\pi RG}{V_s}\dot{x}\right] \quad (7.11)$$

or since $V_s = \sqrt{G/\rho}$ then

$$\tau_{d,elastic} = \frac{1}{2\pi R}\left[GS_{wl}x + 2\pi R\sqrt{G\rho}\dot{x}\right] \tag{7.12}$$

The velocity dependent term is now identical to that in Equation 7.5 but the displacement dependent term remains frequency dependent. The frequency dependency could then be reflected by substitution of Equation 7.8 for the displacement dependant term in Equation 7.12. Instead, it is proposed that the modelling of the pulse type loading should incorporate the static spring constants as presented in Equations 7.6 & 7.7 giving.

$$\tau_{d,elastic} = \frac{Gx}{\zeta R} + \sqrt{G\rho}\dot{x} \tag{7.13}$$

This has been done for several reasons. Based upon the results for shaft resistance obtained in the model study, there was no evidence of a stiffness enhancement up to 50% of the ultimate static capacity during the pulse loading. It is also unclear how to derive the value of a_0 for a transient pulse load when a_0 is based upon idealised harmonic vibration. Additionally, development of the Equation 7.8 was based on frequencies of $0.2 \leq a_0 \leq 0.8$ (Makris & Gazetas, 1993) where it would appear that those associated with the STN type loading are considerably lower.

In Statnamic testing:

$$\tau_{d,elastic} = \frac{(F_{STN} - Ma)}{2\pi RL} \tag{7.14}$$

Thus, the static equivalent force derived from elevated rate pulse loading can be found in the pile's elastic zone using the following equation:

$$F_{static} = F_{STN} - Ma - 2\pi RL\sqrt{G\rho}v \tag{7.15}$$

To apply the new elastic radial damping model and the plastic viscous damping model, it is necessary to define the zones of elastic and plastic pile behaviour. For modelling purposes, a limited static ultimate shaft friction is normally chosen based upon the total stress approach (Michaelides *et al.*, 1997) discussed in Section 5.3.4 (Equation 5.1). As the STN test is designed as a method of determining pile capacity, this approach is not considered acceptable. An alternative approach could be to analyse the STN data to define the static equivalent response in the plastic zone from the viscous damping approach (Equation 7.1). By inspection, it is then possible to see how far the elastic zone found using Equation 7.15 extends.

7.2.2 Proposed tip model

Pile tip response can be represented by Figure 7.5b (Randolph & Simons, 1986) with the spring (K_{base}) and dashpot (C_{base}) constants based upon the response of an elastic semi-infinite half space, referred to as the Lysmer analogue (Das, 1993). The behaviour of the rheological model in Figure 7.5b can be represented by Equations (7.16 & 7.17).

$$F_{base} = K_{base}x + C_{base}\dot{x} + M_{base}\ddot{x} \tag{7.16}$$

$$F_{base} = \frac{2GD_p}{1-\nu}x + \left(\frac{0.8D_p^2}{1-\nu}\sqrt{G\rho}\dot{x}\right)_{elastic} + \left(\frac{0.8D_p^2}{1-\nu}\sqrt{G\rho}\dot{x}\right)_{elastic\ /\ plastic} + 2D_p^3\rho\frac{0.1-\nu^4}{1-\nu}\ddot{x} \tag{7.17}$$

Where

D_p = pile diameter

ν = Poisson's ratio

M_{base} = mass of soil influenced under the pile tip

The application of this equation to the measured tip loads during model STN pulse loading is shown in Figure 7.7. The input of the elastic dashpot was limited by the yielding of the plastic slider shown in Figure 7.5b, which was taken as the point where

STN measured tip loads deviated from the static measured response. The static equivalent tip resistance was hardly influenced by the lumped mass term due to the small mass of soil mobilised below the pile tip. A similar comment could be made for the prototype pile with the input from this term being minimal for STN accelerations even at large diameters. It was assumed that the acceleration of the soil under the pile equalled that of the pile.

As discussed by Randolph & Simons (1986), during plastic deformation at the tip, energy will continue to be propagated into the soil mass. The development of Equation 7.17 attempts to address this by maintaining the elastic-plastic dashpot throughout plastic deformation. Additionally, there is the potential for viscous effects but these have proved difficult to determine due to the mixture of elastic plastic behaviour for the tip compared with the discrete elastic-plastic behaviour of the shaft. Where correction of the tip is required, Equation 7.17 could be used, but it is acknowledged that further research is required for the frequencies associated with STN pulse loading. Due to the problem of separating the elastic and plastic behaviour, Equation 7.17 was applied as suggested by Randolph & Simons (1986) with an elastic and plastic approach. The approach was also modified so that all components of Equation 7.17 were applied throughout the elastic and plastic zones, in effect locking the slider in Figure 7.5b. This is referred to on Figure 7.7 as the "Derived static modified Randolph & Simons (1986)". Equation 7.17 predicts the ultimate capacity and elastic behaviour well, but does not follow the elasto-plastic behaviour.

7.2.3 Shear modulus model for Statnamic analysis

Based upon the findings of Sections 7.2.1 & 7.2.2, a new model for the determination of static equivalent resistance from STN pulse type loads is proposed. This model is applicable to clay soils where the pile has been designed to derive the majority of its capacity from shaft resistance. The model takes the form of two equations that are used as two separate steps to determine the static equivalent pile resistance from Statnamic testing as follows:

Step 1

Prediction of the pile's equivalent ultimate static capacity (plastic behaviour).

$$F_{static(ultimate)} = \frac{F_{STN} - Ma}{(1-\alpha(v)^{\beta} - \alpha(v_s)^{\beta})} \tag{7.18}$$

Step 2

Prediction of pile's behaviour in the elastic zone.

$$F_{static} = F_{STN} - Ma - (2\pi RL\sqrt{G\rho v}) \tag{7.19}$$

Where

v = pile velocity

G = soil shear modulus

ρ = soil density (saturated)

R = pile radius

α & β = damping coefficients determined from the laboratory tests

M = pile mass

a = pile acceleration

L = pile length

v_s = lowest pile penetration rate used in the determination of α & β

Application of the model above to a 30kN pulse test on the model pile in Bed 4 can be seen in Figure 7.8. The shear modulus has been taken as 28MN/m^2 and the saturated density as 1.98Mg/m^3, based upon results from triaxial testing (Balderas-Meca, 2004). It is acknowledged that this is a relatively large strain shear modulus when Randolph & Simons (1986) specified dynamic shear modulus, but small strain shear measurements were not undertaken on the KSS material. The rate parameters were those defined for the pile total resistance in Section 5.4.4. The model in Equation 7.18 & 7.19 in effect includes rate dependent tip components by using the rate parameters derived for the total pile resistance. The predicted ultimate static response (Step 1, Equation 7.18, Figure 7.8) was used as the load limit for the predicted static elastic behaviour (Step 2,

Equation 7.19, Figure 7.8). The results of combining the elastic and plastic predictions are shown in Figure 7.9.

The model appears to work very well throughout the elastic and plastic zones during model pile testing with only a slight discrepancy in the elasto-plastic zone. Based on previous discussion of pile unloading (Section 5.5.9), the proposed model is only valid up to the point of peak loading in the Statnamic test. This would avoid the spike seen at maximum pile displacement (Figures 7.8 & 7.9).

One problem associated with these new approaches is that values are required for the shear modulus and saturated bulk densities. This need for parameter input is often cited as an argument against dynamic pile testing methods, but such parameters may be obtained from the high quality ground investigation that should accompany pile construction. What would be more difficult to obtain are the rate parameters for clay soils.

7.2.4 Testing of the proposed STN analysis method

Based upon the findings of Section 7.2.3, the proposed model for STN analysis incorporating both the elastic and plastic terms of the form shown in Equations 7.18 & 7.19 were used to derive the static equivalent pile resistance from the auger bored pile during the 3000kN STN pulse. Unfortunately, it was found that when the elastic portion of the analysis (Equation 7.19) was applied to the field case, the correction had to be reduced by a factor of 10 before behaviour resembling the static stiffness was obtained. This was equivalent to reducing the average measured dynamic shear modulus from 148MN/m^2 to 1.48MN/m^2. As the elastic model proposed by Randolph & Simons (1986) was designed for dynamic testing with dynamic soil behaviour, the need for such a low modulus associated with relatively large strains would indicate that this velocity dependant radial damping approach is not valid for the frequencies associated with STN testing. Further use of this model with a reduction factor would require additional field tests in clay for validation. Although the formulation proposed by Randolph & Simons (1986) does not appear valid for STN, the concept of an elastic damping phase followed by pile soil interface slip (plastic model) still appears attractive.

If the elastic stiffness during high rate testing was velocity dependant, as suggested by Randolph & Simons (1986) then it is likely that comparable stiffness would be obtained for the field and model tests. As discussed above, this was not the case. If on the other hand the field stiffness was due to inertia, it would not be apparent in the model tests. This is because the mass of the pile and the mobilised soil in the model were relatively small resulting in low inertial pile/soil resistance.

7.2.5 Radial inertia model for Statnamic analysis

It is feasible that, during full scale STN testing the stiffness of the field pile above 50% of the ultimate static resistance is governed by the inertial resistance of the pile and the surrounding soil. Based on this assumption, a new model is proposed which incorporates a lumped mass of soil around the pile, subject to acceleration derived from that of the pile, with Equation 7.1 modified to incorporate a soil inertial term. The model takes the form of two equations that are used as two separate steps to determine the static equivalent pile resistance from Statnamic testing as follows:

Step 1

Prediction of the pile's equivalent ultimate static capacity (plastic behaviour).

$$F_{static(ultimate)} = \frac{F_{STN} - (Ma)_{Pile}}{(1 - \alpha(v)^{\beta} - \alpha(v_{\min})^{\beta})} \tag{7.20}$$

Step 2

Prediction of pile's behaviour in the elastic zone.

$$F_{static(elastic)} = F_{STN} - (Ma)_{Pile} - (Ma)_{Soil} \tag{7.21}$$

The pile behaviour proposed in Section 7.2 by Randolph & Simons (1986) is assumed in that, at some point the pile begins to slip relative to the surrounding soil and the inertial soil behaviour then has a limited effect on the measured loads. An approach to analysis similar to that discussed in Section 7.2.3 can then be used where the static

equivalent response in the plastic zone is first found and is then used to define the extent of soil inertial influence. The results of this approach are shown in Figure 7.10.

The mass of soil influenced by the pile's acceleration was defined from the buried accelerometers surrounding the field pile. As discussed in Section 6.4.6, it was found that the accelerations in the ground had fallen to below 10% of that for the pile at a distance of $6R$ from the pile centre. Thus $6R$ was used to define the outer limit of the accelerating soil mass. To calculate the inertial component of this mass, the magnitude of the acceleration applied was reduced from the pile outwards using the relationship for acceleration dissipation (Equation 6.7). The soil mass itself was then split into individual annular blocks. The corresponding acceleration was then applied to the centre of each radial block.

The method shows considerable improvement of the elastic behaviour prediction from approximately 50% of the ultimate static capacity onwards. Although the prediction looks relatively "clumsy", it has been left as such to avoid appearing manipulated. This was due to the slope of the post yield plastic zone being difficult to determine. Further research is required to develop this analysis method.

The main problems associated with this approach and that originally described by Equation 7.19, is that no component has been included for the tip input to the inertial soil behaviour and that the analysis requires the input of the user to limit the extent of the elastic derived zone. Linking the elastic zone to the plastic zone is more difficult for the field data as the ultimate plastic behaviour occurs at greater displacement than in the model tests. Inclusion of the soil mass would also benefit from the use of computer based analysis where the accelerations of the soil mass can be applied to much smaller soil elements than the spreadsheet based computer analysis used here. Further investigation is required of what soil parameters affect the dissipation of the radial accelerations. If this radial inertial mass was linked to various soil types, then the dissipation magnitude and mass of soil could be obtained for other sites. A simplified version of the inertial soil input may be incorporated by the substitution of Equation 7.22 for the soil inertial term in Equation 7.21.

$$(Ma)_{soil} = \left(35\overline{\rho}\pi R^2 L\right) \times a_{pile} \times 3e^{-3.86} \quad (7.22)$$

Where

R = radius of the pile (m)

L = length of the pile (m)

$\overline{\rho}$ = average soil bulk density along the pile length (kg/m^3, Figure 6.10)

a_{pile} = pile acceleration (m/s^2)

This simplified approach assumes that the accelerations are negligible by $6R$ (Section 6.46, Figure 6.31) and that the profile of acceleration dissipation is uniform along the pile length. Based upon these assumptions, the terms in parenthesis define the mass for a cylinder of soil extending from ground level to pile tip level of a radius equal to $6R$. Again, no tip component is included.

7.3 Recommendations for Statnamic analysis

Based upon the findings of this study it is not possible to recommend the method of STN analysis that can be used in all soil types. Information reviewed in Section 2.0 would suggest that current Statnamic analysis (UPM) performs adequately for piles installed in rock and coarse grained soils. Analysis should be based upon M-UPM or S-UPM used in conjunction with pile instrumentation where piles can no longer be considered as rigid bodies due to length or soil stratigraphy. For piles installed in fine grained soils, derivation of equivalent ultimate static behaviour should be based upon a non-linear parameter based approach similar to that used for the class A prediction (Equation 7.1). Where information is not available to derive the rate parameters, analysis should be based around back figured parameters from static test results in similar soil. These parameters could possibly be obtained in-situ with a specially designed CPT rig (Beazant, 2004). As for the granular soils and rock, instrumentation would also be required for long piles.

Further research is required to investigate the elastic portion of the pile behaviour at STN loading frequencies. This may be in the form of including soil inertia as discussed above. In the short term, it is encouraging to note that the uncorrected STN test results

adequately predict the static pile elastic response up to 50% of the ultimate static pile behaviour. This may be utilised for verification of pile settlements at working loads. Hopefully research in the elastic zone coupled with the creation of a soil damping parameter database will lead to STN being deployed in isolation to test piles in clay.

7.4 Recommendations for STN testing based upon model and field measurements

In undertaking the field study with STN testing, several important issues have been identified associated with the deployment of the STN device and the way in which it is used. When specifying STN testing for piles installed in clay and fine grained soils it must be realised that the applied STN loads must greatly exceed the predicted static ultimate loads. The Grimsby and model tests suggest that the STN peak load must reach at least 1.7 times the predicted ultimate static load.

One problem that may have been particular to this site, or the STN device, was apparent pile movement after the STN loading, as discussed in Section 6.4.1. If this problem was due to the STN piston moving on the pile head, it may be overcome by precise levelling of the pile head before and after each STN test. A more rigorous method would be to mount the photovoltaic cell, which detects the laser reference displacement measuring system, directly on the pile. A further check of the pile's displacement could be made by attaching an accelerometer to the pile, as is standard practice for dynamic testing.

The analysis of results could be improved by increasing data sampling rates to allow greater accuracy in the calculation of velocity and acceleration. By sampling at a higher rate than every millisecond, peak values at the rapid changes seen in the acceleration magnitude would not be omitted. As accelerometers are common in pile testing, it would seem logical to measure the pile acceleration rather than deduce it.

Based on this study and others, the recording of STN data may be slightly misleading in that both the STN load and pile displacement are reduced to zero just prior to the STN test. During preparation of the STN device, the load pack of 18 tonnes is lowered onto the STN piston, which in turn loads the pile. In many of the results presented for STN, the results appear to start at zero load and displacement. The application of the 180kN in some cases is equivalent to the first stage of a maintained load test and the resulting

displacement may give indications of the initial static stiffness. Hence, this equipment preparation stage should be considered as part of the pile loading test, with readings taken throughout.

It is the author's view that, at the present level of understanding and available field data that STN should not be used in isolation for tests in clay soils. Ideally, the test should be used in conjunction with a static test that allows back figured parameters to be derived for the non-linear STN analysis suggested in Equation 7.1, 7.20 & 7.21. This approach is often recommended for other pile testing methods such as dynamic (ICE, 1999 & EC 7, 1997) and other geotechnical tests (CPT).

One area associated with STN testing that requires immediate attention is inclusion of the method in guidance documents and specifications for pile testing for UK use. Detractors would state that the method has no place in the codes of practice but as STN is seeing greater use guidance must be made available. Without such guidance, consultants cannot make an informed assessment of the method's applicability or correctly interpret the results.

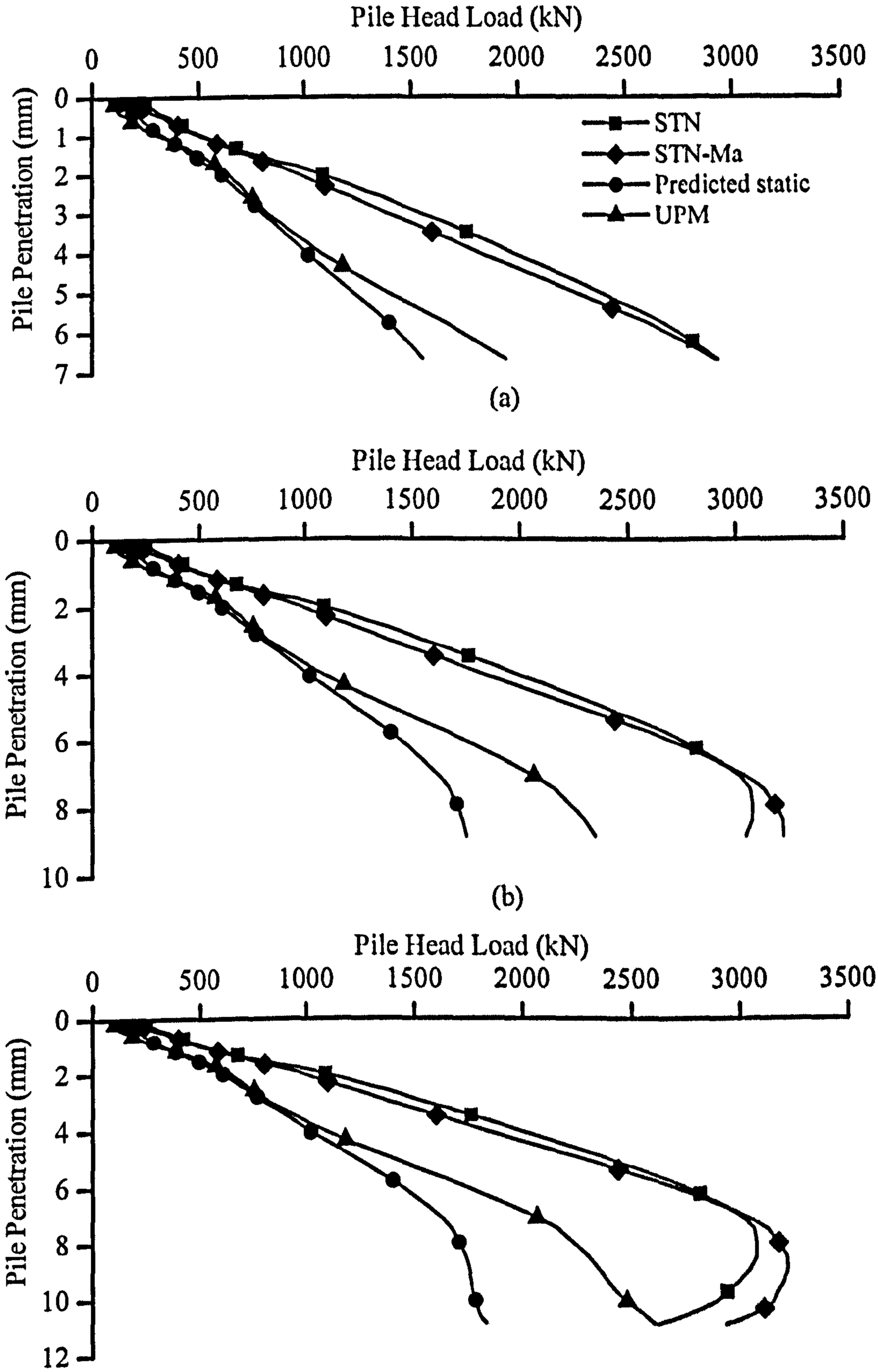

Figure 7.1, Class A prediction of static pile behaviour based on a 3000kN Statnamic test: (a) Stiffness response, (b) Ultimate pile capacity, (c) Comparison with UPM.

Analysis Method	*Derived Static Pile Load (kN)*	*Pile Penetration (mm)*	*Secant Stiffness (kN/mm)*
Predicted static stiffness (Equation 7.1)	1557	6.65	234
For comparison only			
UPM	1940	6.65	291
F_{STN}	2924	6.65	440
F_{STN-Ma}	2915	6.65	438

Table 7.1, Prediction of the auger bored pile static stiffness response from a 3000kN Statnamic test.

Analysis Method	*Derived Static Pile Load (kN)*	*Pile Penetration (mm)*
Predicted ultimate pile capacity (Equation 7.1)	1746	8.85
For comparison only		
UPM	2343	8.85
F_{STN}	3037	8.85
F_{STN-Ma}	3210	8.85

Table 7.2, Prediction of the auger bored pile ultimate static pile capacity from a 3000kN Statnamic test.

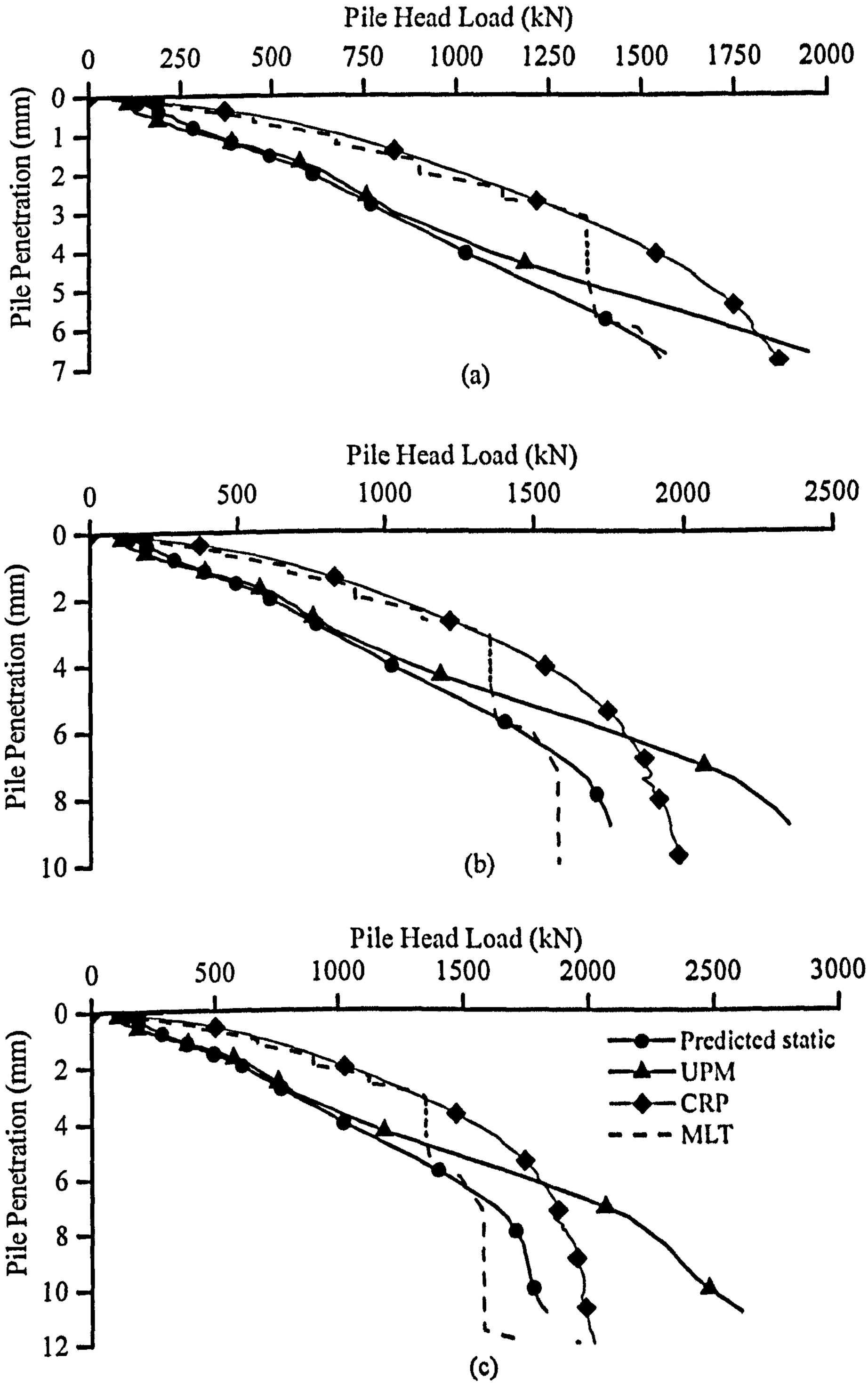

Figure 7.2, Comparison of predicted static response with measured: (a) Stiffness response, (b) Ultimate pile capacity, (c) Comparison with UPM.

Analysis Method	*Derived Static Pile Load (kN)*	*Pile Penetration (mm)*	*Secant Stiffness (kN/mm)*
Measured CRP	1500	3.90	385
Predicted static stiffness (Equation 7.1)	1500	6.32	236
UPM	1500	5.30	283
For comparison only			
F_{STN}	1500	2.89	519
F_{STN-Ma}	1500	3.24	463

Table 7.3, Prediction results from the auger bored pile static stiffness response from a 3000kN STN pulse.

Analysis Method	*Derived Static Pile Load (kN)*	*Pile Penetration (mm)*
Predicted ultimate pile capacity (Equation 7.1)	1746	8.85
Measured static CRP	1946	8.85
UPM	2343	8.85
For comparison only		
F_{STN}	3037	8.85
F_{STN-Ma}	3210	8.85

Table 7.4, Prediction results of the auger bored pile ultimate static pile capacity from a 3000kN STN test.

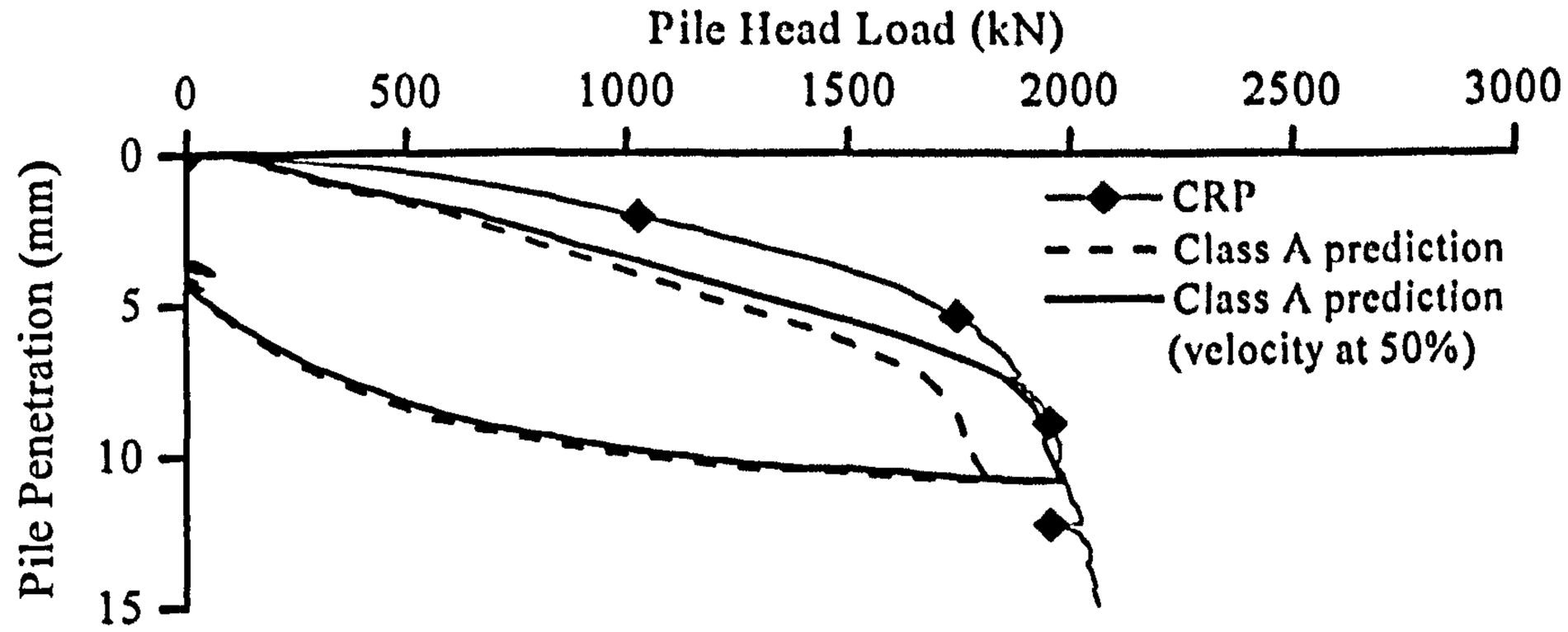

Figure 7.3, Effect of reducing measured velocity on class A prediction results.

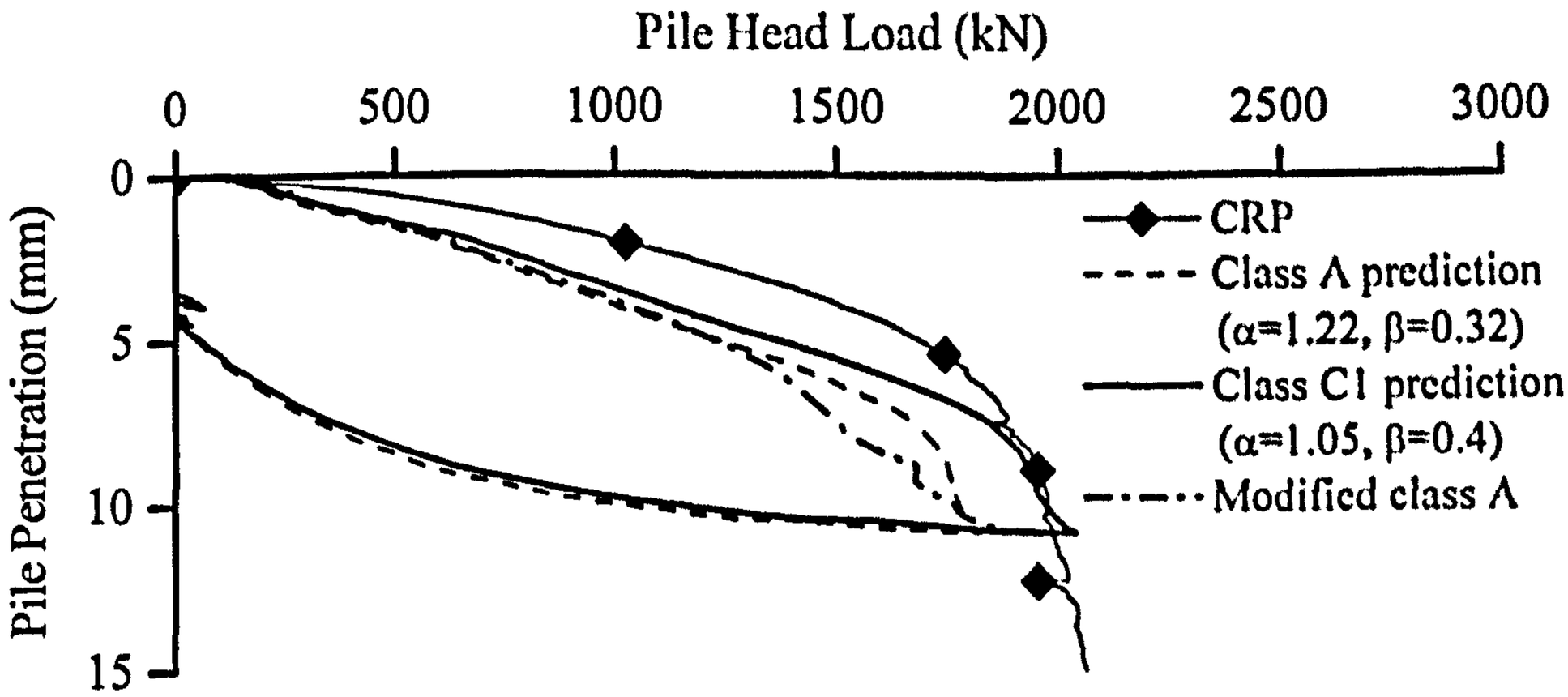

Figure 7.4, Modification of prediction rate parameters to match ultimate measured static pile capacity

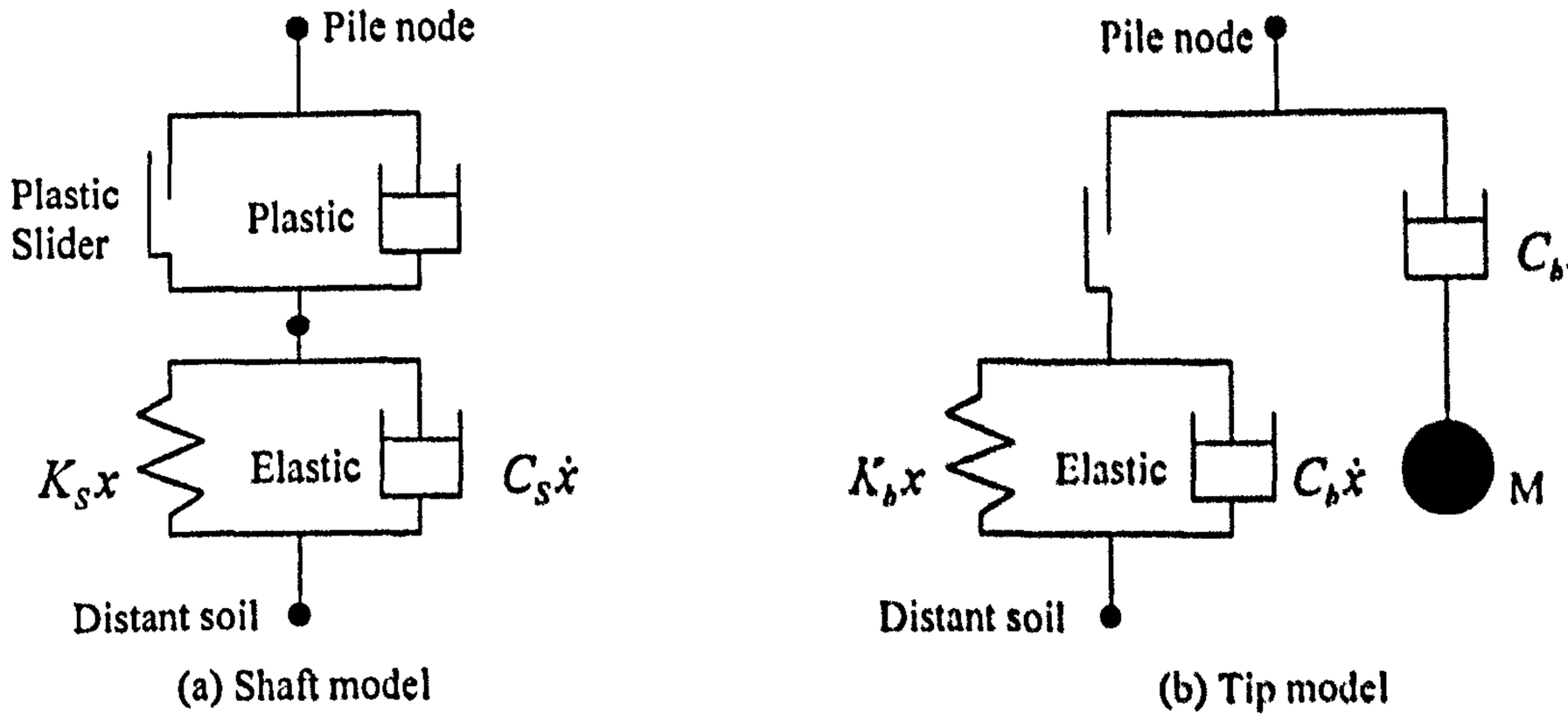

Figure 7.5, Diagrammatic representations of dynamic pile-soil models (Randolph & Deeks, 1992).

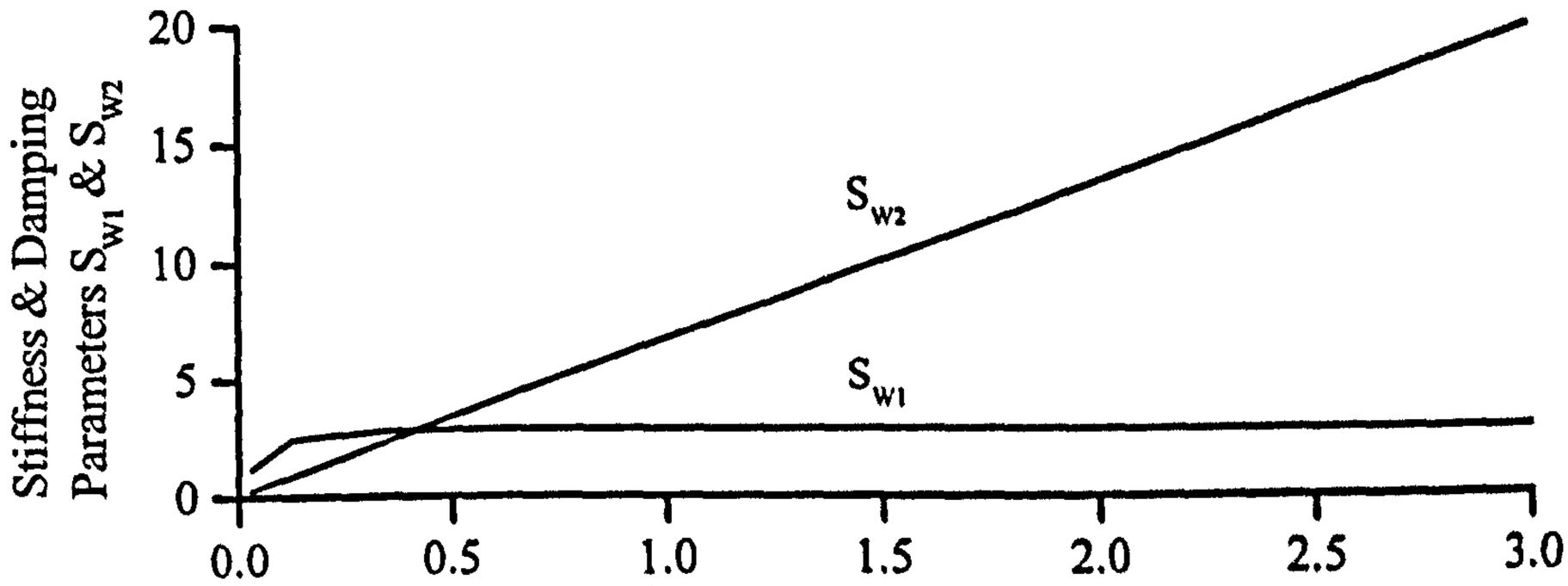

Figure 7.6, Dynamic soil stiffness coefficients (Randolph & Simons, 1986).

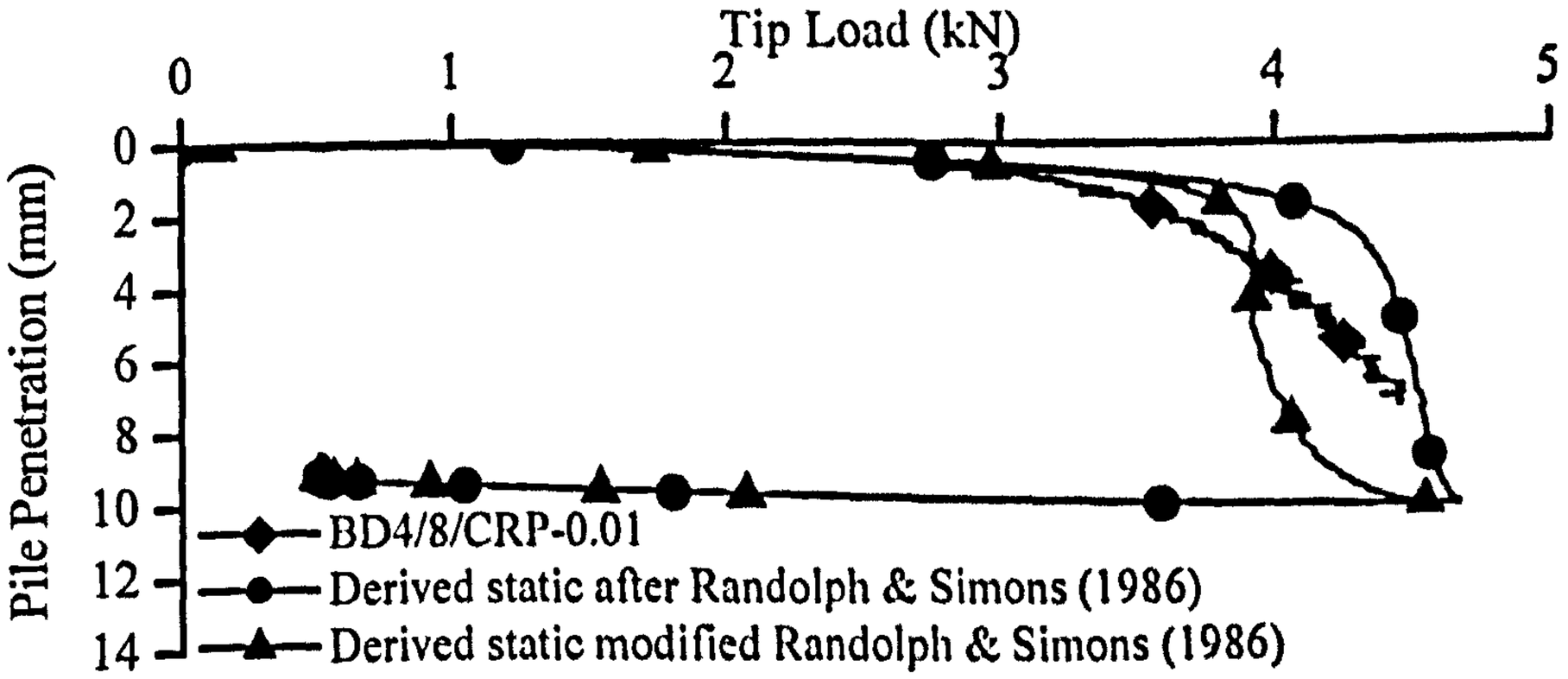

Figure 7.7, Results from model pile testing showing static equivalent tip resistance based upon models by Randolph & Deeks (1992), (BD4/7/STN-30kN).

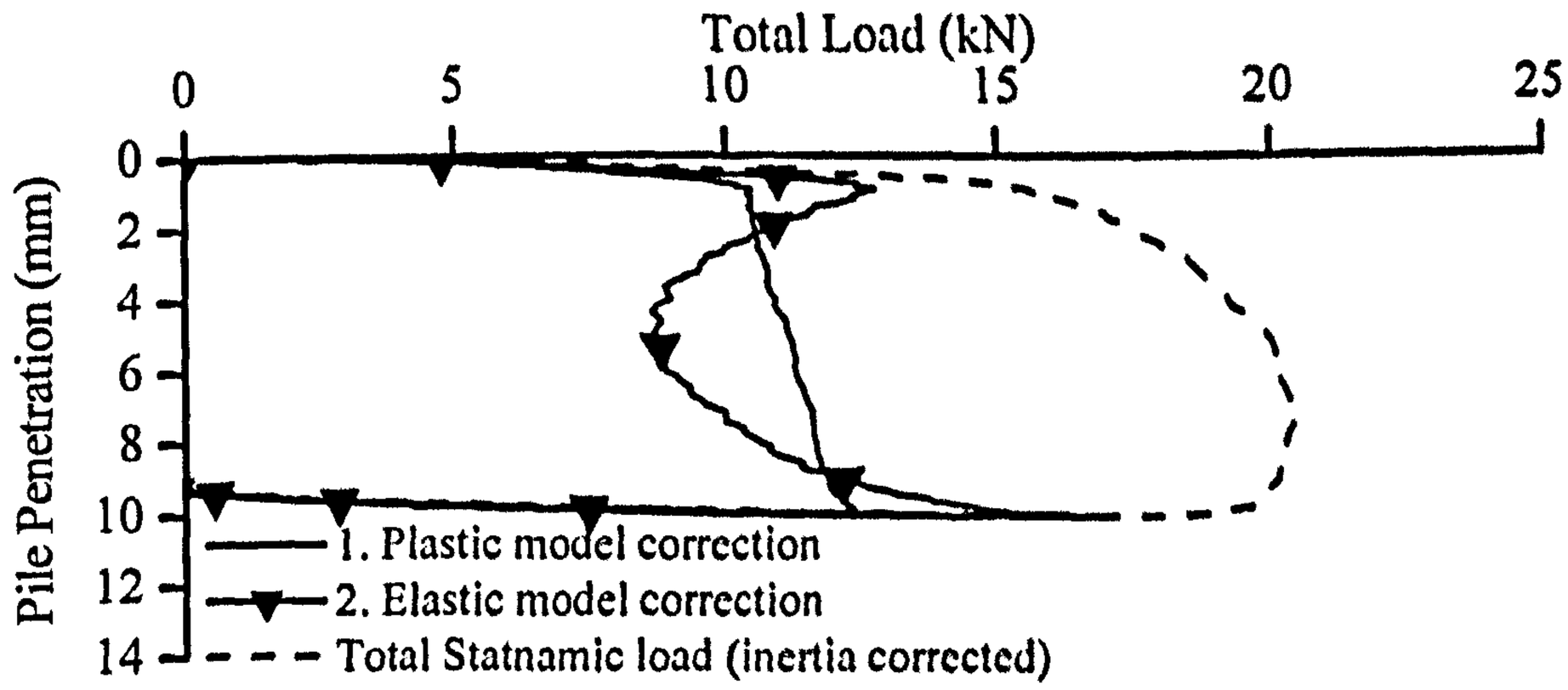

Figure 7.8, Results of model testing showing use of the plastic component of the analysis model to define the limit of elastic correction (BD4/7/STN-30kN).

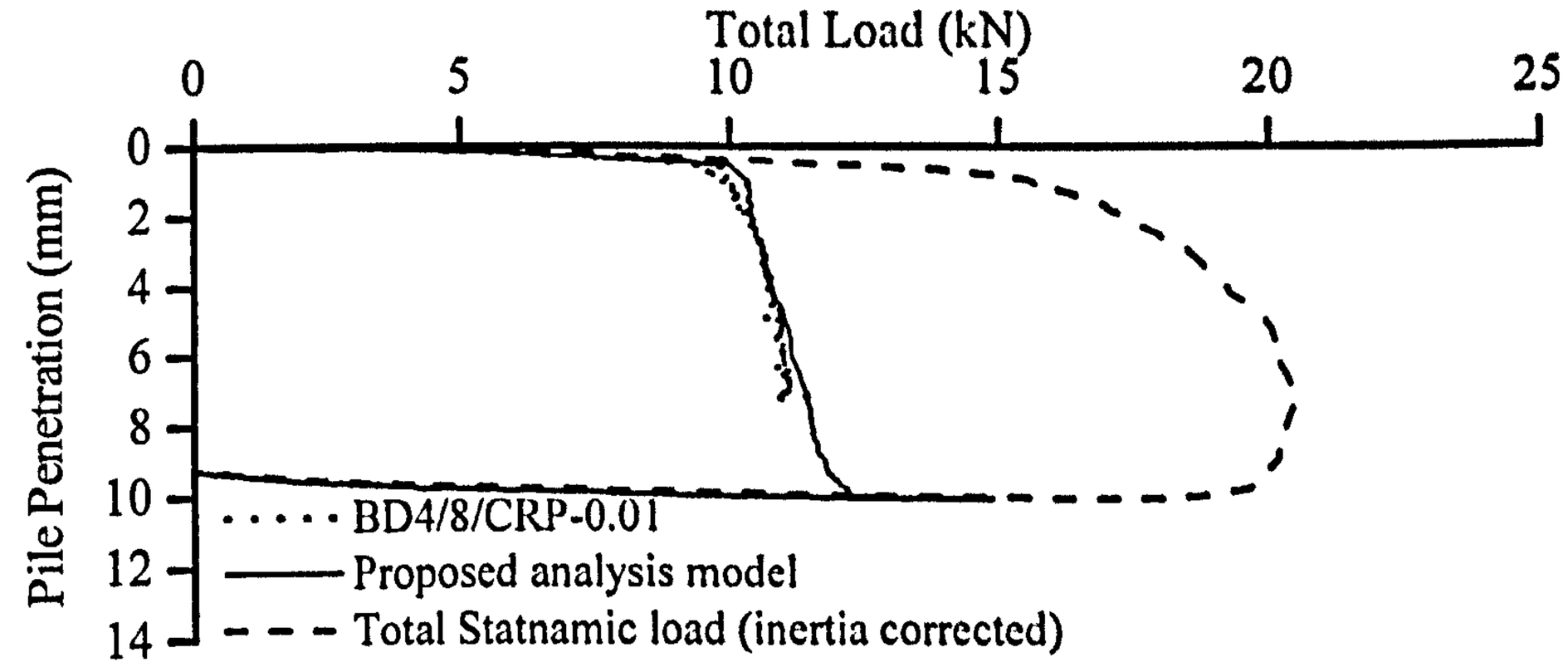

Figure 7.9, Results of model pile testing showing derived static equivalent total load based upon proposed shear modulus model (BD4/7/STN-30kN).

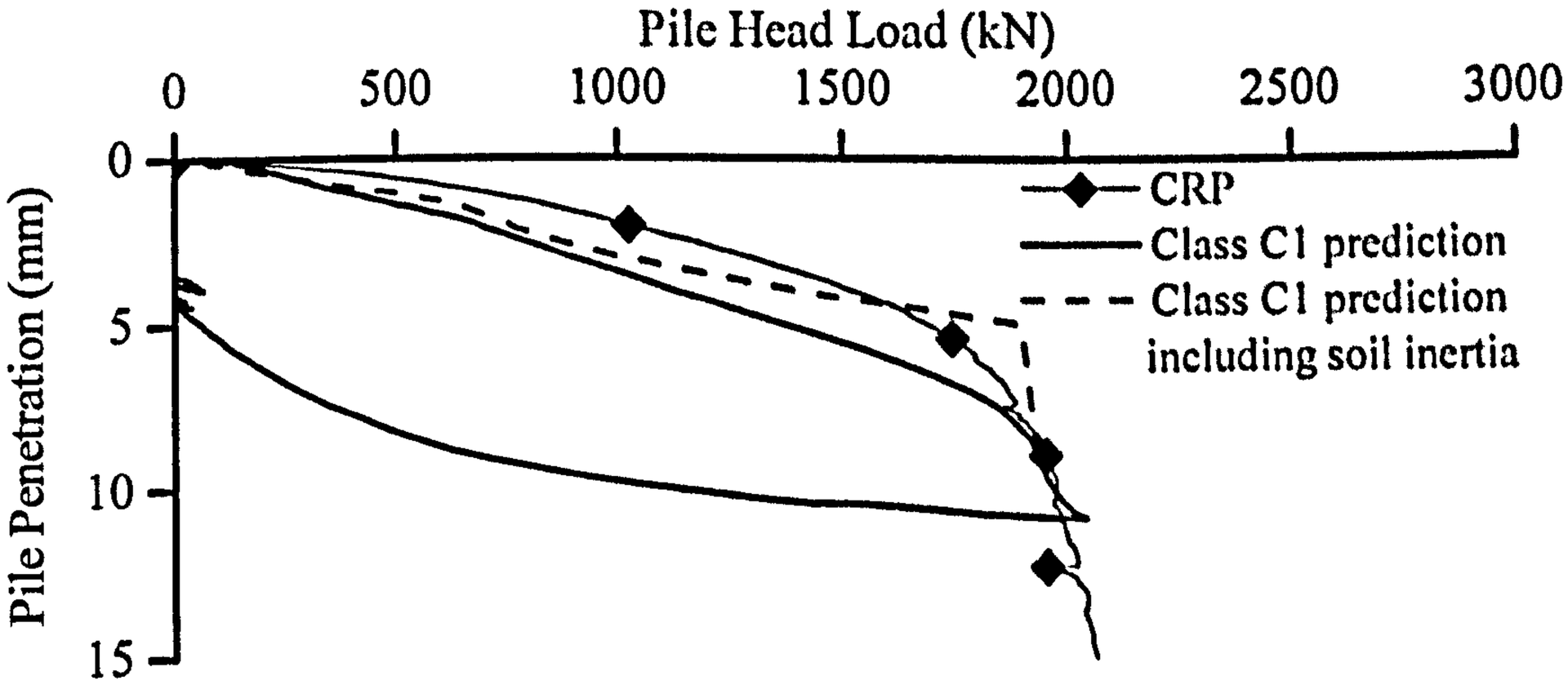

Figure 7.10, Prediction of static behaviour incorporating soil inertia.

8.0 Summary and Conclusions

8.1 Introduction

At the present level of pile design knowledge, it is still necessary to undertake pile load testing. The most recent development in pile load testing is the advent of rapid or kinematic tests such as Statnamic testing which have several benefits over classical forms of foundation load testing. Current analysis of Statnamic tests gives adequate prediction of equivalent static pile behaviour in coarse grained soils but may over predict in fine grained soils whose behaviour is highly non-linear with increasing rates of pile penetration. To improve the analysis of Statnamic tests in these soil types, analysis methods must reflect this non-linearity and give due regard to the influence of soil inertia.

This study has shown that it is possible to use a large clay calibration chamber to carry out a parametric study on the behaviour of a pile under different penetration and loading rates in a fine grained soil. Observations of the mechanisms of soil behaviour have led to the development of new analysis methods that may be used to predict the equivalent static behaviour of full scale piles installed in glacial till. The study findings and conclusions are summarised in the following sections.

8.2 Model pile testing

The following points are a summary of the conclusions made from the results of model pile testing in clay at different rates of pile penetration and simulated Statnamic pile load testing.

1. As the rate of pile penetration during model Constant Rate of Penetration (CRP) testing in the model clay increased so did the pile's ultimate resistance. This rate of penetration dependent behaviour or rate effect can be represented by a modified non-linear rate law as proposed by Randolph & Deeks (1992).
2. The damping or rate constants required to define Randolph & Deeks (1992) modified rate law can be taken as $\alpha = 1.26$ and $\beta = 0.34$ for the total pile head

load based upon the findings of high rate CRP testing. The range of values found for the rate parameters varied from $\alpha = 1.05$ to 1.56 & $\beta = 0.19$ to 0.48. The penetration rate dependant increase in shaft resistance ($\alpha = 2.00$ & $\beta = 0.4$) was much greater than that for the pile's end bearing resistance.

3. Excess pore pressure measured at the interface between the pile and the clay bed was different at different locations on the pile. The excess pore pressure at the pile tip reduced from $0.93\sigma_c$ (where σ_c was the bed confining pressure) at the lowest rate of pile penetration, to $0.004\sigma_c$ at the highest rate. This implies that the effective stress at the pile tip was at its lowest during low rate pile penetration but, increased towards the total confining stress during high rates of pile penetration. Pore pressures measured $15.26R$ (R = pile radius) above the pile tip on the pile's skin were unaffected by rate of pile penetration. It should be noted that the pore pressure response measured during high rate CRP testing was much faster than that predicted by Bond *et al.* (1991) for London clay. Although large pore pressures were measured during high penetration rate model pile testing, it is likely that these were influenced by deformation of the clay calibration chamber.
4. At low rates of penetration, excess pore pressures measured in the clay bed below the pile tip were relatively large ($0.6\sigma_c$). As the rate of pile penetration increased, these pressures reduced and became negative at penetration rates in excess of 50mm/s. For the highest penetration rates, pressures of –100kPa and lower were measured, although this would be influenced by cavitation. Bed excess pore pressures measured between $4.77R$ to $12.91R$ above the pile tip were much smaller than those measured close to the pile tip. For the lowest rates of penetration, the excess pore pressures remained positive throughout pile penetration. At higher rates of pile penetration, the excess pore pressures were negative for the first millimetre of pile penetration. Although large pore pressures were measured during high penetration rate model pile testing, it is likely that these were influenced by deformation of the clay calibration chamber.
5. To produce a permanent model pile penetration equivalent to 10% of the pile's diameter for the soil used in this study, the applied Statnamic loading must be at least 1.5 times the ultimate pile capacity found from low rate CRP testing.

6. Results from model Statnamic loading showed that the load-displacement behaviour was similar to that for low rate CRP testing (0.01mm/s) for up to 60% of the low rate pile-soil elastic response zone. This was without correction for rate effects or inertia. Above this load level, the stiffness measured for Statnamic loading was greater than that for low rate CRP tests.
7. No significant change in either the model pile tip or skin interface pore pressures were measured during the Statnamic event.
8. Excess pore pressures monitored in the clay bed in advance of the pile tip during Statnamic load testing show no significant change. Large positive pore pressures up to $0.75\sigma_c$ were measured 1.22 to 1.61 R above the pile tip.
9. Excess pore pressures measured at the mid height (7.48 to 7.86 R above the tip) of the clay bed during the Statnamic event were similar to those seen during high rate CRP testing whereas, the excess pore pressures measured towards the top of the clay bed were negative but, this was attributed to deformation of the calibration chamber.
10. The dissipation of measured vertical soil accelerations away from the model pile during Statnamic loading may be represented by a two parameter exponential decay. Measured vertical accelerations decayed to less than 10% of the pile's acceleration on exceeding a radial distance of 15 R from the pile's centre line. Additional testing is required to verify this finding.
11. Adequate prediction of equivalent static pile behaviour from model Statnamic testing for the fine grained soil used in this study can be made using a non-linear expression of the form:

$$F_{static} = \frac{F_{STN} - Ma_{(pile)}}{1 + \alpha(v)^{\beta} - \alpha(10^{-5})^{\beta}}$$

Where α and β are defined from CRP testing at varying rates and the lowest rate of CRP penetration is $1\text{x}10^{-5}$m/s.

8.3 Statnamic field study

The following points are a summary of the conclusions from the results of full scale Statnamic and top-down static pile testing at a field research site with piles installed in glacial till.

1. Initial trials suggested that standard Cone Penetration Testing (CPT) equipment advanced at elevated penetration rates may be used to define in-situ rate constants for rapid load pile test analysis. Significant additional testing is required to verify this finding.
2. The accuracy of Statnamic analysis would benefit considerably from the inclusion of an accelerometer at the pile head. This would allow direct measurement of acceleration and provide verification of displacement measurements and velocity calculations.
3. Results from full scale pile load testing in glacial till showed that the stiffness measured during Statnamic, Maintained Load Testing (MLT) and CRP was similar up to 50% of the ultimate static pile capacity derived from CRP testing. Above this level of loading, the stiffness measured for Statnamic loading increased compared with that for low rate CRP tests.
4. Results from pile instrumentation showed that shaft resistance varied considerably between different methods of load testing. From MLT testing, the ultimate shaft resistance varied between 67 and 83kN/m^2, which is 20% lower than that found during CRP testing at 92 to 104kN/m^2. For the largest increment of Statnamic loading the shaft resistance was 34% higher than CRP loading at 96 to 130kN/m^2.
5. Vertical soil accelerations measured at $6.78R$ and $13.45R$ above the pile tip had decayed rapidly within a radial distance $3R$ from the pile centre line and were below 10% of the pile's measured acceleration by $6R$. This reduction in measured vertical acceleration with distance from the pile was adequately represented by a two parameter exponential decay similar to that found during model pile testing.
6. A class A prediction of the equivalent static pile behaviour from Statnamic testing using the non-linear approach proposed for model tests predicted an ultimate static pile capacity that was 10% less than that measured during CRP

testing. This method performed better than the UPM Statnamic analysis, which over predicted by 23%. Both methods of analysis under predict the static pile stiffness by up to 60%.

7. Results from the class A prediction showed that the proposed non-linear analysis method was suitable for the prediction of ultimate static pile capacity. Neither this method nor UPM analysis should be applied to prediction of the elastic load-displacement behaviour for working pile loads.

8. The prediction of equivalent static pile resistance from Statnamic testing needs to be analysed differently in the elastic and plastic zones. In the elastic zone, the enhanced stiffness at loads above 50% of the ultimate static load is thought to be influenced by soil inertial resistance. This can be incorporated in the proposed analysis by an expression of the form:

$$F_{static} = F_{STN} - (Ma)_{pile} - (Ma)_{soil}$$

which is used to predict equivalent static pile behaviour in the elastic zone. The equivalent static behaviour in the plastic zone may be found by using:

$$F_{static} = \frac{F_{STN} - Ma_{(pile)}}{1 + \alpha(v)^{\beta} - \alpha(v_{\min})^{\beta}}$$

9. Results from monitoring of the ground accelerations around the pile shaft showed that the vertical soil inertia could be represented by:

$$(Ma)_{soil} = \left(35\bar{\rho}\pi R^2 L\right) \times a \times 3e^{-3.86}$$

Incorporating this component of vertical soil inertia can improve the prediction of equivalent static soil stiffness for load levels above 50% of the ultimate static capacity. Below 50% of the ultimate static capacity incorporating vertical soil inertia does not significantly improve the prediction.

10. To allow derivation of the equivalent ultimate static pile behaviour from Statnamic testing in the glacial till encountered in this study, the minimum

applied Statnamic loads must be at least 1.7 times the predicted ultimate static capacity.

11. At the present level of understanding and available data, Statnamic testing should not be used in isolation for the load testing of piles in fine grained soils. Ideally, Statnamic load testing should be used in conjunction with a top-down static pile load test that allows back figured parameters to be derived for the proposed non-linear analysis method.

9.0 Recommendations for Further Work

9.1 Improvements to the calibration chamber system

It is recommended that several modifications be made to the existing clay calibration chamber and the bed consolidation arrangements (Section 4.0). The concertina membrane used for one-dimensional consolidation frequently ruptured and its replacement by a hydraulic actuator connected to a piston would be more reliable. Timesavings would be achieved through greater reliability and ease of cell assembly and dismantling. It would also remove the need for the labour intensive fabrication of the large concertina membranes. A similar system to that proposed was used by Smith (1993).

The one-dimensional phase of consolidation would also benefit from an improved top drainage detail to achieve equal discharge from the top and bottom of the sample (Section 4.2.7). Smith (1993) suggested that the creation of high pore pressures during consolidation might promote radial drainage out to the bed-pipe interface and result in bed non-uniformity. To avoid this, he used small increments of consolidation pressure rather than the two single large steps employed here. This approach could be tested in future studies and the effects on bed uniformity assessed. The performance of these improvements and consolidation could then be monitored by automatic monitoring of piston travel and expelled water volumes. Automatic monitoring of the discharged water volumes would also make it easier to identify membrane leaks during the isotropic phase of consolidation.

During the model pile testing, two characteristics of the chamber were identified that may have had a significant effect on the results. These were the influence of chamber deformation on bed pore pressures (Section 5.3.7) and the rigid chamber base on pile end bearing behaviour (Section 5.3.9). The reduction in cell confining and bed pore pressures during elevated rate pile testing was thought to be due to the actuator loading frame being mounted on the chamber top end plate (Figure 4.7). Ideally, the pile loading system should derive its reaction to loading independently from the chamber, thus

preventing deformation of the lid, although this would increase laboratory space requirements. A simpler solution may be to stiffen the top and bottom end plates using braces and to connect the top and bottom bracing together. Remote measurement of the chamber deflections could be undertaken but, such measurements may be difficult to interpret due to very small deflections and electrical noise associated with pile loading. Further investigation of the influence of the cell pressure supply system response time on bed confining pressure is also required.

The use of a chamber with a rigid base is not ideal for a model pile study, even where there is significant pile-base separation, as an artificially stiff boundary condition is imposed. Incorporating an earth pressure cell at the chamber base below the model pile showed that there was a significant jump in load transferred to the base as the rate of loading increased (Section 5.3.9). The proximity of the base may have influenced both the measured tip resistance and the derived shaft resistance. It is recommended that the influence of the rigid chamber base be investigated by incorporating a flexible base. Such a modification would require alteration of the bed instrumentation mounting and drainage. Smith (1993) gives details of a flexible chamber base and drainage system.

One of the major limitations of using the large clay calibration chamber is the long time periods required for bed preparation. This limits the number of beds that can be prepared during a research project. This could be overcome by developing additional one-dimensional consolidation rigs. The improvement of using a hydraulic actuator would also reduce the need to duplicate chamber components for additional consolidation rigs. The major limitation to this development would be laboratory space. Additional testing could also be undertaken by multiple pile installations within each clay bed. This could be achieved by off-centre pile installations. By rotating the chamber top end plate, several pile installations could be carried out in a bed. The actuator loading frame was designed to allow this development.

9.2 Improvements to the model pile and bed instrumentation

The design of the model pile would benefit from improvements in both the skin friction measuring arrangement and the performance of the interface pore water pressure transducers. The skin friction zone accounted for 42% of the typical pile embedded

length (Section 4.3.2). This limited the ability to monitor axial load distribution along the pile and the influence of pile velocity on the load distribution. This may be overcome by fabrication of a new pile section with shorter friction measuring zones or, replacing the existing section with a hollow tube incorporating strain gauges at several locations down the pile length. Although all attempts were made to maintain pile pore pressure transducer saturation during pile installation, the method of installation was not ideal for this. To give greater confidence in the measured pore pressures, the transducer arrangements may benefit from a flushing detail that would allow saturation to be maintained throughout testing, similar to that used during the DOE (1990) study.

An additional development of the pile would be to incorporate radial stress measuring cells. If these were combined with pore pressure measurements, it would be possible to investigate the influence of pile velocity on effective radial stresses. This would lead to greater confidence in the calculation of friction angles and coefficients discussed in Section 5.3.4.

The only significant alteration to the clay bed transducer installations would be to completely encase the accelerometers to remove the suspected influence of bed pore pressure change on accelerometer outputs, as discussed in Section 5.5.7. The units could be encased as used during the full scale pile study (Section 6.3.2).

9.3 Model pile testing

To allow determination of the rate effects during CRP testing a low rate benchmark of pile resistance was defined based upon CRP tests at 0.01mm/s. These were carried out at different elevations during the pile testing sequence (Section 5.4.1). This was used to define the low rate pile resistance at any level during testing. The low rate load varied considerably during the first 40mm of cumulative pile penetration and resulted in considerable scatter in the determination of rate effect parameters (Figures 5.29 & 5.30). Further investigation needs to be made into the most suitable way to define this low rate benchmark. This may be achieved by only undertaking low rate CRP tests in the first 40mm of cumulative pile penetration. Alternatively, miniature CPT testing carried out at the pile's lowest rate parallel to the pile may be used to define a benchmark. This would require modification of the existing chamber arrangement.

As discussed in Section 7.1.4, due to scaling effects between the model pile and the field pile, the low rate pile velocity used in CRP testing may have been too slow. This would result in rate parameters from model testing that would over correct for pile velocity when applied to the field pile. To test the assumption, the effect of changing the velocity used to define the low rate benchmark (Section 5.4.1) on the derivation of rate parameters should be studied. Additionally, simulating the more commonly used MLT test would allow equivalent static pile behaviour found from rapid load testing to be compared with both CRP and MLT tests.

9.4 General laboratory studies

During this research project, the rate dependant behaviour of only two different clays has been studied (KSS & Grimsby Clay). As well as model pile testing, their behaviour at elevated rates has also been studied in triaxial element testing by Balderas-Meca (2004). As it has been shown that individual soil types have different rate dependant behaviour, (Gibson & Coyle, 1968) parameters will be required for analysis of rapid load pile tests depending on soil type. The use of the clay calibration chamber to define parameters for several different soil types is limited due the earlier mentioned clay bed consolidation times. The use of triaxial element testing would be more appropriate for this type of study.

To give flexibility to the analysis of rapid load testing, the findings from such a study would need to identify relationships between commonly determined soil parameters and rate parameters. For initial studies, the variation of parameters such as Atterberg limits and particle size distribution could be studied. If such relationships were identified, it would be possible to determine rate dependant soil characteristics based upon simple laboratory classification tests. This would remove the need for the specialised equipment used in this research study and that used by Balderas-Meca (2004).

9.5 Field studies

As well as the proposed studies to identify rate parameters for a variety of soils, a concurrent study of full scale rapid load testing should be undertaken to assess the results of the laboratory findings. Where field studies are undertaken they would need to focus on determining the influence of soil acceleration on pile resistance, as it is difficult to model this behaviour with small scale laboratory tests. Results from such a

study would allow the radius of soil influenced and dissipation of acceleration to be determined. This behaviour could then be linked to soil parameters and used to improve the analysis proposed in Section 7.2.5. This type of study may also be suitable for centrifuge testing.

Although it may be possible to link soil rate behaviour to fundamental soil properties, verification by in-situ testing would add confidence to rapid load testing analysis methods. An investigation into using currently available CPT equipment to determine rate parameters for the Grimsby site is discussed in Section 6.2.3. Initial findings based upon limited testing were encouraging, with the need to undertake more tests and reduce the rate of the slowest test being identified as possible improvements. The small wheel drive type CPT rigs designed for offshore testing (Beazant, 2004) may prove more suitable for this type of study due to the ability to vary penetration velocity. Where information is required for load tests of higher frequencies (dynamic) then similar studies could be based upon the Standard Penetration Test (SPT) or Dynamic Penetration Testing (DPT).

9.6 Rapid load testing analysis

In the short term, rate parameters for the analysis method proposed in Section 7.2.5 could be obtained by back analysis of existing rapid load pile testing in fine grained soils. Such a study would be dependent on the availability of rapid load testing data and ground investigation information. Experience during this study for UK use of the Statnamic test would suggest that it is rarely used in fine grained soils. Additionally, where the Statnamic test has been used, it was as a result of unforeseen problems encountered during top-down static pile testing. Such circumstances make information difficult to obtain because of commercial confidentiality.

Improvements to the analysis method proposed in Section 7.2.5 could be made in several ways. The analysis would benefit from full automation by development of a suitable computer based software package. This software would automatically select the point where pile behaviour changed from elastic to plastic based upon the definition of ultimate pile behaviour found by Equation 7.20 (Section 7.2.5). The calculation of the soil inertial component of elastic pile behaviour could also be undertaken. The software

should be developed such that the only inputs were Statnamic measured data and some limited simple soil parameters such as Atterberg limits.

One area that has been given little regard in this research project is the separate consideration and modelling of the pile tip behaviour. Future research should include the development of a model of analysis specifically for the tip component of pile resistance at elevated rates. Although it was found that the rate effect for the tip was greatly reduced when compared with the shaft, no investigation has been made of the influence of soil inertia below the pile tip. Such an investigation could be incorporated in further calibration chamber testing or field trials.

Appendix 1: A summary of rate effect models

A summary of rate effect models found during the study.

Originator	*Rate law*	*Test conditions*	*Soil type*
Taylor (1942)*	$\tau = \overline{\eta}\dot{e}$	Oedometer (Secondary consolidation)	Clay
Smith (1962)*	$R_{dynamic} = R_{static}(1 + Jv)$	Dynamic pile penetration (Wave Equation Analysis)	
Marayama and Shibata (1964)*	$\dot{\varepsilon} = \beta\tau_0 \sinh(\alpha\tau/\tau_0)$	Creep deformation	Clay
Barden (1965)*	$\tau = \beta(\dot{e})^{1/N}$	Oedometer (Secondary consolidation)	
Yong & Japp (1967)	$\tau = \tau_0 + \alpha_0 e^{\frac{\varepsilon_f - \varepsilon}{\gamma}} \log\frac{\dot{\varepsilon}}{\dot{\varepsilon}_0}$	Triaxial tests Rates = 80 to 1600mm/s	Kaolinite Grundite
Gibson & Coyle (1968)	$\frac{R_d}{R_s} = 1 + Jv^N$	Triaxial tests, unconsolidated & undrained Rates up to 3246mm/s	Sand Sandy Clay Clay
Dayal & Allen (1975)	$\frac{q_{cd}}{q_c} = 1 + K_L \log\left(\frac{v}{v_s}\right)$	Cone penetration at constant rates Rates = 1.3 to 811mm/s	Pottery clay Silica sand
Heerema (1979)	$\tau = \alpha_2 + \alpha_3 v^{0.2}$	Simple shear Rates = 0.0008 to 1000mm/s	Sand & Clay
Lithkouhi & Poskitt (1980)	$\frac{R_d}{R_s} = 1 + Jv^N$ $\left(R_d/R_s = 1 + \alpha\sinh^{-1}\beta v\right)$	Model piles driven into clay targets. Rates = 0.3-1750mm/s	Clay
Bea (1982)	$\frac{R_d}{R_s} = \alpha_1 + \alpha_2 \log\frac{\dot{P}}{\dot{P}_s}$	Pile load tests & elevated rate laboratory tests	Cohesive soils
Poskitt & Leonard (1982)	As per Lithkouhi & Poskitt	As above. Rates = 0.2 to 2000mm/s	Cowden Clay
Briaud *et al.* (1984)	$c_{u1}/c_{u2} = (t_{f2}/t_{f1})^N$ $N = 0.028 + 0.00060w$ $N = 0.035 + 0.00066I_p$ $N = 0.036 + 0.046I_L$	Simple shear and rod shear tests plus literature review.	Clay soils
Randolph & Deeks (1992)	$\tau_d = \tau_s\left[1 + \alpha\left(\frac{\Delta v}{v_0}\right)^{\beta}\right]$	Literature review	Sand & Clay
Soga & Mitchell (1996)	$q_f/q_{f(ref)} = (\dot{\varepsilon}_1/\dot{\varepsilon}_{1(ref)})^{\beta}$	Triaxial compression tests Rates = 0.0008mm/s	Pancone Clay
Triantafyllidis (2001)	$R_s/R_d = 1 - I_v \ln(v/v_s)$ $I_v = -7 + 2.55\ln(w_L)$	Multiaxial testing	Clayey soils

**References obtained from Lithkouhi & Poskitt (1980)*

Appendix 2: Model pile testing information

KSS Material information

Details of materials and suppliers used to manufacture KSS material. Specifications are those provided by the individual material supplier.

KAOLIN

Speswhite powder china clay

Supplier: Whitchem Limited
Address: 23 Albert Street
Newcastle-under-Lyme
Staffordshire
ST5 1JP
UK
Phone: 01782 711777
Fax: 01782 717290

Material information

Particle size distribution	
53 microns (BS 300 mesh residue) max. (%)	0.02
20 microns (%)	0.1
10 microns max. (%)	0.5
2 microns (%)	80.0±3
Specific gravity	2.6
Specific surface area (m^2/g)	11

SILT

Oakamoor HPF4 silica flour, high purity quartz sand. Dry ground.

Supplier: Hepworth Minerals and Chemicals Limited
Address: Brookside Hall
Sandbach
Cheshire
UK
Phone: 01270 752601
Fax: 01270 752600

Material information

Particle size distribution

150 microns (%)	1.5
125 microns (%)	3.6
106 microns (%)	6.5
75 microns (%)	16.3
53 microns (%)	29.6
40 microns (%)	46.2
30 microns (%)	55.7
20 microns (%)	66.6
10 microns (%)	79.5
5 microns (%)	87.6
Bulk density (kg/m^3)	1400
Surface area (m^2/g)	0.25
Source	Oakamoor, Staffordshire
Geology	Upper Millstone Grit

SAND
Buckland P30 silica sand

Supplier: Hanson Aggregates
Address: Quarry Hill Road
Borough Green
Sevenoaks
Kent
TN16 8RW
UK
Phone: 01732 789100
Fax: 01732 885601
Web: www.hanson-aggregates.com

Material information

Particle size distribution

699 microns (%)	0.5
500 microns (%)	3.5
355 microns (%)	20.2
250 microns (%)	69.5
211 microns (%)	86
152 microns (%)	98
150 microns (%)	100
Bulk density (kg/m^3)	1490-1610
Specific gravity	2.5
Source	Heath & Reach, Bedfordhsire
Geology	Lower Greensand

Calibration equipment

Details of the different equipment used to calibrate the instrumentation used during this study.

Transducer	*Calibration device*	*Comment*
Druck PDCR81 mini pore pressure transducer	FIG240 Bundenburg nitrogen dead weight tester with an air water interface.	Transducers were calibrated in the saturation cell described in Section 4.2.8. Transducers located in the clay bed.
Druck 810 & Kulite XT123 pressure transducers	FIG380L Bundenburg oil dead weight tester	Druck 810 located cell top and side. Kulites located in the pile.
Entran load cell, ELHS-T4M	15kN proving ring (PR4873). Load applied by Amsler 100kN universal testing machine.	Transducer located at pile tip (Figure 4.8). Transducer calibrated as installed in pile tip.
Pile skin friction load cells	As above.	Transducer calibrated as complete pile unit.
Hydraulic actuator load cell	As above.	Cell located between pile and the hydraulic actuator (Figure 4.7).
Actuator displacement transducer	Mitutoyo 300mm vernier calliper	Transducer located within the hydraulic actuator.
Pile LVDT displacement transducer	Mitutoyo digital micrometer head (0-50mm)	

Model pile testing procedure

MODEL CRP TESTING

Pile connection and Kelsey K7500 servo controller set up procedure from CRP testing

A, Hydraulic pump start up and connection of actuator to pile

1, Check K7500 is in unload and displacement mode prior to starting any testing.
2, Check initial K7500 settings are as follows:

Menu			
Gains	Disp	Servo	1.20
		Proportional	1.20
		Derivative	0.00
Limits	Disp	Upper stop	To suit current pile position
		Upper warn	As above
		Lower warn	-70.00mm
		Lower stop	-75.00mm
	Action (master)	As per stored parameters	
Set Gen	Test Bias	As required for test	
	Start/stop times	Static fade in	As required for test rate
		Static fade out	Nominal 3000 seconds

3, Check the pile is clamped and that the LVDT has enough travel for the test drive length. Do not start the pump if the actuator is in contact with the pile.
4, Check the hydraulic pump pressure bleed valve is fully open.
5, Start the hydraulic pump and use the Kelsey to bring the pump into low pressure mode followed by high pressure mode. Slowly close the pump pressure bleed valve.
6, Using the set Kelsey point function withdraw the actuator to its full extent.
7, Slowly move the actuator load connection plate to within 10mm of the pile load connection plate and install clamping bolts but do not tighten.
8, Use Kelsey inching pendant to bring the loading plates just into contact and tighten up the bolts.

B, CRP pile test

1, Remove the pile clamp.
2, Adjust the gains to suit the test rate (see following table). This must be done very slowly with continuous adjustment of the set point to minimise accidental loading.
3, Check new set point against required bias and adjust as necessary.
4, Press start on Kelsey.
5, On the test reaching the required displacement press stop.
6, Quickly but carefully reduce gains to pre test levels.
7, Remove bolts from pile/actuator loading plates.
8, Adjust static fade out time to 60 seconds.
9, When the pile has reached its pre test displacement use the set point to move the actuator to its highest position.
10, Clamp the pile.
11, Slowly open the pump pressure bleed valve and set the Kelsey to unload.
12, Shut down the pump.

MODEL STATNAMIC TESTING

C, Statnamic pile test

1, Follow the CRP pile connection instructions first.
2, Check initial K7500 settings are as follows:

Menu			
Set Gen	Test type	External	
	Test bias	0.1kN	
	Cycle counter	None	
	Elapsed timer	4 hour (nominal)	
	Elapsed timer	Reset	
	Test mode	Load	
	Start/stop times	Static fade in	5msecs
		Dynamic fade in	3msecs
		Dynamic fade out	3msecs
		Static fade out	5msecs
	Action (master)	Pause	
Limits	Load	Upper stop	To suit test
		Upper warn	As above
	Displacement	Upper stop	As above
		Upper warn	As above

3, Remove pile clamp.
4, Select load control on control mode.
5, Adjust the gains to suit the test load (see following table). This must be done very slowly with continuous adjustment of the set point to minimise accidental loading.
6, Press start on Kelsey.

7, Press stop on Kelsey as soon as the test is complete.
8, Select displacement control.
9, Remove bolts from pile/actuator loading plates.
10, Adjust static fade out time to 60 seconds.
11, When the pile has reached its pre test displacement use the set point to move the actuator to its highest position.
12, Clamp the pile.
13, Slowly open the pump pressure bleed valve and set the Kelsey to unload.
14, Shut down the pump.

Gain settings

Optimum PID gain settings for the Kelsey K7500 servo hydraulic controller found for each different pile test.

Test type	*Rate (mm/s)*	*Load (kN)*	*Gain settings*			
			Servo	*Proportional*	*Integral*	*Differential*
CRP	0.01		4.00	3.66		0.50
	10		3.00	3.00		0.65
	25		1.90	3.50		0.80
	100		1.60	3.50		0.90
	200		1.45	3.50		0.94
	350		1.35	3.50		0.90
	500		1.30	3.50		0.90
STN		10	1.10	0.80	4.00	
		15	1.10	0.80	4.00	
		20	1.10	0.78	4.00	
		25	1.10	0.76	4.00	
		30	1.10	0.75	4.00	

These values are considered the optimum gains to be used for each test type. Note that these values will require adjustment between different beds.

Appendix 3: Summary of bed transducer locations

Summary of embedded transducer positions for each individual bed

Bed No.: 2
Bed final height: 996mm

Transducer	*Initial depth (mm)*	*Final depth (mm)*	*Initial radial position*	*Final radial position*	*Position relative to pile tip (z/R)*
PP1	246	231	3.71R	1.77R	16.32 to 19.20
PP2	245	231	6.86R	5.31R	16.32 to 19.20
PP3	239	231	10.02R	8.66R	16.32 to 19.20
PP4	516	508	3.71R	4.14R	8.40 to 11.28
PP5	516	512	6.85R	7.66R	8.30 to 11.20
PP6	516	507	9.97R	9.91R	8.44 to 11.31
PP7	805	809	No reading	1.86R	-0.19 to 2.69
PP8	421	423	No reading	1.23R	10.84 to 13.71
AC17	517	503	3.74R	3.00R	8.55 to 11.43
AC18	516	502	6.85R	6.49R	8.58 to 11.46

Bed No.: 3
Bed final height: 1002mm

Transducer	*Initial depth (mm)*	*Final depth (mm)*	*Initial radial position*	*Final radial position*	*Position relative to pile tip (z/R)*
PP1	257	246	2.14R	1.43R	12.46 to 16.17
PP2	259	309	3.71R	2.86R	10.66 to 14.37
PP3	257	248	5.29R	4.57R	12.40 to 16.12
PP4	527	513	2.14R	2.37R	4.83 to 8.54
PP5	527	518	3.71R	3.83R	4.69 to 8.40
PP6	527	522	5.29R	4.77R	4.57 to 8.29
PP7	744	741	2.14R	1.94R	-0.60 to 2.72
PP8	746	741	5.14R	3.60R	-0.60 to 2.72
AC17	507	498	3.74R	2.77R	6.34 to 9.66
AC18	507	498	6.85R	6.14R	6.34 to 9.66

Bed No.: 4
Bed final height: 1016mm

Transducer	*Initial depth (mm)*	*Final depth (mm)*	*Initial radial position*	*Final radial position*	*Position relative to pile tip (z/R)*
PP1	271	263	2.14R	2.34R	12.94 to 16.29
PP2	271	265	3.71R	3.00R	12.89 to 16.23
PP3	271	256	5.29R	4.14R	13.14 to 16.49
PP4	541	534	2.14R	2.43R	5.20 to 8.54
PP5	541	535	3.71R	3.71R	5.17 to 8.51
PP6	541	533	5.29R	5.06R	5.23 to 8.57
PP7	761	No reading	2.14R	No reading	-1.29 to 2.06
PP8	761	No reading	5.14R	No reading	-1.29 to 2.06
AC17	761	771	3.74R	3.37R	-1.57 to 1.77
AC18	761	773	6.85R	6.63R	-1.63 to 1.71

Bed No.: 5
Bed final height: 1018mm

Transducer	*Initial depth (mm)*	*Final depth (mm)*	*Initial radial position*	*Final radial position*	*Position relative to pile tip (z/R)*
PP1	543	531	5.29R	5.06R	5.38 to 8.70
PP2	543	536	2.14R	2.06R	5.26 to 8.58
PP3	543	532	3.71R	3.63R	5.06 to 8.38
PP4	273	269	2.14R	3.09R	12.89 to 16.21
PP5	273	266	3.71R	3.34R	12.97 to 16.29
PP6	273	265	5.29R	4.09R	13.00 to 16.32
PP7	763	761	2.14R	1.94R	-1.17 to 2.24
PP8	763	758	5.14R	3.37R	-1.08 to 2.24
AC17	763	766	3.74R	3.43R	-1.31 to 2.01
AC18	Accelerometer installed in the pile				

PP = Pore Pressure transducer
AC = Accelerometer
Z = Height above pile tip
R = Pile radius

Appendix 4: Field site borehole logs

Borehole logs from Grimsby field test site ground investigation

T.L.P. Ground Investigations. — **Borehole Record** — Cable Tool Boring 180mm dia. to base

Location : Expanded Piling Ltd., Cheapside Works, North Thoresby. **Borehole No. 1.**

Carried out For The University of Sheffield, Department of Civil & Structural Engineering. **Ground Level** **Co-ordinates** **Date :** 24.05.2001.

Description	Reduced Level	Legend	Depth & Thickness	Samples/Tests: Depth	Sample Type	Sample No.	Test	Field Records
Brown, mottled rust brown silty, slightly sandy clay containing fragments of brick, small stones and other assorted gravel. Made Ground.			(0.30) 0.30	0.20	D	1.		
				0.40	D	2.		
Firm to stiff, light orange brown, mottled light grey, silty, sandy Clay containing assorted fine gravel.			(0.60) 0.90	0.85	U	1.		60 blows.
Stiff, brown, mottled light grey, silty, sandy Clay containing assorted fine gravel.			(1.10)	1.55	D	3.	SPT	3,4,5,6,7,8.
			2.00	2.00	U	2.		99 blows.
Stiff, dark brown, occasionally mottled light grey, silty, slightly sandy Clay containing chalk and other assorted gravel.				2.65	D	4.	SPT	2,2,3,3,5,7.
				3.10	U	3.		55 blows.
Glacial Till (Boulder Clay).				3.70	D	5.	SPT	2,2,3,4,4,5.
				4.20	U	4.		50 blows.
firm to stiff between 5.00m and 7.50m.				4.80	D	6.	SPT	1,1,2,2,3,5.
				5.30	U	5.		47 blows.
				6.00	D	7.	SPT	1,1,2,2,3,4.
				6.50	U	6.		40 blows.
				7.20	D	8.	SPT	1,2,3,3,4,4.
				7.70	U	7.		52 blows.
				8.55	D	9.	SPT	2,2,3,4,4,5.
				9.15	U	8.		43 blows.
				9.65	D	10.	SPT	2,2,3,4,5,6.
				10.45	U	9.		48 blows.

S.P.T.: Where full penetration has not been achieved the number of blows for the quoted penetration is given (Not 'N' value)

Depths: All depths and reduce levels in metres. Thickness given in brackets in depth column.

Samples/Test Key.
D Disturbed Sample
B Bulk Sample
W Water Sample
U Undisturbed Core sample
S Standard Penetration Test
V Vane Test

Remarks
No groundwater seepages were encountered within the depth penetrated. Borehole casing advanced to a depth of 5.65m. b.g.l.

Logged by: S.T.
Scale: 1:50
Fig.

T.L.P. Ground Investigations.	Borehole Record Cable Tool Boring 150mm. dia. to base	Location : Expanded Piling Ltd., Cheapside Works, North Thoresby.	Borehole No. 1.
Carried out For The University of Sheffield. Department of Civil & Structural Engineering.		Ground Level	Co-ordinates	Date : 25.05.2001.

Description	Reduced Level	Legend	Depth & Thickness	Samples/Tests: Depth	Sample: Type	Sample: No.	Test	Field Records
As previous sheet								
Stiff, dark brown, silty, slightly sandy Clay containing fragments of chalk and other assorted sub rounded gravel.				11.15	D	11.	SPT	2,2,4,5,6,6.
				11.75	U	10.		52 blows.
Glacial Till (Boulder Clay).				12.60	D	12.	SPT	2,3,3,5,5,6.
				13.20	U	11.		50 blows.
				13.90	D	13.	SPT	2,3,4,5,7,8.
				14.60	U	12.		58 blows.
				15.30	D	14.	SPT	2,3,5,6,8,8.
				15.85	U	13.		55 blows.
				16.50	D	15.	SPT	2,3,4,5,6,8.
				17.05	U	14.		70 blows.
				17.80	D	16.	SPT	2,4,5,7,8,9.
				18.45	U	15.		70 blows.
				19.10	D	17.	SPT	2,4,5,6,7,8.
				19.75	U	16.		60 blows.
			20.35	End of Borehole.				

Groundwater Observations.
No groundwater seepages were encountered within the depth penetrated.
Standpipe installed in dry hole at 12.80m. b.g.l.

S.P.T.: Where full penetration has not been achieved the number of blows for the quoted penetration is given (Not 'N' value) Depths: All depths and reduce levels in metres. Thickness given in brackets in depth column.	Samples/Test Key. D Disturbed Sample B Bulk Sample W Water Sample U Undisturbed Core sample S Standard Penetration Test V Vane Test	Remarks	Logged by S.T. Scale 1:50 Fig.

T.L.P. Ground Investigations. — **Borehole Record** — Cable Tool Boring 150mm. dia. to base

Location : Expanded Piling Yard, North Thoresby, N. E. Linca. — Borehole No. 2.

Carried out For The University of Sheffield. Department of Civil & Structural Engineering. — Ground Level — Co-ordinates — Date : 27.03.2002.

Description	Reduced Level	Legend	Depth & Thickness	Samples/Tests: Depth	Samples: Type	Samples: No.	Test	Field Records
Loose, assorted brick and concrete rubble in a matrix of brown silty and sandy 'soil'.			0.23	(0.23)				
Brown, silty, sandy clay containing fragments of coal, sandstone, brick and other assorted gravel. **Made Ground.**			0.50	(0.27)				
Firm to stiff ,brown, silty, slightly sandy Clay containing occasional small fragments of coal, sandstone, old red sandstone and other assorted gravel			0.90	(0.40)				
				1.05 - 1.75	U	1.		
Glacial Till (Boulder Clay.)				1.80 - 2.50	U	2.		
Stiff to very stiff, brown, mottled orange brown and grey silty, slightly sandy Clay containing occasional small fragments of chalk and other assorted gravel			(3.00)	2.50 - 3.20	U	3.		
				3.25 - 3.95	U	4.		
			3.90	4.05 - 4.75	U	5.		
Generally stiff, dark brown, silty, slightly sandy Clay containing occasional small fragments of chalk, coal and other assorted gravel				4.90 - 5.60	U	6.		
				5.70 - 6.40	U	7.		
Glacial Till (Boulder Clay.)				6.50 - 7.20	U	8.		
				7.25 - 7.95	U	9.		
				8.00 - 8.70	U	10.		
				8.80 - 9.50	U	11.		
Thin lens of wet, brown, silty **Sand.**			9.25					
				9.70 - 10.40	U	12.		

S.P.T. : Where full penetration has not been achieved the number of blows for the quoted penetration is given (Not 'N' value)

Depths: All depths and reduce levels in metres.

Samples/Test Key.

D Disturbed Sample
B Bulk Sample
W Water Sample
U Undisturbed Core sample
S Standard Penetration Test
V Vane Test

Remarks

Logged by

Scale

Fig.

T.L.P. Ground Investigations	Borehole Record Cable Tool Boring 150mm. dia. to base	Location : Expanded Piling Yard, North Thoresby, N. E. Lincs.	Borehole No. 2.
Carried out For	The University of Sheffield. Department of Civil & Structural Engineering.	Ground Level	Co-ordinates	Date : 27.03.2002.

Description	Reduced Level	Legend	Depth & Thickness	Samples/Tests: Depth	Samples: Type	Samples: No.	Test	Field Records
Dark brown, silty, slightly sandy Clay containing occasional small fragments of chalk, coal and other assorted gravel				10.60 - 11.30	U	13		
				11.40 - 12.10	U	14		
				12.25 - 12.95	U	15		
				13.08 - 13.76	U	16		
				13.85 - 14.55	U	17		
				14.70 - 15.40	U	18		
			15.40	End of Borehole.				

Observations.
Slight groundwater seepage was encountered at 9.25 emanating from a thin lens of water bearing silty sand.
After 15 mins no water had accumulated in the base of the borehole.
On completion borehole remained dry after borehole casing was withdrawn.

S.P.T.: Where full penetration has not been achieved the number of blows for the quoted penetration is given (Not 'N' value) Depths: All depths and reduce levels in metres.	Samples/Test Key. D Disturbed Sample B Bulk Sample W Water Sample U Undisturbed Core sample S Standard Penetration Test	Remarks	Logged by Scale Fig.

Appendix 5: Class A prediction documents

Original class A prediction documentation as submitted prior to static pile testing

THE UNIVERSITY OF SHEFFIELD
Department of Civil & Structural Engineering

Sir Frederick Mappin Building
Mappin Street
Sheffield S1 3JD

Tel: +44 (0) 114 222 5741
Fax: +44 (0) 114 222 5700
Email: a.f.l.hyde@sheffield.ac.uk
Internet: http://www.shef.ac.uk

Adrian Hyde BSc, PhD, MICE, CEng
Senior Lecturer

27 January 2003

Professor Malcolm Bolton
Schofield Centre
Department of Engineering
University of Cambridge
High Cross
Madingley
Cambridge
CB3 0EL

Dear Malcolm

Prediction of Static Pile Behaviour from Statnamic Testing

Please find enclosed the prediction of the load displacement behaviour under constant rate of penetration (CRP) conditions for a test pile installed in glacial clay at Expanded Piling's plant yard near Grimsby. PMC Ltd carried out rapid load (Statnamic) pile tests on 14th and 15th January 2003. We have modified the load-displacement behaviour recorded during these tests based on damping characteristics derived from laboratory element and model tests carried out under the supervision of Mike Brown the Research Associate on this EPSRC funded project.
We ask that you keep this data until we supply you with the CRP test results which will be supplied by PMC in due course. We anticipate carrying out the CRP and MLT tests on our pile in the week commencing 3rd February.

Yours sincerely

Adrian

Adrian FL Hyde

THE QUEEN'S ANNIVERSARY PRIZES
1998 2000

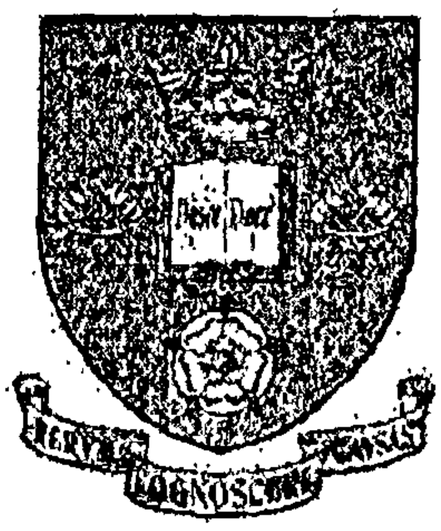

GEOTECHNICAL ENGINEERING
RESEARCH GROUP

University of Sheffield
Department of Civil &
Structural Engineering

The Prediction of Static Pile Behaviour from Statnamic Testing of an Auger Bored Pile in Glacial Clay- Static Pile Testing Results

Adrian Hyde, Bill Anderson, Michael Brown & Juan Balderas-Meca

Submitted to Prof. Malcolm Bolton
(Department of Engineering, University of Cambridge)

Final Submission: 28/01/03

The prediction of static pile behaviour from Statnamic testing of an auger bored pile in glacial clay.

Introduction

The object of this prediction exercise is to derive the equivalent static pile response from a rapid load pile (Statnamic) test. The Statnamic test applies a test load to a pile by means of an upward accelerating mass above the pile. The duration of the load (approximately 180ms) is sufficient to eliminate stress wave effects for all but the slenderest of piles but generates additional damping forces in clay soils. The models used to correct for this damping effect are empirical and based upon three years of experimental model pile testing and rapid load triaxial testing in the geotechnics laboratory at Sheffield (Balderas Meca, 2002, Brown *et al.*, 2002).

A fully instrumented 600mm diameter auger bored test pile has been installed to 12m by Expanded Piling in a uniform deposit of glacial clay at Waltham on the outskirts of Grimsby. Statnamic testing was carried out on 14th and 15th January 2003.

Prediction History

14-15/01/03	Statnamic testing completed
28/01/03	Prediction forwarded to Prof. Malcolm Bolton.
03/02/03	Anticipated start of static testing

Loading regime

The pile was subject to a series of Statnamic loads as shown:

1000kN
1500kN
2000kN
1500kN
2500kN
3000kN

The load displacement curves for these tests are shown in Figure.1 with the pile tests set at zero for the beginning of each new cycle. The Class A predictions of pile stiffness and ultimate capacity have been based on the Statnamic curve for 3000kN loading.

The static loading programme will utilise both Constant Rate of Penetration (CRP) and Maintained Load Testing (MLT). Initially CRP testing will be carried out with a pile penetration rate of 0.01mm/s. The pile will then be left for a minimum of 48 hours prior to MLT testing. The static loading will be carried out in accordance with the ICE Specification for Piling and Embedded Retaining Walls (ICE, 1997).

Nature of prediction

A model based on Constant Rate of Penetration (CRP) testing at varying rates using model piles in a clay calibration has been used to predict the CRP behaviour of the full scale pile. The calibration chamber contained an artificial clay bed of kaolin mixed with silt and sand (KSS). This model will be used for the Class A prediction.

Triaxial tests at various strain rates on the KSS material from the calibration chamber and the glacial clay from the full scale test site have been used to compare damping or rate effect coefficients for the two materials.

An analysis has also been carried out using the widely used Unloading Point Method (UPM) for comparison. This model assumes damping effects are negligible when the pile velocity is zero and from this derives a constant damping coefficient with which the load displacement data is corrected. Since this method ignores the non-linear nature of the variation of damping with velocity, we do not believe that this method gives a reliable prediction of static pile capacity. See Appendix 1 for further details of this method.

Prediction method

The Statnamic load is F_{STN} given by:

$$F_{STN} = F_s\left[1+\alpha(v)^{\beta}-\alpha\left(10^{-5}\right)^{\beta}\right]+Ma$$

where:

F_{STN} is the measured Statnamic force on the head of the pile.
F_s is the predicted load in a CRP pile test carried out at a displacement rate of 10^{-5} m/s
α and β are damping coefficients determined from the laboratory pile tests
M is the mass of the pile
a is the acceleration of the pile
v is the velocity of the pile in m/s

Thus:

$$F_s = \frac{F_{STN}-Ma}{1+\alpha(v)^{\beta}-\alpha\left(10^{-5}\right)^{\beta}}$$

The values of the damping coefficients derived from the model pile tests were:
$\alpha = 1.22$
$\beta = 0.32$

These values for α & β are derived directly from model pile tests in an artificial clay consisting of Kaolin, Sand & Silt (KSS). The validity of applying parameters derived from this material to the full-scale pile in the glacial clay has been justified by variable rate triaxial testing on both clays that gave similar coefficients for both materials (Balderas Meca, 2002). (Table 1)

Table 1 Damping coefficients from triaxial rate effect tests

	Artificial Clay (KSS)	Glacial clay
α	0.77	0.78
β	0.20	0.21

Pile static stiffness response predictions (Figure 2, Table 2)

Figure 2, shows the load displacement curves for the 3000kN Statnamic load cycle. The full Class A static prediction compared with the UPM static prediction and the original Statnamic data are presented. Table 2 shows the load and displacement co-ordinates for the end of each of the curves to aid comparison with the static results.

Table 2 Predictions of the static pile test load /displacements

Model	Derived Static Pile Load (kN)	Pile Head Displacement (mm)
Class A prediction	**1557**	**6.65**
For comparison only		
UPM	1940	6.65
F_{STN}	2924	6.65
F_{STN}-Ma	2915	6.65

Ultimate static predictions (Figure 3, Table 3)

It is difficult to predict the ultimate static capacity based upon the Statnamic data. This is because it is not clear that the full shaft and end bearing capacities of the bored pile were reached at the Statnamic device's maximum capacity of 3000kN. Examination of the full Statnamic load displacement curve corrected for inertia (Figure 3) suggests that the ultimate load may have been reached at the maximum value of F_{STN}-Ma. Based on this tentative conclusion the pile displacement was obtained at the maximum measured load on the curve of F_{STN}-ma versus displacement. The corresponding load was then corrected for damping and has been presented in Table 3 as the ultimate pile capacity.

Table 3 Predictions of the ultimate pile capacity

Model	Derived Static Pile Load (kN)	Pile Head Displacement (mm)
Predicted Ultimate pile load capacity	**1746**	**8.85**
For comparison only		
UPM	2343	8.85
F_{STN}	3037	8.85
F_{STN}-Ma	3210	8.85

Summary of the Prediction

1. The Class A prediction for static stiffness response of the pile predicted from Statnamic testing is shown in Figure 2. The displacement at a load of 1557kN will be 6.65mm.

2. The ultimate static pile capacity is given in Figure 3. The ultimate load will be 1746kN at 8.85mm.

References

Balderas Meca, J. 2002. Rate effects in rapid loading of clays. *BGA 7th Young Geotechnical Engineers' Symp.-Diversity in Geotechnics, Dundee, UK, 17-19th July, 2002.*

Brown, M.J., Hyde, A.F.L. & Anderson, W.F. 2002. The influence of loading rate on pile behaviour in clay. In R. Philips, P.J. Guo & R. Popescu (eds), *Physical Modelling in Geotechnics – ICPMG'02, ST John's, Newfoundland, Canada, 10-12 July, 2002*: 667-672. Rotterdam, A.A. Balkema.

Gibson, G.C. & Coyle, H.M. 1968. Soil damping constants related to common soil properties in sands and clays (Bearing Capacity for Axially Loaded Piles). *Texas Transportation Institute Research Report* 125-1 (Study 2-5-67-125). Texas: Texas A&M University.

The Institution of Civil Engineers. 1997. Specification for piling and embedded retaining walls. 1st ed. London, UK, Thomas Telford Publishing.

Kusakabe, O. & Matsumoto, T. 1995. Statnamic tests of Shonan test program with review of signal interpretation. *Statnamic Seminar; Proc. intern., Vancouver, 1995*: 113-122.

Middendorp, P. 1993. First experiences with Statnamic load testing of foundation piles in Europe. In F.C. Townsend (eds), *Deep Foundations on Bored and Auger Piles, 1993*: 265-272. Rotterdam, A.A. Balkema.

Appendix 1

UPM prediction

The present standard method of analysis referred to as the "Unloading Point Method" UPM, (Middendorp, 1993, Kusakabe & Matsumoto, 1995).

UPM suggested ultimate

The ultimate load suggested by the UPM method that assumes full mobilisation is given below with the model values at the corresponding pile displacement. The load values quoted refer to the point of maximum load found by UPM. The predicted load outputs have been quoted at the displacement corresponding to maximum UPM load.

Model	Derived Static Pile Load (kN)	Pile Head Displacement (mm)
Predicted Ultimate pile load capacity	1825	10.83
For comparison only		
UPM	2602	10.83
STN	2616	10.83
STN-ma	2927	10.83

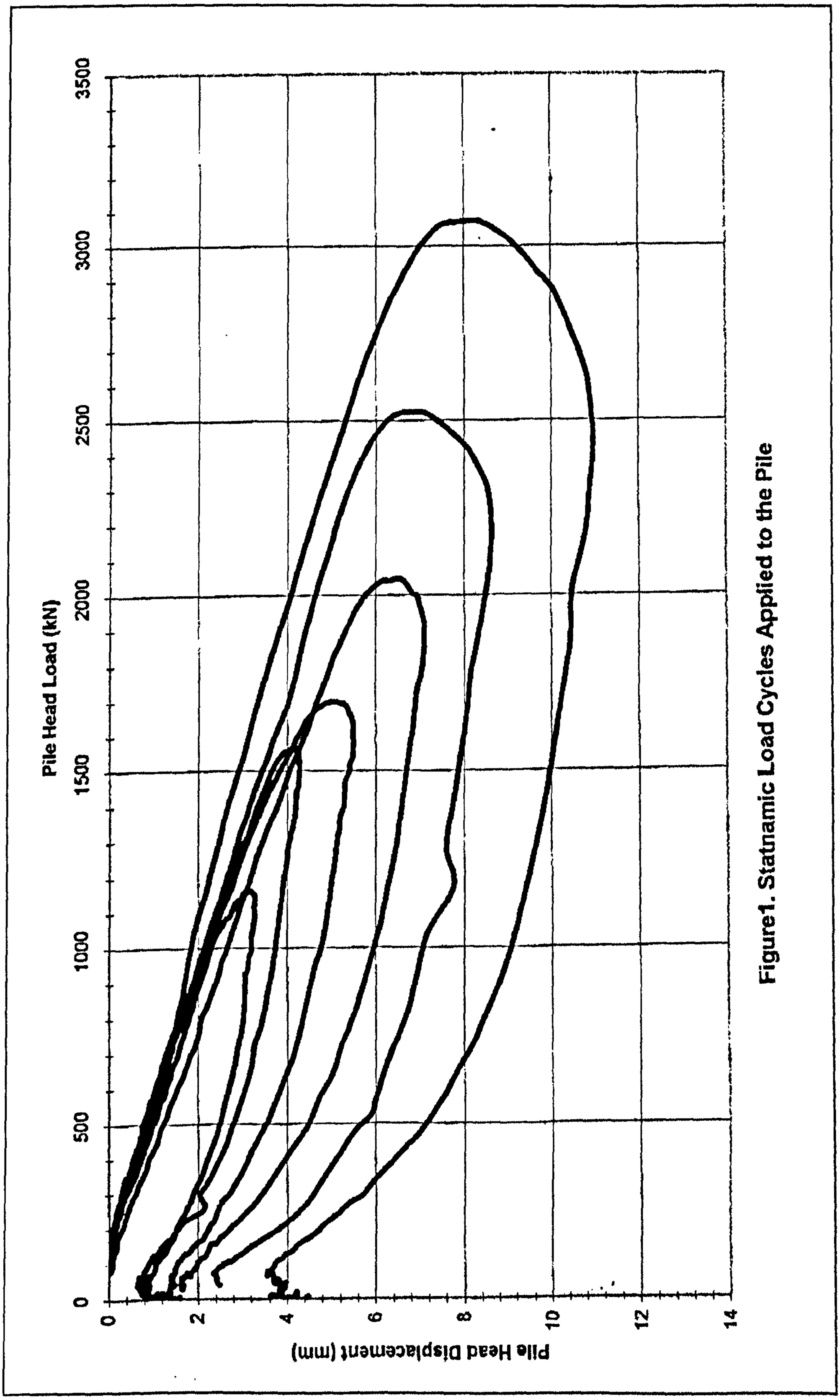

Figure1. Statnamic Load Cycles Applied to the Pile

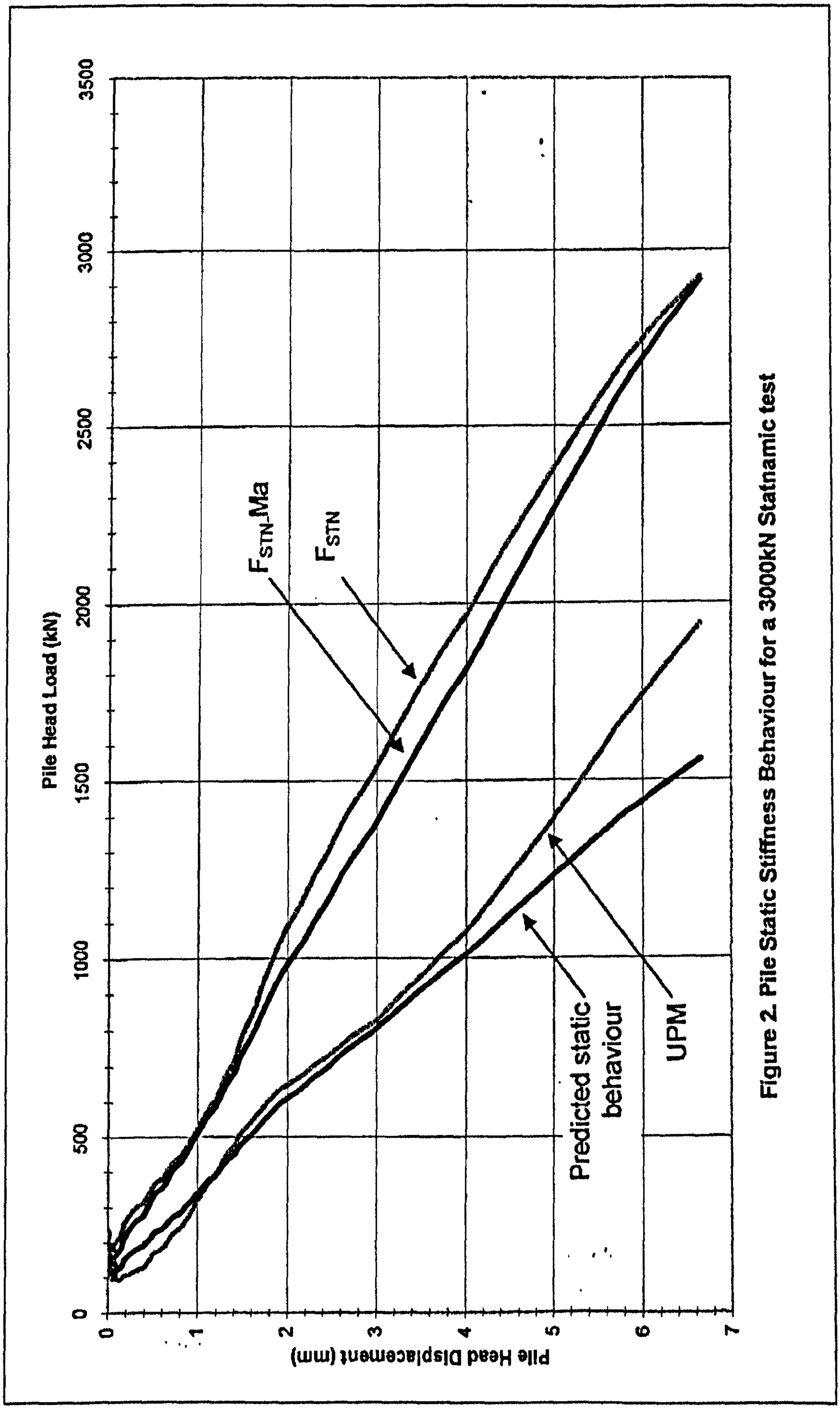

Figure 2. Pile Static Stiffness Behaviour for a 3000kN Statnamic test

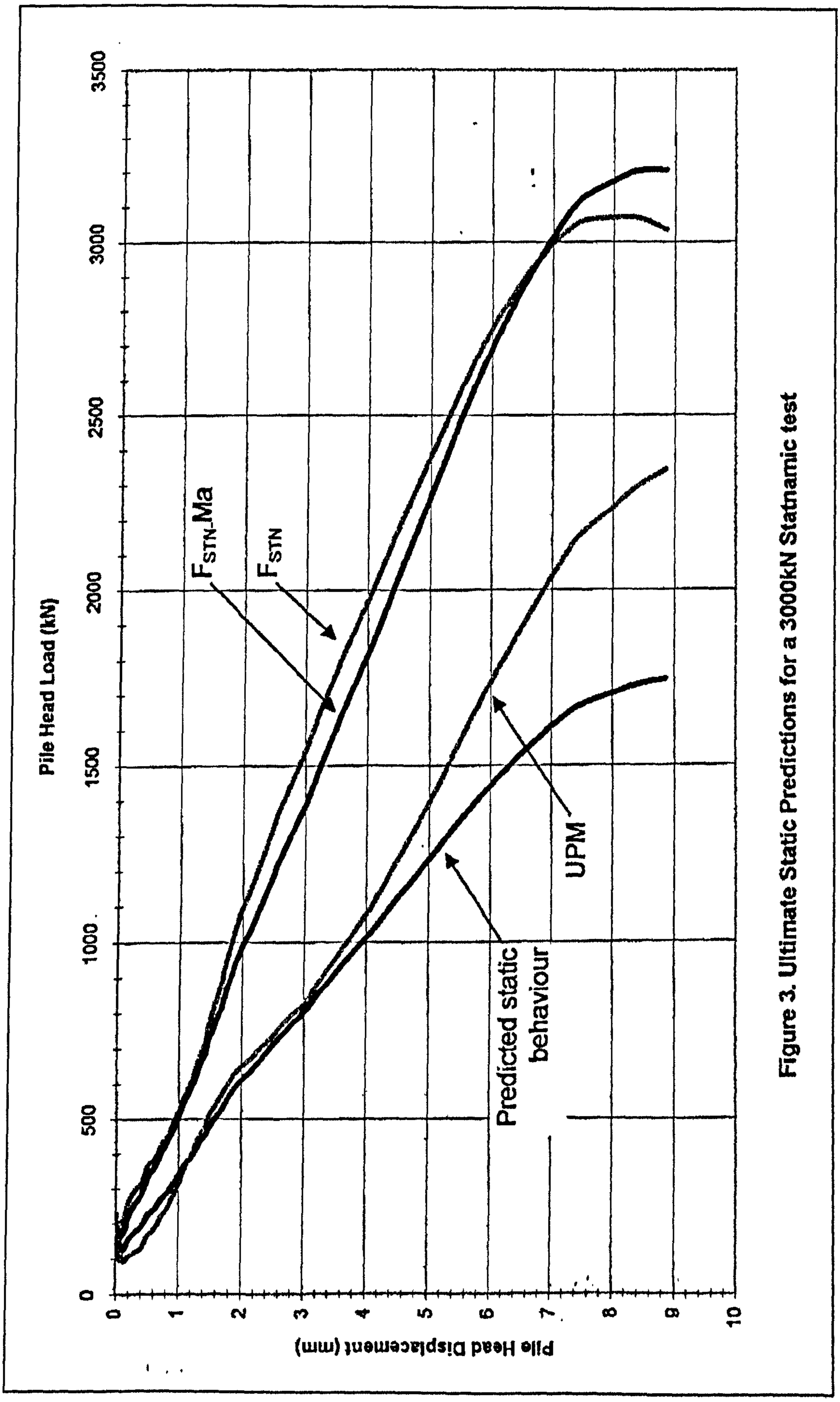

Figure 3. Ultimate Static Predictions for a 3000kN Statnamic test

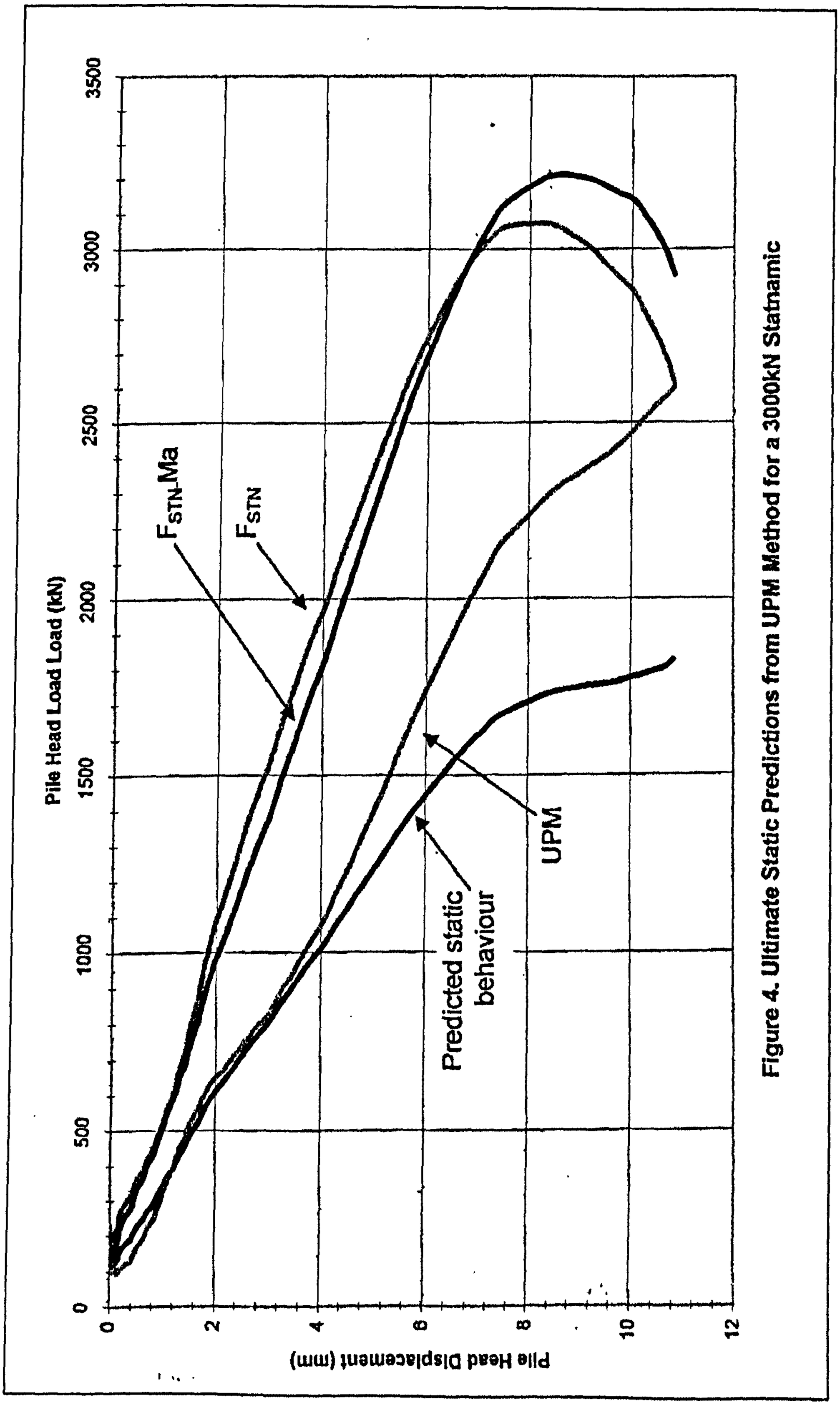

Figure 4. Ultimate Static Predictions from UPM Method for a 3000kN Statnamic

References

AMERICAN STANDARD TESTING METHODS. Standard test method for piles under static axial compressive load. ASTM D1143-81:1994.

ANDERSON, W.F. (1974) The use of multistage triaxial tests to find the undrained strength parameters of stony boulder clay. Proc. Inst. Civil Engineers, Vol. 57, Issue N Part 2, June 1974. pp. 367-372.

ANDERSON, W.F., YONG, K.Y. & SULAIMAN, J.I. (1985) Shaft adhesion on bored and cast-in-situpiles. Proc. Int. Conf. on Soil Mechanics and Foundation Engineering, 11th, San Francisco, 12-16 August 1985. Rotterdam, A.A. Balkema. pp. 1333-1336.

ANDERSON, W.F., PYRAH, I.C. & FRYER, S.J. (1989) Creep and consolidation effects in pressuremeter tests in fine grained soils-Clay calibration chamber specification and clay bed preparation. University of Sheffield, Dept. of Civil & Structural Engineering, Sheffield, UK. November 1989. Report 50996/4, SERC Research Grant GR/D 48162.

ANDERSON, W.F., PYRAH, I.C. & FRYER, S.J. (1991) A clay calibration chamber for testing field devices. ASTM Geotechnical Testing Journal, Vol. 14, No. 4, December 1991. pp. 440-450.

ANDERSON, W.F., BROWN, M.J., HYDE, A.F.L. & BALDERAS MECA, J. (2003) A laboratory study of Statnamic testing of piles in clays. Proc. Int. Conf. on Advances in Soft Soil Engineering and Technology, 2nd, Putrajaya, Malaysia, 2-4 July 2003. pp. 117-127.

ANONYMOUS (1996) Piling. Ground Engineering Journal, Vol. 29, No. 8, October 1996. pp. 18-21.

ANONYMOUS (1997) Test of two worlds (Piling). Ground Engineering Journal, Vol. 30, No.10, November 1997. pp. 28-31.

ANONYMOUS (1999) Uncertainty principle (Pile predictions). Ground Engineering Journal, Vol. 32, No.11, November 1999. pp. 32-34.

ANONYMOUS (2000) Hammering it home (Dynamic pile testing). Ground Engineering Journal, Vol. 33, No.9, September 2000. pp. 25-26.

ATKINSON, J.H. (1993) An introduction to the mechanics of soils and foundations through critical state soil mechaninc s. 1st ed. UK, McGraw-Hill Int., 1993.

BADONI, D. & MAKRIS, N. (1997) Pile-to-pile interaction in the time domain- non-linear axial group response under harmonic loading. Geotechnique, Vol. 47, No. 2, 1997. pp. 299-317.

BALDERAS-MECA, J. (2004) Rate effects in rapid loading of clay soils. PhD Thesis, University of Sheffield, UK, 2004 (In preparation).

BARDEN, L. (1965) Consolidation of clay with non-linear viscosity. Geotechnique, Vol. 15, No. 4, 1965. pp. 345-362.

BEA, R.G. (1982) Soil strain rate effects on axial pile capacity. Proc. Int. Conf. On Numerical Methods in Offshore Engineering, 2nd, 1985. pp. 107-131.

BEAZANT, G. (2004) Testing the water. Ground Engineering Journal, Vol. 37, No.1, January 2004. pp. 20-21.

BELL, A (2001) Investigation into the increase in capacity with time of precast piles driven into stiff overconsolidated clay. MSc Thesis, University of Sheffield, UK 2001.

BELL, F.G. (1987) Ground engineer's reference book. 1st ed., London, Butterworth & Co. pp. 58/3-58/13.

BERMINGHAM, P.A., EALY, C.D. & WHITE, J.K. (1994) A comparison of Statnamic and static field tests at seven FHWA sites. Proc. HTE. Int. Conf. on Design & Construction of Deep Foundations, 1994. pp. 616-630.

BERMINGHAM, P.A. & WHITE, J. (1995) Pyrotechnics and the accurate prediction of Statnamic peak loading and fuel charge size. Proc. of Int. Statnamic Seminar, 1st Vancouver, Canada, 27-30 September 1995. pp. 1-12.

BERMINGHAM, P.A. (1999) Motivation for developing Statnamic testing. Private Communication, January 1999.

BERRIDGE, N.G. & PATTISON, J. (1994) Geology of the country around Grimsby and Partington, British Geological Survey. 1983, Memoir.

BOND, A.J. & JARDINE, R.J. (1991) Effects of installing displacement piles in a high OCR clay. Geotechnique, Vol. 41, No. 3, 1991. pp. 341-363.

BOND, A.J., JARDINE, R.J. & DALTON, J.C.P. (1991) Design and performance of the Imperial College instrumented pile. ASTM Geotechnical Testing Journal, Vol. 14, No. 4, December 1991. pp. 413-424.

BORGHI, X., WHITE, D.J., BOLTON, M.D. & SPRINGMAN, S. (2001) Empirical pile design based on cone penetrometer data: An explanation for the reduction of unit base resistance between CPTs and piles. Proc. Int. Conf. on Deep Foundations Practice, 5th, Singapore, 4-6 April 2001. pp. 125-132.

BRIAUD, J.L., GARLAND, E. & FELIO, G.Y. (1984) Rate of loading parameters for vertically loaded piles in clay. Proc. of the Annual Offshore Technology Conference, 16th, Houston, Texas, 7-9 May 1984. pp. 407-412.

BRITISH STANDARDS INSTITUTION. Methods of test for soils for civil engineering purposes. BS1377:1990.

BRITISH STANDARDS INSTITUTION. Part 121: Testing concrete-Method for determination of static modulus of elasticity in compression. BS1881:1983.

BRITISH STANDARDS INSTITUTION. Code of practice for foundations. BS8004:1986.

BROUWER, J.J.M. (2002) Guide to cone penetration testing on shore and near shore. 1st ed., Lankelma Limited, UK.

BROWN, D.A. (1994) Evaluation of static capacity of deep foundations from Statnamic testing. ASTM Geotechnical Testing Journal, Vol.17, No. 4, December 1994. pp. 403-414.

BROWN, M.J., HYDE, A.F.L. & ANDERSON, W.F. (2002) The influence of loading rate on pile behaviour in clay. In R. Philips, P.J. Guo & R. Popescu (eds), Int. Conf. On Physical Modelling in Geotechnics ICPMG'02, Newfoundland, Canada, 10-12 July, 2002. Rotterdam, A.A. Balkema. pp. 667-672.

BROWN, M.J. (2003) Research Developments-Progress Report. Ground Engineering Journal. Vol. 36, No.4, April 2003. pp. 31-32.

BURLAND, J.B. & TWINE, D. (1988) The shaft friction of bored piles in terms of effective strength. In W.F. van Impe (eds), Proc. Int. Geotechnical Seminar on Deep Foundations on Bored and Auger Piles, 1st, Ghent, 7-10 June 1988. Rotterdam, A.A. Balkema. pp. 411-420.

CASAGRANDE, A & SHANNON, W.L. (1948) Stress deformation and strength characteristics of soils under dynamic loads. Int. Conf. on Soil Mechanics and Foundation Engineering, 2nd, Vol. 5, 1948. pp. 29-34.

CASAGRANDE, A & WILSON, S.D. (1951) Effect of rate of loading on the strength of clays and shales at constant water content. Geotechnique, Vol. 2, No. 3, June 1951. pp. 251-263.

CHANDLER, R.J. & MARTINS, J.P. (1982) An experimental study of skin friction around piles in clay. Geotechnique, Vol. 32, No. 2, 1982, pp. 119-132.

CHOW, F. (1997) Fiona Chow asks is pile design progressing? Ground Engineering Journal, Vol. 30, No.10, November 1997. pp. 3.

CLAYTON, C.R.I. & BICA, A.V.D. (1993) The design of boundary-type total stress cells. Geotechnique, Vol. 43, No. 4, 1993. pp. 523-535.

COOKE, R.W. & WHITAKER, T. (1961) Experiments on model piles with enlarged bases. Geotechnique, Vol. 11, No. 1, March 1961. pp. 1-13.

COOKE, R.W. (1978) Influence of residual installation forces on the stress transfer and settlement under working loads of jacked and bored piles in cohesive soils. In Raymond Lundgren (ed), Symp. on the Behaviour of Deep Foundations, Boston, USA, 25-30 June 1978, ASTM, ASTM STP 670. pp. 231-249.

COOP, M.R. & WROTH, C.P. (1989) Field studies of an instrumented model pile in clay. Geotechnique, Vol. 39, No. 4, 1989. pp. 679-696.

CRAIG, .R.F (1992) Soil Mechanics. 5th ed. London, UK, Chapman & Hall, 1992.

DANZIGER, B.R., COSTA, A.M., LOPES, F.R. & PACHECO, M.P. (1999) Back ananlysis of offshore pile driving with an improved soil model. Geotechnique, Vol. 49, No. 6, 1999. pp. 777-799.

DAS, .B.M. (1993) Principles of soil dynamics. 1st ed. Boston, USA, PWS-KENT Publishing Co., 1993.

DAYAL, U. & ALLEN, J.H. (1975) The effect of penetration rate on the strength of remoulded clay and sand samples. Canadian Geotechnical Journal, No. 12, 1975. pp. 336-348.

DELPAK, R, ROBINSON, R.B. & OMER, J.R. (1998) Assessment of the performance of large diameter, bored, cast in-situ piles formed in Mercia Mudstone. CIRIA Conf. The Engineering Properties of the Mercia Mudstone Group, Derby, UK, 25 November 1998, London, CIRIA, 2000/1. pp. 36-63.

DEPARTMENT OF ENERGY (1990) Research on the behaviour of displacement piles in an overconsolidated clay. Dept. of Energy (DOE)-Offshore Technology. Prepared by Imperial College, London. HMSO Publications Centre, London. Report OTH 89 296.

DUNNICLIFF, J & GREEN, G.E. (1988) Geotechnical instrumentation for measuring field performance. 1st ed., USA, John Wiley & sons, 1988.

EIKSUND, G. & NORDAL, S. (1996) Dynamic model pile testing with pore pressure measurements. In F.C. Townsend, M. Hussein & M.C. McVay (eds), Int. Conf. on the Application of Stress-Wave Theory to Piles, 5th, Orlando, Florida, 11-13 September 1996. pp. 1-11.

EIKSUND, G (2003) Dynamic model pile testing rig specification and performance. Private Communication. July 2003.

EL NAGGAR, M.H. & NOVAK, M. (1994) Non-linear model for axial dynamic pile response. ASCE Journal of Geotechnical Engineering, Vol. 120, No. 2, February, 1994. pp. 308-329.

ENGLAND, M & FLEMING, W.G.F (1994) Review of foundation testing methods and procedures. Proc. Inst. Civil Engineers: Geotechnical Engineering Journal. Vol. 107, No.3, July 1994. pp. 135-142.

ENGLAND, M. (2000) Personal correspondence. 19th July 2000.

ENGLAND, M (2003) O for another loading test. Ground Engineering Journal: European Foundations, No. 19, Summer 2003. pp 24-26.

EPOSITO, G., COURAGE, W.M.G. & FOUKEN, R.J. van. (2000) Application of the stress wave method to automatic signal matching and to Statnamic predictions. In S. Niyama & J. Beim (eds), Int. Conf. on the Application of Stress Wave Theory to Piles, 6th, Sao Paulo, Brazil, 11-13 September 2000, Rotterdam, A.A. Balkema. pp. 575-581.

EUROCODE 7 (1997) Geotechnical design. Part 1: General Rules (together with United Kingdom application document) BRITISH STANDARDS INSTITUTION. DD ENV 1997-1:1994.

FERAHIAN, R.H. (1977) Static bearing capacity of piles from dynamic measurements. Proc. Inst. Civil Engineers, Part 1, No.62, 1977. pp. 655-662.

FLEMING, W.G.F, WELTMAN, A.J., RANDOLPH, M.F. & ELSON, W.K. (1992) Piling Engineering. 2nd ed., Glasgow, UK, Blackie & Son Ltd, 1992.

FLEMING, W.G.F & ENGLAND, M. (2001) Locking pile behaviour (Meeting report). Ground Engineering Journal. Vol. 34, No.1, January 2001. pp. 30-33.

FLEMING, W.G.F. (1996) Ken Fleming assess the present major issues in the pile testing industry. Ground Engineering Journal. Vol. 29, No.8, October 1996. pp. 2.

FYLDE ELECTRONIC LABORATORIES, LTD. (1999) Micro Analogue 2. Preston, UK, Fylde Electronic Laboratories Ltd., 1999. User Manual.

GARBIN, E.J. (1999) Data interpretation for axial Statnamic testing and the development of the Statnamic Analysis Workbook. MSc Thesis, University of South Florida, USA, 1999.

GIBSON, G.C. & COYLE, H.M. (1968) Soil damping constants related to common soil properties in sands and clays (Bearing Capacity for Axially Loaded Piles). Texas A&M University, Texas, USA, Texas Transportation Institute. September 1968. Research Report 125-1, Study 2-5-67-125.

GUDEHUS, G (1981) Bodenmechanik. Institute of Soil Mechanics and Foundation Mechancis, University of Karlsruhe, Germany. (No longer in print, in German).

HANNA, T.H. (1973) Foundation instrumentation. 1st ed., Switzerland, Trans Tech S.A., 1973.

HEEREMA (1979) Relationship between wall friction, displacement velocity and horizontal stress in clay and in sand, for pile driveability analysis. Ground Engineering Journal, January 1979. pp. 55-65.

HIRD, C.C & MOSELEY, V.J. (2000) Model study of seepage in smear zones around vertical drains in layered soil. Geotechnique, Vol. 50, No. 1, 2000. pp. 89-97.

HOLEYMAN, A.E. (1988) Modelling of dynamic behaviour at the pile base. Int. Conf. on the Application of Stress Wave Theory to Piles, 3rd, Ottawa, Canada. pp. 174-185.

HOLEYMAN, A.E. (1992) Keynote Lecture: Technology of pile dynamic testing. In F.B.J. Barends (ed), Int. Conf. on the Application of Stress Wave Theory to Piles, 4th, The Hague, The Netherlands, 21-24 September 1992. Rotterdam, A.A. Balkema, 1992. pp. 195-215.

HOLEYMAN, A.E., COUVREUR, J.M. & CHARUE, N. (2001) Results of dynamic and kinetic pile load tests and outcome of an international prediction event. In A.E. Holeyman (ed), Screw Piles-Installation and Design in Stiff Clay, edited by, Belgium, Swets & Zeitlinger. pp. 247-273.

HORVATH, R.G. (1995) Influence of loading rate on the capacity of a model pile in clay. Canadian Geotechnical Journal, Vol. 32, 1995. pp. 364-368.

HORVATH, R.G. & STOLLE, D. (1996) Frustrum confining vessel for testing model piles. Canadian Geotechnical Journal, Vol. 33, 1996. pp. 499-504.

HOULSBY, G.T. (1984) Boundary conditions in the test chamber. Seminar on cone penetration testing in the laboratory, University of Southampton, UK, November, 1984, Vol. 2. pp. 22-24.

HUANG, A, HOLTZ, R.D. & CHAMEAU, J.L. (1988) A calibration chamber for cohesive soils. ASTM Geotechnical Testing Journal, Vol. 11, No. 1, March 1988. pp. 30-35.

HUMPHESON, C. & SEAMAN, J.W. (1992) Dynamic testing of large diameter bored underreamed piles in London Clay. Piling: European Practice and Worldwide Trends, Thomas Telford, London, 1992. pp. 198-205.

HYDE, A.F.L., ROBINSON, S.A. & ANDERSON W.F. (2000) Rate effects in clay soils and their relevance to Statnamic pile testing. In O. Kusakabe, F. Kuwabara & T. Matsumoto (eds), Int. Statnamic Seminar, 2nd, Tokyo, Japan, 28-30 October 1998. Rotterdam, A.A. Balkema. pp. 303-309.

JAMES, R.C. (1967) The effect of electro osmosis on the bearing capacity of bored piles in clay soils. PhD Thesis, University of Sheffield, UK, 1967.

KATTI, D.R., TANG, J. & YAZDANI, S. (2003) Undrained response of clays to varying strain rates. ASCE Journal of Geotechnical and Geoenvironmental Engineering, Vol. 129, No. 3, March 2003. pp. 278-282.

KING, G.J.W., DICKIN, E.A., LYNDON, A. & WEI, M.J. (2000) The influence of rate of loading on the behaviour of continuous-flight-auger bored piles in soft clay. Geotechnical and Geological Engineering Journal, Vol. 18, 2000. pp. 139-153.

KISTLER INSTRUMENTS CORP. (1997) Power supply/coupler type 5134A/5134M2. Hampshire, UK, Kistler Instruments Corp., 1997. Operating Instructions B125134Ae-4.97.

KUSAKABE, O & MATSUMOTO, T (1995) Statnamic tests of Shonan test program with review of signal interpretation, Proc. of 1st Int Statnamic Seminar, Vancouver, Canada, 27-30 September 1995. pp. 113-122.

LAMBE, T.W. (1973) Predictions in soil engineering. Geotechnique, Vol. 23, No. 2, 1973. pp. 149-202.

LEE, F.K. (1990) Frequency response of diaphragm pore pressure transducers in dynamic centrifuge model tests. ASTM Geotechnical Testing Journal, Vol. 13, No. 3, September 1990. pp. 201-207.

LEFEBVRE, G. & LEBOEUF, D. (1987) Rate effects and cyclic loading of sensitive clays. ASCE, Journal of Geotechnical Engineering, Vol. 113, No. 5, May 1987, pp. 476-489.

LEINENKUGEL, H.J. (1976) Deformations- und festigkkeitsverhalten bindiger erdstoffe. Institue for Soil Mechanics and Foundation Mechanics, University of Karlsruhe, Germany, Vol. 66. (in German).

LEMOS, L.J.L. & VAUGHAN, P.R. (2000) Clay-interface shear resistance. Geotechnique, Vol. 50, No. 1, 2000. pp. 55-64.

LEWIS, C.L. (1999) Analysis of axial Statnamic testing by the segmental unloading point method. MSc Thesis, University of South Florida, USA, 1999.

LITKOUHI, S. & POSKITT, T.J. (1980) Damping constants for pile driveability calculations. Geotechnique, Vol. 30, No. 1, 1980. pp. 77-86.

LOADTEST (2003) www.loadtest.com. Company website.

LUNNE, T., ROBERTSON, P.K. & POWELL, J.J.M (1997) Cone penetration testing in geotechnical practice. 1st ed. London, UK, Blackie Academic and Professional, 1997.

LUPINI, J.F., SKINNER, A.E. & VAUGHAN, P.R. (1981) The drained residual strength of cohesive soils. Geotechnique, Vol. 31, No. 2, 1981. pp. 181-213.

LYNDON, A., WEI, M.J., PRICE, G. & STANSFIELD, L. (1993) Strain measurement in CFA bored piles in soft clay. In W.F. van Impe (ed), Proc Int. Geotechnical Seminar on Deep Foundations on Bored and Auger Piles, 2nd, Ghent, Belgium, 01-04 January, 1993. Rotterdam, A.A. Balkema. pp. 413-416.

MAKRIS, N. & GAZETAS, G. (1993) Displacement phase difference in a harmonically oscillating pile. Geotechnique, Vol. 43, No. 1, 1993. pp. 135-150.

MARAYAMA, S. & SHIBATA, T. (1964) Flow and stress relaxation of clays. Int. Union of Theoretical and Applied Mechanics Symp. on Rheology and Soil Mechanics, Grenoble.

MATSUMOTO, T., FUJITA, K., KUSAKABE, O., OKAHARA, M. KAWABATA, N. & NISHIMURA, S. (2000) Dynamic load testing and Statnamic load testing for acceptance and design of driven piles. In. S. Niyama & J. Beim (eds), Int. Conf. on the Application of Stress Wave Theory to Piles, 6th, Sao Paulo, Brazil, 11-13 September 2000, Rotterdam, A.A. Balkema. pp. 335-343.

McKINLAY, D.G., TOMLINSON, M.J. & ANDERSON, W.F. (1974) Observations on the undrained strength of glacial till. Geotechnique, Vol. 24, No. 4, 1974. pp. 503-516.

McMANUS, K.J. & KULHAWY, F.H. (1991) A cohesive soil for large-size laboratory deposits. ASTM Geotechnical Testing Journal, Vol. 14, No. 1, March 1991. pp. 26-34.

McVAY, M.C., KUO, C.L. & GUISINGER, A.L. (2003) Calibrating resistance factor in the load and resistance factor design of Statnamic load testing. University of Florida, Florida, USA, Florida Department of Transportation. March 2003. Research Report 4910-4504-823-12, Contract BC354, RPWO#42.

MENDOZA, M.J., LUNA, O.J., IBARRA, E. & ROMO, M.P. (2001) Small-scale models of friction piles in soft marine clay. Proc. Int. Conf. on Soil Mechanics and Foundation Engineering, 15th, Istanbul 27-31 August 2001, Vol. 2. A.A. Balkema, Rotterdam, 2001. pp. 1307-1310.

MICHAELIDES, O., GAZETAS, G., BOUCKOVALAS, G. & CHRYSIKOU, E. (1997) Approximate non-linear dynamic axial response of piles. Geotechnique, Vol. 48, No. 1, 1997. pp. 33-53.

MIDDENDORP, P., BERMINGHAM, P. & KUIPER, B. (1992) Statnamic load testing of foundation piles. In F.B.J. Barends (ed), Int. Conf. on the Application of Stress Wave Theory to Piles, 4th, The Hague, The Netherlands, 21-24 September 1992. Rotterdam, A.A. Balkema, 1992. pp. 581-588.

MIDDENDORP, P. (1993) First experiences with Statnamic load testing of foundation piles in Europe. In W.F. van Impe (ed), Proc Int. Geotechnical Seminar on Deep Foundations on Bored and Auger Piles, 2nd, Ghent, Belgium, 01-04 January, 1993. Rotterdam, A.A. Balkema. pp. 265-272.

MIDDENDORP, P. & BIELEFELD, M.W (1995) Statnamic load testing and the influence of stress wave phenomena. Proc. of Int Statnamic Seminar, 1st, Vancouver, Canada, 27-30 September 1995. pp. 207-220.

MIDDENDORP, P. (2000[a]) Keynote lecture: Statnamic the engineering of art. In S. Niyama & J. Beim (eds), Int. Conf. on the Application of Stress Wave Theory to Piles, 6th, Sao Paulo, Brazil, 11-13 September 2000, Rotterdam, A.A. Balkema. pp. 551-562.

MIDDENDORP, P. (2000[b]) Statnamic tests gain ground (Pile testing). Ground Engineering Journal. Vol. 33, No.9, European Foundations Supplement (Winter 2000), September 2000. pp. 16-17.

MIDDENDORP, P., GINNEKEN, G.J.J. van & FOEKEN R.J. van. (2000) The advantages and disadvantages of dynamic load testing and Statnamic load testing. In S. Niyama & J. Beim (eds), Int. Conf. on the Application of Stress Wave Theory to Piles, 6th, Sao Paulo, Brazil, 11-13 September 2000. Rotterdam, A.A. Balkema. pp. 625-632.

MOLLER, B. & BERGDAHL, U. (1981) Dynamic pore pressure during pile driving in fine sand. Proc. Int. Conf. on Soil Mechanics and Foundation Engineering, 10th, Stockholm, Sweden, 15-19 June 1981. Rotterdam A.A. Balkema. pp. 791-794.

MORRISON, P.R.J. & TAYLOR, R.N. (1994) Modelling of foundations in a rising groundwater environment. Proc. Int. Conf. on Soil Mechanics and Foundation Engineering, 13th, New Delhi, India, 5-10 January 1994. Rotterdam, A.A. Balkema. pp. 655-658.

MULLINS (2002) Innovative load testing systems subgroup, Statnamic testing critical evaluation of Statnamic test data. University of South Florida, National Cooperative Highway Research Program.

MULLINS, G., LEWIS, C.L. & JUSTASON, M.D (2002). Advancements in Statnamic data regression techniques. In M.W. O'Neill (ed), Proc. ASTM Conf. Int. Deep Foundations Congress, 2002, Florida, ASTM Geotechnical Special Publication No.116, Vol. 2. pp 915-930.

NATIONAL INSTRUMENTS CORP. (1999) Multifunction I/O boards for PCI bus computers. UK, National Instruments Corp., 1999. PCI E Series User Manual.

NICOLA, A.D. & RANDOLPH, M.F. (1999) Centrifuge modelling of pipe piles in sand under axial loads. Geotechnique, Vol. 49, No. 3, 1999. pp. 295-318.

NISHIMURA, S. & MATSUMOTO, T. (1995) Wave propagation analysis during Statnamic loading of a steel pipe. Proc. of 1st Int Statnamic Seminar, Vancouver, Canada, 27-30 September 1995. pp. 23-33.

OLSON, R.E. & PAROLA, J.F. (1967) Dynamic shearing properties of compacted clay. Proc. of Int. Symp. on Wave Propagation and Dynamic Properties of Earth Materials, University of New Mexico, 23-25 August 1967. University of New Mexico Press, Albuquerque, New Mexico, 1967, pp. 173-182.

OMER, J.R. (2002) Pile testing: Toe load cell design. Private Communication, 29 April 2002.

OS, A.G. van & LEUSSEN, W. van (1987) Basic research on cutting forces in sand. ASCE Journal of Geotechnical Engineering, Vol. 113, No. 12, December 1987. pp. 1501-1516.

OSTERBERG, J.O. (1999) What has been learned about drilled shafts from the Osterburg load test. Deep Foundations Institute Annual Meeting (DFI), October 1999. pp. 2.

PAIKOWSKY, S.G. & CHERNAUSKAS, L.R. (1996) Soil inertia and the use of pseudo viscous damping parameters. In F.C. Townsend, M. Hussein & M.C. McVay (eds), Int. Conf. on the Application of Stress Wave Theory to Piles, 5th, Orlando, Florida, 11-13 September 1996. Rotterdam, A.A. Balkema, 1992. pp. 203-216.

PALMER, A.C. (1999) Speed effects in cutting and ploughing. Geotechnique, Vol. 49, No. 3, 1999. pp. 285-294.

PETERSON, R.W. & ARULMOLI, K. (1991) The shaft friction of bored piles in terms of effective strength. In A.B. Huang (ed), Proc. Int. Symposium on Calibration Chamber Testing, 1st, Potsdam, New York, 28-29 June 1991. New York, Elsevier, 1991. pp. 329-337.

PENUMADU, D. & CHAMEAU, J.L. (1998) Interpretation of model pressuremeter test using automated clay calibration chamber data. ASTM Geotechnical Testing Journal, Vol. 21, No. 1, March 1998. pp. 18-30.

PMC (2003) Company website. www.piletest.co.uk.

POSKITT, T.J. & LEONARD, C. Effect of velocity on penetrometer resistance. Proc. of the European Symposium on Penetration Testing, 2nd, Amsterdam, Holland, 24-27 May 1982. pp. 331-336.

POULOS, H.G. & DAVIS (1980) Pile foundation analysis and design. New York, John Wiley & Sons.

POULOS, H.G. (2000) Pile testing-from the designer's viewpoint. In O. Kusakabe, F. Kuwabara & T. Matsumoto (eds), Int. Statnamic Seminar, 2nd, Tokyo, Japan, 28-30 October 1998. Rotterdam, A.A. Balkema. pp. 3-21.

PROCTER D.C. & KHAFFI, J.H. (1987) Cyclic axial displacement tests on model piles in clay. Geotechnique, Vol. 37, No. 4, 1987. pp. 505-509.

RANDOLPH, M.F. (1983) Design considerations for offshore piles. In S.G. Wright (ed), ASCE Int. Conf. Geotechnical Practice in Offshore Engineering, Austin, Texas, 27-29 April 1983. pp. 422-439.

RANDOLPH, M.F. & SIMONS, H.A. (1986) An improved soil model for one-dimensional pile driving analysis. Int. Conf. On Numerical Methods in Offshore Piling, 3rd, Nantes, France, 21-22 May 1986. Paris, Editions Technip. pp. 3-17.

RANDOLPH, M.F. & DEEKS, A.J. (1992) Dynamic and static soil models for axial response. In F.B.J. Barends (ed), Int. Conf. on the Application of Stress Wave Theory to Piles, 4th, The Hague, The Netherlands, 21-24 September 1992. Rotterdam, A.A. Balkema. pp. 3-14.

RANDOLPH, M.F. (2003) Science and empiricism in pile foundation design. Geotechnique, Vol. 53, No. 10, 2003. pp. 847-875.

RAUSCHE, F., GOBLE, G.G. & LIKINS, G.E. (1985) Dynamic determination of pile capacity. ASCE Journal of Geotechnical Engineering, Vol. 111, No. 3, March 1985. pp. 367-383.

REIDING, F.J. (1992) Computer-integrated pile test equipment. In F.B.J. Barends (ed), Int. Conf. on the Application of Stress Wave Theory to Piles, 4th, The Hague, The Netherlands, 21-24 September 1992. Rotterdam, A.A. Balkema. pp. 311-317.

RICHARDSON, A.M. & WHITMAN, R.V. (1963) Effect of strain rate upon undrained shear resistance of a saturated remoulded fat clay. Geotechnique, Vol. 13, No. 4, 1963. pp. 310-324.

RICKETTS, G.A. (2002) Seismic testing at Waltham Grimsby. Soil Mechanics, UK, University of Sheffield. November 2002. Report L2145.

ROSSATO, G., NINIS, L. & JARDINE, R.J. (1992) Properties of some kaolin based model clay soils. ASTM Geotechnical Testing Journal, Vol. 15, No. 2, June 1992. pp. 166-179.

ROSSATO, G., NINIS, L. & JARDINE, R.J. (1994) On stress-strain and strength properties of model soils. Int. Conf. on Soil Mechanics and Foundation Engineering, 14th, New Delhi, India, 1994. pp. 389-392.

ROWE, P.W. & BARDEN, L. (1966) A new consolidation cell. Geotechnique, Vol. 16, No. 2, June 1966. pp. 162-170.

SANGTIAN, N (2001) Miniature piezocone tests and effects of smear due to vertical penetration in layered soils. PhD Thesis, University of Sheffield, UK, Semptember, 2002.

SCHMERTMANN, J.H., HAYES, J.A., MOLNIT, T. & OSTERBERG, J.O. (1998) O-Cell testing case histories demonstrate the importance of bored pile (drilled shaft) construction technique. Proc. Int. Conf. On Case Histories in Geotechnical Engineering, 4th, St Louis, Missouri, USA, 9-12 March, 1998. pp. 1103-1115.

SEIDEL, J.P. (1996) The use of the signal matching approach to the analysis of Statnamic tests. In Townsend, M. Hussein & M.C. McVay (eds),.Int. Conf. on the Application of Stress Wave Theory to Piles, 5th, Orlando, Florida, 11-13 September, 1996. Rotterdam, A.A. Balkema. pp. 1051-1061

SHEERAN, D. & KRIZEK, R.J. (1971). Preparation of homogeneous soil samples by slurry consolidation. Journal of Materials, Vol. 6, No. 2. pp. 356-373.

SKEMPTON, A.W. (1948) Vane tests in the alluvial plain of the River Forth near Grangemouth. Geotechnique, Vol. 1, No. 2, December 1948. pp. 111-118.

SKEMPTON, A.W. & BISHOP, A.W. (1950) The measurement of the shear strength of soils. Geotechnique, Vol. 2, No. 2, December 1950. pp. 90-108.

SKEMPTON, A.W. (1985) Residual strength of clays in landslides, folded strata and the laboratory. Geotechnique, Vol. 35, No. 1, 1985. pp. 3-18.

SMITH, E.A.L. (1962) Pile-driving analysis by the wave equation. ASCE, Journal of Soil Mechanics and Foundation division, Vol. 127, Part I (Paper No. 3306), pp. 1145-.

SMITH, M.G. (1993) A Laboratory study of the Marchetti Dilatometer. PhD Thesis, University of Oxford, Keble College, UK, 1993.

SOGA, K. & MITCHELL, J.K. (1996) Rate dependant deformation of structured natural clays. Proc. of the ASCE National Convention- Measuring and Modelling Time Dependant Soil Behaviour, Washington DC, 10-14 Nov 1996. New York, ASCE. Geotechnical Special Publication 61. pp. 243-257.

SOUDAIN, M (2002) Ground control to Mr Brown. Ground Engineering Journal, Vol. 35, No. 12, December 2002. pp. 28-29.

STAIN, R.T. (1992) SIMBAT – a dynamic load test for bored piles. Piling: European Practice and Worldwide Trends, London, Thomas Telford, 1992. pp. 198-205.

STEENFELT, J.S., RANDOLPH, M.F. & WROTH, C.P. (1981) Instrumented model piles jacked into clay. Proc. Int. Conf. on Soil Mechanics and Foundation Engineering, 10th, Stockholm, 15-19 June 1981, Vol. 2. Rotterdam, A.A. Balkema. pp. 857-864.

TAYLOR, D.W. (1942) Research on consolidation of clays. Massachusetts Institute of Technology, Dept. of Civil & Sanitary Engineering, Serial 82.

THE INSTITUTION OF CIVIL ENGINEERS. (1997) Specification for piling and embedded retaining walls. 1st ed. London, UK, Thomas Telford Publishing, 1997.

THE STEEL CONSTRUCTION INSTITUTE. (1997) Steel bearing piles guide. 1st ed. A.R. Biddle, Ascot, UK, The Steel Construction Institute, 1997. Publication No. P156.

TAKE, W.A. & VALSANGKAR, A.J. (2001) Earth pressures on yielding retaining walls of narrow backfill width. Canadian Geotechnical Journal, Vol. 38, 2001. pp. 1220-1230.

TAYLOR, P.T. (1966) Age effects on shaft resistance and effect of loading rate on load distribution of bored piles. PhD Thesis, University of Sheffield, UK, 1966.

TAYLOR, R.N. (1995) Geotechnical Centrifuge Technology.1st ed., Glasgow, Blackie Academic and Professional, Taylor, R.N (ed).

TEH, C.I. & HOULSBY, G.T. (1991) An analytical study of the cone penetration test in clay. Geotechnique, Vol. 41, No. 1, 1991. pp. 17-34.

TIKA, T.E., VAUGHAN, P.R. & LEMOS, L.J.L. (1996) Fast shearing of pre-existing shear zones in soil. Geotechnique, Vol. 46, No. 2. 1996. pp. 197-233.

TOMLINSON, M.J. (1994) Pile design and construction practice. 4th ed. London, UK, E & FN Spon,1994.

TOMLINSON, M.J. (2001) Foundation design and construction. 7th ed. Edinburgh, UK, Pearson Education Ltd, 2001.

TRENTER, N.A. (1999) Engineering in glacial tills. Dept. Environment Transport and the Regions (DETR) & Construction Industry Research and Information (CIRIA), CIRIA, London, UK. 1999. CIRIA Report C504.

TRIANTAFYLLIDIS, T. (2001) On application of the Hiley formula in driving long piles. Geotechnique, Vol. 51, No. 10, 2001. pp. 891-895.

VAUGHAN, J. (1975) Application of B&K equipment to strain measurements. Bruel & Kjaer (UK) Ltd, Harrow, October 1975.

VEGA, J.F. (2001) Tensile properties of heat damaged concrete. PhD Thesis, University of Sheffield, UK, November, 2001.

WEELE, A.F.van (1993) Keynote Lecture: Quality assessment foundation piles after installation. In W.F. van Impe (ed), Proc Int. Geotechnical Seminar on Deep Foundations on Bored and Auger Piles, 2nd, Ghent, Belgium, 01-04 January, 1993. Rotterdam, A.A. Balkema. pp. 459-467.

WELTMAN, A.J & HEALY, P.R. (1978) Piling in Boulder Clay and other glacial tills, DOE & CIRIA Piling Group, November, 1978., London, CIRIA. Report No. PG5.

WELTMAN, A.J (1980) Pile load testing procedures, DOE & CIRIA Piling Group, March 1980. London, CIRIA. Report No. PG7.

WHITAKER, T. (1964) Load cells for measuring the base loads in bored piles and cylinder foundations. Building Research Station, current papers, Engineering Series No. 11.

WHITAKER, T. & COOKE, W.C. (1966) An investigation of the shaft and base resistances of large bored piles in London Clay. Building Research Station, current papers, Engineering Series No. 31, Reprint of paper presented at Symp. On Large Bored Piles, Inst. Of Civil Engineers, London, 22nd February, 1966.

WHEELER, P. (2000) Behaviour problems (Design and reality). Ground Engineering Journal, European Foundations Supplement (Spring 2000). pp. 24-25.

WHITE, D (2002) An investigation into the behaviour of pressed in piles. PhD Thesis, University of Cambridge, UK, 2002.

WHITMAN, R.V. (1957) The behaviour of soils under transient loadings. Proc. Int. Conf. on Soil Mechanics and Foundation Engineering, 4th, 1957. pp. 207-210.

WILLIAMSON, I.T. (1983) South Humberside project. British Geological Survey. (1983), Technical Report.

WOOD, T (2003) An investigation into the validation of pile performance using Statnamic tests. MSc Thesis, Imperial College, London, UK, 2003.

WROTH, C.P., CARTER, J.P. & RANDOLPH, M.F. (1979) Stress changes around a pile driven in cohesive soil. Recent developments in the design and construction of piles, 1979, Institution of Civil Engineers, London. pp. 345-354.

YONG, R.N. & JAPP, R.D. (1967) A flow law for clays in dynamic compression. Proc. Int. Symp. on Wave Propagation and Dynamic Properties of Earth Materials, Alberquerque, USA, 23-25 Aug 1967. New Mexico, University of New Mexico Press. Pp. 183-188.

ZHU, J.G. & YIN, J.H. (2000) Strain rate dependent stress strain behaviour of overconsolidated Hong Kong marine clay. Canadian Geotechnical Journal, No. 37, 2000. pp. 1272-1282.